LATE WINTER SNOW AND ICE CHARACTERISTICS OF FIRST-YEAR FLOES IN THE BELLINGSHAUSEN AND AMUNDSEN SEAS, ANTARCTICA

Results of Investigations During R.V. *Nathaniel B. Palmer* Cruise NBP 93-5 in August and September 1993

M.O. Jeffries[1], A.P. Worby[2], K. Morris[1], W.F. Weeks[1], B. Hurst-Cushing[1], R. Jaña[3] and H.R. Krouse[4]

[1]Geophysical Institute, University of Alaska Fairbanks
[2]Antarctic CRC, University of Tasmania
[3]Instituto Antartico Chileno
[4]Department of Physics & Astronomy, University of Calgary

Geophysical Institute, University of Alaska Fairbanks
Report UAG-R-325

February 1997

TABLE OF CONTENTS

ABSTRACT

In August and September 1993, the R.V. *Nathaniel B. Palmer* operated for 37 days in the pack ice of the Bellingshausen and Amundsen seas supporting a sea ice research program, which included snow cover characterization, snow and ice thickness measurements and ice core analysis. The objective of the study was to improve our knowledge of the conditions and processes that contribute to first–year sea ice development and ice thickness variability in this region, and their impact on active microwave backscatter from the ice.

The mean snow density was 247kg/m^3. The principal snow type was composed of facetted crystals and depth hoar (48%), indicating strong temperature gradient metamorphism had been common. Ice layers (9%) indicated that snow metamorphism also included melting. Wet snow and slush layers (6%) at the base of the snow cover, with a mean salinity of 21.6‰, were due to seawater flooding of the snow/ice interface and brine wicking. Negative freeboard values, i.e., the water level was above the ice surface which was flooded with seawater, occurred at 18% of the drill holes on the snow and ice thickness transects. The majority of snow depth values (76%) ranged from 0.05–0.35m. The mean snow depth value was 0.23±0.16 m. The majority of ice thickness values (62%) ranged from 0.3–0.8m. The mean ice thickness was 0.90±0.64m. Both the ice thickness and snow depth probability density functions have long tails of high values: the ice thickness distribution due to thickening by rafting and ridging, and the snow depth distribution due to snow drift formation on the flanks of ridge sails and other protuberances at the surface. In addition to the widespread flooding of the snow/ice interface, there was strong flooding potential, as indicated by the large number (59%) of freeboard values in the range 0–0.05m. Three types of floe, X, Y and Z, are classified according to their coefficients of ice thickness variation. Their snow depth, ice thickness, draft and freeboard characteristics, and structural composition are described.

Ice <0.5m thick was colder (mean temperature: –3.9°C) than ice ≥0.5m thick (mean temperature: –2.8°C), mainly because it had a thinner snow cover and was, therefore, less well insulated from the atmosphere than the thicker ice. Ice <0.5m thick was also more saline (mean salinity: –7.3‰) than ice ≥0.5m thick (mean salinity: 5.6‰), primarily because the thicker ice was older and had undergone greater brine loss. The temperature–ice thickness and the salinity–ice thickness relationships each have an abrupt change of slope at 0.5m. In ice ≥0.5m thick, mean core salinity was largely independent of ice thickness and generally lower than Arctic ice of similar age and thickness. The composite salinity profile for ice <0.5m thick was close to the *C* shape that is typical of Arctic first–year ice. Ice ≥0.5m thick, however, had a characteristic *S* shape profile with the highest values at the top due to snow ice formation, and a trend to lower values towards the bottom due to brine loss. Much of the brine loss may have been due to gravity drainage, since the majority of brine volumes were >5%, a value at which brine pockets coalesce and gravity drainage occurs.

Ice crystal texture and $\delta^{18}O$ values show that the major structural components of the floes were frazil ice (44%), congelation ice (25%) and snow ice (25%). The frazil ice originated primarily in the pancake cycle. Frazil and congelation ice layers both had an average thickness of 0.12m, indicating that neither reached a substantial thickness by thermodynamic growth alone; each thickened primarily by dynamic processes, i.e., deformation. The snow ice layers had a mean thickness of 0.2m and indicated that, by the end of winter, the thermodynamic development of the ice cover was dominated by seawater flooding of the snow/ice interface and snow ice formation. Snow ice layers were composed of 7–13% snow, which contributed to 2–4% of the total ice mass.

1. INTRODUCTION

Knowledge of the spatial and temporal variability of the thickness distribution of the Antarctic sea ice cover is essential for understanding the role of the pack ice in modifying atmosphere–ocean interactions and exchanges of heat, mass and momentum, their influence on ocean and climate variability from the local to global scale, and the biological productivity of the ice and ocean. Fundamental to the understanding of the ice thickness distribution is a knowledge of the dynamic (ridging and rafting) and thermodynamic (freezing and melting) processes that contribute to the development of the sea ice cover under the influence of atmospheric and oceanic forcing.

The pack ice is a mobile mix of ice of different thicknesses, plus open water in leads and polynyas. High air–sea heat exchange and rapid new ice formation occur in open water areas (Maykut, 1978; Worby and Allison, 1991) and the associated salt fluxes profoundly affect the ocean salinity budget, water mass formation and circulation (Gordon and Huber, 1990; Fahrbach et al., 1991). The ridges that result from deformation contain most of the pack ice mass even though they constitute a relatively small area of the pack ice (Allison and Worby, 1994; Worby et al., in press). Deformation affects the bottom roughness, which determines the drag coefficient and influences the exchange of momentum between the ice and ocean (Andreas et al., 1993).

The first comprehensive Antarctic sea ice thickness data set, from the eastern Weddell Sea, showed that undeformed first–year ice with a preferred thickness of 0.5–0.6m was significantly thinner than ice of a similar age in the Arctic (Wadhams et al., 1987). Subsequently, in the western Weddell Sea, even deformed first–year ice was found to be thinner than similar Arctic ice (Lange and Eicken, 1991a). The pack ice off East Antarctic has thickness characteristics similar to those of the eastern Weddell Sea (Allison et al., 1993; Allison and Worby, 1994; Worby and Massom, 1995). Prior to 1993, little was known of sea ice thickness variability in the Pacific sector of the Southern Ocean, between the Antarctic Peninsula and Victoria Land, i.e, the Ross, Amundsen and Bellingshausen seas. Since then, a considerable amount of data has been obtained in this region during dedicated sea ice research cruises aboard the R.V. *Nathaniel B. Palmer* (Worby et al., 1994, 1996; Jeffries and Adolphs, 1997; Jeffries et al., 1995, in press)

The snow depth distribution is also of some importance. Snow is an effective insulator which, depending on snow depth and thermal conductivity, reduces heat transfer from the base of the ice to the snow/ice interface and thus basal ice growth rates (Maykut 1978, 1986). Snow depth and wetness affect the albedo of the snow surface and thus its radiative properties and the surface energy balance (Andreas and Makshtas, 1985; Allison et al., 1993). Snow depth variability influences the surface roughness, which determines the drag coefficient and the exchange of momentum between the atmosphere and the ice (Andreas et al., 1993). The snow cover also controls the amount of light available for phytoplankton growth within and below the sea ice (Sullivan et al., 1985; Garrison et al., 1986; Eicken, 1992a).

One of the key roles of the snow cover on Antarctic sea ice, and one which sets it apart from Arctic snow/sea ice interactions, is to contribute to the thickening of the ice by snow ice formation at the snow/ice interface. The widespread occurrence of this process was first documented in the Weddell Sea (Lange et al., 1990; Eicken et al., 1994) and has since been shown to be widespread in the East Antarctic pack ice (Worby and Massom, 1995). The freezing of slush and the formation of snow ice at the snow/ice interface, and the associated brine exchange between the snow/ice interface and the underlying ocean in autumn, provide a significant salt flux to the upper ocean (Lytle and Ackley, 1996). They also contribute to the establishment of a productive ice surface algal community (Fritsen et al., 1994). The introduction of seawater at the snow/ice interface also has a significant effect on passive and active microwave signatures of the ice cover (Comiso et al., 1989; Lytle et al., 1996).

Increased snowfall, seawater flooding of the snow/ice interface, and resultant increased ice temperatures might have contributed to the summer sea ice anomalies observed in the Bellingshausen and Amundsen seas between 1988 and 1991 (Jacobs and Comiso, 1993). On the other hand, numerical model simulations indicate that, while increased snow accumulation rates do lead to a thinner, more porous and thus weaker ice cover, they might also enhance snow–ice formation once seawater flooding has occurred and contribute to the survival of perennial sea ice covers in areas such as the western Weddell Sea and the Bellingshausen Sea (Eicken et al., 1995).

To understand the relationship between sea ice and climate requires a knowledge of the seasonal and regional variability of the snow and ice processes and air–ice–ocean interactions that contribute to sea ice growth and decay. Numerical models can not provide a complete understanding of sea ice processes, air–ice–ocean interactions and their role in climate variability. Currently, the information that can be gleaned from satellites is limited by ambiguities in the remotely sensed signatures of sea ice and their dependence on surface properties and processes. Direct observations of sea ice processes and interactions are necessary to increase the knowledge and understanding of sea ice growth and decay, and they are increasing as research vessels spend a greater amount of time in the pack ice in all seasons. Ship–based programs include measurements of the snow and ice thickness, and the examination of the structure and properties of ice cores, which are a record of some of the conditions and processes that have contributed to ice growth and decay since the initial formation of the ice cover. Such information can, in turn, provide forcing and validation fields for numerical models, and improve the understanding of sea ice remote sensing signatures.

The late winter pack ice in the Bellingshausen and Amundsen Seas was studied for the first time in August and September 1993, during a cruise aboard the R.V. *Nathaniel B. Palmer*. The objective of the study was to improve our knowledge of the conditions and processes that contribute to first–year ice development and ice thickness variability in this region, and their impact on active microwave backscatter from the ice. Some of the results of the study have been discussed already in a number of publications: snow cover characteristics (Jeffries et al., 1994c); snow and ice thickness distributions (Worby et al., 1994, 1996); ice core structure and stable isotopic composition (Jeffries et al., 1994c, 1997); active microwave backscatter signatures (Jeffries et al. 1995; Morris and Jeffries, 1995, in press; Morris et al., 1996).

The purpose of this report is to provide a complete overview of the results of the ice floe sampling and investigation program in August and September 1993. The report contains data that have already been presented in the papers described above, as well as data that are being published for the first time. This is primarily a data report, and while we make some comparisons with other Antarctic sea ice zones and attempt to place the data in the context of the current knowledge of Antarctic sea ice processes, neither the comparisons nor the discussion are exhaustive. We hope that the report will prove to be useful to those interested in field investigations, remote sensing and/or modelling of Antarctic sea ice processes.

2. STUDY AREA AND METHODS

This investigation was conducted from the R.V. *Nathaniel B. Palmer*, which operated for 37 days in August and September 1993 in the pack ice of the Bellingshausen and Amundsen seas between latitudes 66.75° and 70.3°S, and longitudes 77° and 110°W (Figures 1 and 2). The study included snow cover characterization (temperature, density, stratigraphy and snow type, oxygen isotopic composition), snow and ice thickness profiling (snow depth, ice thickness, draft and freeboard) and ice core analysis (temperature, salinity, brine volume, structure and stable oxygen isotopic composition).

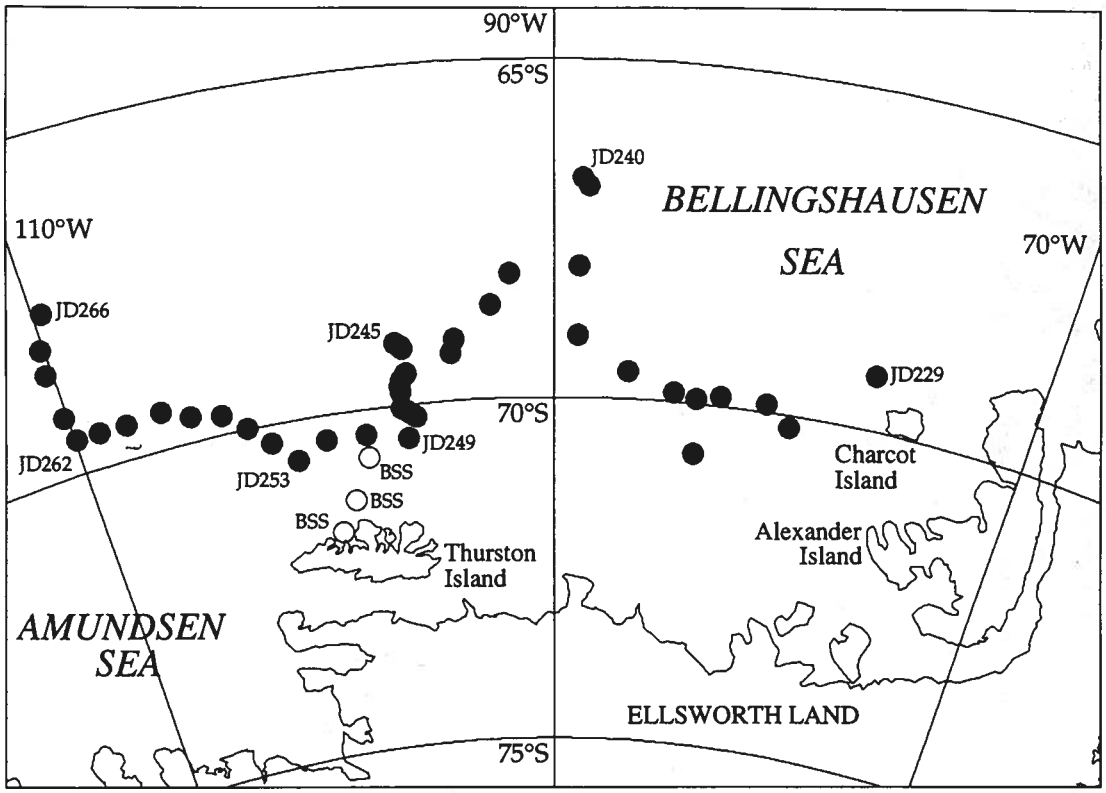

Figure 1. Map of the study area showing the track of the R.V. Nathaniel B. Palmer in the pack ice of the Bellingshausen and Amundsen seas in August and September 1993. The solid circles identify the location of the floes that were investigated for this study. The alpha–numeric code with some of the circles is the Julian Date on which the sampling was done, e.g., JD 240 is 28 August. Additional information on the types of investigation done on each floe is presented in Figure 2. The open circles marked BSS identify the location of floes that were sampled in March 1992 during a previous cruise (Jeffries et al., 1994a).

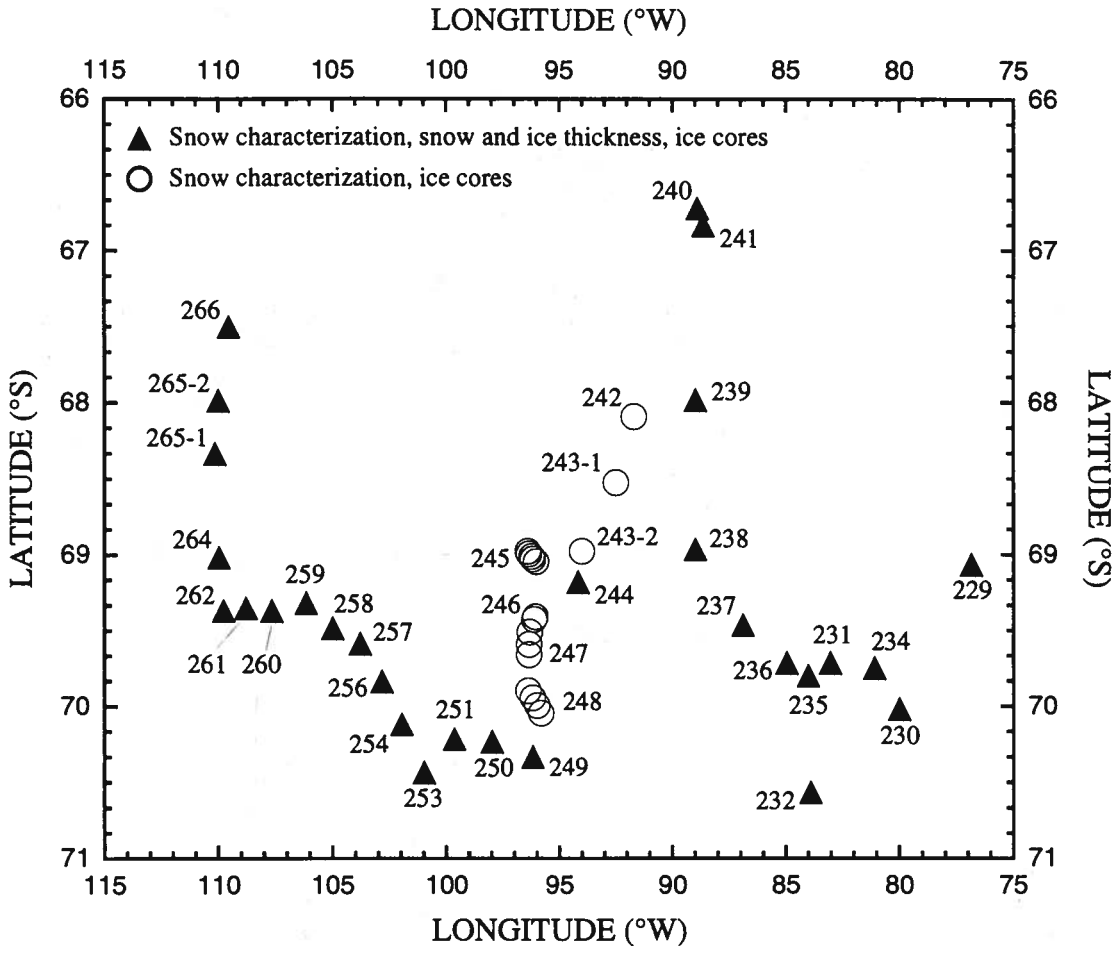

Figure 2. Map showing the location and date (Julian Day) of investigation of ice floes studied. The open circles identify the floes that were investigated during the period when a significant swell was propagating through the pack ice and breaking previously large/massive floes into small floes with typical dimensions of 5–20m across.

When possible, the measurements and observations described above were made on all floes on a daily basis. The exception to this occurred between 30 August (day 242) and 5 September (day 248) when a swell propagating through the pack ice broke up the previously large/massive floes into much smaller floes typically 5–20m across. It has since been determined from ERS–1 SAR data that the swell penetrated as far as 400km into the pack ice from the ice edge (Morris and Jeffries, in press). During this period, when the conditions were either too hazardous and/or the floes were too small to be occupied by the entire party (6–8 individuals), only snow cover characterization and ice coring were completed on as many as five different floes each day. On day 244, the swell subsided briefly and it was possible for the entire party to work on a rare piece of undeformed sheet ice. Figure 2 identifies those floes where only snow cover characterization and ice coring were possible.

Ice and snow thickness measurements obtained by drilling provide information on small scale (10–100 m) variations in ice and snow thickness and, together with ice structure data, can be used to determine the processes of ice floe development. A total of 1113 direct measurements of snow depth, ice thickness, draft and freeboard were made at holes drilled in the ice at equi–distant intervals along 80–150m long transects across 29 different floes. Each transect was from a floe representative of the surrounding pack, and included measurements across any ridged ice that was present. We are confident that the data set includes a reasonably good representation of the thicker, ridged ice, but we recognize that it contains an inadequate representation of ice <0.2m due to our reluctance to work on such thin ice. Holes were drilled at 2.5m intervals across most floes, but on some the interval was reduced to 1m.

Sixty–three pairs of ice cores were obtained from 50 different ice floes. Each core had a diameter of 0.1m and the distance between pairs of cores was ≤0.3m. One core was used for immediate measurements of temperature and salinity, and the other for crystal structure and stable isotope analysis for identification of growth processes. An additional 16 cores were obtained from some of the floes for temperature and salinity measurements only. The base of each core was examined for the presence of a friable skeletal layer that indicates active congelation ice formation. Only one of the floes where cores were obtained was multiyear ice. The structure and isotopic composition of this core (248–4b) is described and illustrated in the Appendix (pages A–32 and A–34). Otherwise, this report focusses on the first–year ice data.

Each pair of cores was given a unique identification number beginning NBP 95–3 (the cruise number) followed by the Julian Day and the number in the sequence of cores obtained that day. For example, core NBP 95–3/245–3 was the third core to be obtained on day 245 (2 September) during cruise NBP 95–3. Each salinity/temperature core was given the affix *a*, and each structure/isotopes core was given the affix *b*. Thus, cores NBP 95–3/245–3*a* and 245–3*b* were the third pair of salinity/temperature and structure/isotopes cores to be obtained on day 245.

As soon as the first ice core was removed from the floe, temperatures were measured along its length with a thermistor probe and digital thermometer. The first two measurements were at depths of 0.05m and 0.1m below the surface, and all subsequent measurements were at 0.1m intervals. The ice was then cut into two 0.05m long sections at the top and into 0.1m long sections below that. Each section was sealed in a plastic bucket and returned to the ship where the ice was melted. The salinity of the melted samples was measured with a Beckmann salinity meter (Model RB5-349A Solubridge, accuracy 2% of reading) calibrated with Standard Seawater. Brine volumes were calculated from the temperature and salinity data according to the method of Cox and Weeks (1983). The initial brine volume calculations assumed an ice density of 900kg/m^3; the implications of those data with respect to the possible role of vertical brine exchange in flooding of the snow/ice interface are described briefly in Jeffries et al. (in press). Subsequently, an ice density of 920kg/m^3 (Eicken et al., 1994) was assumed and those brine volume data are reported here.

The second ice core was returned to the ship for ice crystal structure analysis in the cold–room operating at a temperature of –15°C. This involved: (1) cutting vertical thick sections with a thickness of 2–3mm along the entire length of each core; (2) illuminating the vertical sections between crossed polarizers to reveal the crystal structure; and (3) logging the structure of each vertical section, and compiling a profile of structure variations from the top to the bottom of the core. The remaining pieces of ice were analyzed by Christian Fritsen, University of Southern California, for his study of nutrients and biological productivity in the ice.

Once the structural analysis was complete, samples were cut from each core according to the structural variations and the samples were melted for stable oxygen isotope analysis. A total of 524 samples were analyzed. The oxygen isotopic composition of each sample ($^{18}O/^{16}O$ ratio), measured by mass spectrometer, is expressed as $\delta^{18}O$ in per mil (‰) units. $\delta^{18}O$ is the difference between the ratio of the heavy (^{18}O) to light (^{16}O) isotopes in the sample (s) and the isotopic ratio of a standard, in this case V–SMOW (Vienna–Standard Mean Ocean Water, $\delta^{18}O = +0.07‰$), i.e.,

$$\delta^{18}O = \{ ([^{18}O/^{16}O]_S / [^{18}O/^{16}O]_{V\text{–}SMOW}) - 1 \} \times 10^3$$

All the snow and ice thickness profiles, ice core temperature, salinity, brine volume and stable isotope profiles, and ice core structure diagrams are illustrated in the Appendix.

A total of 118 snow pits were investigated on the same floes where ice cores were obtained; 79 of those snow pits were located at the sites where cores were retrieved. The digital thermometer and probe were used to measure the temperature at the snow surface and at the snow/ice interface. To minimize the effects of solar radiation, the probe was always shaded for the surface temperature measurements, and for the snow/ice interface temperature measurement the full length of the probe (10cm) was always pushed under the snow on the shady side of the snow pit. Density was measured by weighing a known volume ($100cm^3$) of snow and those samples (115 total) were subsequently melted for salinity and stable isotope analysis. The snow stratigraphy was recorded, including the occurrence and thickness of layers of ice, facetted crystals/depth hoar and wet snow/slush. The snow salinity was determined from electrical conductivity measurements made using a Rosemount Analytical Conductivity Bridge (Model RC–20, accuracy 0.25% of reading) calibrated with Standard Seawater.

A total of thirty–six sea water samples obtained during CTD/bottle casts were analyzed for their oxygen isotopic composition. The seawater samples were from the upper 15m of the water column adjacent to the different floes from which ice cores had been obtained. The seawater stable isotope data are useful in connection with the interpretation of the ice core stable isotope variability.

The snow, ice and water $\delta^{18}O$ data are used to differentiate between granular snow ice and granular frazil ice, and to determine the fraction of snow contributing to the snow ice layers and to the entire ice thickness. Lange et al. (1990) described a model to determine the fraction of snow and meteoric ice in Weddell Sea ice. Here we use a simplified version of that model that was used to determine the snow fraction and meteoric ice fraction of late summer ice cores in the Bellingshausen/Amundsen region (Jeffries et al., 1994a).

The model has the form

$$f_s + f_{sw} = 1 \qquad (1)$$

$$f_s\delta_s + f_{sw}\delta_{sw} = \delta \qquad (2)$$

where f_s is a snow fraction, f_{sw} is a seawater fraction, δ_s is the mean $\delta^{18}O$ value of the snow, δ is the mean $\delta^{18}O$ value of the ice layer for which the snow fraction is being determined, and δ_{sw} is a seawater $\delta^{18}O$ value. For δ_s we use values of –17‰, –13.2‰ and –9.4‰, i.e., the mean snow $\delta^{18}O$ value ± 1 standard deviation (–13.2±3.8‰), to calculate f_s values. We do this to allow for the variability of snow $\delta^{18}O$ values that arises from atmospheric processes that affect the isotopic ratio of the moisture prior to and during precipitation events, and from factors such as metamorphism, wind erosion and redeposition that affect the isotopic composition of the snow cover once it has been deposited on the floes. Although the mean $\delta^{18}O$ value of the seawater samples was –0.9‰, we use a value of 0.0‰ for δ_{sw}. This allows for isotopic fractionation (α = 1.009) during the formation of snow ice, which is implicit in our choice of 0.0‰ as the isotopic criterion for differentiating between snow ice and frazil ice.

3. SNOW COVER CHARACTERISTICS AND PROPERTIES

3.1 Snow pit depth

The depth of the snow pits varied between 0.03m and 0.82m, but the majority were <0.5m deep. The mean value was 0.22±0.14m. These values are consistent with the much greater number of snow depth values obtained along the snow and ice thickness transects (section 4.1) and indicate that the depth of the snow pits was representative of the snow cover thickness on the floes that were investigated.

3.2 Snow types and stratigraphy

For the purpose of describing the snow types and stratigraphy we use a simple classification of four categories: slush/wet snow, ice layers, facetted grains and depth hoar, "other snow". Slush and wet snow, which occurred primarily at the base of the snow cover, resulted mainly from seawater flooding of the snow/ice interface and also brine wicking. The slush was easy to recognize and the wet snow, often comprised of intact snow grains unaltered by the wetting, was characterized by a grey appearance. Facetted grains and depth hoar crystals are a consequence of temperature gradient metamorphism. The "other snow" category refers to any snow that does not fall into the other three categories, and includes new snow, and older snow that has not been subject to temperature gradient metamorphism. The latter often occurred as wind slab.

Wet snow and slush occurred in 35% of the snow pits. The widespread occurrence of wet snow/slush is consistent with the frequent observation of flooding along the snow and ice thickness transects (section 4.1). The snow pits contained an average of 6.3% wet snow/slush. As a function of the total depth of snow examined in all the snow pits, the snow cover was composed of 6% wet snow/slush.

Facetted grains and depth hoar occurred in 81% of the snow pits. The snow pits contained an average of 48% facetted grains/depth hoar. As a function of the total depth of snow examined in all the snow pits, the snow cover was composed of 55% facetted grains/depth hoar. Skeletal depth hoar, comprising loose accumulations of cupped and columnar crystals with dimensions of as much as 3-5 mm and voids (1–2 mm) between crystals, was observed in 59% of the snow pits. Skeletal depth hoar represents an advanced stage of metamorphism in older snow that has been subject to strong negative temperature gradients (section 3.3).

Ice layers occurred in 74% of the snow pits. The majority of pits had at least one ice layer, and occasionally as many as four ice layers. The snow pits contained an average of 9.1% ice layers. As a function of the total depth of snow examined in all the snow pits, the snow cover was

composed also of 9.1% ice layers. The ice layers had an average thickness of 2.7cm and extended horizontally for distances of metres. Since air and snow surface temperatures exceeded 0°C on a number of occasions during the cruise, the ice layers might be melt features. In addition, when relatively warm, moist marine air flows over the pack ice, there is likely to be condensation onto the cold snow cover, resulting in the formation of surface crusts and ice layers. Horizontal ice layers also are often associated with depth hoar formation (Colbeck, 1991).

"Other snow" occurred in 83% of the snow pits. The snow pits contained an average of 36% "other snow". As a function of the total depth of snow examined in all the snow pits, the snow cover was composed of 30% "other snow".

The amounts of each snow type described above are similar to those reported in the East Antarctic pack ice (Worby and Massom, 1995).

The density values of the snow samples varied between 108kg/m^3 and 467kg/m^3, with a mean value of 247kg/m^3. These values are lower than those reported in the East Antarctic pack ice (Worby and Massom, 1995), but similar values have been reported in the Weddell Sea (Garrity, 1992; Eicken et al., 1994).

The probability density function of snow density values (Figure 3a) shows that the majority of values occur in the range 175–325kg/m^3 with a mode of 225–250kg/m^3. Figures 3b and 3c show the probability density functions for the depth hoar and "other snow" categories respectively. The depth hoar PDF is more peaked and has a narrower range of values than the "other snow", but there is no statistically significant difference between their mean values; 235±54kg/m^3 (depth hoar) and 255±70 kg/m^3 ("other snow"). The similarity between the densities of each snow type is peculiar inasmuch as the depth hoar might be expected to have a much lower density. However, it is possible that brine wicking into the depth hoar, either directly from the ice surface or from slush layers, might add sufficient mass to increase the weight and thus the density of the depth hoar. This is discussed further in section 3.2.

3.3 Salinity and $\delta^{18}O$

The range of salinity values for all the snow samples was 0.02–36.3‰, with a mean value of 8.65±10.6‰. The probability density function for all the salinity values has a distinct peak in the 0–5‰ category and a long tail of higher values (Figure 4a). The mean salinity value and the shape of the PDF are similar to those reported in the East Antarctic pack ice (Worby and Massom, 1995).

The range of $\delta^{18}O$ values for all the snow samples was –23.3 to –0.6‰, with a mean value of –11.9±4.7‰. The probability density function for all the $\delta^{18}O$ values has a fairly normal distribution, with the majority of values falling in the range –16 to –8‰ (Figure 4c).

The wet snow and slush have a mean salinity of 21.6±7.9‰. When those samples are excluded from the snow salinity data set, the range of snow salinity values is 0.02–29.2‰, with a mean value of 4.8±8.0‰. However, the salinity PDF (Figure 4b) does not differ significantly from that of the entire snow salinity data set. A long tail of high values remains and we attribute this to brine wicking up into the snow cover either directly from the ice surface or from the slush layers. Brine might move into the snow without discolouring it and creating the moist, grey appearance that was our criterion for the identification of wet snow.

The wet snow and slush have a mean $\delta^{18}O$ value of –4.9±2.0‰. Excluding those samples from the snow $\delta^{18}O$ data set leaves the PDF without any values less than –6.0‰ (Figure 4d). The range

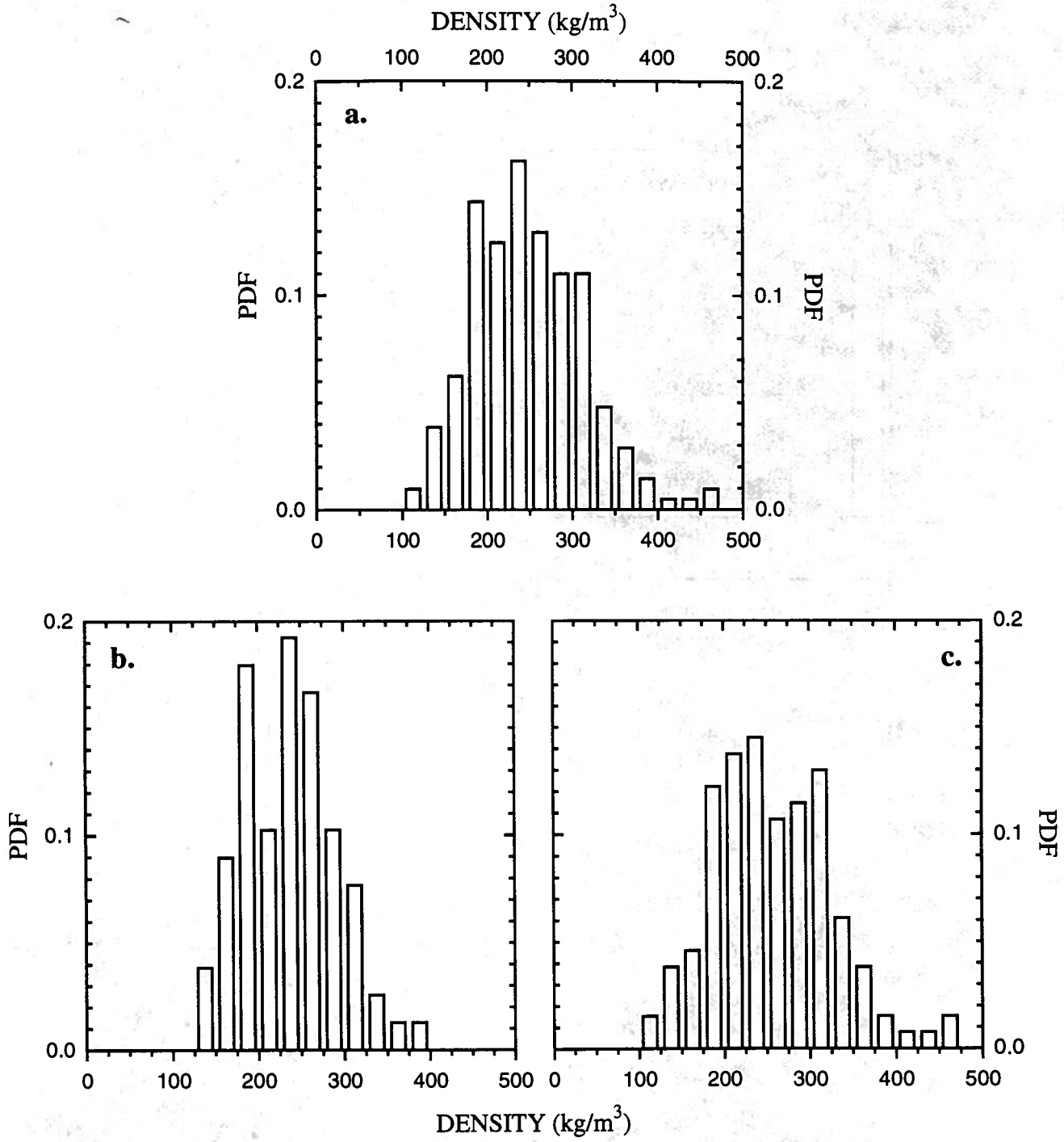

Figure 3. Probability density functions (PDF) of density of (a.) all snow samples, (b.) depth hoar samples, and (c.) "other snow" samples.

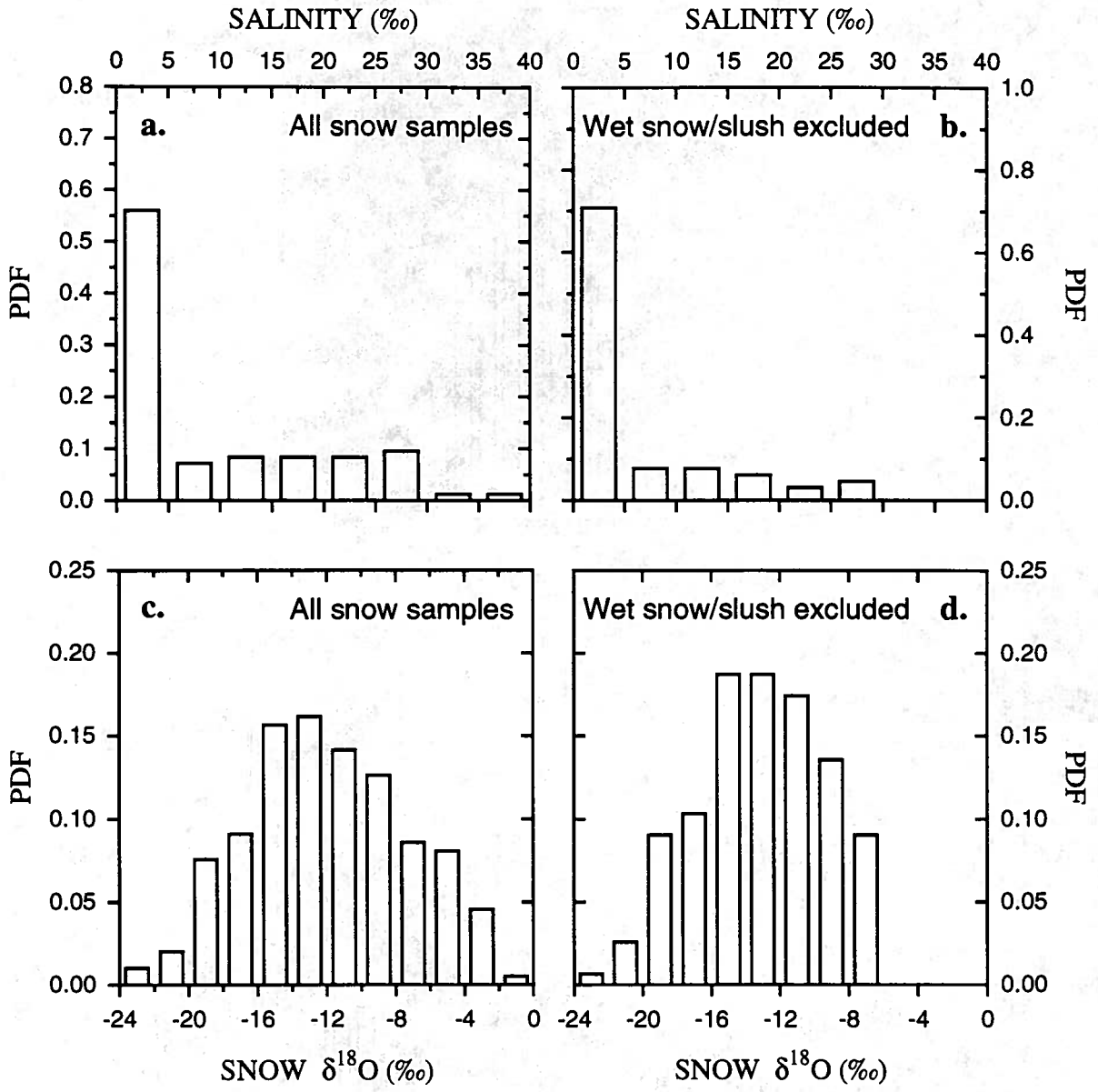

Figure 4. Probability density functions (PDF) of salinity (top) and $\delta^{18}O$ (bottom) values in the snow cover. Graphs (a.) and (c.) represent all the snow samples. Graphs (b.) and (d.) exclude the wet snow and slush at the base of the snow cover.

of $\delta^{18}O$ values for these snow samples is –23.3 to –6.0‰, with a mean value of –13.2±3.8‰. We use this value for calculating the fraction of snow in the ice cores, as described in section 5.5.4.

3.4 Temperature

Snow surface temperatures ranged from –25.3° to 0°C, with a mean value of –11.8±7.6°C. These values reflect the temperature conditions in which the work on floes was undertaken, since the snow surface temperature responds quickly to air temperature variability. On the other hand, temperatures at the snow/ice interface are higher and have a narrower range than those at the snow surface (Figure 5a), and they respond more slowly to air temperature variability due to the insulating properties of the snow cover (Figure 5c).

The snow/ice interface temperatures ranged from –13.3 to –2°C, with a mean value of –4.7±2.3°C. A similar value has been reported in the East Antarctic pack ice (Worby and Massom, 1995). The majority of snow/ice interface temperatures were between –8°C and –2°C (Figure 5a). In the 10 instances where snow/ice interface temperatures were <–8°C, the snow depth was ≤0.1m (mean value 0.05±0.02m) and thus provided significantly less insulation than a deeper snow cover. The relationship between the snow surface and snow/ice interface temperatures is similar to that reported in the eastern Weddell Sea (Comiso et al., 1989).

The temperature difference between the snow surface and the snow/ice interface varied between –21.6°C and 3.3°C, with a mean value of –7.0±7.0°C. A negative value indicates that the snow surface temperature is lower than the snow/ice interface temperature, and this occurred at 78% of the snow pits. The temperature gradients in the snow cover varied between –2.4°C/cm and 0.3°C/cm, with a mean value of –0.4°C/cm. The temperature gradients were quite a strong function of the snow depth (Figure 5c). Temperature gradients at 76% of the snow pits were steeper than –0.1°C/cm, the critical value for kinetic crystal growth and formation of facetted crystals and depth hoar (Colbeck, 1982).

4. SNOW DEPTH AND ICE THICKNESS VARIABILITY

4.1 Snow depth, ice thickness, draft and freeboard distributions

The snow depth, ice thickness, draft and freeboard data for each floe are summarized in Table 1. Probability density functions (PDFs) of all the snow depth, ice thickness, draft and freeboard data are shown in Figure 6.

The snow depth PDF (Figure 6a) has a mode of 0.05–0.10m and 76% of the values occur in the range 0.05–0.35m. The mean snow depth value is 0.23±0.16m. The thicker snow in the tail of the distribution primarily represents snow that had accumulated on the flanks of ridges, which act as snow fences and cause drifts to form. This phenomenon is illustrated by the snow and ice profiles of the strongly ridged floe in Figure 7.

The dominant features in the ice thickness distribution (Figure 6c) are the mode at 0.4–0.5m and the narrow range of thickness categories that contain the bulk of the measured values. Almost 62% of the observations fall in the range 0.3–0.8m. Thickness values of this magnitude can be attained by thermodynamic processes alone in Antarctica, particularly in landfast ice zones (e.g., Jeffries et al., 1993; Worby and Massom, 1995). However, as the structure analysis shows (section 5.5), most of the ice investigated for this study had been subject to deformation, which plays a key role in thickening the ice cover. The mean ice thickness is 0.90±0.64m. The large standard deviation with respect to the mean for all the data and for the individual ice floes

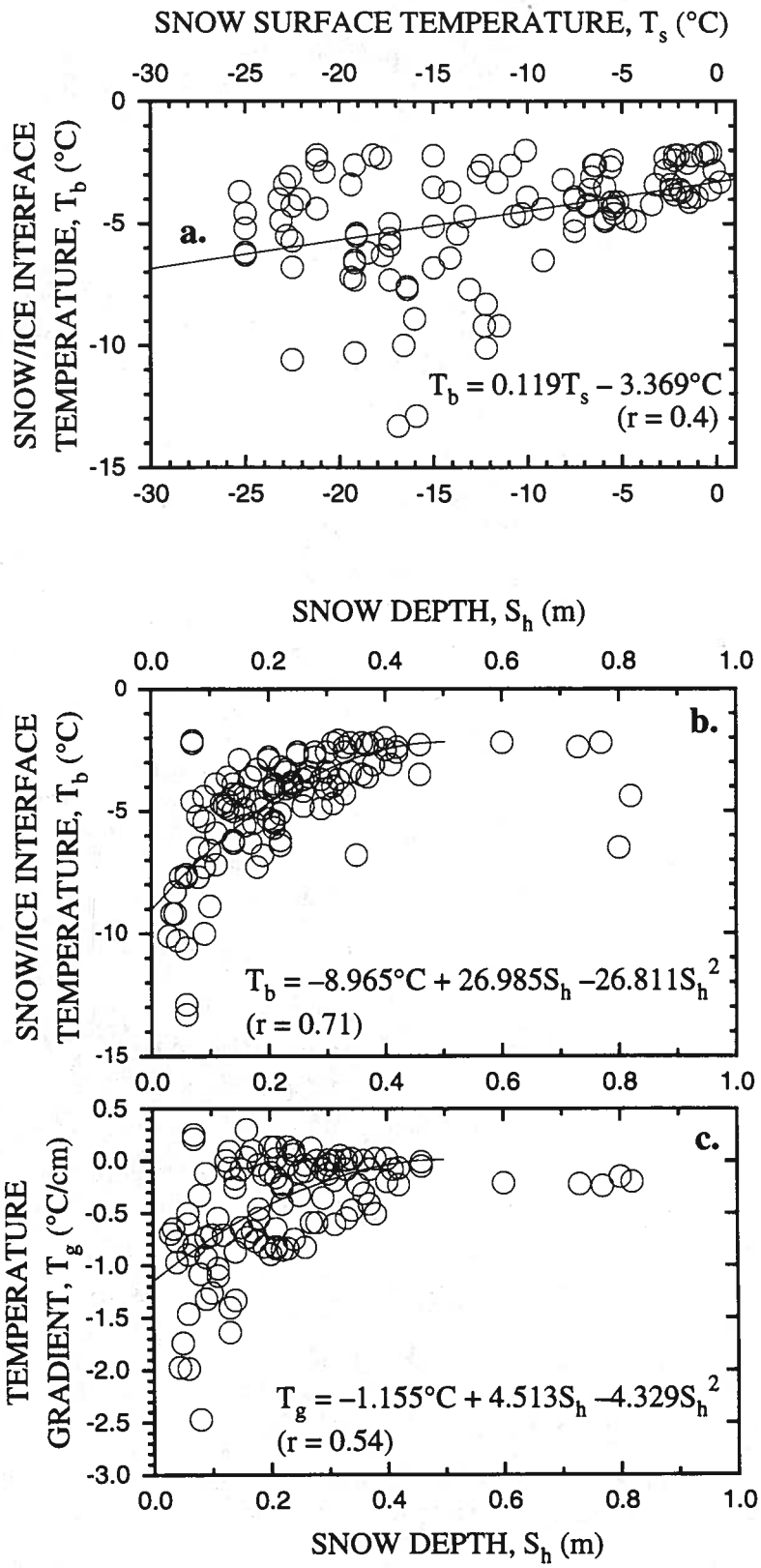

Figure 5. Scatter plots and regression equations of the relationships between (a.) the snow/ice interface temperature and the snow surface temperature, (b.) the snow/ice interface temperature and the snow depth, and (c.) snow depth and temperature gradient in the snow cover. Plot (a.) has a linear regression curve. Plots (b.) and (c.) have second–order polynomial regression curves.

Table 1. Summary of descriptive statistics (mean ± 1 standard deviation) of floe type, snow depth, ice thickness, draft and freeboard of each floe, the number of measurements (n), and the coefficient of ice thickness variation.

Floe Number & Type	Snow Depth (m)	Ice Thickness (m)	Draft (m)	Freeboard (m)	n	Coefficient of Ice Thickness Variation
229, C	0.28 ± 0.15	1.53 ± 0.79	1.41 ± 0.78	0.11 ± 0.11	53	0.51
230, C	0.23 ± 0.09	2.30 ± 1.48	2.07 ± 1.29	0.21 ± 0.27	26	0.64
231, C	0.20 ± 0.07	0.91 ± 0.43	0.85 ± 0.41	0.05 ± 0.04	21	0.47
232, B	0.35 ± 0.11	0.93 ± 0.20	0.91 ± 0.21	0.02 ± 0.04	41	0.22
234, C	0.23 ± 0.11	1.00 ± 0.63	0.94 ± 0.56	0.05 ± 0.10	41	0.63
235, C	0.20 ± 0.06	0.71 ± 0.30	0.68 ± 0.30	0.02 ± 0.02	41	0.42
236, C	0.32 ± 0.23	1.18 ± 1.05	1.10 ± 0.94	0.07 ± 0.07	49	0.88
237, B	0.55 ± 0.12	1.48 ± 0.43	1.46 ± 0.43	0.01 ± 0.02	40	0.29
238, B	0.09 ± 0.05	0.42 ± 0.16	0.40 ± 0.15	0.02 ± 0.04	61	0.38
239, B	0.04 ± 0.01	0.34 ± 0.09	0.32 ± 0.08	0.02 ± 0.02	41	0.26
240, B	0.20 ± 0.10	0.54 ± 0.17	0.52 ± 0.17	0.01 ± 0.03	41	0.31
241, C	0.24 ± 0.10	0.72 ± 0.41	0.71 ± 0.40	0.00 ± 0.04	53	0.56
244, A	0.06 ± 0.01	0.36 ± 0.03	0.35 ± 0.03	0.01 ± 0.01	41	0.08
249, B	0.57 ± 0.13	1.33 ± 0.73	1.37 ± 0.76	-0.04 ± 0.07	36	0.54
250, C	0.31 ± 0.05	0.81 ± 0.24	0.88 ± 0.22	-0.06 ± 0.07	41	0.29
251, C	0.32 ± 0.60	0.85 ± 0.51	0.86 ± 0.51	-0.01 ± 0.02	41	0.60
253, B	0.36 ± 0.10	0.91 ± 0.26	0.90 ± 0.25	0.00 ± 0.03	51	0.28
255, C	0.30 ± 0.06	0.92 ± 0.45	0.90 ± 0.43	0.01 ± 0.04	32	0.48
256, B	0.18 ± 0.08	0.84 ± 0.29	0.81 ± 0.28	0.02 ± 0.02	41	0.34
257, C	0.06 ± 0.03	0.65 ± 0.37	0.60 ± 0.35	0.04 ± 0.03	37	0.56
258, B	0.18 ± 0.06	0.75 ± 0.17	0.72 ± 0.17	0.02 ± 0.01	42	0.22
259, C	0.10 ± 0.04	0.58 ± 0.11	0.54 ± 0.11	0.03 ± 0.02	41	0.18
260, C	0.13 ± 0.05	0.54 ± 0.24	0.52 ± 0.23	0.02 ± 0.01	42	0.44
261, C	0.27 ± 0.08	0.85 ± 0.41	0.83 ± 0.41	0.01 ± 0.03	41	0.48
262, C	0.13 ± 0.08	0.98 ± 0.48	0.92 ± 0.46	0.06 ± 0.03	43	0.48
264, C	0.18 ± 0.08	1.02 ± 0.72	0.97 ± 0.66	0.05 ± 0.07	40	0.70
265-1, B	0.22 ± 0.04	0.67 ± 0.14	0.66 ± 0.13	0.01 ± 0.01	9	0.21
265-2, B	0.16 ± 0.07	0.77 ± 0.19	0.74 ± 0.19	0.02 ± 0.05	15	0.25
266, B	0.18 ± 0.08	0.65 ± 0.20	0.63 ± 0.19	0.01 ± 0.02	12	0.31

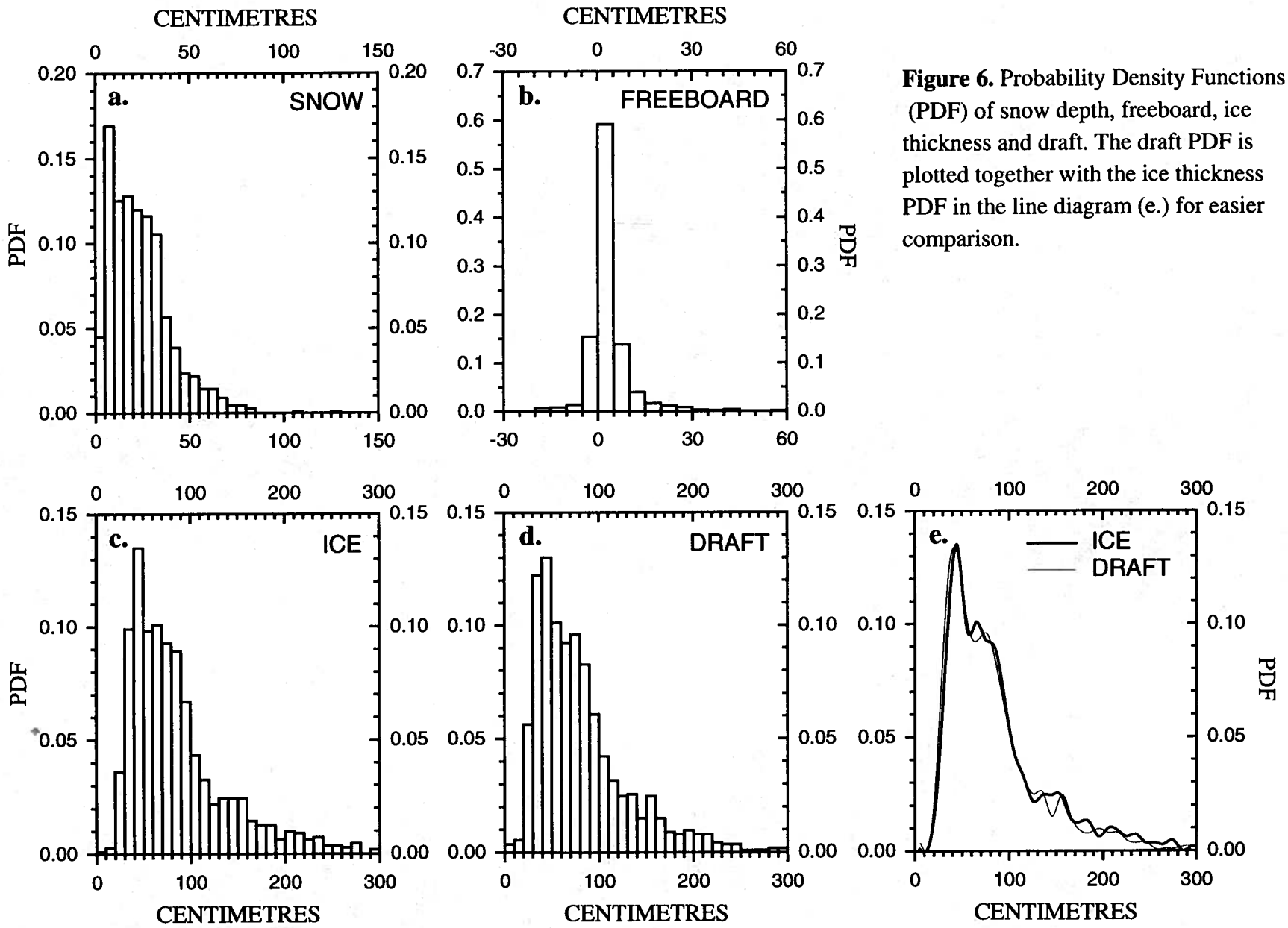

Figure 6. Probability Density Functions (PDF) of snow depth, freeboard, ice thickness and draft. The draft PDF is plotted together with the ice thickness PDF in the line diagram (e.) for easier comparison.

(Table 1) is an indication of the high degree of sea ice thickness variability that results from deformation by ridging and rafting.

Much of the variability in the ice thickness data is due to the bottom roughness of the floes. A characteristic feature of all the ice thickness profiles is the considerable irregularity of the undersurface compared to the relatively level upper surface. This is true of the ridged and rafted floes, as observed elsewhere in the Antarctic pack ice (Wadhams et al., 1987; Lange and Eicken, 1991a; Andreas et al., 1993; Allison and Worby, 1994). Figure 7 illustrates a floe with distinct ridges at distances of 20m and 80m along the transect. The deep keels at these points are associated with sails at the ice surface. The sails are less exaggerated and are usually narrower and have vertical dimensions 3 to 5 times less than the keels. Figure 8 illustrates the ice thickness profile of a floe formed by the rafting of ice cakes, while Figure 9 illustrates the ice thickness profile resulting from rafting of level, 0.3m thick congelation ice (see pages A–47 to A–50). Both floes have a very irregular bottom surface compared to the snow/ice interface. Figure 9 is particularly interesting, as it illustrates that rafting is not just a simple process of one piece of ice riding over another, but that the ice can break into blocks which pile up to form a substantial keel.

The draft distribution (Figure 6d) is very similar to but lags slightly behind, i.e., to the left of, the ice thickness distribution (Figure 6e), i.e., in most cases the ice thickness exceeds the draft. This is evident in the freeboard distribution (Figure 6b), where almost 82% of the values are ≥0m. In other words, 18% of the drill holes had a negative freeboard and the snow/ice interface was flooded with seawater. Similar values indicating widespread flooding of the snow/ice interface have been reported elsewhere in the Antarctic pack ice: 15–38% in the Weddell Sea (Wadhams et al., 1987; Ackley et al., 1990; Lange and Eicken, 1991b); 40–53% in the East Antarctic pack ice (Worby and Massom, 1995); 29% in the western Ross Sea (Jeffries and Adolphs, in press).

It is noteworthy that 59% of the freeboard values occurred in the 0–5cm range, which suggests that there was strong potential for flooding. This potential can be realized by additional snow accumulation or redistribution of the existing snow cover (Ackley et al., 1990). Figure 10 is an example of a floe where the snow/ice interface was flooded along almost the entire length (75%) of the drilling transect. The maximum height of the water surface above the ice surface was 0.24m at a distance of 67.5m (Figure 10). Seawater flooding of the snow/ice interface contributes to the high snow salinity values illustrated in Figure 4.

As noted above, snow depth and ice thickness across a floe can be extremely variable due to the effects of deformation and snow drift. At ridge sails in particular, where ice thickness is usually at a maximum, snow thickness can be negligible, while on the ridge flanks the snow cover may be thicker than elsewhere on the floe (e.g. Figure 11). Even on rafted floes, the depth of the snow cover may be determined by the topography or the process of floe formation. For example, the deepest snow on Floe 229 (Figure 8) occurs on some of the thinnest ice at a distance of 0.20–25m and appears to have drifted and accumulated on the margin of the thicker, heavily rafted ice. On Floe 257 (Figure 9), the snow peak at a distance of 54m was the consequence of a "bulldozer" effect – a result of the ice pushing snow ahead of it as it rafted across the adjacent ice surface.

Because of processes such as the erosion and redeposition of snow, there is considerable scatter and a poor correlation between snow depth and ice thickness at point measurements across a floe, as shown for all the individual measurements (Figure 11a; correlation coefficient = 0.47). On the other hand, the correlation between *mean* snow depth and *mean* ice thickness for individual floes is much higher, as an entire floe is closer to hydrostatic equilibrium than individual points across the floe (Figure 11b).

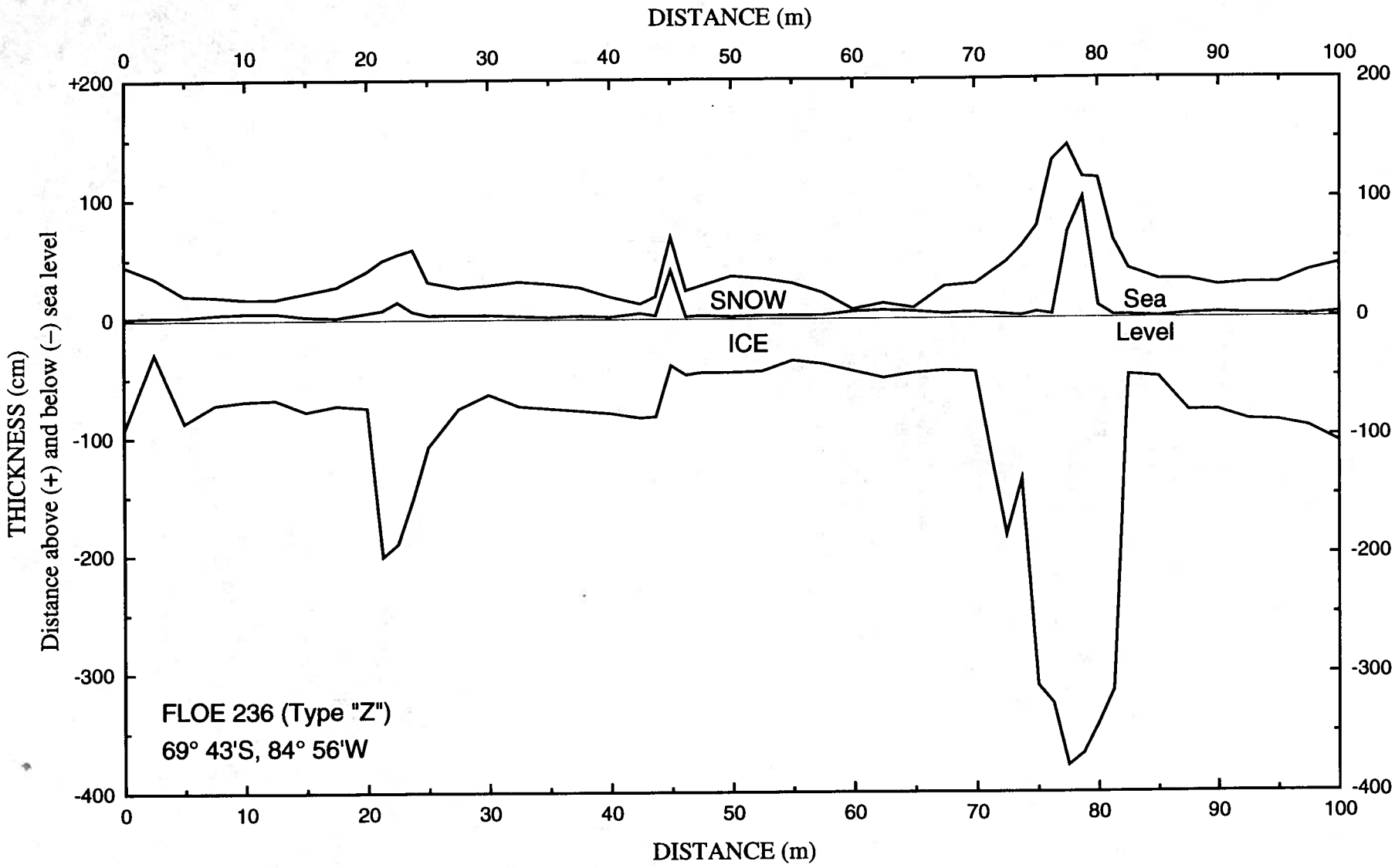

Figure 7. Snow and ice thickness profiles of a ridged floe. The thin, horizontal line at 0m represents sea level.

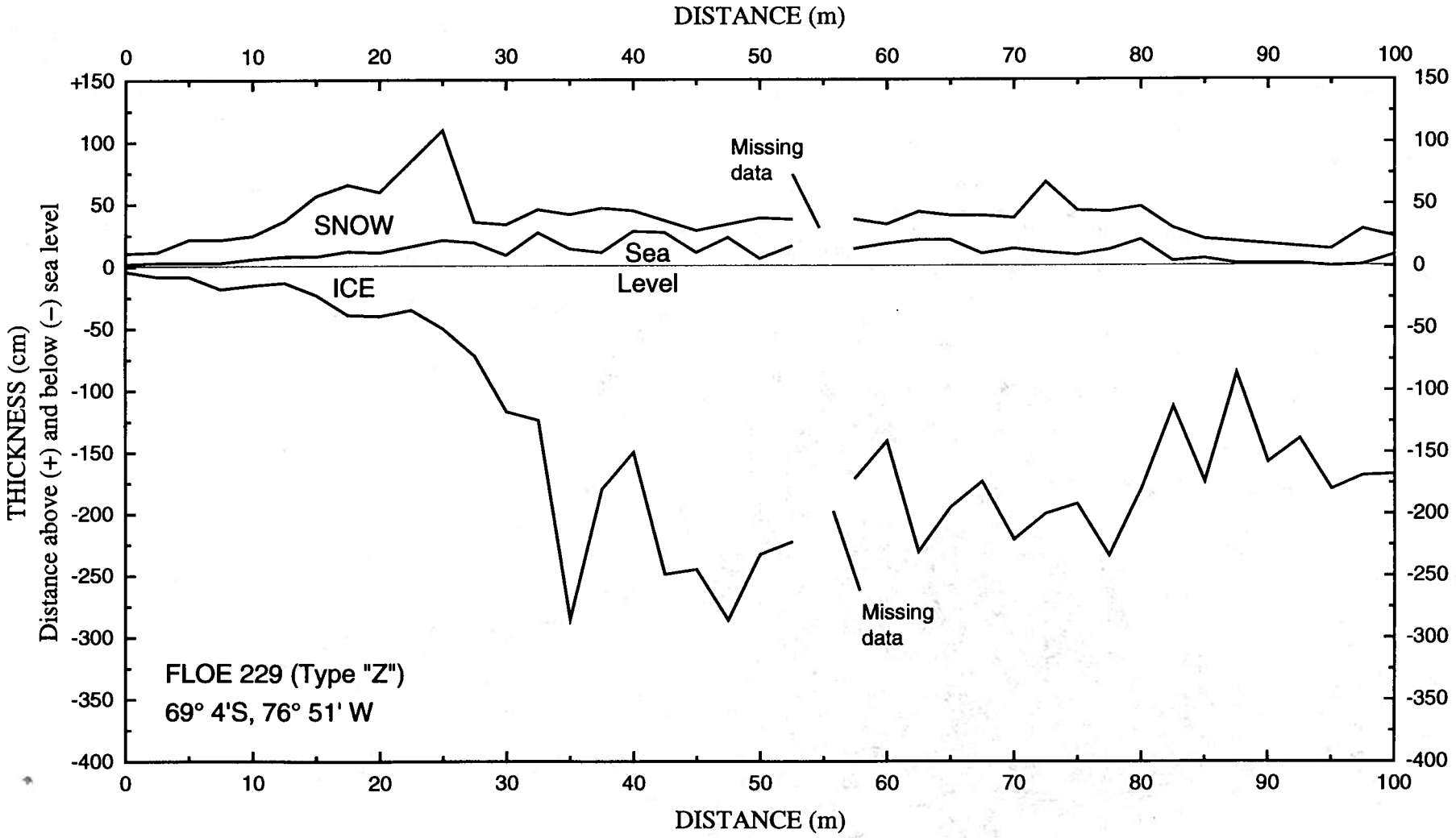

Figure 8. Snow and ice thickness profiles of a floe composed of rafted cakes. The thin, horizontal line at 0m represents sea level.

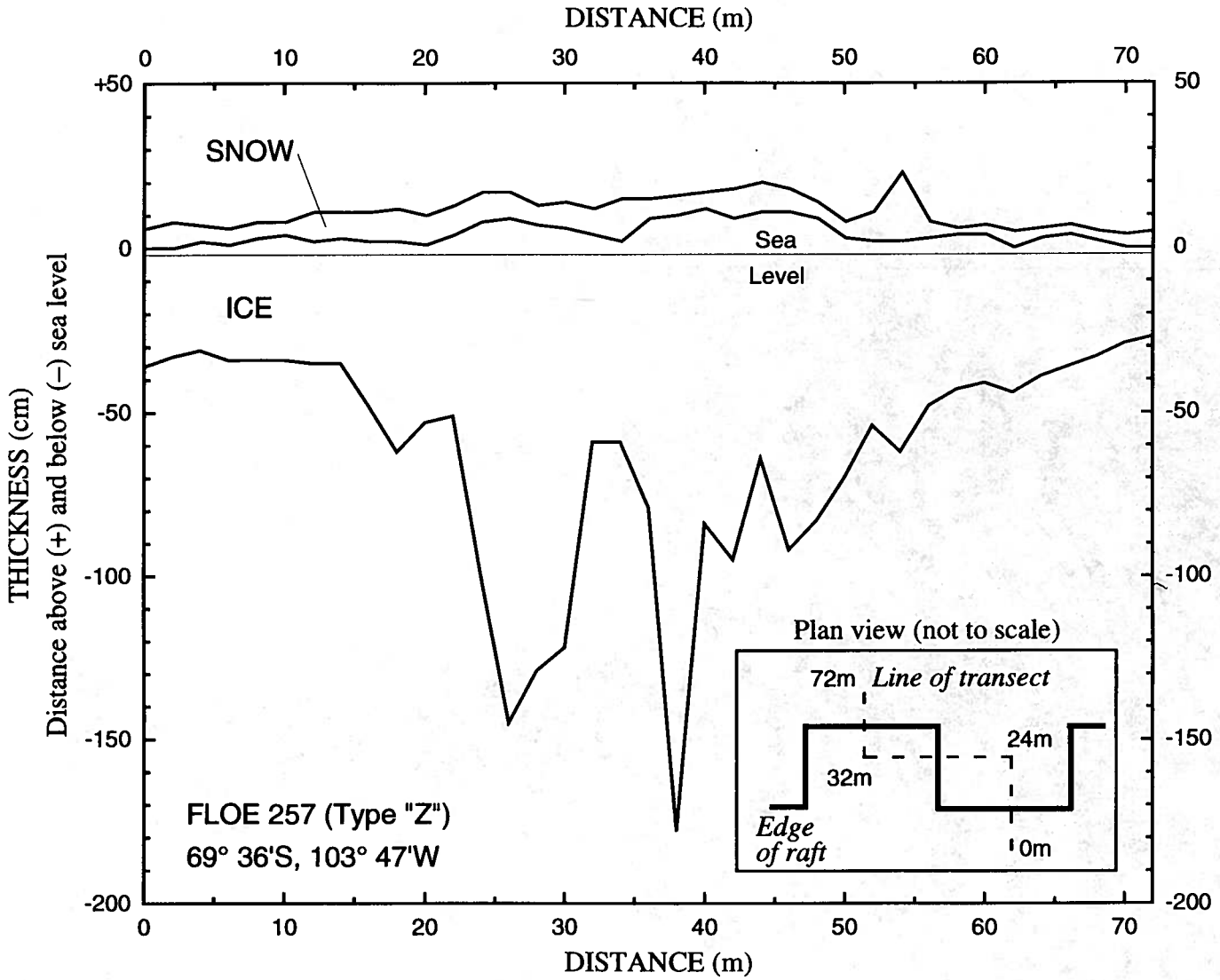

Figure 9. Snow and ice thickness profiles of a rafted floe. The inset shows a plan view of the location of the transect (dashed line) in relation to the edge of the raft (solid line). The thin, horizontal line at 0m thickness represents sea level.

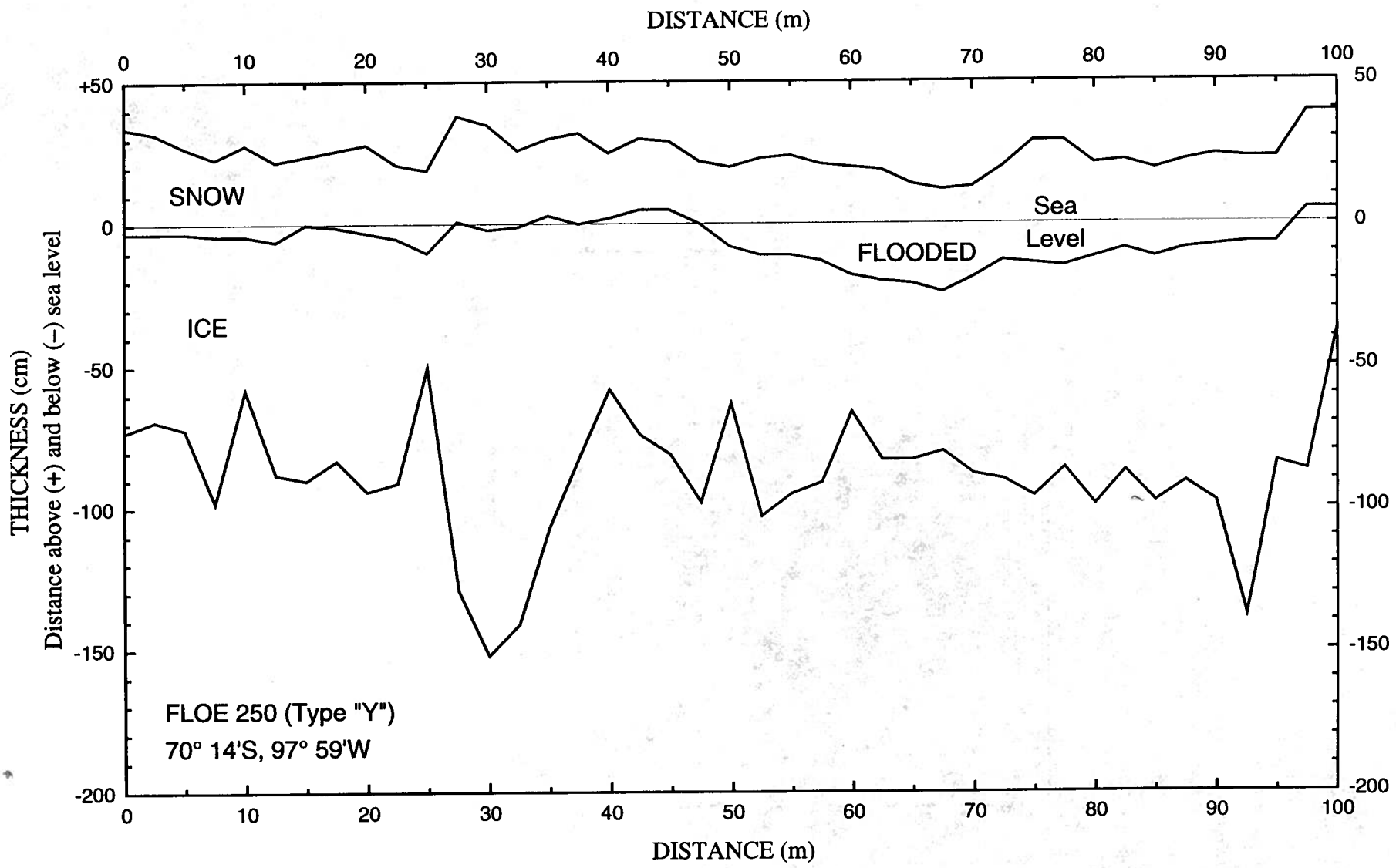

Figure 10. Snow and ice thickness profiles of a floe with extensive seawater flooding at the snow/ice interface. The thin, horizontal line at 0m represents sea level.

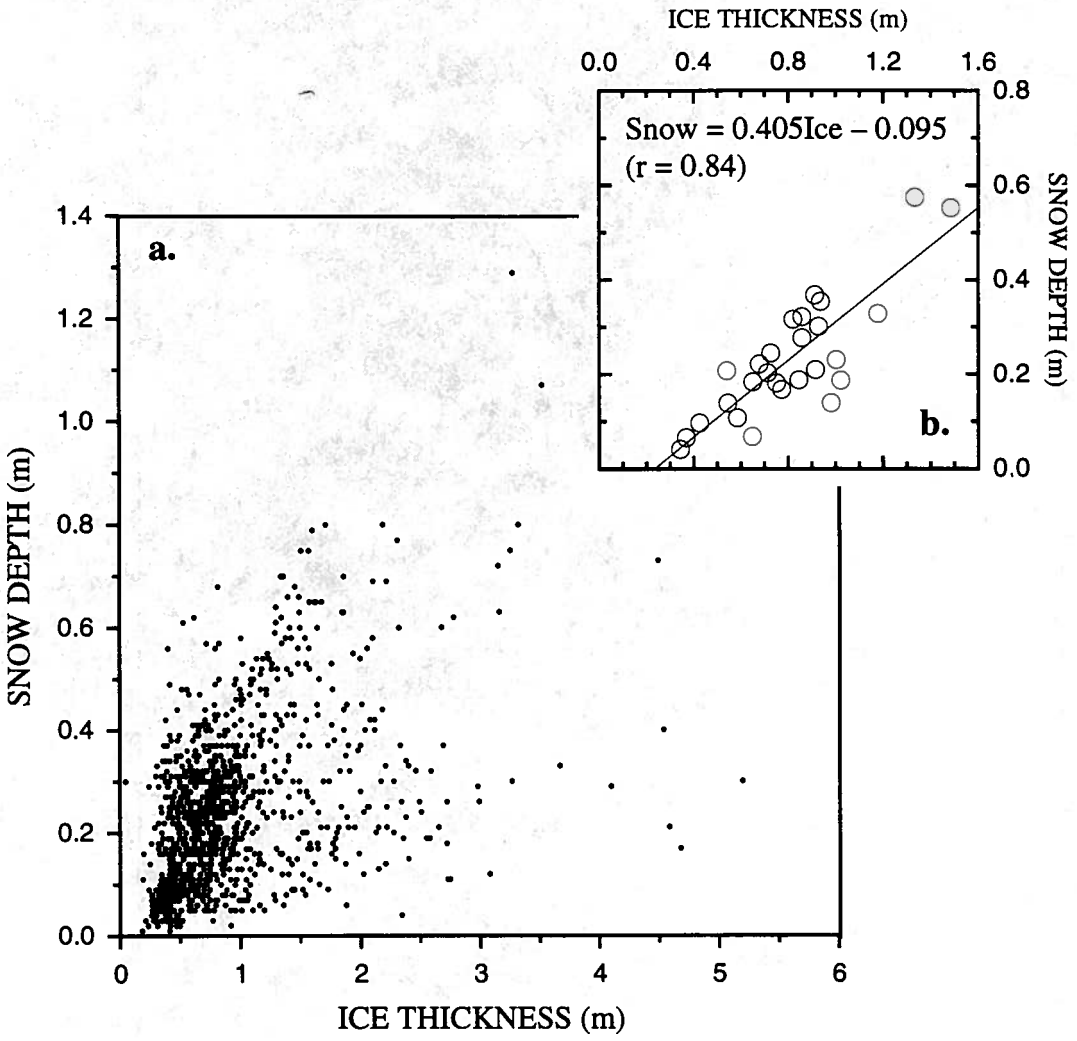

Figure 11. (a.) scatter plot of the 1,113 individual snow depth and ice thickness data points, and (b.) scatter plot and regression line for the mean snow depth and mean ice thickness of the individual ice floes.

4.2 Floe classification and snow and ice thickness

The PDFs illustrated in Figure 6 provide a general summary of the variability of snow depth, ice thickness, draft and freeboard for the entire study area. Within this data set there might be additional information on the characteristics of individual floes or sets of floes that could provide greater insight into the processes that contribute to the development of the ice cover.

Lange and Eicken (1991a) classified three different floe types (I, II and III) in the north–western Weddell Sea, but the criteria on which the classification was based are unclear. We classifiy different floe types according to the variability of the ice thickness. The parameter that is used for this objective classification is the coefficient of ice thickness variation, σ/x, where σ is the standard deviation of the mean ice thickness and x is the mean ice thickness. The higher the coefficient of variation the greater the variability of the ice thickness. A floe is classified as Type X, Y or Z, according to whether its σ/x value occurs in the range 0–0.19, 0.2–0.39 and ≥ 0.4 respectively. The higher the σ/x value, the greater the variability of ice thickness. There are 2, 12 and 15 Type X, Type Y and Type Z floes, respectively (Table 1).

The snow depth, ice thickness, draft and freeboard data for each floe type are summarized in Table 2. Probability density functions for snow depth, ice thickness, draft and freeboard of each floe type are illustrated in Figure 12.

Table 2. Summary of descriptive statistics (mean ± 1 standard deviation) of snow depth, ice thickness, draft and freeboard for Type X, Y and Z floes, and the number of measurements (*n*) in each floe category.

Floe Type	Snow Depth (m)	Ice Thickness (m)	Draft (m)	Freeboard (m)	*n*
X	0.08 ± 0.03	0.47 ± 0.13	0.45 ± 0.12	0.02 ± 0.02	82
Y	0.23 ± 0.16	0.73 ± 0.38	0.72 ± 0.38	0.01 ± 0.04	451
Z	0.24 ± 0.15	0.98 ± 0.72	0.94 ± 0.67	0.04 ± 0.09	580

4.2.1 Type X Floes

Detailed comments on the Type X floes are difficult to make since only two floes and fewer than 100 data points occur in this category. The few available data indicate that these are the thinnest floes with the least snow cover. The snow depth and ice thickness values have a narrow range. There are very few negative freeboard values, but there is a high flooding potential.

4.2.2 Type Y Floes

Figure 10 illustrates the snow and ice thickness profile of a Type Y floe. The snow depth PDF for these floes has a mode of 0.05–0.10m and 78% of the values are ≤0.35m. A short tail includes snow depths up to 0.8m. The ice thickness PDF is bi–modal, with peaks at 0.4–0.5m and 0.7–0.8m, plus a tail of higher values. Almost 73% of the ice thickness values occur in the range 0.2–0.9m. Negative freeboards occurred at 20% of the drill holes on these floes. The 67% of values in the 0–0.05m range indicates a high flooding potential.

The ice thickness PDF and the mean ice thickness of the Type Y floes are similar to those of the Type II floes identified in the north–western Weddell Sea (Lange and Eicken, 1991a). The Weddell Type II floes were described as lightly deformed first–year ice. This is an appropriate description of the Type Y floes, which include moderately rafted and moderately ridged ice, which contribute to the tail of the ice thickness distribution. It is possible that the first peak (0.4–

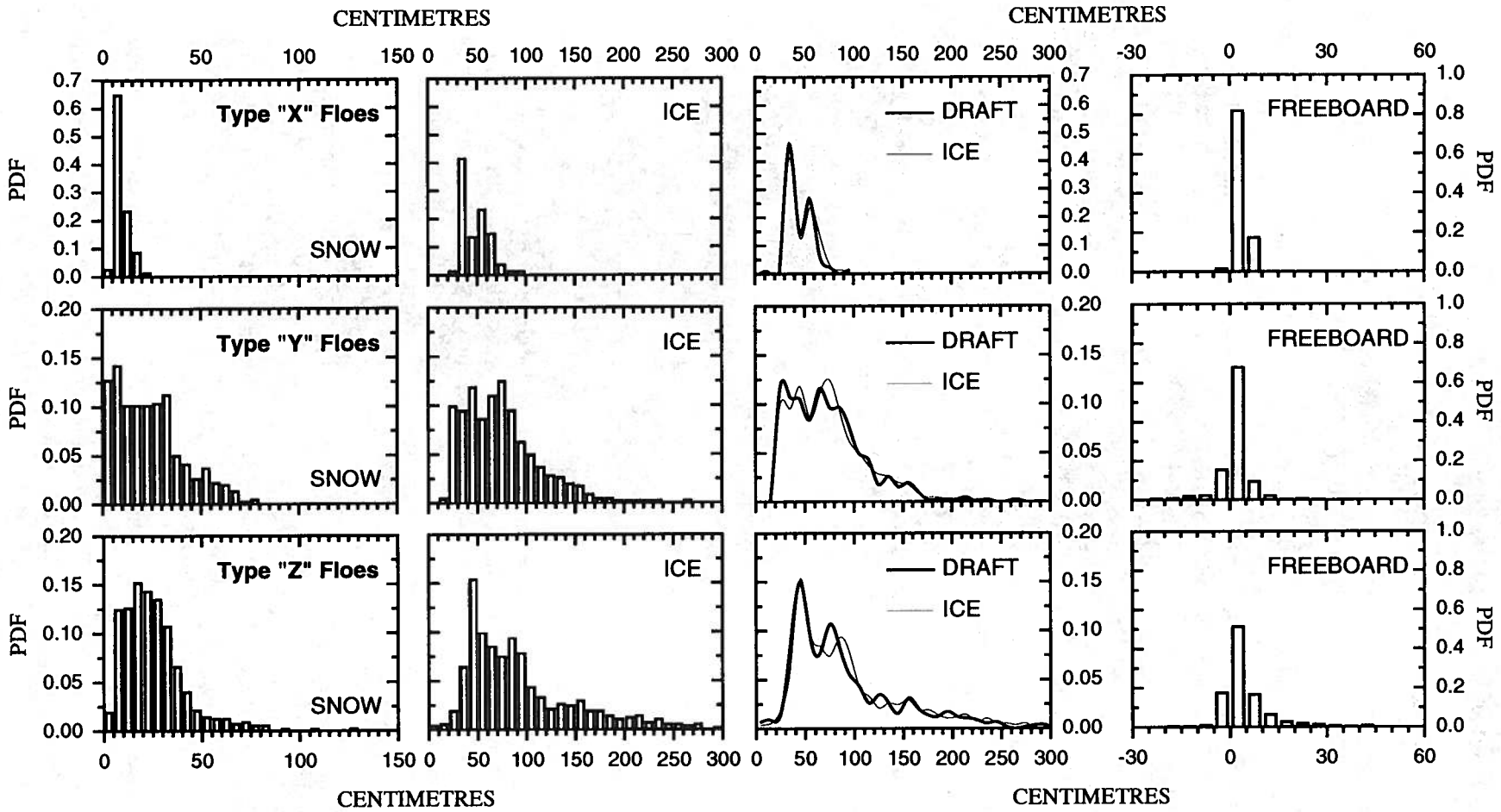

Figure 12. Probability density functions (PDF) of snow depth, ice thickness, draft and freeboard in Type "X", "Y" and "Z" floes. Note that the snow depth, ice thickness/draft and freeboard PDFs each have different vertical scales. The ice thickness and draft PDFs are plotted together in the line diagrams for easier comparison.

0.5m) in the ice thickness distribution includes undeformed, thermodynamically thickened ice. If this is the case, then 0.4–0.5m might be the maximum thickness attainable by such ice before it is deformed and thicker ice categories are created.

The snow depth on the Type Y floes is deeper than on the Weddell Sea Type II floes, where most of the values occurred in the range 0.05–0.125m (Lange and Eicken, 1991a). The snow depths and how they compare with Weddell Sea data are discussed briefly in the next section on Type Z floes.

4.2.3 Type Z Floes

The snow and ice thickness profiles of three different Type Z floes are illustrated in Figures 7, 8 and 9. These include one ridged floe (Figure 7) and two rafted floes (Figures 8 and 9).

The snow depth PDF has a mode of 0.15–0.2m and 78% of the values occur in the range 0.05–0.35m. The tail of the snow depth PDF is much longer than that for Type Y floes and includes a few values exceeding 1.2m. Like the Type Y floes, the ice thickness PDF for the Type Z floes is bi–modal with peaks at 0.4–0.5m and 0.8–0.9m. Over 60% of the values occur in the range 0.3–1.0m, and 33% of the values occur in the long tail of ice >1m thick. The tail also has a small peak at 1.5–1.6m. Negative freeboards occurred at 19% of the drill holes, i.e., the same as on the Type Y floes. The Type Z floes have a lower flooding potential than the Type Y floes, i.e, there are fewer values in the 0–0.05m range. They also have a larger number of high positive values than the Type Y floes.

As with the Type Y floes, the PDF mode at 0.4–0.5m in the Type Z floes probably includes some undeformed, thermodynamically thickened ice. Otherwise, the Type Z floes include a large amount of deformed ice. The ice thickness PDF for the Type Z floes is similar to that described for heavily deformed Type I floes in the north–western Weddell Sea (Lange and Eicken, 1991a). 'Heavily deformed' is an appropriate description for the Type Z floes, although they have a lower mean ice thickness than the Type I floes. This heavy or strong deformation includes ridging (Figure 7) and rafting (Figures 8 and 9). That rafted ice should occur in the same category as ridged ice is evidence that rafting creates thick ice with a high variance.

The snow depth PDFs for Type Y and Z floes are quite similar, and there is no significant statistical difference between the mean snow depth values. Type Y floes have deeper snow than Weddell Type II floes, but the snow on Type Z floes is not as deep as on Weddell Type I floes (Lange and Eicken, 1991a). However, the combined average snow depth for the Weddell Type I and II floes is 0.24m, i.e., the same as the Type Y and Z floes. Thus, in late winter/spring, any regional differences in snow accumulation may be related more to how the snow is distributed on the ice surface than to differences in precipitation. The snow depth values in both regions are undoubtedly conservative, as some of the original precipitation has been entrained into the floes by snow ice formation. Snow ice in the Bellingshausen/Amundsen region is discussed in section 5.5.3.

5. ICE CORE CHARACTERISTICS

5.1 Ice core length

The ice cores obtained for analysis of ice structure and stable isotopic composition had a mean length of 0.84±0.53m (range 0.14 to 2.24m). The ice cores obtained for salinity, temperature and brine volume measurements had a mean length of 0.68±0.44m (range 0.14 to 2.24m). The latter mean value is lower than that for the structure cores because the data set includes a greater

number of samples from thin, new ice. Regardless of these minor differences, the core length values are consistent with the much greater number of ice thickness values obtained along the snow and ice thickness transects (section 4.1) and indicate that the ice cores were representative of the ice thickness of the floes that were investigated.

5.2 Salinity

The individual salinity values are presented in probability density functions in Figure 13. There are two PDFs: one for ice <0.5m thick and one for ice >0.5m thick. The data have been divided into these categories because, as Figures 14a and 14b show, the relationships between mean salinity and thickness and between mean temperature and thickness each have an abrupt change of slope at 0.5m.

The PDF for ice <0.5m thick is bi–modal with peaks at 7–8‰ and 12–13‰. The latter is primarily associated with new ice samples ≤0.1m thick. The mean salinity of ice <0.5m thick is 7.3±2.7‰ with a range of 3.0–19.0‰. The PDF for ice ≥0.5m thick has a single peak and is skewed to the left of the PDF for ice <0.5m thick. The mode is at 4–5‰. The mean salinity for ice ≥0.5m thick is 5.6±1.8‰ with a range of 1.9–12.8‰.

The mean salinity of each ice core as a function of ice core length (ice thickness) is plotted in Figure 14a. The break in slope at a thickness of 0.5m is apparent. In ice <0.5m thick, bulk salinities decrease rapidly as ice thickness increases. In ice ≥0.5m, the slope and correlation of the relationship are negligible and the mean salinity and ice thickness appear to be independent of one another.

The mean salinity and ice thickness data are plotted in Figure 14d together with the regression curves for winter Arctic ice (Cox and Weeks, 1974). This comparison indicates that (1) salinity values in the Bellingshausen/Amundsen ice <0.5m thick are similar to those of Arctic ice of the same thickness, while (2) salinity values in ice >0.5m thick are generally lower than those of Arctic ice of the same thickness. The comparison with the Arctic ice may be an indication that the salinity of Bellingshausen/Amundsen ice <0.5m thick was largely a function of the same processes that determine the salinity of Arctic ice of the same thickness. These include brine loss by brine expulsion as the ice undergoes rapid cooling (Weeks and Ackley, 1982). As Figure 14b and 16a show, the lowest temperatures occur in the ice <0.5m thick. On the other hand, the apparent independence of salinity and thickness in ice ≥0.5m thick might indicate that the salinity of this ice is influenced less by the factors that influence the salinity of Arctic ice of this thickness than it is by factors that are more specific to Antarctic sea ice growth processes and environment. These include snow ice formation and the oceanic heat flux (Eicken, 1992b).

Eicken (1992b) suggested that to fully understand the bulk salinity of Antarctic sea ice it is neccesary to examine the salinity profiles, i.e., the distribution of salinity between the top and bottom of the ice, as well as the mean salinity–thickness relationship. Composite or mean salinity profiles for three thickness categories (<0.5m, 0.5 to 1.0m, >1.0m) are shown in Figure 15. Because of the wide range of thickness values in ice ≥0.5m thick, two composite profiles have been compiled, each for a narrower range of thicknesses. This reduces biasses that might be introduced by combining data from cores of significantly different length.

Of the three composite salinity profiles, the profile for ice ≤0.5m thick most closely resembles the *C* shape that is often associated with Arctic sea ice salinity profiles (Weeks and Lee, 1958, 1962; Nakawo and Sinha, 1981). That such a profile should occur in ice <0.5m thick in the Bellingshausen/Amundsen seas is perhaps additional evidence that its salinity is primarily a function of those processes which influence the salinity of Arctic ice of the same thickness. The salinity profiles for the other two categories can be best described as *S*–shaped with a trend to lower values towards the base of the ice. The salinity of the topmost layers is twice that of the

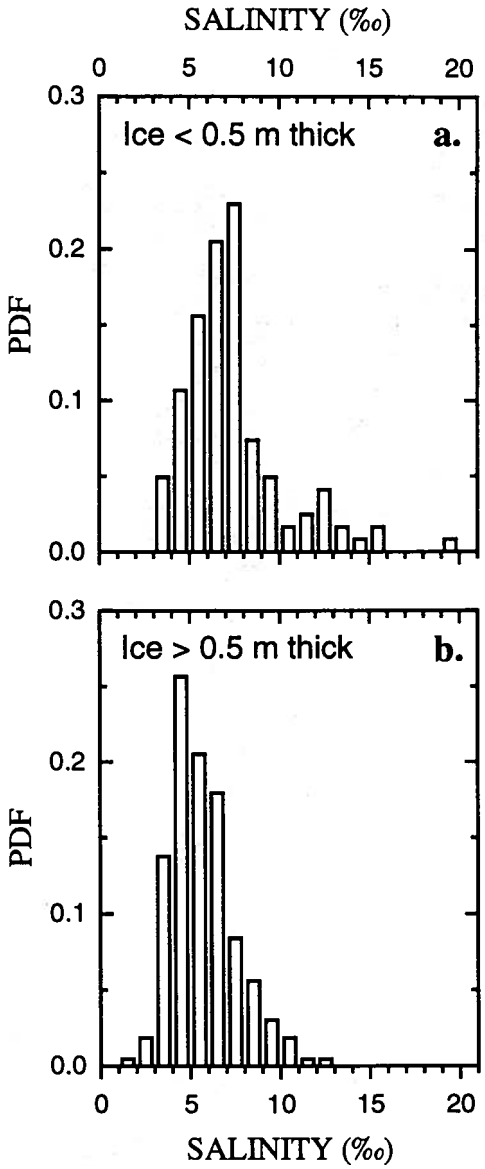

Figure 13. Probability density functions (PDF) of salinities in (a.) ice < 0.5m thick and (b.) ice > 0.5m thick.

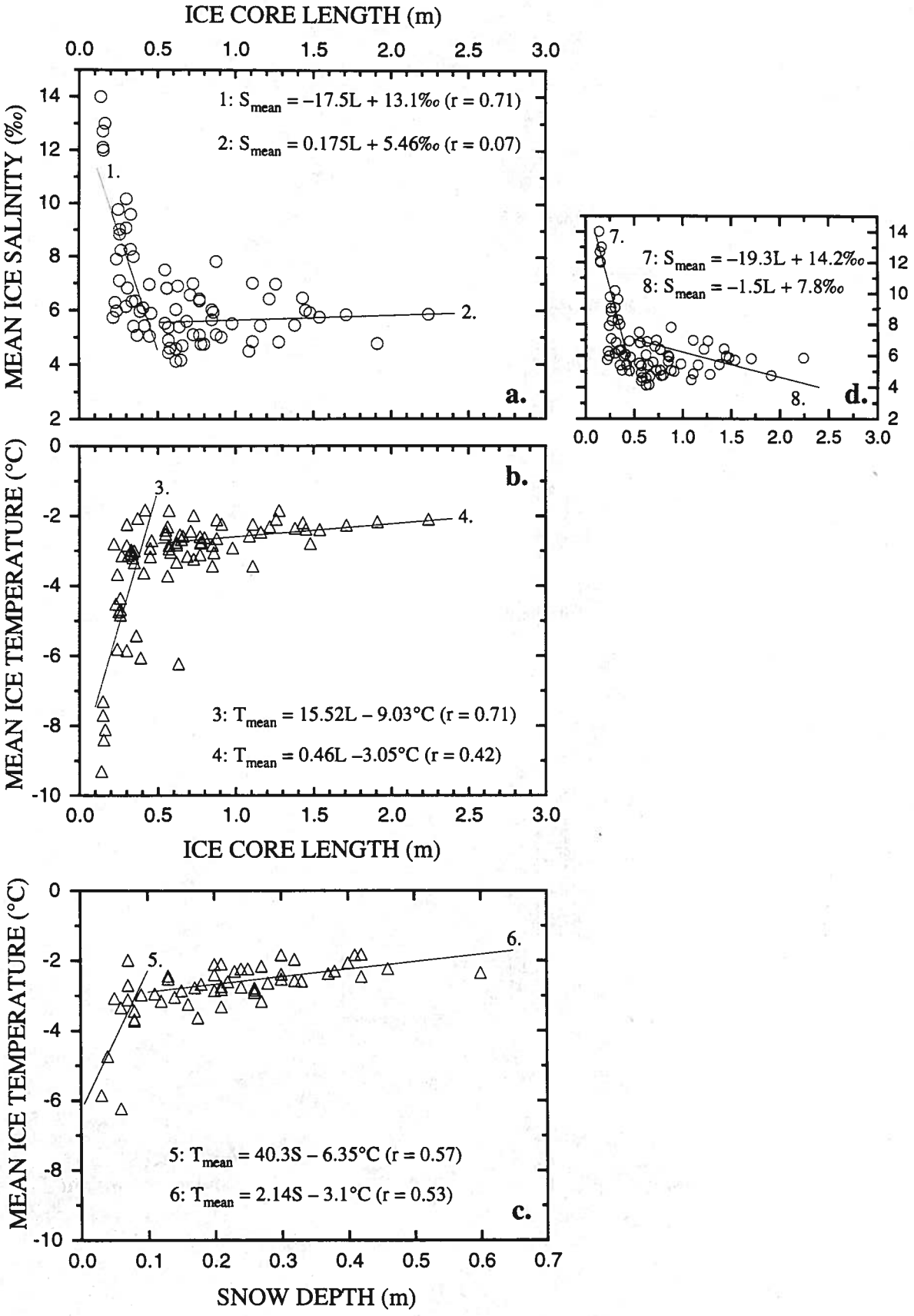

Figure 14. Scatter plots and regression equations for the relationships between (a.) mean ice salinity and ice core length, (b.) mean ice temperature and ice core length and (c.) mean ice temperature and snow depth. Plot (d.) compares the salinity–core length data with the regression curves for winter Arctic sea ice (Cox and Weeks, 1974).

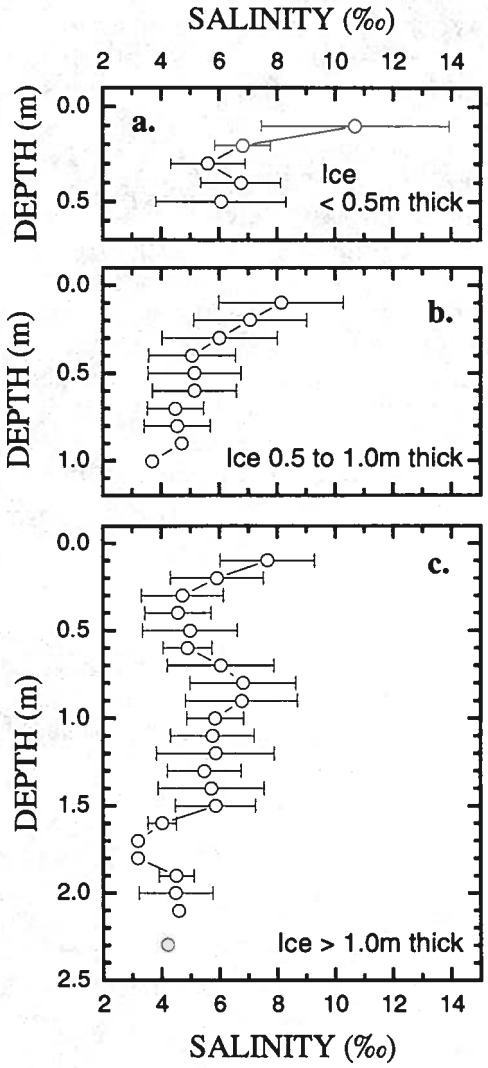

Figure 15. Composite salinity profiles for three different ice thickness categories.

lowermost layers. Such *S*–shaped salinity profiles are common in the Weddell Sea (Eicken, 1992b)

The high salinity at the top of the *S*–shaped profiles can be attributed primarily to snow ice formation (Eicken, 1992b), which was common throughout the study area (see section 5.5.3). The freezing of the seawater at the snow/ice interface creates highly saline ice, perhaps because freezing rates are faster due to lower snow/ice interface temperatures (Figure 5) than are normally associated with seawater freezing; consequently, more brine is entrapped in the snow ice. Furthermore, the snow ice may retain more brine over the course of time because downward brine loss is impeded by the ice below (Eicken, 1992b).

The low salinity values at the bottom of the *S*–shaped profiles may be due to a combination of slow ice growth, or even stagnation of growth, a high oceanic heat flux and the insulating effect of the snow cover (Eicken, 1992b). As Figure 14c shows, the ice ≥0.5m thick was well insulated. A substantial salt loss from the lower ice layers can also occur when an ice cover is established rapidly and is then maintained at a fairly constant thickness for the remainder of the season (Eicken, 1992b). The ice investigated for this study might actually have been thinning. Only six ice cores had a basal skeletal layer that indicated that there was active congelation ice growth at the time of sampling, and they were primarily new ice samples from leads. The scalloping that was evident at the bottom of many cores indicated that melting was occurring at the base of thicker floes. This would also contribute to the low salinity values at the base of the ice, since it would remove any recently grown, high salinity ice.

5.3 Temperature

The individual temperature values are presented in probability density functions in Figure 16. There are two PDFs: one for ice <0.5m thick and one for ice >0.5m thick. The data have been divided into these categories because, as Figures 14a and 14b show, the relationships between mean temperature and thickness and between mean salinity and thickness have an abrupt change of slope at 0.5m.

The PDF for ice <0.5m thick has a mode at –3 to –2°C and a moderate tail of low values. The tail of low values primarily represents new ice which has little or no insulating snow cover. The mean temperature of ice <0.5m thick is –3.9±2.0°C, with a range of –10.3 to –1.4°C. The PDF for ice ≥0.5m thick is more peaked than the PDF for ice ≤0.5m thick. The mode is also –3 to –2°C°C, but there are far fewer low temperature values in the tail. The mean ice temperature for ice ≥0.5m thick is –2.8±1.2° with a range of –12.9 to –1.3°C.

The mean temperature of each ice core as a function of ice core length (ice thickness) is plotted in Figure 14b. The break in slope at a thickness of 0.5m is apparent. In ice <0.5m thick, mean temperature decreases rapidly as ice thickness increases. In ice ≥0.5m, the relationship has a much lower slope but temperature remains a function of thickness as indicated by the moderately high correlation coefficient.

The plot of mean ice temperature as a function of snow depth is evidence of the key role that the snow cover plays in determining ice temperatures (Figure 14c). This is particularly true of the ice <0.5m thick, where a small increase in the depth of snow leads to a significant increase in the ice temperature. Once the snow depth exceeds 0.1m, the addition of more snow has less impact on the temperature of the underlying ice. These field observations demonstrate the role of the snow cover in insulating the sea ice and its potential to affect heat conduction and heat fluxes, as originally modelled by Maykut (1978, 1986).

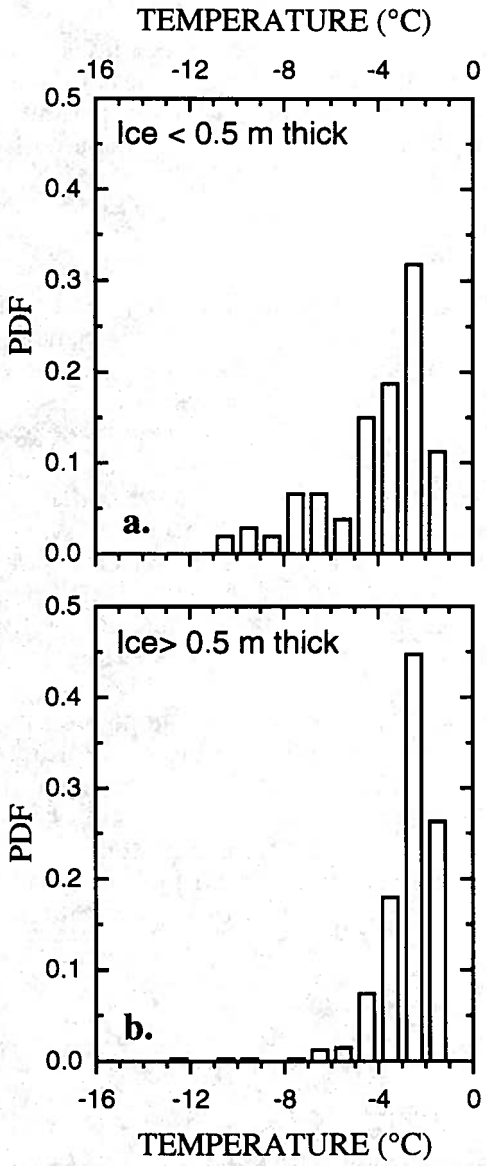

Figure 16. Probability density functions (PDF) of temperatures in (a.) ice < 0.5m thick and (b.) ice > 0.5m thick.

Composite temperature profiles provide a picture of the distribution of temperatures between the top and the bottom of the ice (Figure 17). Regardless of ice thickness, the temperature profile is not linear. The effects of the deeper snow cover on thicker ice (Figure 11) are evident in the decrease in temperatures and temperature gradients in the upper layers of the ice (Figure 17). Also, as the ice thickens, the thickness of the cold upper layer decreases as a proportion of the total ice thickness and there is an increase in the thickness of the lower layer where the ice is almost isothermal and close to the melting point. These temperature characteristics might explain why little active congelation ice growth was observed at the base of the floes.

5.4 Brine volume

The probability density function for all brine volumes is shown in Figure 18. The largest proportion of the values occur in the range 7.5–12.5%. The mean value is 11.9±5.1% and the range is 0.1–35.1%. Slightly more than 95% of the brine volume values are ≥5%. This value is significant because at these brine volumes, brine pockets coalesce, gravity drainage occurs and, as brine drains out of the ice at the base, it may be replaced by seawater (Cox and Weeks, 1975).

Composite brine volume profiles provide a picture of the distribution of liquid brine within the ice cover (Figure 19). The highest brine volumes occur in the lower layers of ice >1m thick (Figure 19c). Such high brine volumes would increase the permeability of the ice, and brine exchange between the ice and seawater would lower the ice salinity and increase the ice temperature; hence the lower layer of isothermal ice near its melting point (Figure 17c) and the overall trend to lower salinities towards the base of the ice (Figure 15).

Of the 95% of the brine volume values ≥5%, most of them occurred in 85% of the ice cores that were obtained. The PDF for these cores is shown in Figure 18b. In other words, most of the cores had brine volumes ≥5% along their entire length. This is reflected in the composite brine volume profiles where few of the standard deviation bars have minima <5% (Figure 19). The implication of this phenomenon is that there was potential for brine exchange between the base and the top of the ice at most of the sampling sites. This can contribute to flooding of the snow/ice interface, which can be enhanced by the increased density of the brine that is rejected as snow ice forms (Fritsen et al., 1994)

5.5 Structure and stable isotopes

5.5.1 General structural characteristics

The ice cores were composed primarily of granular and columnar ice and it was typical for the cores to be composed of many layers of one or both ice types. This multiple layering of each ice type was a characteristic structural feature of the majority of the cores regardless of spatial sampling scale, i.e., it was observed in multiple cores obtained from a single floe (Figure 20a), from floes spaced a few kilometres apart (Figure 20b) and in cores obtained from floes spaced hundreds of kilometres apart (Figure 20c). See the appendix for illustrations of the structure of all the ice cores that were analyzed. Jeffries et al. (1994a) also reported the occurrence of multiple layering and structural complexity in floes in this region. It is evidence of the dynamic nature of the ice growth environment where deformation (rafting and ridging), play a key role in thickening the ice cover after initial thermodynamic ice formation.

Any given layer of granular or columnar ice was often composed of numerous sub–layers stacked one upon the other. In granular ice, the sub–layers were distinguished from one another by differences in crystal size and/or sharp boundaries. Multiple layering of granular frazil ice is illustrated by, for example, core 245-5 (Figure 20b) and core 230–1 (page A–2). For a

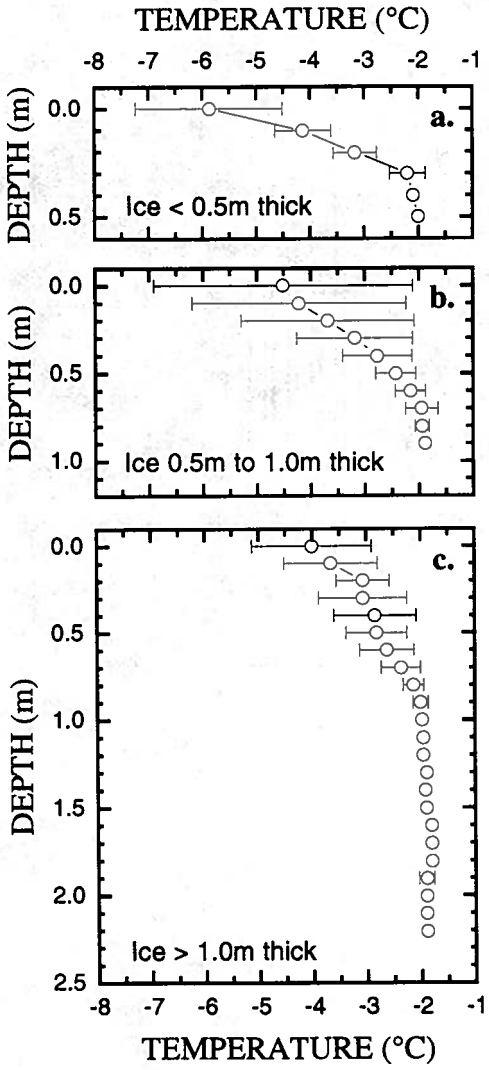

Figure 17. Composite ice temperature profiles for three ice thickness categories.

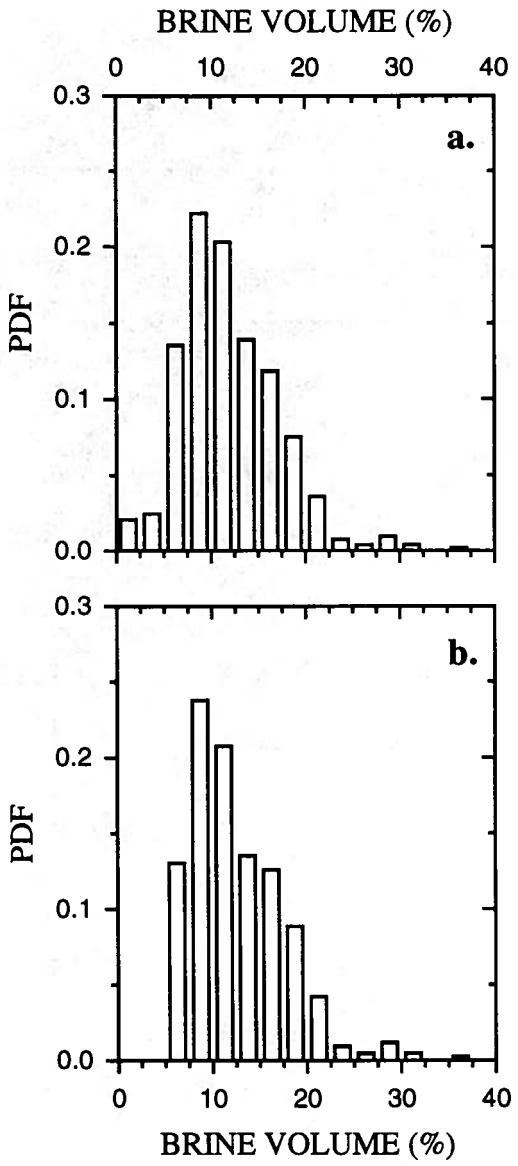

Figure 18. Probability density functions (PDF) of brine volumes in (a.) all ice cores and (b.) only those cores in which the brine volume was >5% along the entire length of each core.

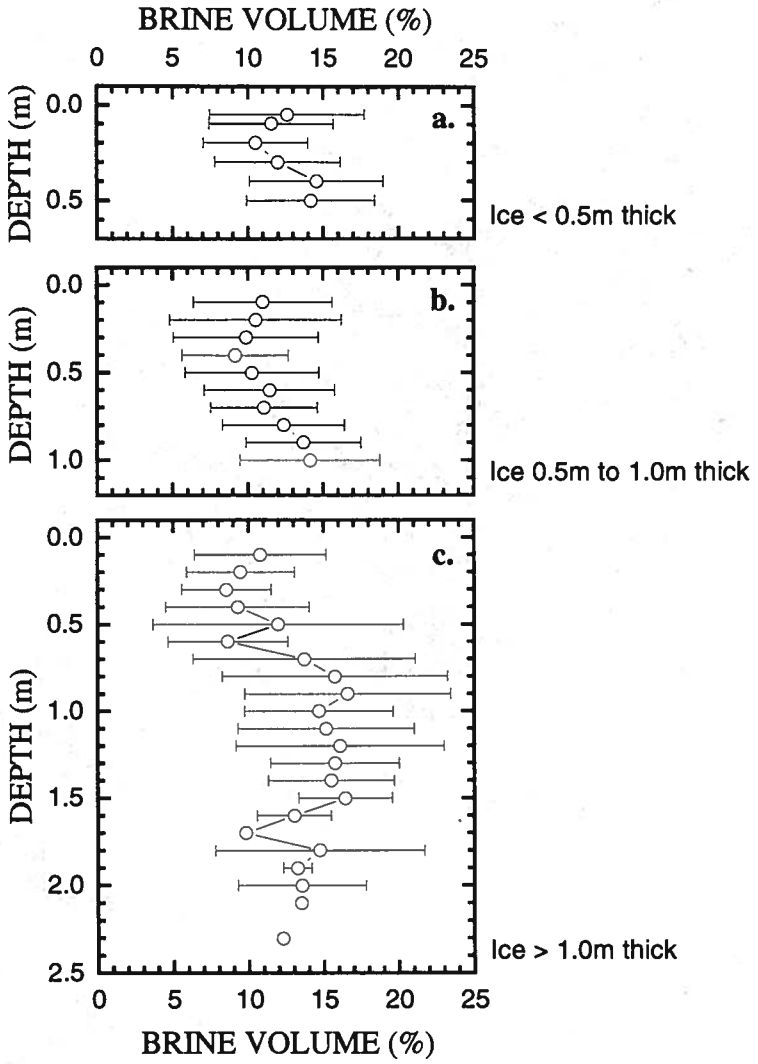

Figure 19. Composite brine volume profiles for three ice thickness categories.

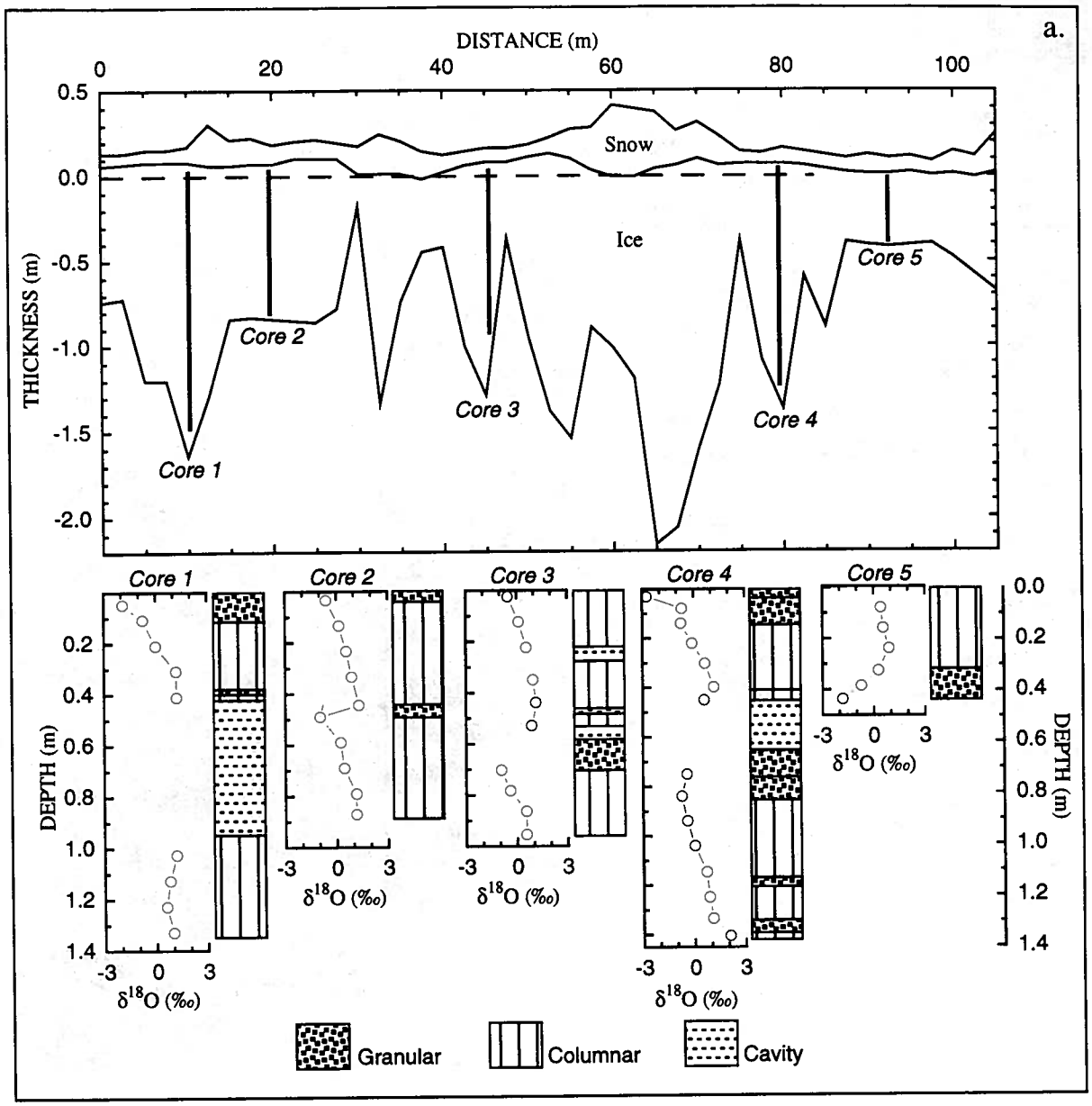

Figure 20a. Snow and ice thickness profiles of Floe 262 (Type Z), and oxygen isotope profiles and structure diagrams for five ice cores.

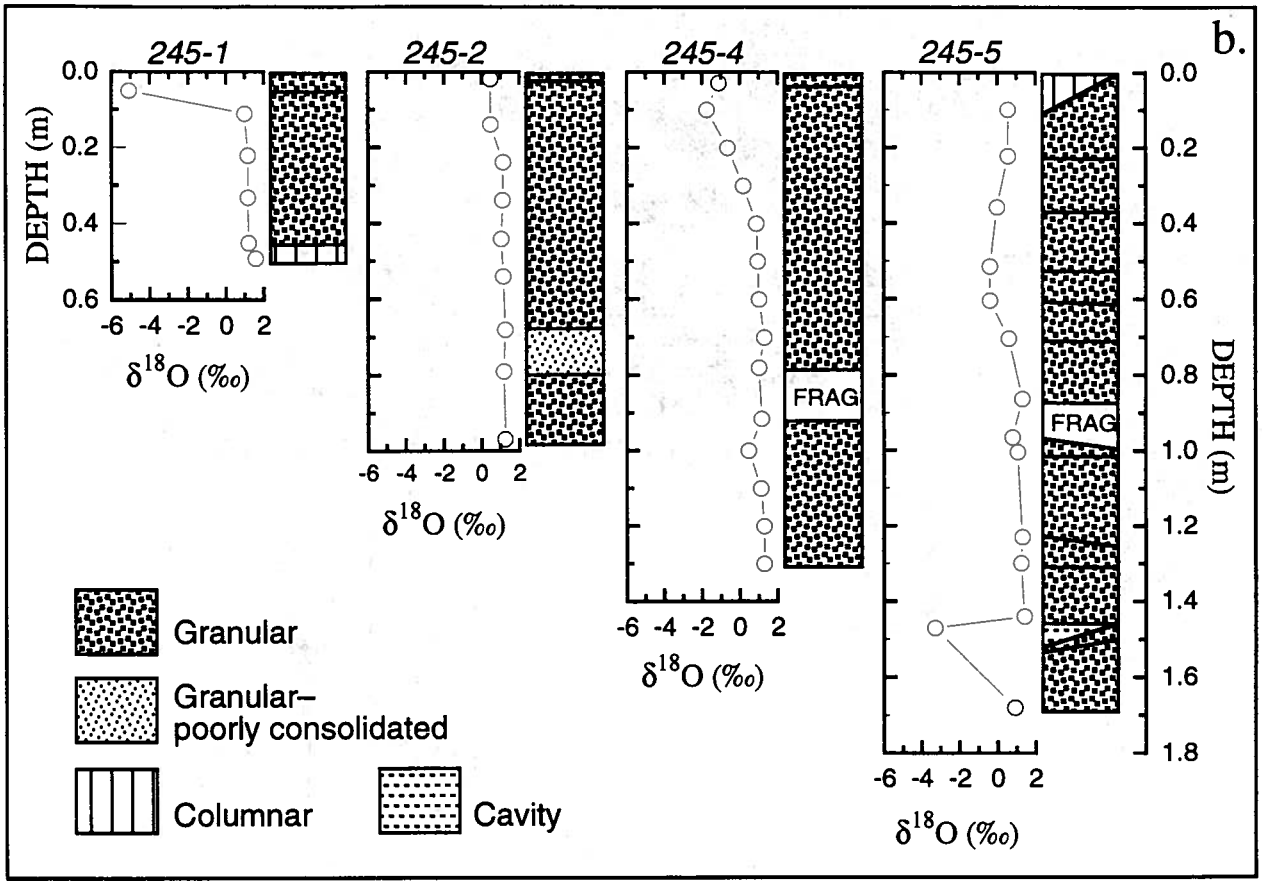

Figure 20b. Oxygen isotope profiles and structure diagrams for ice cores obtained on the same day from different floes spaced 4–6km apart. The abbreviation FRAG. denotes fragmented ice.

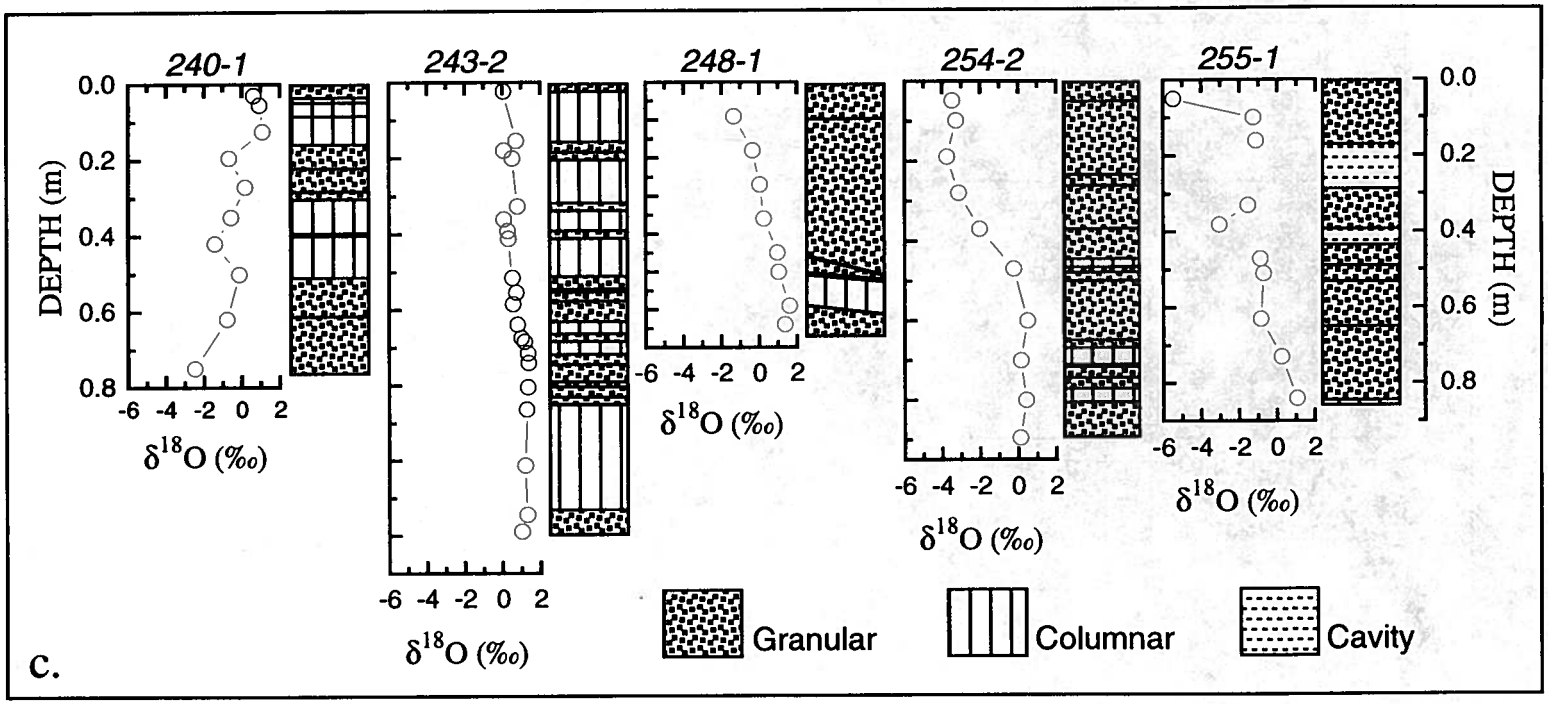

Figure 20c. Oxygen isotope profiles and structure diagrams for selected ice cores obtained from different floes spaced tens to hundreds of kilometres apart.

photographic illustration of sharp boundaries between granular ice sub–layers that characterize a pancake formed by rafting, see Lange et al. (1989: Fig. 3).

The boundaries between the columnar ice sub–layers were often evident as sharp discontinuities in crystal growth and changes in column width. This suggested that an original columnar ice layer had been fractured and the resultant sub–layers had been stacked on top of each other. This is particularly well illustrated by rafted floe 257 (Figure 9 and pages A–47 to A–50) and also by floe 262 (Figure 20a). Occasionally, columnar ice layers tilted over at an angle were observed (e.g. floe 257, p. A–48). For photographic examples of tilted congelation ice layers see Jeffries et al. (1994a: Figs. 5 and 8). Twenty nine of the cores (46%) had a basal layer of columnar ice; only six of those had a skeletal layer that indicated that there was active ice growth at the time of sampling.

Three ice cores contained layers of poorly consolidated granular ice sandwiched between layers of fully consolidated granular ice (Fig. 20b). The cores of the poorly consolidated granular ice remained intact, but the ice was very porous. Individual grains were still visible as the ice crystals were continuing to freeze together. Thus, these cores were sufficiently unconsolidated that they could be crushed by hand. Subsequent stable isotope analysis showed these layers to have originated as frazil ice.

Some cores contained thin layers of fragmented ice composed of angular, randomly oriented crystals that appeared to be fragments of columnar ice that had lost its original structure, probably during ice deformation. Cavities were also encountered within some floes and severel had vertical dimensions exceeding 0.5m (e.g., core 1, floe 262, Fig. 20a). Occasionally, a skeletal layer was observed growing down from the roof of a cavity, i.e, evidence that columnar ice growth was occurring in the cavity. The cavities also are the result of deformation and indicate that the ice had not consolidated completely since the deformation had occurred.

5.5.2 $\delta^{18}O$ data and profiles

The probability density function for all first–year ice $\delta^{18}O$ data is shown in Figure 21a. The values vary between –6.6‰ and +2.0‰, with a mean value of 0.0±1.3‰. The majority of the $\delta^{18}O$ values are greater than the seawater value of –0.9‰, as would be expected due to isotopic fractionation and heavy isotope (^{18}O) enrichment of the solid phase during freezing (e.g., O'Neil, 1968). However, 14.7% of the $\delta^{18}O$ values are lower than the seawater $\delta^{18}O$ value. Furthermore, as the composite $\delta^{18}O$ profile comprising the $\delta^{18}O$ data for all the ice cores shows, the most negative $\delta^{18}O$ values occur primarily in the uppermost ice layers and that the variability decreases as a function of increasing depth (Figure 21). Eicken et al. (1994) illustrated a similar profile in Weddell Sea ice. The negative $\delta^{18}O$ values in the uppermost layers are a consequence of seawater flooding the snow/ice interface and the entrainment of snow into the floe by snow ice formation. This is consistent with the observation that negative freeboard values occurred at 56% of the ice core sampling sites, and at 18% of the drill holes along the ice thickness transects.

The $\delta^{18}O$ profiles of individual ice cores show that the most negative $\delta^{18}O$ values occurred primarily in granular ice layers, i.e., snow ice, in the uppermost parts of the cores (Fig. 2). There were also numerous cases where the most negative $\delta^{18}O$ values occurred in granular ice layers some distance below the surface, often sandwiched between columnar and granular ice layers with more positive $\delta^{18}O$ values, e.g., core 2 on floe 262 (Fig. 2a) and core 240–1 (Fig. 2c). In one case, core 5 on floe 253 (Fig. 2a), the most negative $\delta^{18}O$ values are in granular ice at the base of a core that is otherwise composed of columnar ice. These sub–surface, isotopically negative layers occurred in 15 cores and are probably a result of the burial of snow ice layers by rafting (Lange and Hubberten, 1992). In 13 cores snow ice was the predominant ice type, and in one core (232–2b, page A–4) it comprised 100% of the core length.

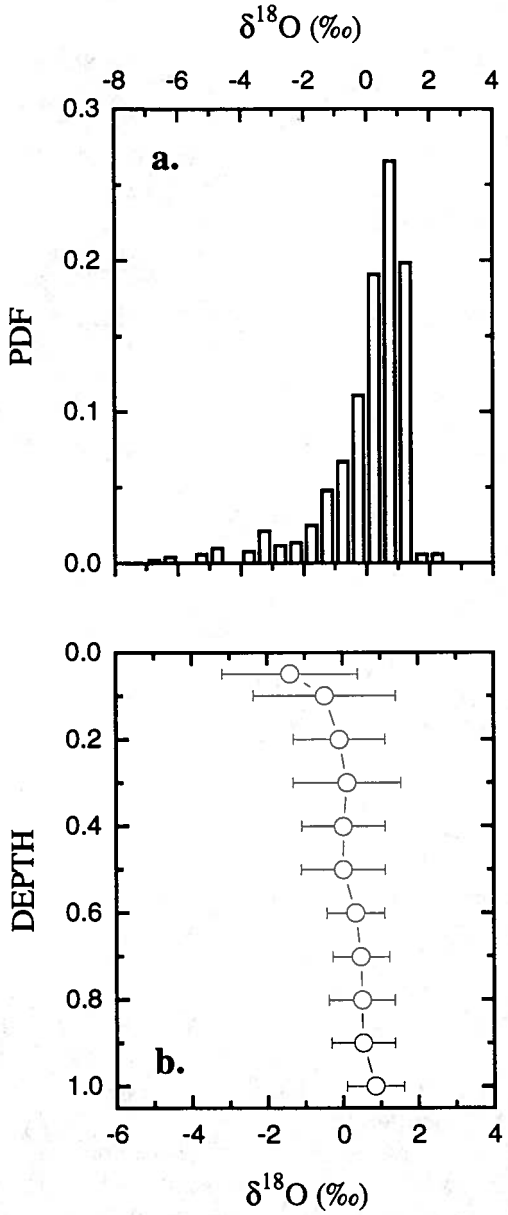

Figure 21. Probability density functions (PDF) of (a.) $\delta^{18}O$ values in all the ice cores, and (b.) a composite $\delta^{18}O$ profile for all the ice cores (the depth scale is normalized).

The ice thickness distribution represented by the ice core lengths has three distinct modes: <0.5m, 0.5–1.0m and >1.0m. Average $\delta^{18}O$ profiles for each of these categories show the trend from moderately negative $\delta^{18}O$ values in the surface layers to more positive $\delta^{18}O$ values at the base of the ice (Figure 22). The occurrence of moderately negative $\delta^{18}O$ values at the surface of each of these thickness categories indicates that snow ice occurrence is independent of ice thickness. Unlike the composite $\delta^{18}O$ profile for all the cores, which has the greatest variability in the uppermost layers (Figure 21), the profiles in Figure 22 show some high variability layers far below the surface, e.g. at 0.3m and 0.4m in the >1.0m category (Figure 22c). These are due to the occurrence of sub–surface or "buried" snow ice layers with more negative $\delta^{18}O$ values.

5.5.3 Structural composition, layer thickness variability and thickening of the ice cover

The columnar texture of congelation ice and the characteristics of fragmented ice are easily distinguished from ice with a granular texture. To identify the layers and amount of snow ice and frazil ice in each core requires stable isotope data, since each has a granular texture and it is difficult to differentiate between them unambiguously on the basis of crystal textures alone (Lange et al., 1990). We assume that any granular ice with a $\delta^{18}O$ value <0‰ is snow ice, an approach taken by other investigators (Lange et al., 1990; Eicken et al., 1994; Worby and Massom, 1995).

The 63 cores that were analyzed for structure and isotopic composition have a total length of 52.08m. The contributions of snow ice, frazil ice, columnar ice, fragmented ice and cavities to the structural composition of the total length of core are presented in Table 3. Cavities, although they are not ice, are part of the total ice thickness and thus are included in the calculation of the structural composition of the ice floes. The average amount of each ice type per core is presented in Table 3. Whether the structural composition is considered in absolute or average terms, the results show that the floes were dominated by granular ice of frazil origin, while the amount of columnar ice only slightly exceeds the amount of granular ice of snow ice origin.

Table 3. Structural composition of first–year ice cores as (1.) a function of the total length of core analyzed and (2.) an average amount of each ice type per core.

	Snow Ice (%)	Frazil Ice (%)	Congelation Ice (%)	Cavities (%)	Fragmented Ice (%)
1.	23.8	44.3	25.5	5.5	0.9
2.	23.2	40.6	32.5	3.6	0.1

The structural composition of the Type A, B and C floes is summarized in Table 4. Care must be exercised in the intepretation of these data because: (1) not all the ice cores obtained during the cruise are included, since the floe types are not known for the period when the swell adversely affected the investigation and no snow and ice thickness data were obtained; and (2) only one core was obtained from most floes, with the exception of floe 253 (Type B) and floes 257 and 262 (Type C), where 4–5 cores were obtained from each floe. Nevertheless, some interesting patterns emerge. Snow ice makes a significant contribution to the mass of each ice type, as suggested by the composite $\delta^{18}O$ profiles for different thickness categories (Figure 22). The cavities increase in importance as the ice thickness and variability increase. This is not surprising in that the thicker the ice the more likely it is that it has been deformed, thereby increasing the likelihood that cavities will be created.

The thickness of the many thin layers of granular and columnar ice that make up ice cores in the East Antarctic pack ice have been presented as evidence of the important role of dynamic processes in thickening the ice cover (Worby and Massom, 1995). With the aid of stable isotopes

Table 4. Structural composition of Type A, B and C floes as (1.) a function of the total length of core analyzed and (2.) an average amount of each ice type per core.

Floe Type		Snow Ice (%)	Frazil Ice (%)	Congelation Ice (%)	Cavities (%)	Fragmented Ice (%)
A	(1.)	34.1	7.7	58.2	–	–
	(2.)	25.2	5.3	69.5	–	–
B	(1.)	37.2	40.3	16.9	3.4	2.2
	(2.)	33.5	41.0	22.8	1.5	1.2
C	(1.)	24.2	32.4	33.8	9.4	0.2
	(2.)	29.2	30.6	34.7	5.4	0.1

we can distinguish between granular snow ice and granular frazil ice, and determine the thickness of snow ice layers and frazil ice sub–layers. These data, together with data on the thickness of the columnar ice sub–layers, can help us to better determine the relative roles of the dynamic and thermodynamic processes that contribute to the development of the pack ice.

The thickness of the surface and buried snow ice layers in each of the 51 cores in which they occur are illustrated in Figure 23. Snow ice makes up between 1% and 100% of these cores. The thickness distributions for the surface and buried snow–ice layers are shown in Figures 24a and 24b; the layer thickness distributions are similar, with the majority of values being <0.4m thick, and there is no significant difference between the mean values. The thickness distributions for the sub–layers that make up the columnar and frazil ice layers are shown in Figures 24c and 24d. Most values are <0.2m and the mean layer thickness of the frazil and congelation ice is about 60% of the snow–ice layer thickness.

The snow ice layers were often composed of numerous sub–layers, e.g., core 231–1b (page A–3), but the snow ice layer thickness distributions represent the total thickness of each snow ice layer in each core and not the many thinner sub–layers. These will form as snow ice accumulates by multiple flooding and snow ice formation events. The individual snow ice sub–layers represent thermodynamic thickening, and the total thickness of each snow ice layer represents the maximum snow ice layer thickness attained by thermodynamic thickening. On the other hand, we interpret the multiple layering of many thin sub–layers in the frazil ice and congelation ice as being the result primarily of dynamic thickening; consquently, it is the thickness of the sub–layers that represents the maximum thickness attained by thermodynamic thickening. For example, the sub–layers in frazil ice probably represent rafted pancakes, and those in congelation ice represent rafted nilas and young ice. The pancakes, nilas and young ice represent the original, thermodynamically–thickened building blocks of the total thickness of each frazil ice and congelation ice layer, which owe their total thickness primarily to dynamic processes

The amounts and ratio of frazil to congelation ice observed in the ice cores are similar to those observed in other sea ice zones of the Southern Ocean (Gow et al., 1982, 1987; Jacka et al., 1987; Lange et al., 1989; Jeffries and Weeks, 1992; Allison and Worby, 1994). Much of the frazil ice that forms elsewhere on the Southern Ocean contributes to the "pancake cycle" which plays a key role in the development of the ice cover (Wadhams et al., 1987; Lange et al., 1989). Pancake ice and rafting were widespread in the outer parts of the pack ice during the 1993 cruise, and the many thin sub-layers of frazil ice in the cores suggest that pancake formation and rafting played an important role in the development of the ice floes that were studied.

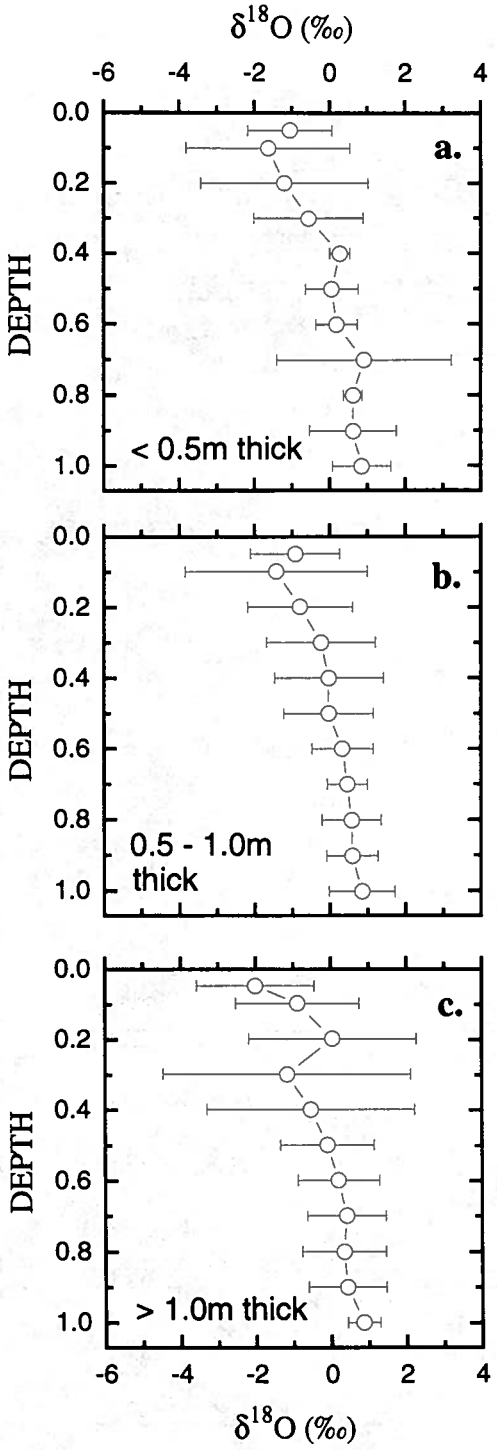

Figure 22. Composite $\delta^{18}O$ profiles for three ice thickness categories. The depth scale is normalized.

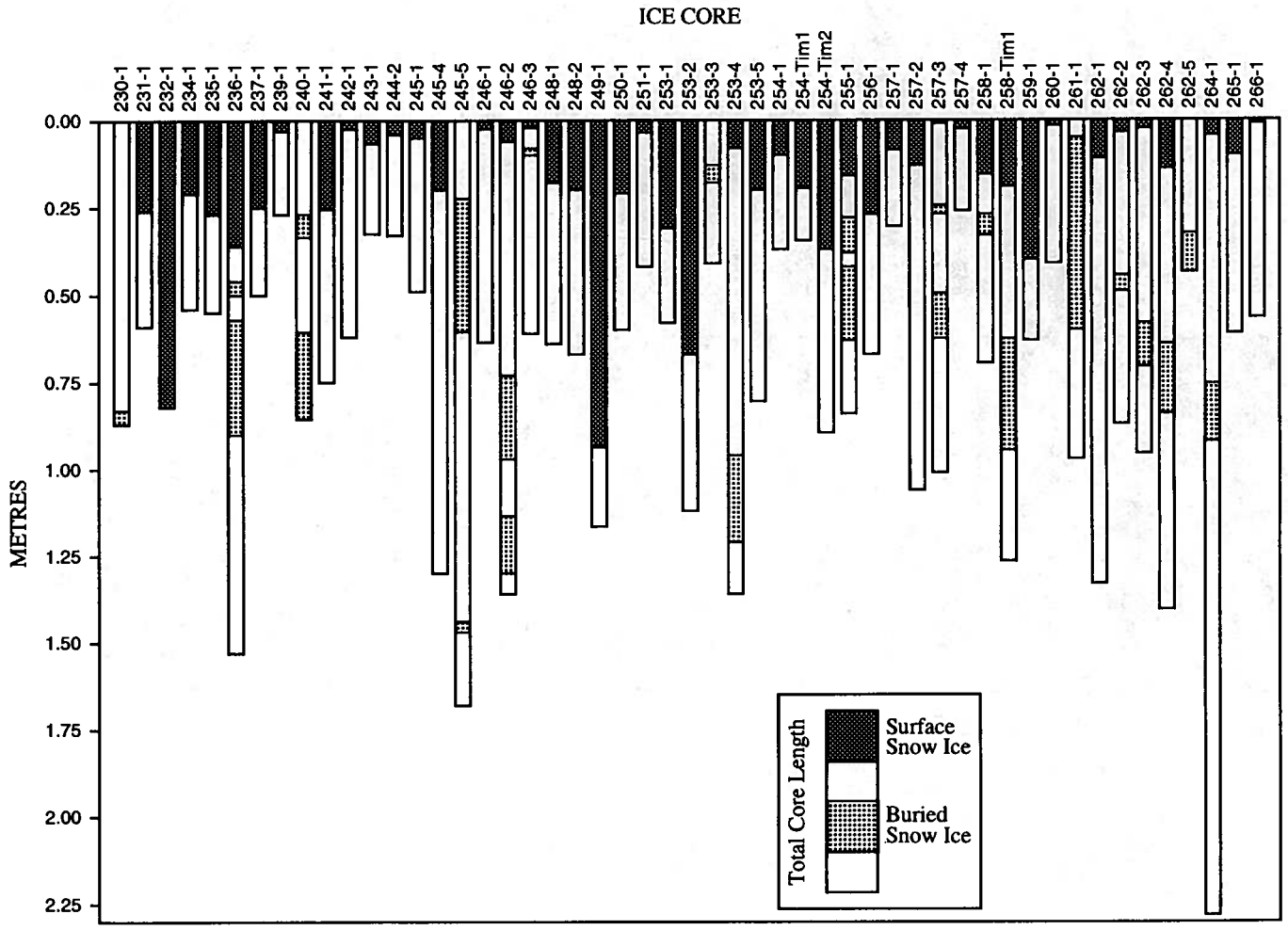

Figure 23. Diagrammatic representation of ice core length and the thickness of surface and buried snow ice layers.

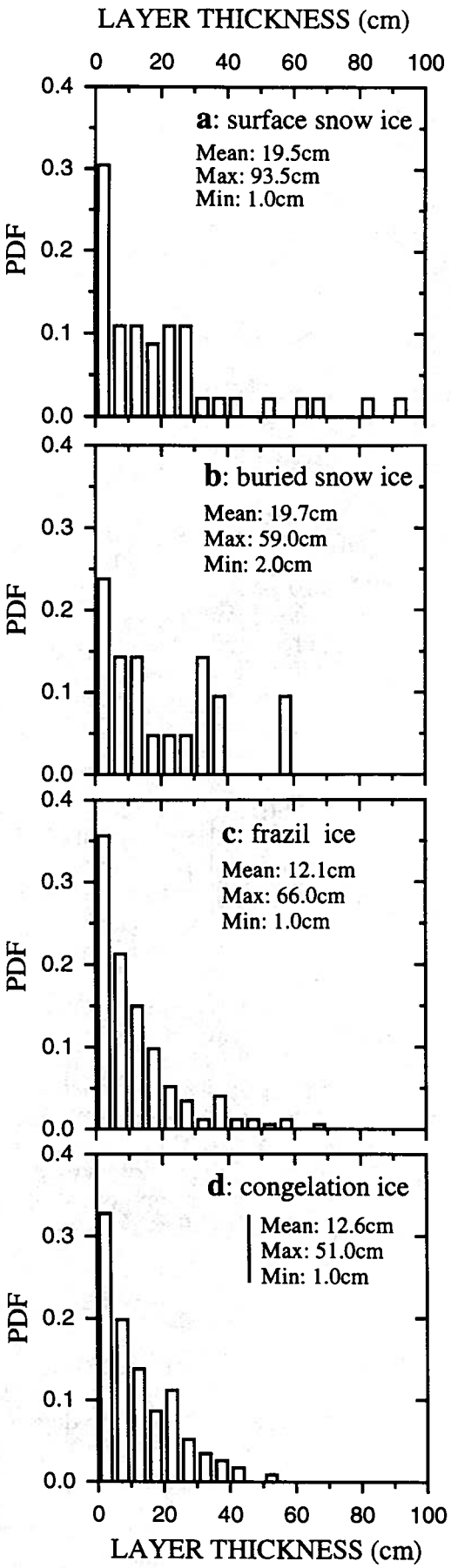

Figure 24. Probability density functions (PDF) of the thickness of individual snow ice, frazil ice and congelation ice layers in ice cores.

The many thin congelation ice sub–layers observed in the cores probably resulted from the rafting of nilas and/or young ice, as occurs elsewhere in Antarctica shortly after initial ice formation on leads and polynyas (Eicken and Lange, 1989; Allison and Worby, 1994). In the Weddell Sea, the typical congelation ice layer thickness in first–year ice is between 0.2m and 0.3m (Lange and Eicken, 1991b). The congelation ice layers in the Bellingshausen/Amundsen cores are thinner than those in the Weddell Sea ice, perhaps indicating that they are rafted even sooner after initial formation than those in the Weddell Sea. The frazil and congelation ice layers are equally thin, which suggests that pancakes also do not develop to a significant thickness before being rafted.

The oxygen isotope data for the Bellingshausen/Amundsen cores are in stark contrast to the first investigation of the oxygen isotopic composition of Weddell Sea ice, where few negative $\delta^{18}O$ values were observed (Gow et al., 1987). The frequent occurrence of moderately negative $\delta^{18}O$ values in the late winter Bellingshausen/Amundsen cores is similar to subsequent investigations in the Weddell Sea (Lange et al., 1990; Eicken et al., 1994, 1995) and the East Antarctic pack ice (Allison and Worby, 1994; Worby and Massom, 1995) and a consequence of seawater flooding and snow–ice formation.

Snow–ice formation contributes a smaller amount to the total ice mass than frazil ice formation, but a similar amount as columnar ice growth. However, the larger quantities of frazil ice and the columnar ice occur in a greater number of thinner sub–layers than the snow–ice layers. Although the initial formation of the frazil ice and congelation ice layers represents thermodynamic thickening, the amount and multiple layering of frazil and congelation ice observed in the cores is primarily the result of dynamic processes, i.e., rafting and ridging. The greater thickness of the snow ice layers compared to those of the frazil and congelation ice sub–layers indicates that, by late winter, snow ice formation has made a greater contribution to the thermodynamic thickening of the total ice mass than frazil and congelation ice formation.

The significance of snow ice formation for the thickening of the ice cover in the Bellingshausen/Amundsen seas is demonstrated also by the fact that its contribution (24%, Table 3) is generally greater than amounts reported elsewhere. It is over three times that reported in the eastern Weddell Sea in July and August (7%: Lange et al., 1990) and greater than most of the average values reported from four cruises in the East Antarctic pack ice: 9% in May, 23% and 30% in October and 19% in November (Allison and Worby, 1994; Worby and Massom, 1995).

The large amount of snow ice might be related to the occurrence of basal melting as indicated by scalloping and the general absence of skeletal layers and active basal ice growth. This would remove both frazil ice and congelation ice, and lead to a relative increase in the snow ice component and its contribution to the thermodynamic thickening of the ice cover; hence the large number of cores in which snow ice was the predominant ice type. Furthermore, thinning the ice would effectively increase the snow load and increase the potential for further flooding and snow ice formation. In time, this "conveyor belt", in which ice is melted off the bottom and snow ice is added at the surface, could lead to a situation where snow ice is the major component of the total ice thickness, as has been observed in the Weddell Sea in late winter (S. F. Ackley and V. Lytle, personal communication, 1995).

5.5.4 Snow fractions

The isotopic mass balance model (equations 1 and 2) is applied to each granular ice layer with a $\delta^{18}O$ value < 0‰, i.e., each snow ice layer, to obtain the f_s value for that layer. The f_s values for each core are illustrated in Figure 25. The mean values vary between 7% and 13% depending on the choice of snow $\delta^{18}O$ value (Table 5).

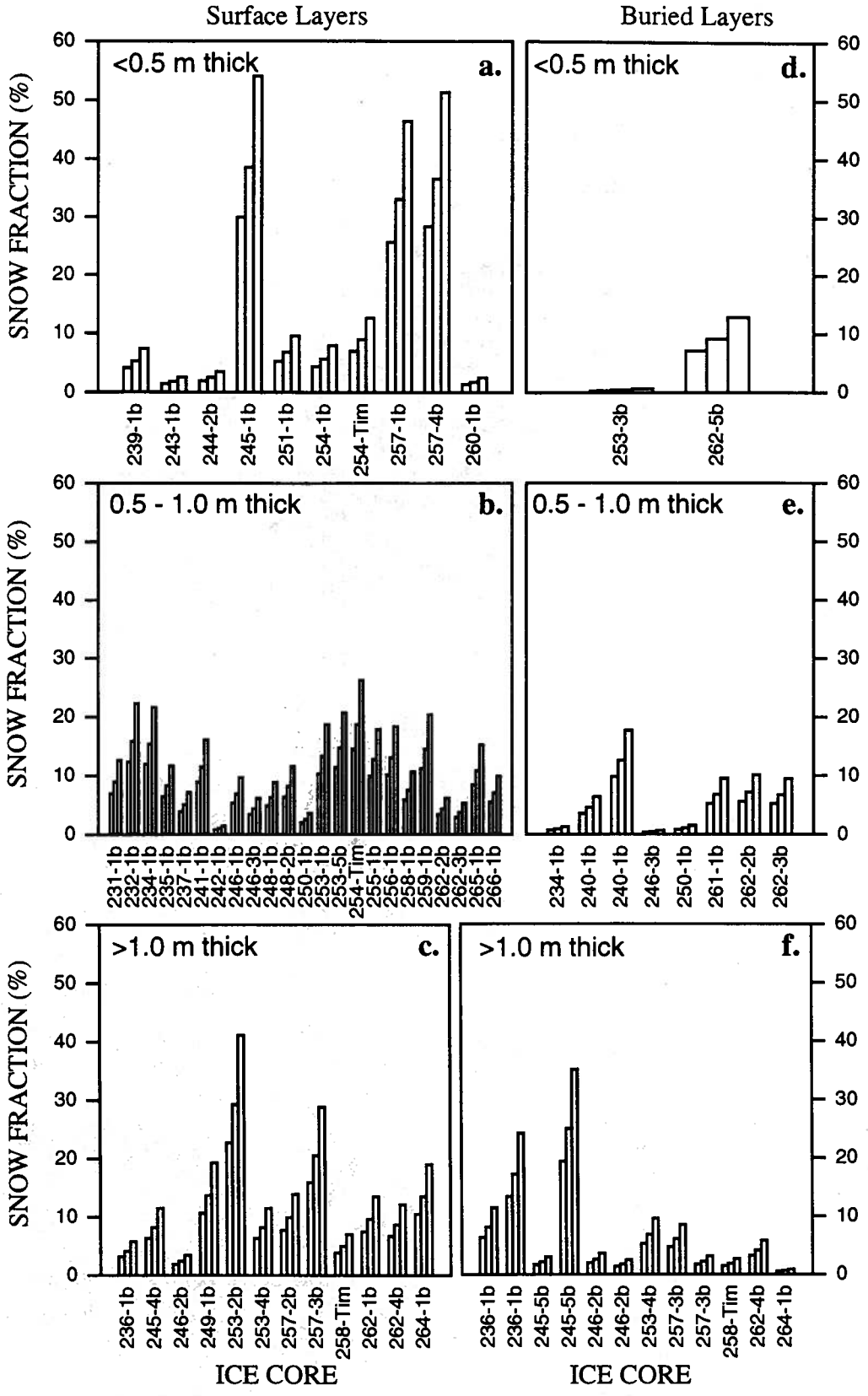

Figure 25. Variability of the snow fraction (f_s) of surface (a, b, c) and buried (d, e, f) snow ice layers in three different ice thickness categories.

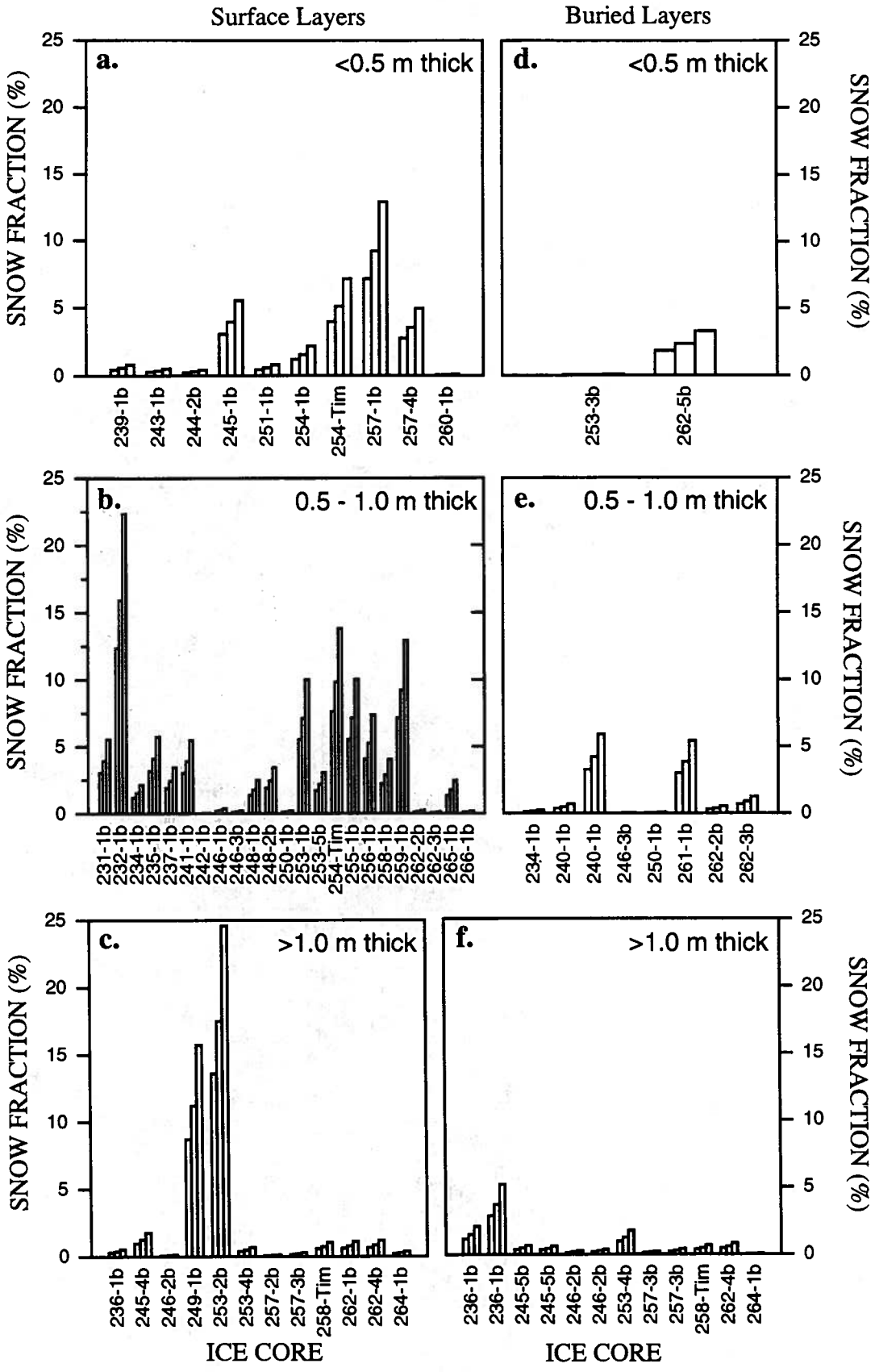

Figure 26. Variability of the snow fractions illustrated in Figure 25 as a function of ice core length, i.e., F_m values. Graphs (a.), (b.) and (c.) represent the surface snow ice layers. Graphs (d.), (e.) and (f.) represent buried snow ice layers.

The snow fraction of the total core, F_m, is calculated according to

$$F_m = f_s\,(h_i/h_c) \qquad (3)$$

where f_s is the snow fraction of the snow ice, h_i is the thickness of the snow ice layer and h_c is the core length. The F_m values for each core are illustrated in Figure 26. The mean F_m values vary between 2% and 4% depending on the choice of snow $\delta^{18}O$ value (Table 5).

Table 5. Mean snow fractions (f_s) of the snow ice and their contribution to the snow fraction (F_m) of the ice cores as a function of using different snow $\delta^{18}O$ values as input to equations (1) and (2).

	δ_s, –17.0‰	δ_s, –13.2‰	δ_s, –9.4‰
Surface snow ice, f_s (%)	8.5	10.9	15.3
Buried snow ice, f_s (%)	4.5	5.8	8.2
Surface + Buried, f_s (%)	7.2	9.2	13.0
Surface snow ice, F_m (%)	2.4	3.1	4.4
Buried snow ice, F_m (%)	0.8	1.0	1.4
Surface + Buried, F_m (%)	2.4	3.1	4.4

The minimum f_s values (those calculated using the minimum snow $\delta^{18}O$ value of –17.0‰) are not significantly different from those reported using the same criterion in the Weddell Sea, i.e., 2–7% (Lange et al., 1990). The F_m values contributed by the snow ice also are similar to those observed in the Weddell Sea, i.e., 3% (Lange et al., 1990) and 4% (Eicken et al., 1994, 1995).

6. SUMMARY & CONCLUSION

In August and September 1993 we completed the first thorough investigation of the snow cover characteristics, snow and ice thickness distribution, and properties and structure of first–year ice floes in the Bellingshausen and Amundsen seas. The results of this investigation have increased our knowledge of the nature of the late winter snow and ice cover, and understanding of the processes that contribute to ice formation and thickening.

The snow cover was a complex mixture of different snow types and properties that reflected the variable environmental conditions and processes that had contributed to its metamorphosis. These include the extremes of (1) cold, continental air conditions that lead to strong temperature gradients and depth hoar formation, and (2) warm, moist, marine air conditions that cause melting and the formation of ice layers. Wet snow and slush are also common at the base of the snow cover as a result of seawater flooding at the snow/ice interface and brine wicking.

Seawater flooding at the snow/ice interface had contributed to significant snow ice formation. The ice core data indicated that, by the end of winter, snow ice had made a greater contribution to the thermodynamic thickening of the ice cover than either frazil ice or congelation ice formation. Snow ice layers were composed of 7–13% snow, which amounted to 2–4% of the total ice mass. Although these values seem quite modest, the contribution of snow is significant and may be due a combination of a high snow load at the ice surface and melting at the bottom. The latter, which

melts frazil and/or congelation ice off the bottom, enhances the importance of flooding, snow entrainment and snow ice formation in the thermodynamic thickening of the ice cover.

Frazil ice was the most common component of the floes, which probably reflects the important role that the pancake cycle played in floe formation. The amount of congelation ice was almost half the amount of frazil ice, which might indicate that the relatively calm conditions required for congelation ice formation are less common that than the more dynamic conditions that favour frazil ice formation and the pancake cycle. The dynamic nature of the ice growth environment is reflected in the average thickness (0.12m) of frazil and congelation ice layers, which suggests that neither attains a significant thickness by thermodynamic growth before being subject to deformation, i.e., rafting and ridging.

The important role that deformation played in the thickening of the ice cover is reflected in the snow and ice thickness data and profiles. The mean thickness of individual floes and of the entire data set has a large standard deviation, and most of that variability is accounted for by the roughness of the bottom surface of the floes. Ridging produces massive keels with much smaller surface sails, but even rafting can greatly increase the ice mass and thickness variability below the waterline without significantly increasing the surface topographic variability. Nonetheless, the ice surface topography is sufficient to affect the snow depth distribution, primarily as a consequence of snow drift accumulation on the flanks of ridge sails and other protuberances.

In addition to influencing seawater flooding of the snow/ice interface and snow ice formation, the snow depth distribution had a major impact on the properties of the underlying ice. The insulating properties of the snow cover were particularly evident in the relationships between snow depth and snow/ice interface temperatures, and snow depth and mean ice temperatures. Ice temperatures were sufficiently high that most brine volume values exceeded 5%, thus promoting brine pocket coalescence and brine drainage. While this reduced the salinity of the lower ice layers, snow ice formation promoted high salinity values in the uppermost ice layers; the result was a characteristic *S*–shaped salinity profile in ice ≥0.5m thick. Thinner ice had a salinity profile that resembled a *C* shape, where higher values at the bottom might have remained if there had been less melting of the most recently formed ice.

ACKNOWLEDGEMENTS

This study was supported by Grant 9117721 from the National Science Foundation (NSF), Office of Polar Programs. B. H.–C. was supported in part by an REU (Research Experience for Undergraduates) supplement to this grant. Chris Fritsen, Russ Nilson, Tim Quakenbush and Chuah Teong Sek assisted with the snow and ice thickness measurements, the ice core drilling and numerous other aspects of the investigation. Captain Joe Borkowski, the officers and crew of the R. V. *Nathaniel B. Palmer*, and Antarctic Support Associates personnel contributed to a successful and enjoyable cruise. NSF, the Australian Antarctic Division and the Antarctic CRC made it possible for A.P.W. to participate in the study, and NSF and Instituto Antartico Chileno made it possible for R.J. to participate in the cruise. The Stable Isotope Laboratory, University of Calgary, is supported in part by grants from the Natural Sciences and Engineering Research Council of Canada.

REFERENCES

Ackley, S. F., M. A. Lange and P. Wadhams. 1990. Snow cover effects on Antarctic sea ice thickness. In, *Sea Ice Properties and Processes*, S. F. Ackley and W. F. Weeks (editors), CRREL Monograph 90–1, pp. 16–21.

Allison, I., R. E. Brandt and S. G. Warren. 1993. East Antarctic sea ice: Albedo, thickness distribution and snow cover. *Journal of Geophysical Research*, 98 (C7), 12,417–12,429.

Allison, I. and A. P. Worby. 1994. Seasonal changes in sea ice characteristics off East Antarctica. *Annals of Glaciology*, 20, 195–201.

Andreas, E. L. and A. P. Makshtas. 1985. Energy exchange over Antarctic sea ice in the spring. *Journal of Geophysical Research*, 90(C4), 7199–7212.

Andreas, E. A, M. A. Lange, S.F. Ackley and P. Wadhams. 1993. Roughness of Weddell Sea ice and estimates of air-ice drag coefficient. *Journal of Geophysical Research*, 98(C7), 12439–12452.

Colbeck, S. C. 1982. An overview of seasonal snow metamorphism. *Reviews of Geophysics and Space Physics*, 20(1), 45–61.

Colbeck, S. C. 1991. The layered character of snow covers. *Reviews of Geophysics*, 29(1), 81–96.

Comiso, J. C., T. C. Grenfell, D. L. Bell, M. A. Lange and S. F. Ackley. 1989. Passive microwave in situ observations of winter Weddell Sea ice. *Journal of Geophysical Research*, 94(C8), 10891–10905.

Cox, G. F. N. and W. F. Weeks. 1974. Salinity variations in sea ice. *Journal of Glaciology*, 13(67), 109–120.

Cox, G. F. N. and W. F. Weeks. 1975. Brine drainage and initial salt entrapment in sodium chloride ice. *CRREL Research Report* 345, pp. 1-46.

Cox, G. F. N. and W. F. Weeks. 1983. Equations for determining gas and brine volumes in sea ice. *Journal of Glaciology*, 29(102), 306–316, 1983.

Eicken, H. 1992a. The role of sea ice in structuring Antarctic ecosystems. *Polar Biology*, 12, 3-13.

Eicken, H. 1992. Salinity profiles of Antarctic sea ice: field data and model results. *Journal of Geophysical Research*, 97(C10), 15545–15557.

Eicken, H. and M. A. Lange. 1989. Development and properties of sea ice in the coastal regime of the southeastern Weddell Sea. *Journal of Geophysical Research*, 94(C6), 8193–8206.

Eicken, H., M. A. Lange., H.–W. Hubberten, and P. Wadhams. 1994. Characteristics and distribution patterns of snow and meteoric ice in the Weddell Sea and their contribution to the mass balance of sea ice. *Annales Geophysicae*, 12 (1), 80–93.

Eicken, H., H. Fischer and P. Lemke. 1995. Effects of the snow cover on Antarctic sea ice and potential modulation of its response to climate change. *Annals of Glaciology*, 21, 369–376.

Fahrbach, E., M. Knoche and G. Rohardt. 1991. An estimate of water mass transformation in the southern Weddell Sea. *Marine Chemistry*, 35(1–4), 25–44.

Fritsen, C. H., V. I. Lytle, S. F, Ackley and C. W. Sullivan. 1994. Autumn bloom of Antarctic pack–ice algae. *Science*, 266(5186), 782–784.

Garrison, D. L., C. W. Sullivan and S. F. Ackley. 1986. Sea ice microbial community studies in the Antarctic. *Bioscience*, 36(4), 243–250.

Garrity, C. 1992. Characterization of snow on floating ice and case studies of brightness temperature changes during the onset of melt. In, *Microwave Remote Sensing of Sea Ice*, F. D. Carsey (editor), Geophysical Monograph 68, AGU, Washington, D.C., pp. 313–328.

Gordon, A. L. and B. A. Huber. 1990. Southern Ocean Winter Mixed Layer. *Journal of Geophysical Research*, 95(C7), 11655–11672.

Gow, A. J., S. F. Ackley, W. F. Weeks and J. W. Govoni. 1982. Physical and structural characteristics of Antarctic sea ice. *Annals of Glaciology*, 3, 113–117.

Gow, A. J., S. F. Ackley, K. R. Buck and K. M. Golden. 1987. Physical and structural characteristics of Weddell Sea pack ice. *CRREL Report* 87–14.

Haas, C and T. Viehoff. 1994. Sea ice observations in the Bellingshausen/Amundsen Sea: shipboard observations and satellite imagery during ANT XI/3. Berichte aus em Fachbereich Physik, Report 51, Alfred–Wegener–Institut.

Jacka, T. H., I. Allison, R. Thwaites and J. C. Wilson. 1987. Characteristics of the seasonal sea ice zone of East Antarctica and comparison with satellite observations. *Annals of Glaciology*, 9, 85-91.

Jacobs, S. S. and J. C. Comiso. 1993. A recent sea–ice retreat west of the Antarctic Peninsula. *Geophysical Research Letters*, 20(12), 1171–1174.

Jeffries, M. O. and W. F. Weeks. 1992. Structural characteristics and development of sea ice in the western Ross Sea. *Antarctic Science*, 5(1), 63–75.

Jeffries, M. O. and U. Adolphs. In press. Early winter snow and ice thickness distribution, ice structure and development of the western Ross Sea pack ice between the ice edge and the Ross Ice Shelf. *Antarctic Science*, 1997.

Jeffries, M. O., W. F. Weeks, K. Morris and R. A Shaw. 1993. Structural characteristics of congelation ice and platelet ice and their role in the development of Antarctic landfast sea ice. *Journal of Glaciology*, 39, 223–238.

Jeffries, M. O., R. A. Shaw, K. Morris, A. L. Veazey and H. R. Krouse. 1994a. Crystal structure, stable isotopes ($\delta^{18}O$) and development of sea ice in the Ross, Amundsen and Bellingshausen Seas, Antarctica. *Journal of Geophysical Research*, 99(C1), 985–995.

Jeffries, M. O., K. Morris, A. L. Veazey and H. R. Krouse. 1994b. Depositional environment of the snow cover on West Antarctic pack ice floes. *Annals of Glaciology*, 20, 33–38.

Jeffries, M. O., K. Morris, A. P. Worby and W. F. Weeks. 1994c. Late winter characteristics of the seasonal snow cover on sea ice floes in the Bellingshausen and Amundsen Seas. *Antarctic Journal of the United States*, 29(1), 9–10.

Jeffries, M. O., T. S. Chuah and K. Morris. 1995. C–band radar backscatter from antarctic first–year sea ice: I *In situ* scatterometer measurements. *Antarctic Journal of the United States*, 30(1–4), 24–26.

Jeffries, M. O., A. P. Worby, K. Morris and W. F. Weeks. 1997. Seasonal variations in the properties and structural composition of sea ice and snow cover in the Bellingshausen and Amundsen seas, Antarctica. *Journal of Glaciology*, in press.

Kawamura, T., K. I. Ohshima, S. Ushio and T. Takizawa. 1993. Sea–ice growth in Ongul Strait, Antarctica. *Annals of Glaciology*, 18, 97–101.

Kawamura, T., T. Takizawa, K. Ohshima and S. Ushio. In press. Physical, structural and isotopic characteristics and growth processes of sea ice in Lützow–Holm Bay, Antarctica. *Journal of Geophysical Research*.

Lange, M. A. and H. Eicken. 1991a. The sea ice thickness distribution in the northwestern Weddell Sea. *Journal of Geophysical Research*, 96(C3), 4821–4837.

Lange, M. A. and H. Eicken. 1991b. Textural characteristics of sea ice and the major mechanisms of ice growth in the Weddell Sea. *Annals of Glaciology*, 15, 210–215.

Lange, M. A. and H.–W. Hubberten. 1992. Isotopic composition of sea ice as a tool for understanding sea ice processes in the polar regions. In, *Physics and Chemistry of Ice*, edited by N. Maeno and T. Hondoh, Sapporo, Japan, Hokkaido University Press, 399–405.

Lange, M. A., S. F. Ackley, P. Wadhams, G. S. Dieckmann and H. Eicken. 1989. Development of sea ice in the Weddell Sea. *Annals of Glaciology*, 12, 92–96.

Lange, M. A., P. Schlosser, S. F. Ackley, P. Wadhams and G. S. Dieckmann. 1990. ^{18}O concentrations in sea ice of the Weddell Sea, Antarctica. *Journal of Glaciology*, 36(124), 315-323.

Lytle, V. I. and S. F. Ackley. 1996. Heat flux through sea ice in the western Weddell Sea: convective and conductive transfer processes. *Journal of Geophysical Research*, 101(C4), 8853–8868.

Lytle, V. I., K. C. Jezek, S. P. Gogineni and A. R. Hosseinmostafa. 1996. Field observations of microwave backscatter from Weddell Sea ice. *International Journal of Remote Sensing*, 17(1), 167–180.

Maykut, 1978. Energy exchange over young sea ice in the central Arctic. *Journal of Geophysical Research*, 83(C7), 3646–3658.

Maykut, G. 1986. The surface heat and mass balance. In, *The Geophysics of Sea Ice*, N. Untersteiner (editor), Plenum Press, New York, pp. 395–463.

Morris, K. and M. O. Jeffries. 1995. C–band radar backscatter from antarctic first–year sea ice: II ERS–1 SAR measurements. *Antarctic Journal of the United States*, 30(1–4), 26–28.

Morris, K., M. O. Jeffries and S. Li. 1996. Sea ice characteristics and backscatter variability in the Bellingshausen Sea, Antarctica. Proceedings of the Fourth Circumpolar Symposium on Remote Sensing of the Polar Environments, 29 April–1 May, Lyngby, Denmark. European Space Agency Special Publication, ESA SP–391, pp. 113–117.

Morris, K. and M. O. Jeffries. In press. Sea ice characteristics and seasonal variability of ERS–1 SAR backscatter in the Bellingshausen Sea. *Antarctic Research Series*, 1997.

Nakawo, M. and N. K. Sinha. 1981. Growth rate and salinity profile of first–year sea ice in the High Arctic. *Journal of Glaciology*, 27(96), 315–330.

O'Neil, J. R. 1968. Hydrogen and oxygen isotope fractionation between ice and water. *Journal of Physical Chemistry*, 72(10), 3683–3684.

Panov, V. V. and V. I. Fedotov. 1977. Pripay vostochnoy Antarktidy (Fast ice of the East Antarctic). *Trudy Sovietskoy Antarkticheskoy Ekspeditsii*, 63, 130pp.

Sullivan, C. W., A. C. Palmisano, S. T. Kottmeier, S. M. Grossi and R. L. Moe. 1985. The influence of light on growth and development of the sea ice microbial community in McMurdo Sound, Antarctica. In, *Fourth SCAR Symposium on Antarctic Biology, Nutrient Cycles and Food Webs*, W. R. Siegfried, P. R. Condy and R. M. Laws (editors), Springer–Verlag, Berlin, pp. 84–88.

Wadhams, P., M. A. Lange and S. F. Ackley. 1987. The ice thickness distribution across the Atlantic sector of the Antarctic Ocean in midwinter, *Journal of Geophysical Research*, 92(C13), 14,535–14, 552.

Weeks, W. F. and O. S. Lee. 1958. Observations on the physical properties of sea ice at Hopedale, Labrador, *Arctic*, 11(3), 134–155.
Weeks, W. F. and O. S. Lee. 1962. The salinity distribution in young sea ice. *Arctic*, 15(2), 134–155.
Weeks, W. F. and S. F. Ackley. 1982. The growth, structure and properties of sea ice. *CRREL Monograph* 82–1.
Worby, A. P. and I. Allison. 1991. Ocean–atmosphere energy exchange over thin, variable concentration Antarctic pack–ice. *Annals of Glaciology*, 15, 184-190.
Worby, A. P., W. F. Weeks, M. O. Jeffries, K. Morris and R. Jaña. 1994. Late winter sea ice and snow thickness distributions in the Bellingshausen and Amundsen Seas. *Antarctic Journal of the United States,* 29(1), 13–15.
Worby, A. P., M. O. Jeffries, K. Morris, W. F. Weeks and R. Jaña. In press. The thickness distribution of sea ice and snow cover during late winter in the Bellingshausen and Amundsen Seas, Antarctica. *Journal of Geophysical Research,* 101(C12), 28,441-28,455.
Worby, A. P. and R. Massom. 1995. The structure and properties of sea ice and snow cover in East Antarctic pack ice. Hobart, Tasmania, *Antarctic CRC Research Report*, 7.

APPENDIX

Snow and Ice Thickness Profiles and Ice Core Characteristics

NBP 93-5 FLOE 229

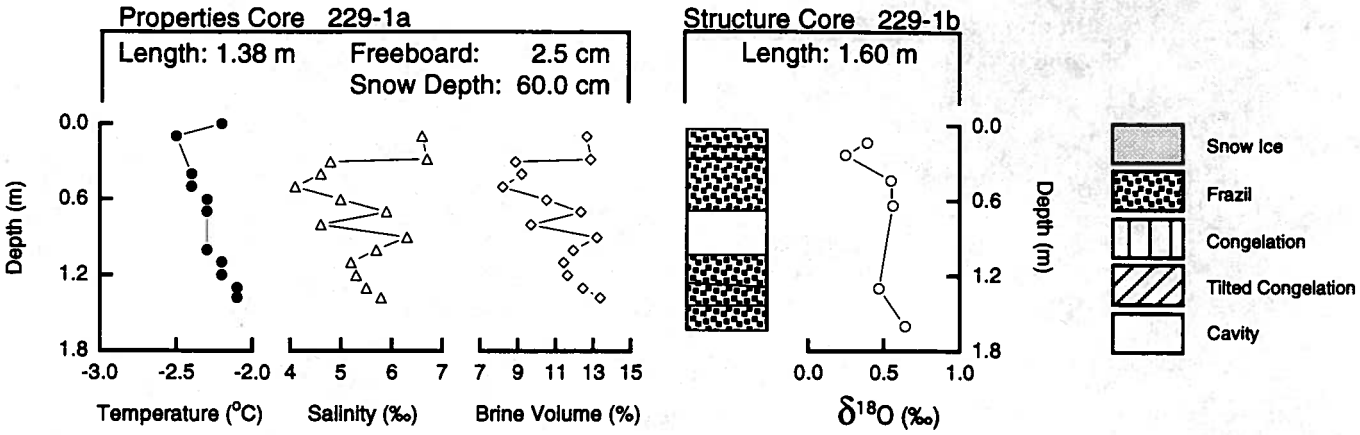

Position: 69° 04.10' S, 76° 51.00' W
Date: 17 August 1993

Mean Ice Thickness: 196.6 ± 52.8 cm
Mean Snow Thickness: 25.4 ± 11.0 cm
Mean Freeboard: 11.7 ± 11.9 cm
Floe Type: C

Salinity min: 4.1 ‰
Salinity max: 6.7 ‰
Salinity mean: 5.4 ‰

$\delta^{18}O$ min: 0.25 ‰
$\delta^{18}O$ max: 0.64 ‰
$\delta^{18}O$ mean: 0.48 ‰

Snow Ice: 00.0 %
Frazil Ice: 78.1 %
Congelation: 00.0 %
Cavity: 21.9 %

Snow Fraction
f_s: 0.00 %
F_m: 0.00 %

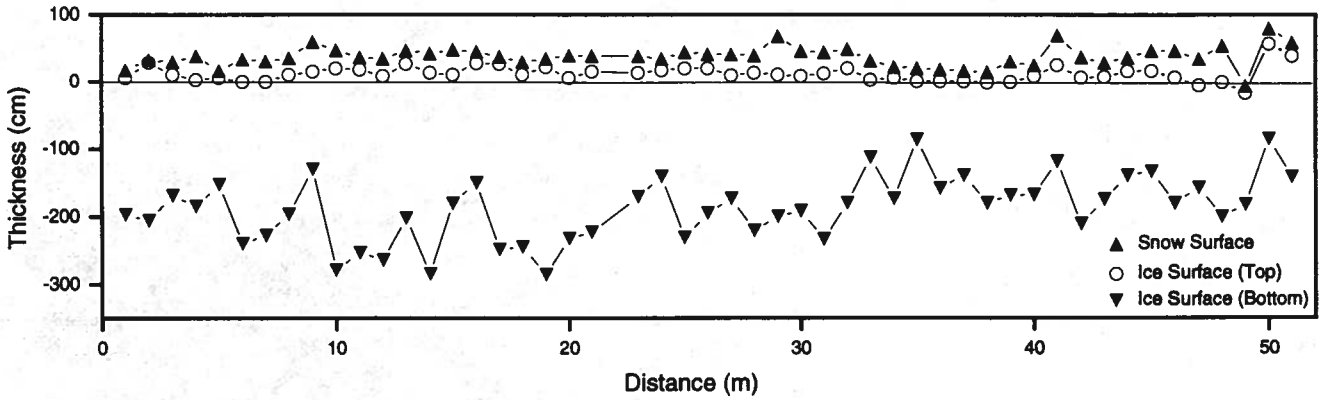

NBP 93-5 FLOE 230

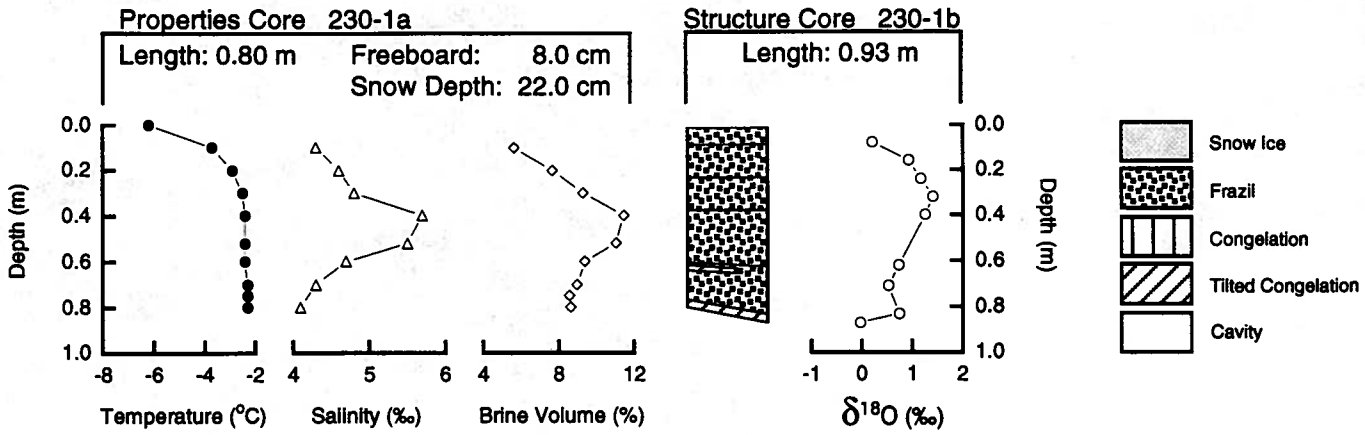

Position: 70° 01.70' S, 79° 59.50' W
Date: 18 August 1993

Mean Ice Thickness: 230.7 ± 148.1 cm
Mean Snow Thickness: 23.0 ± 9.6 cm
Mean Freeboard: 22.0 ± 27.1 cm
Floe Type: C

Salinity min: 4.1 ‰
Salinity max: 5.7 ‰
Salinity mean: 4.7 ‰

$\delta^{18}O$ min: -0.03 ‰
$\delta^{18}O$ max: 1.41 ‰
$\delta^{18}O$ mean: 0.77 ‰

Snow Ice: 00.0 %
Frazil Ice: 94.5 %
Congelation: 5.5 %
Cavity: 00.0 %

Snow Fraction
f_s: 0.00 %
F_m: 0.00 %

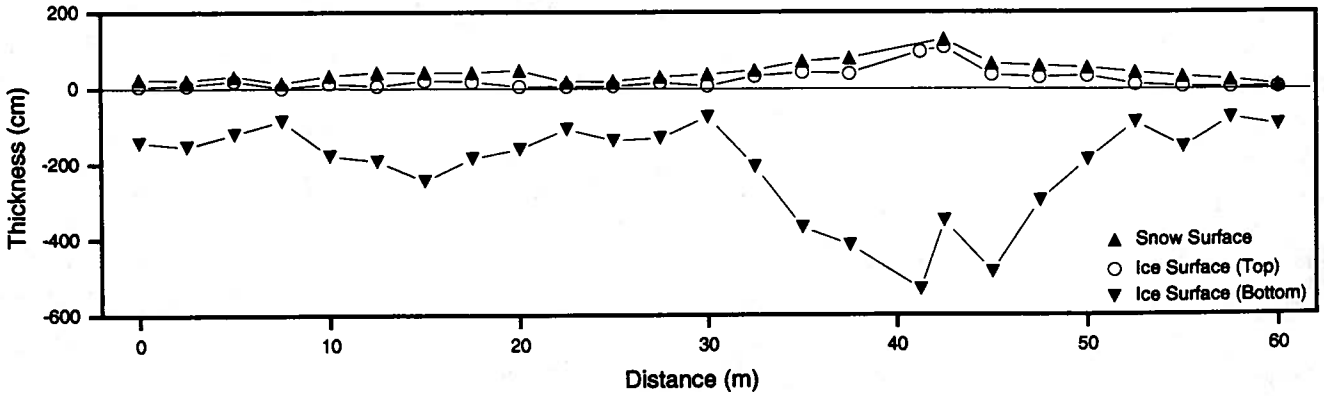

NBP 93-5 FLOE 231

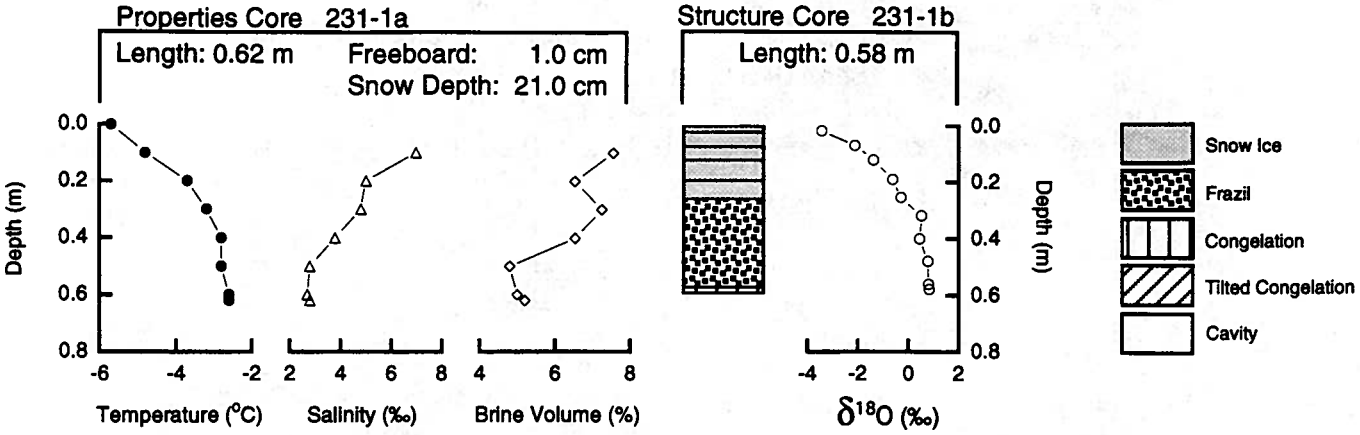

Position: 69° 48.00' S, 84° 00.50' W
Date: 19 August 1993

Mean Ice Thickness: 91.6 ± 43.8 cm
Mean Snow Thickness: 20.9 ± 7.8 cm
Mean Freeboard: 5.7 ± 4.8 cm
Floe Type: C

Salinity min: 2.7 ‰
Salinity max: 7.0 ‰
Salinity mean: 4.1 ‰

$\delta^{18}O$ min: -3.42 ‰
$\delta^{18}O$ max: 0.84 ‰
$\delta^{18}O$ mean: -0.43 ‰

Snow Ice: 44.0 %
Frazil Ice: 52.6 %
Congelation: 3.4 %
Cavity: 00.0 %

Snow Fraction
f_s: 8.99 %
F_m: 3.95 %

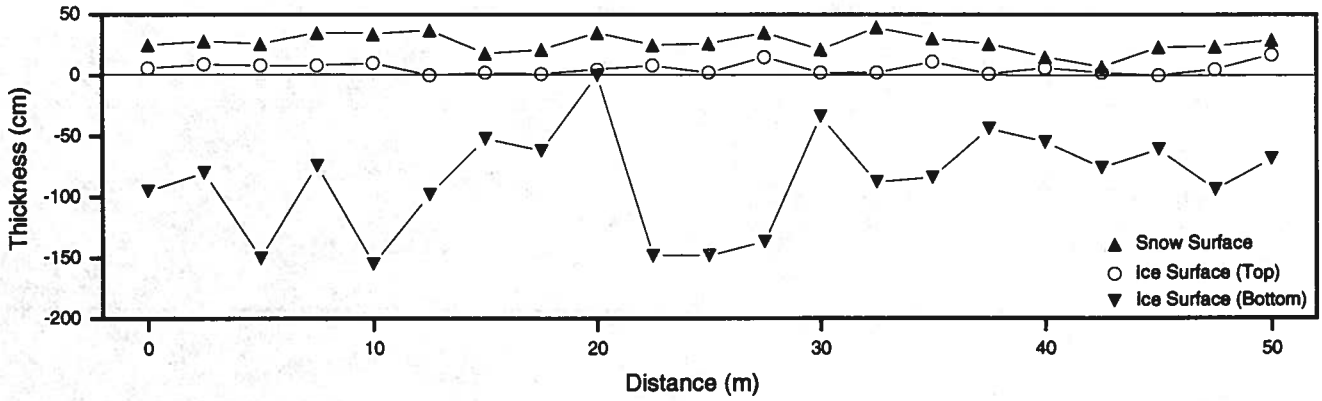

NBP 93-5 FLOE 232

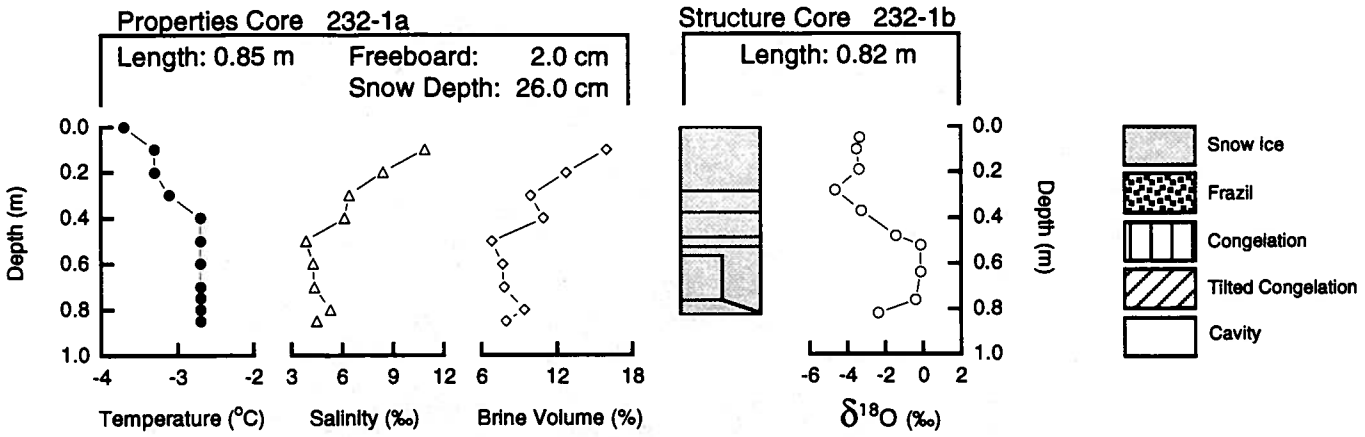

Position: 70° 34.50' S, 83° 54.60' W
Date: 20 August 1993

Mean Ice Thickness: 93.8 ± 20.9 cm
Mean Snow Thickness: 35.4 ± 11.4 cm
Mean Freeboard: 2.2 ± 4.2 cm
Floe Type: B

Salinity min: 3.8 ‰
Salinity max: 10.9 ‰
Salinity mean: 6.0 ‰

$\delta^{18}O$ min: -4.65 ‰
$\delta^{18}O$ max: -0.13 ‰
$\delta^{18}O$ mean: -2.25 ‰

Snow Ice: 100.0 %
Frazil Ice: 00.0 %
Congelation: 00.0 %
Cavity: 00.0 %

Snow Fraction
f_s: 15.92 %
F_m: 15.92 %

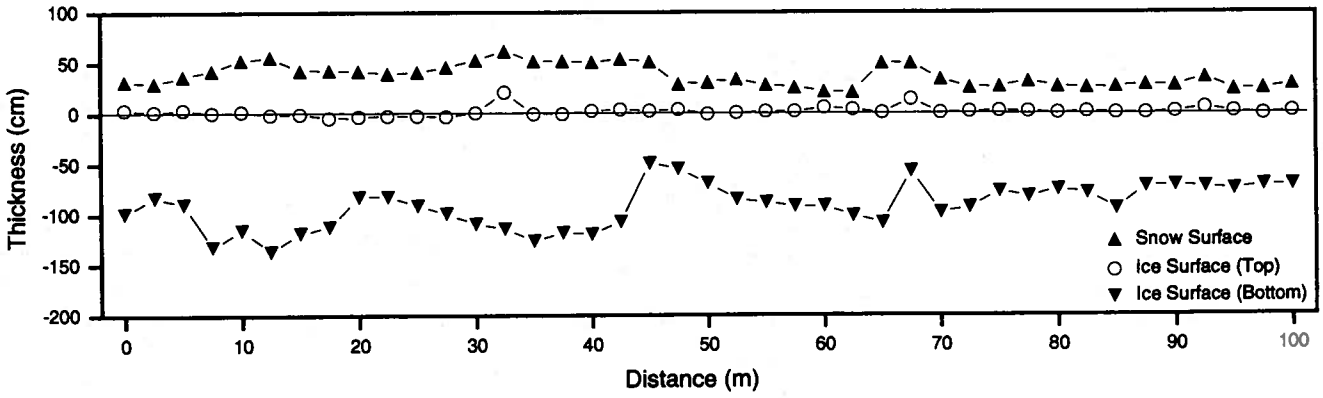

NBP 93-5 FLOE 234

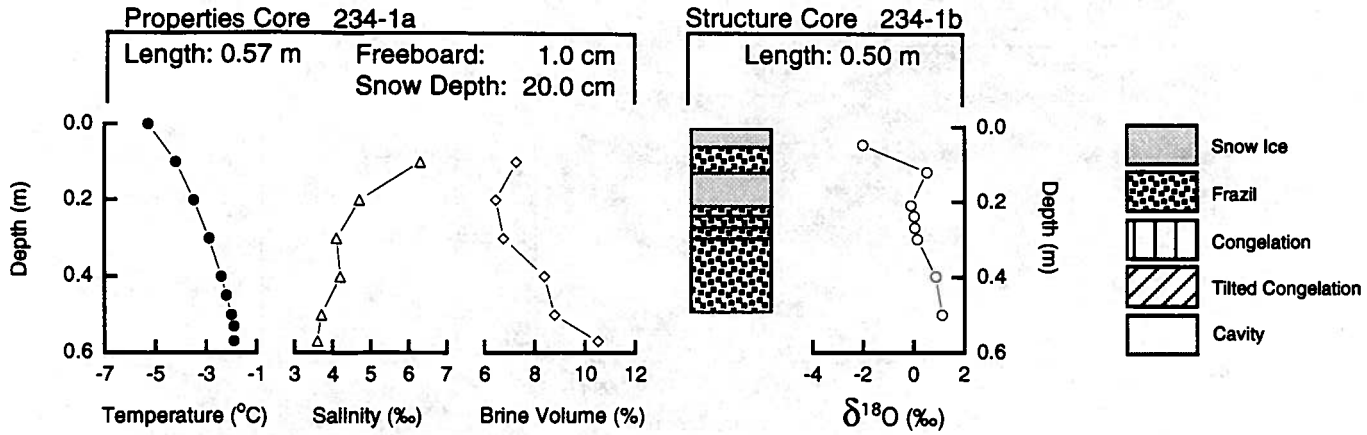

Position: 69° 45.60' S, 81° 05.70' W
Date: 22 August 1993

Mean Ice Thickness: 100.6 ± 63.0 cm
Mean Snow Thickness: 23.1 ± 11.9 cm
Mean Freeboard: 5.8 ± 10.7 cm
Floe Type: C

Salinity min: 3.6 ‰
Salinity max: 6.3 ‰
Salinity mean: 4.4 ‰

$\delta^{18}O$ min: -2.04 ‰
$\delta^{18}O$ max: 1.13 ‰
$\delta^{18}O$ mean: 0.06 ‰

Snow Ice: 28.0 %
Frazil Ice: 72.0 %
Congelation: 00.0 %
Cavity: 00.0 %

Snow Fraction
f_s: 6.10 %
F_m: 1.71 %

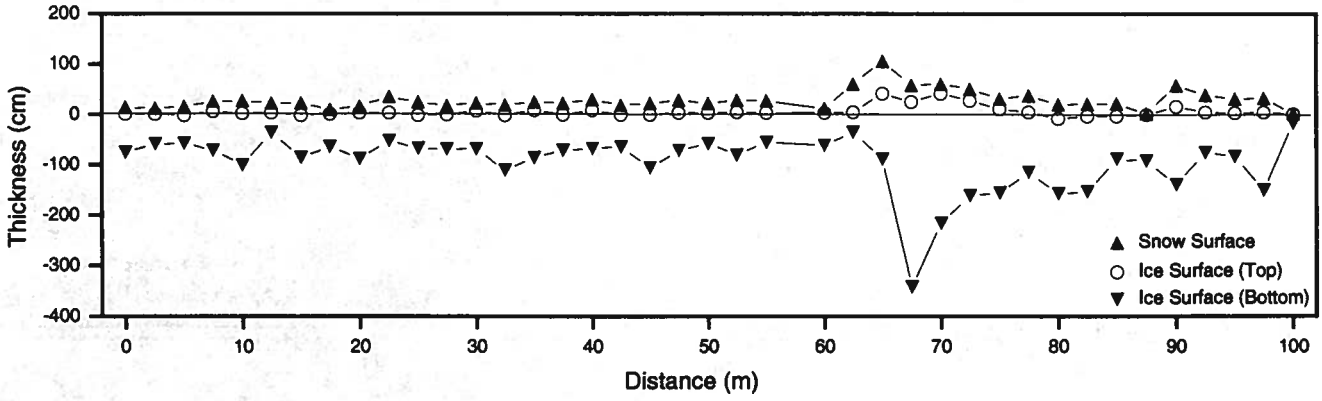

NBP 93-5 FLOE 235

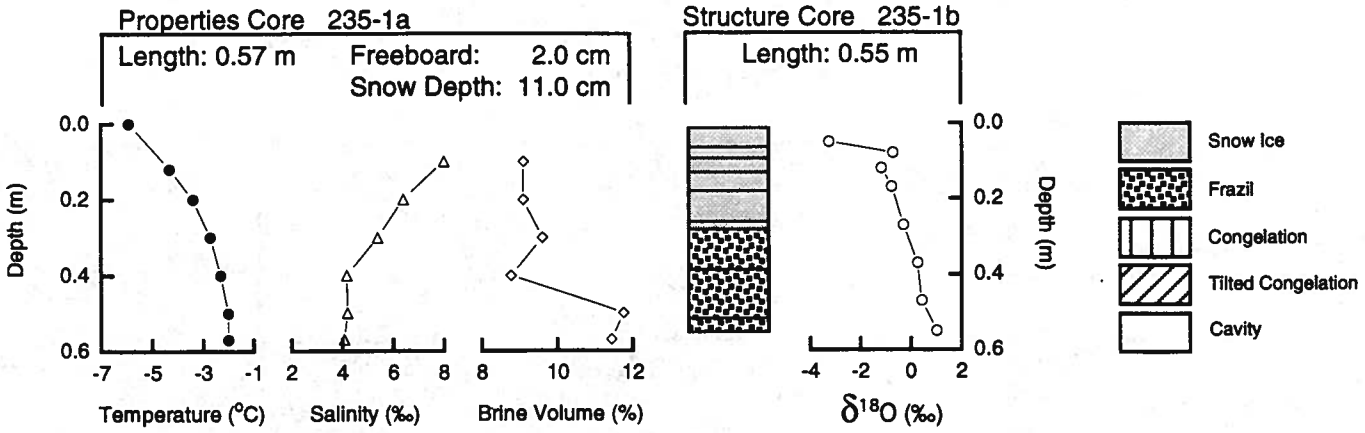

Position: 69° 43.90' S, 81° 01.00' W
Date: 23 August 1993

Mean Ice Thickness: 71.3 ± 30.9 cm
Mean Snow Thickness: 20.2 ± 6.2 cm
Mean Freeboard: 2.8 ± 2.0 cm
Floe Type: C

Salinity min: 4.1 ‰
Salinity max: 8.0 ‰
Salinity mean: 5.4 ‰

$\delta^{18}O$ min: -3.24 ‰
$\delta^{18}O$ max: 1.03 ‰
$\delta^{18}O$ mean: -0.56 ‰

Snow Ice: 49.1 %
Frazil Ice: 50.9 %
Congelation: 00.0 %
Cavity: 00.0 %

Snow Fraction
f_s: 8.35 %
F_m: 4.10 %

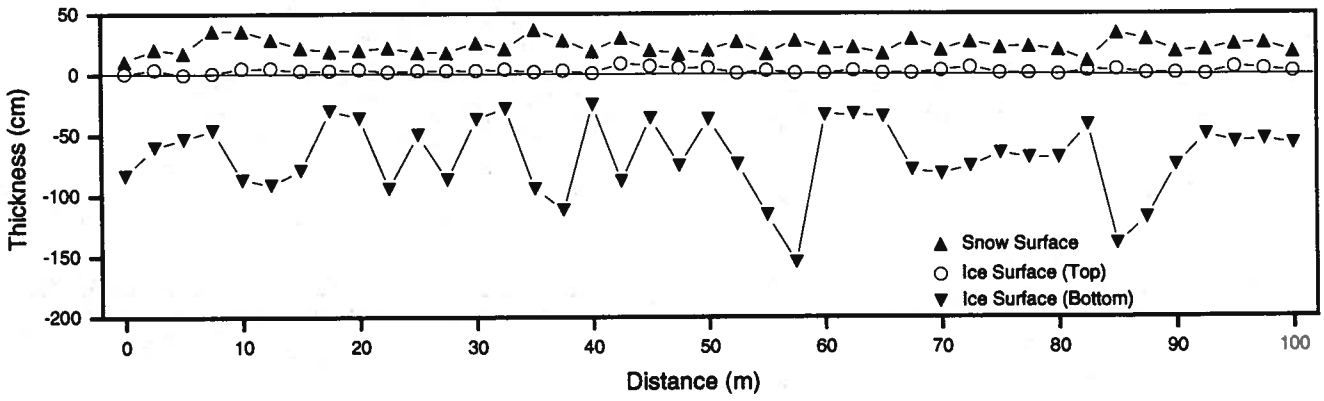

NBP 93-5 FLOE 236

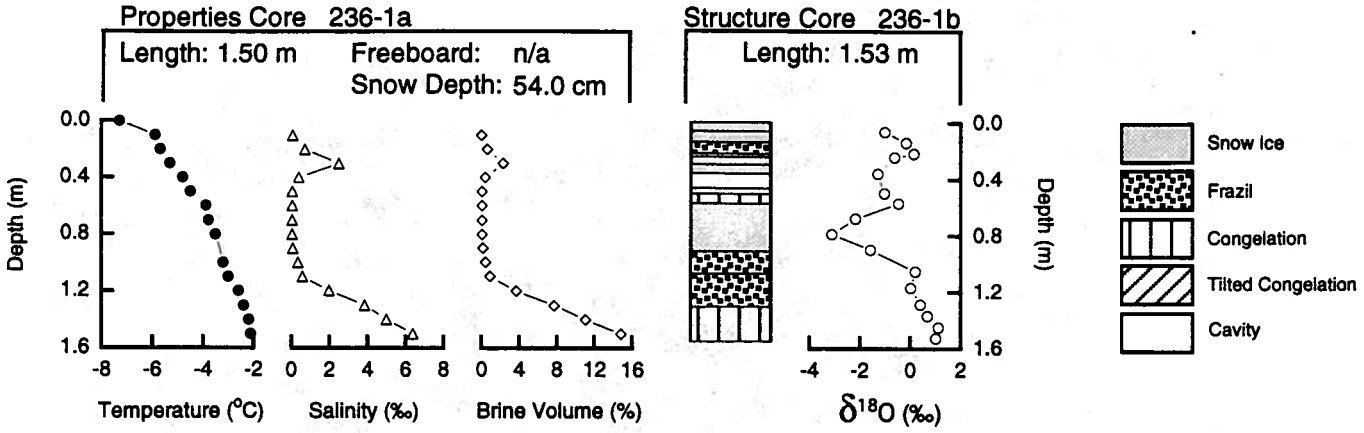

Position: 69° 43.87' S, 84° 56.85' W
Date: 24 August 1993

Mean Ice Thickness: 118.2 ± 105.3 cm
Mean Snow Thickness: 32.8 ± 23.7 cm
Mean Freeboard: 7.2 ± 17.6 cm
Floe Type: C

Salinity min: 0.0 ‰
Salinity max: 6.4 ‰
Salinity mean: 1.5 ‰

$\delta^{18}O$ min: -3.10 ‰
$\delta^{18}O$ max: 1.11 ‰
$\delta^{18}O$ mean: -0.48 ‰

Snow Ice: 42.5 %
Frazil Ice: 30.7 %
Congelation: 20.3 %
Cavity: 6.5 %

Snow Fraction
f_s: 11.4 %
F_m: 5.6 %

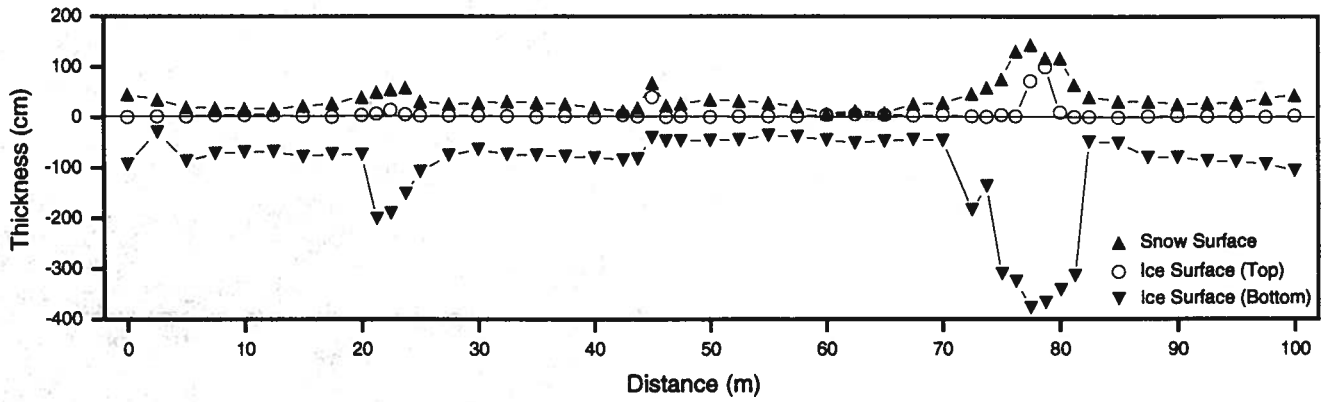

NBP 93-5 FLOE 237

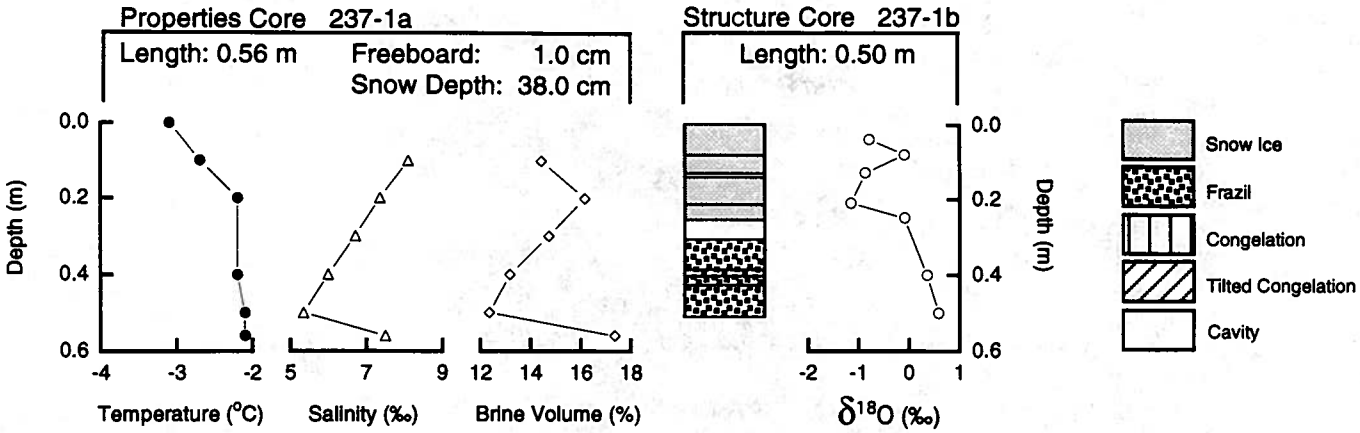

Position: 69° 28.35' S, 86° 54.10' W
Date: 25 August 1993

Mean Ice Thickness: 148.6 ± 43.8 cm
Mean Snow Thickness: 55.3 ± 12.3 cm
Mean Freeboard: 1.8 ± 2.3 cm
Floe Type: B

Salinity min: 5.3 ‰
Salinity max: 8.1 ‰
Salinity mean: 6.8 ‰

$\delta^{18}O$ min: -1.15 ‰
$\delta^{18}O$ max: 0.59 ‰
$\delta^{18}O$ mean: -0.29 ‰

Snow Ice: 48.0 %
Frazil Ice: 40.0 %
Congelation: 00.0 %
Cavity: 12.0 %

Snow Fraction
f_s: 5.11 %
F_m: 2.45 %

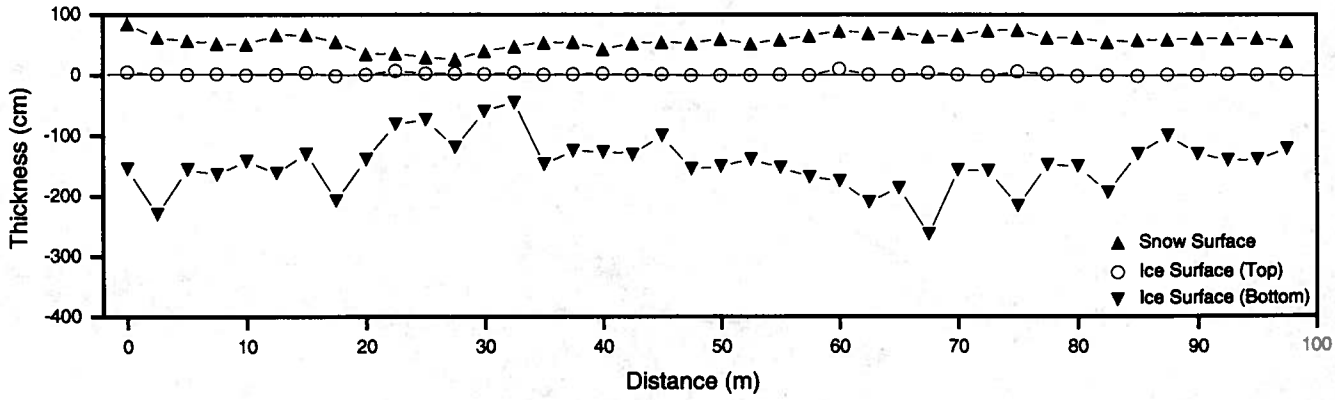

NBP 93-5 FLOE 238

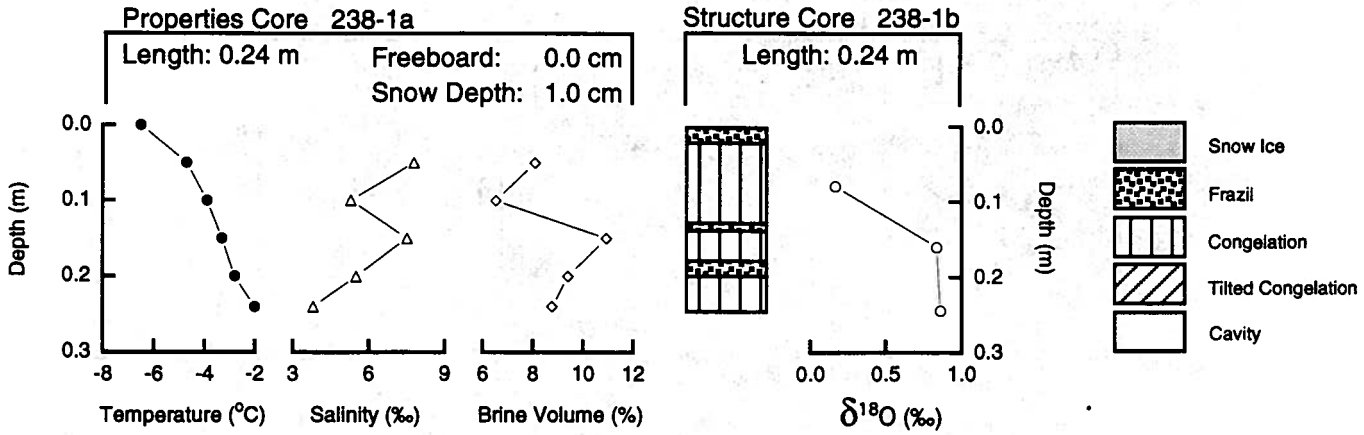

Position: 68° 58.48' S, 88° 59.66' W
Date: 26 August 1993

Mean Ice Thickness: 42.6 ± 17.0 cm
Mean Snow Thickness: 9.7 ± 6.0 cm
Mean Freeboard: 2.2 ± 4.4 cm
Floe Type: B

Salinity min: 3.8 ‰
Salinity max: 7.8 ‰
Salinity mean: 6.0 ‰

$\delta^{18}O$ min: 0.17 ‰
$\delta^{18}O$ max: 0.86 ‰
$\delta^{18}O$ mean: 0.62 ‰

Snow Ice: 00.0 %
Frazil Ice: 20.4 %
Congelation: 79.6 %
Cavity: 00.0 %

Snow Fraction
f_s: 0.00 %
F_m: 0.00 %

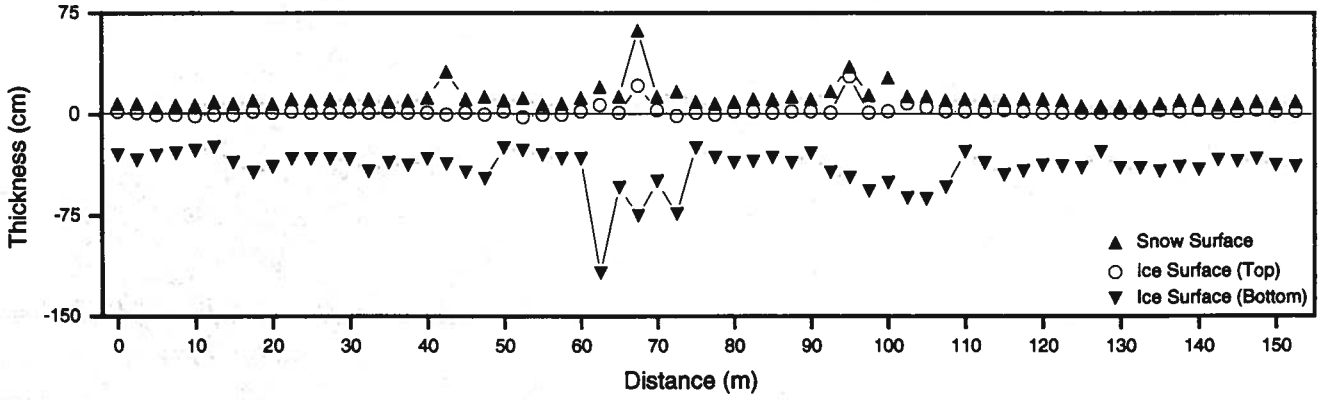

NBP 93-5 FLOE 239

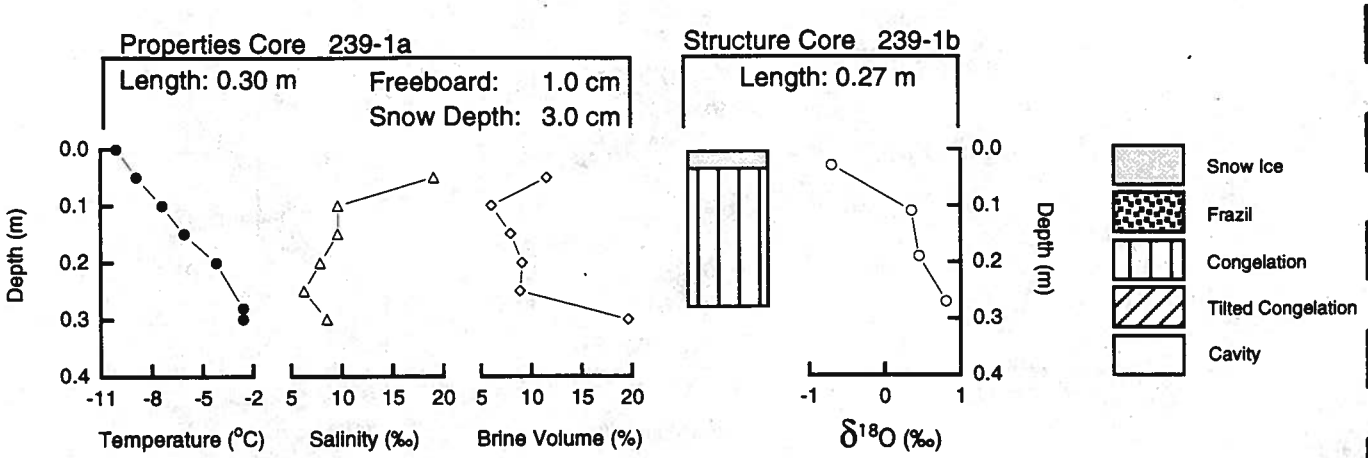

Position: 67° 59.72' S, 88° 59.00' W
Date: 27 August 1993

Mean Ice Thickness: 34.5 ± 9.1 cm
Mean Snow Thickness: 4.1 ± 1.6 cm
Mean Freeboard: 2.2 ± 2.4 cm
Floe Type: B

Salinity min: 6.3 ‰
Salinity max: 19.1 ‰
Salinity mean: 10.2 ‰

$\delta^{18}O$ min: -0.69 ‰
$\delta^{18}O$ max: 0.81 ‰
$\delta^{18}O$ mean: 0.23 ‰

Snow Ice: 11.1 %
Frazil Ice: 00.0 %
Congelation: 88.9 %
Cavity: 00.0 %

Snow Fraction
f_s: 5.27 %
F_m: 0.59 %

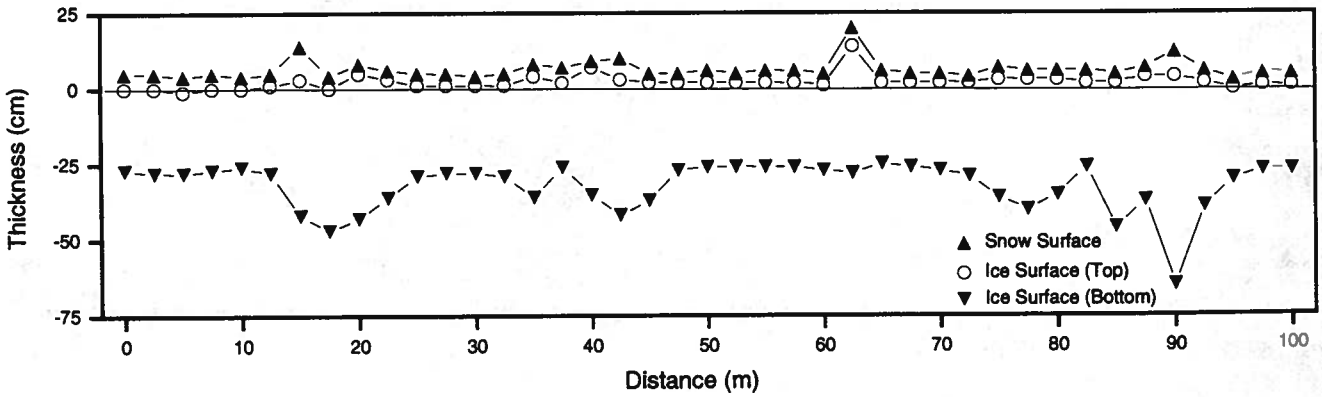

NBP 93-5 FLOE 240

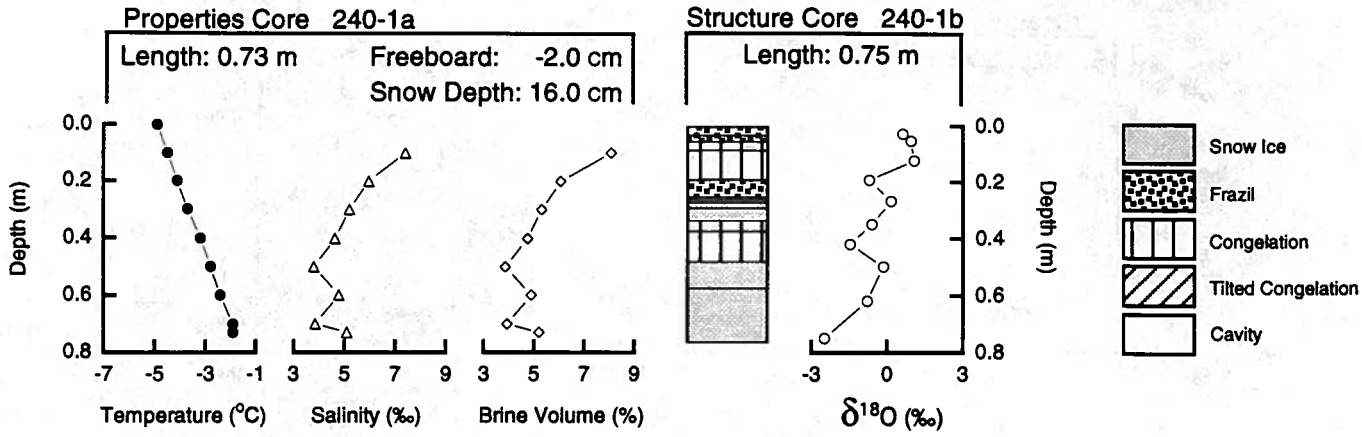

Position: 66° 43.15' S, 88° 53.79' W
Date: 28 August 1993

Mean Ice Thickness: 54.0 ± 17.1 cm
Mean Snow Thickness: 20.7 ± 10.0 cm
Mean Freeboard: 1.2 ± 3.4 cm
Floe Type: B

Salinity min: 3.8 ‰
Salinity max: 7.4 ‰
Salinity mean: 5.1 ‰

$\delta^{18}O$ min: -2.48 ‰
$\delta^{18}O$ max: 1.07 ‰
$\delta^{18}O$ mean: -0.33 ‰

Snow Ice: 44.0 %
Frazil Ice: 17.3 %
Congelation: 38.7 %
Cavity: 00.0 %

Snow Fraction
f_s: 10.65 %
F_m: 4.68 %

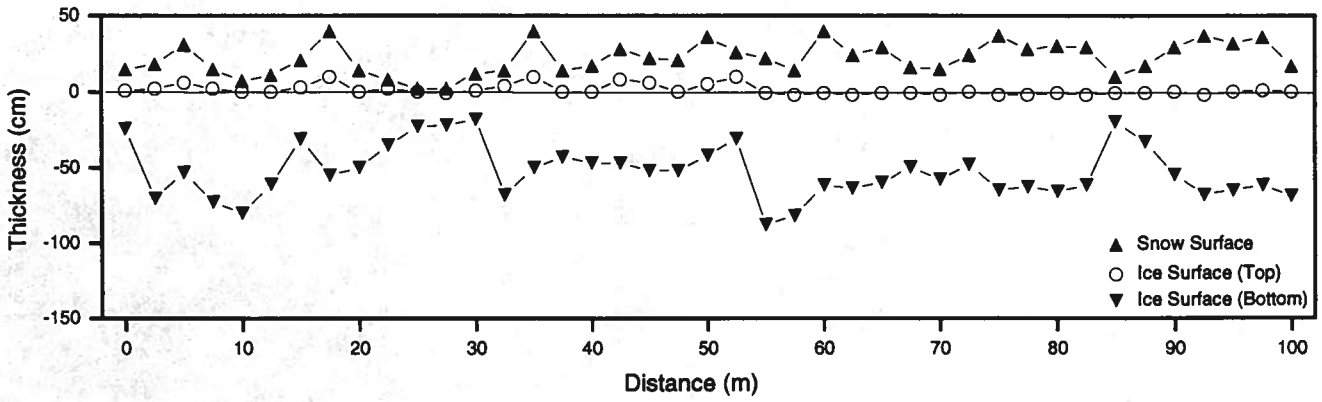

NBP 93-5 FLOE 241

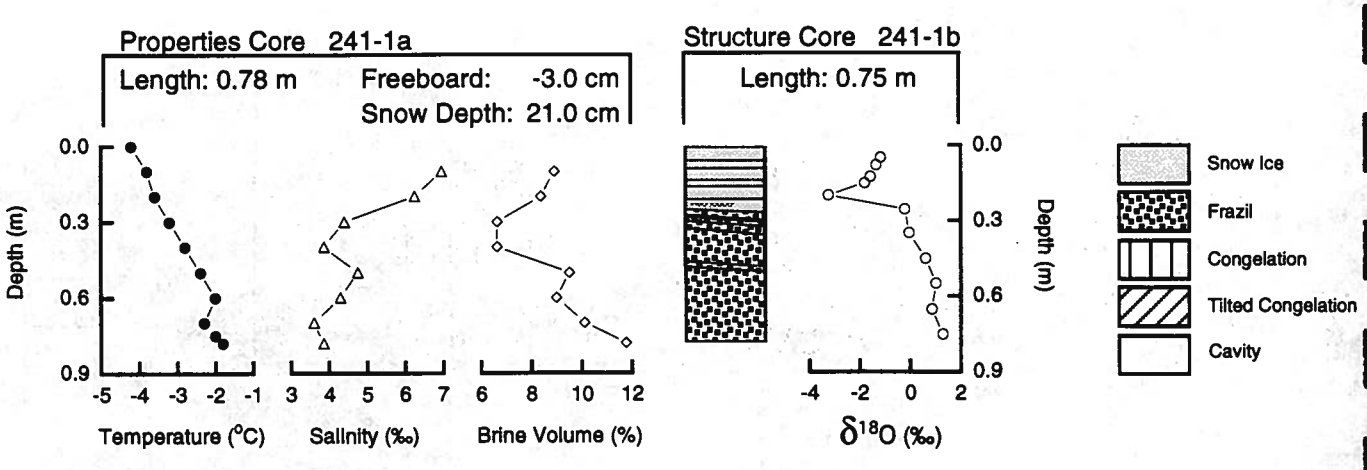

Position: 66° 50.00' S, 88° 39.10' W
Date: 29 August 1993

Mean Ice Thickness: 72.4 ± 41.5 cm
Mean Snow Thickness: 24.4 ± 10.9 cm
Mean Freeboard: 0.7 ± 4.8 cm
Floe Type: C

Salinity min: 3.6 ‰
Salinity max: 6.9 ‰
Salinity mean: 4.7 ‰

$\delta^{18}O$ min: -3.24 ‰
$\delta^{18}O$ max: 1.29 ‰
$\delta^{18}O$ mean: -0.51 ‰

Snow Ice: 34.0 %
Frazil Ice: 66.0 %
Congelation: 00.0 %
Cavity: 00.0 %

Snow Fraction
f_s: 11.51 %
F_m: 3.91 %

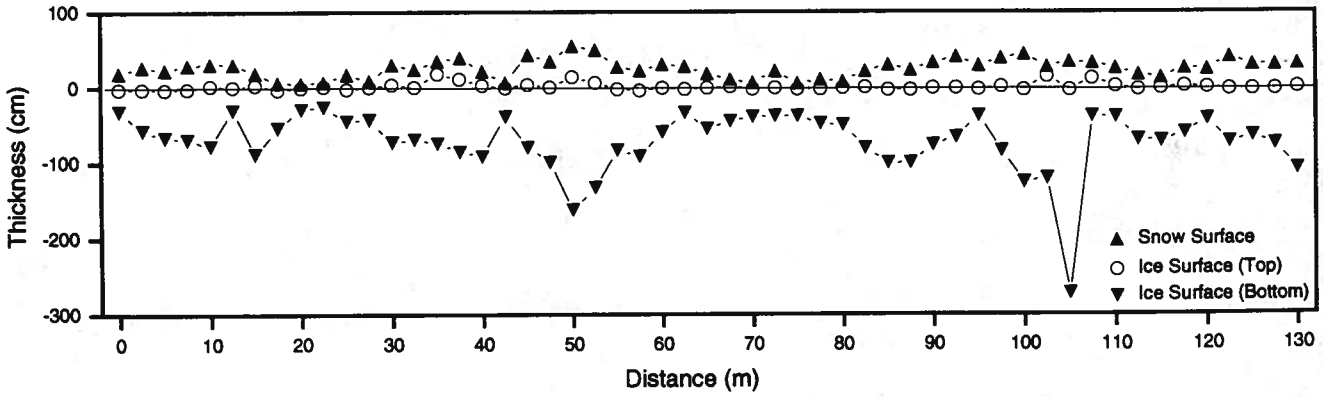

NBP 93-5 FLOE 242

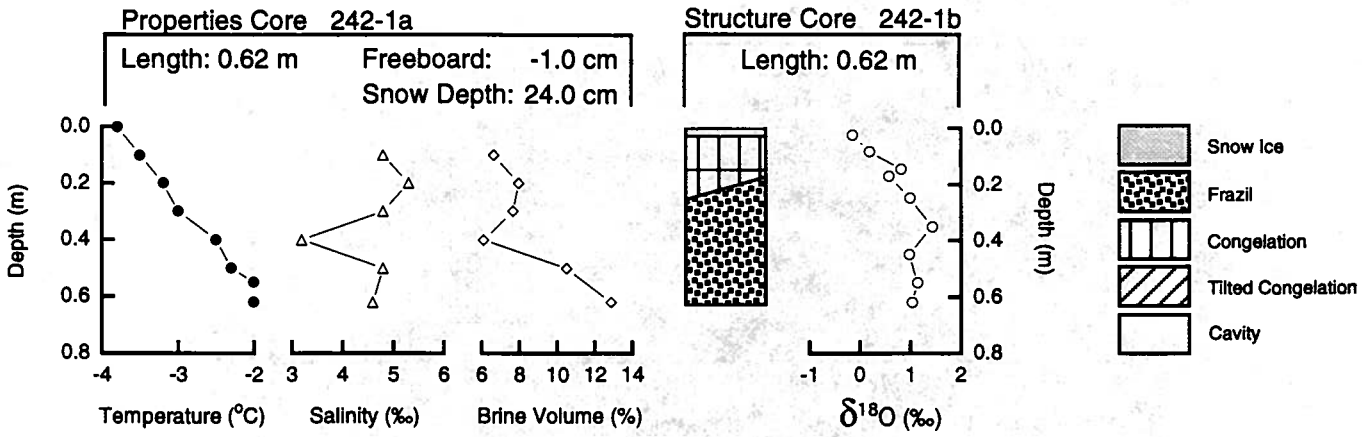

Position: 68° 06.20' S, 91° 41.80' W
Date: 30 August 1993

Mean Ice Thickness: n/a
Mean Snow Thickness: n/a
Mean Freeboard: n/a
Floe Type: n/a

Salinity min: 3.2 ‰
Salinity max: 5.3 ‰
Salinity mean: 4.6 ‰

$\delta^{18}O$ min: -0.14 ‰
$\delta^{18}O$ max: 1.43 ‰
$\delta^{18}O$ mean: 0.78 ‰

Snow Ice: 4.0 %
Frazil Ice: 66.1 %
Congelation: 29.9 %
Cavity: 00.0 %

Snow Fraction
f_s: 1.05 %
F_m: 0.04 %

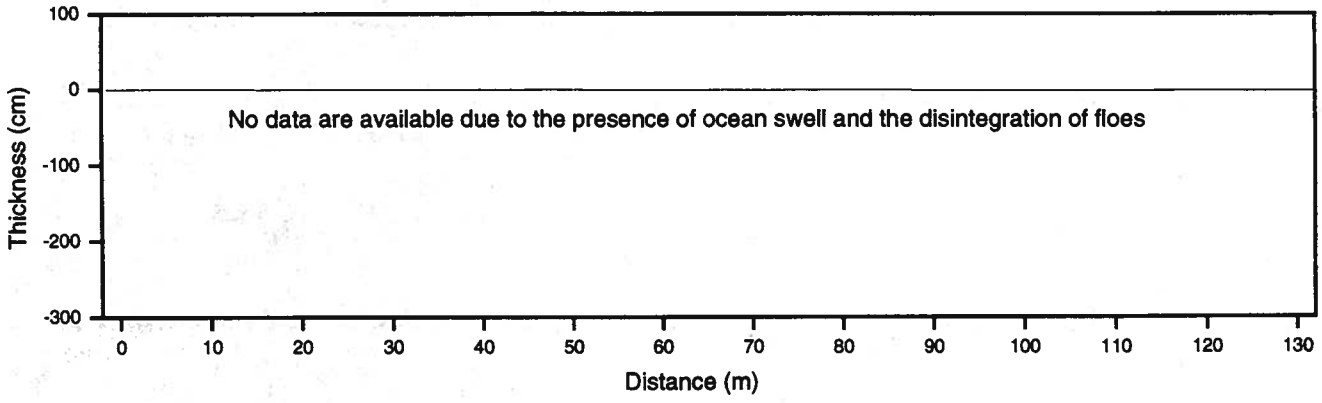

NBP 93-5 FLOE 243

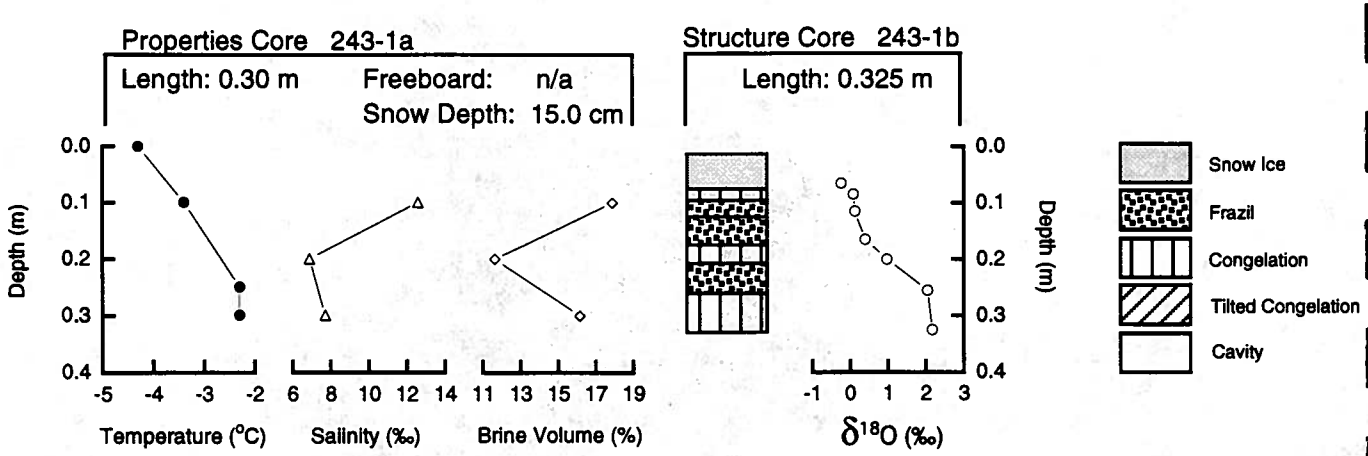

Position: 68° 32.30' S, 92° 29.50' W
Date: 31 August 1993

Mean Ice Thickness: n/a
Mean Snow Thickness: n/a
Mean Freeboard: n/a
Floe Type: n/a

Salinity min: 6.9 ‰
Salinity max: 12.6 ‰
Salinity mean: 9.1 ‰

$\delta^{18}O$ min: -0.24 ‰
$\delta^{18}O$ max: 2.17 ‰
$\delta^{18}O$ mean: 0.80 ‰

Snow Ice: 20.0 %
Frazil Ice: 41.5 %
Congelation: 38.5 %
Cavity: 00.0 %

Snow Fraction
f_s: 1.82 %
F_m: 0.36 %

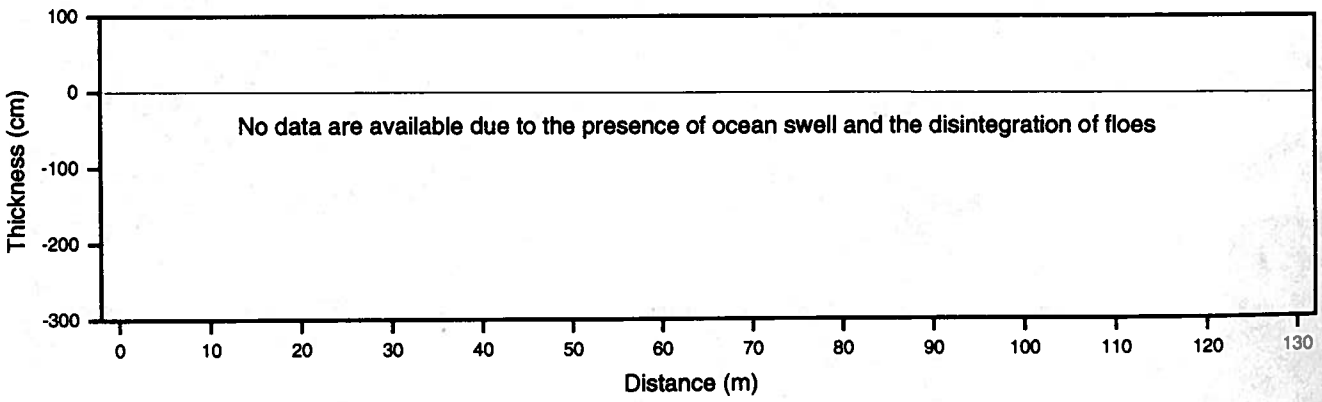

NBP 93-5 FLOE 243

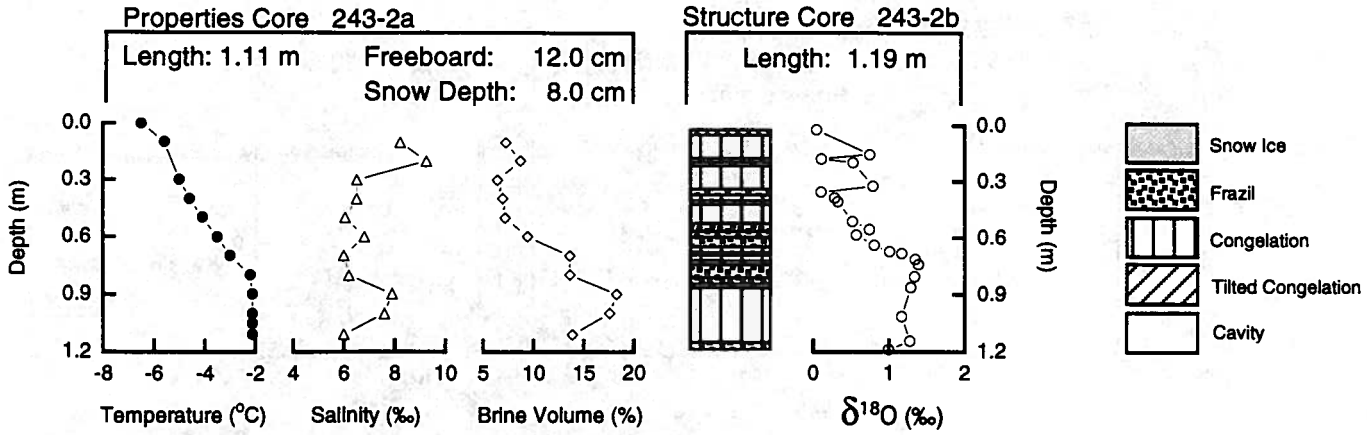

Position: 68° 32.30' S, 92° 29.50' W
Date: 31 August 1993

Mean Ice Thickness: n/a
Mean Snow Thickness: n/a
Mean Freeboard: n/a
Floe Type: n/a

Salinity min: 6.0 ‰
Salinity max: 9.2 ‰
Salinity mean: 7.0 ‰

$\delta^{18}O$ min: 0.04 ‰
$\delta^{18}O$ max: 1.39 ‰
$\delta^{18}O$ mean: 0.79 ‰

Snow Ice: 00.0 %
Frazil Ice: 37.8 %
Congelation: 62.2 %
Cavity: 00.0 %

Snow Fraction
f_s: 0.00 %
F_m: 0.00 %

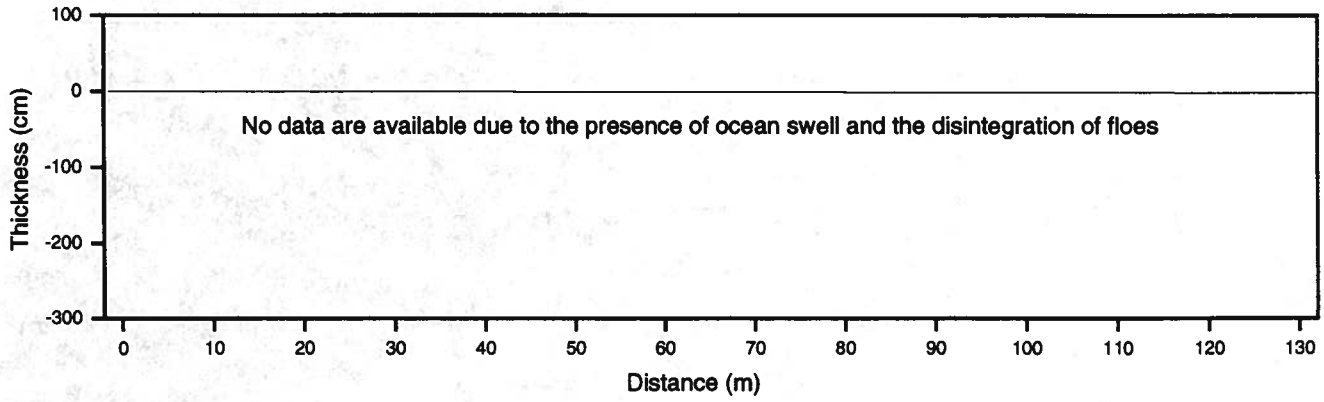

NBP 93-5 FLOE 244

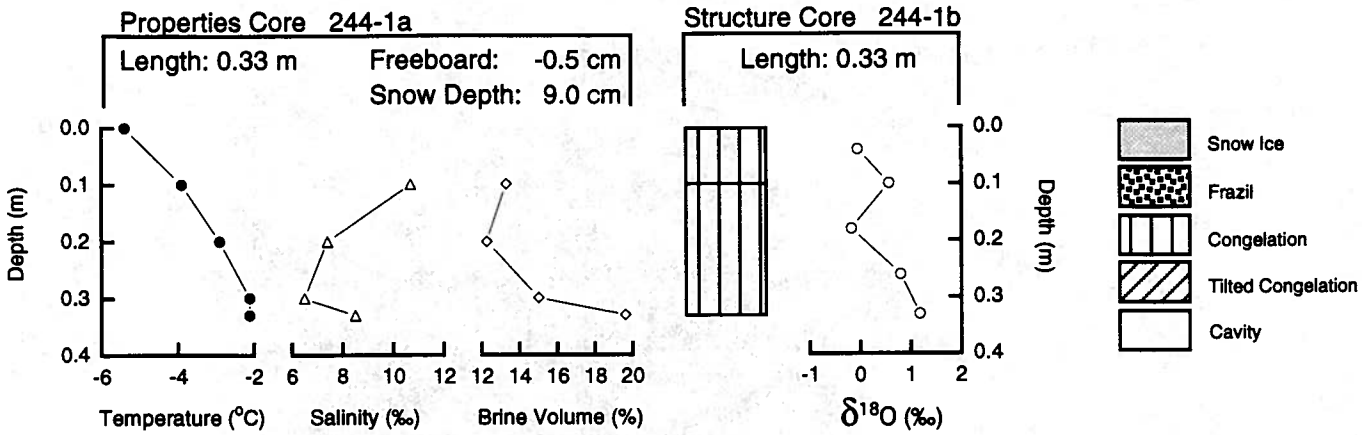

Position: 69° 11.40' S, 94° 10.20' W
Date: 1 September 1993

Mean Ice Thickness: 36.9 ± 3.4 cm
Mean Snow Thickness: 6.6 ± 1.5 cm
Mean Freeboard: 1.2 ± 0.8 cm
Floe Type: A

Salinity min: 6.5 ‰
Salinity max: 10.7 ‰
Salinity mean: 8.3 ‰

$\delta^{18}O$ min: -0.18 ‰
$\delta^{18}O$ max: 1.18 ‰
$\delta^{18}O$ mean: 0.46 ‰

Snow Ice: 00.0 %
Frazil Ice: 00.0 %
Congelation: 100.0 %
Cavity: 00.0 %

Snow Fraction
f_s: 0.00 %
F_m: 0.00 %

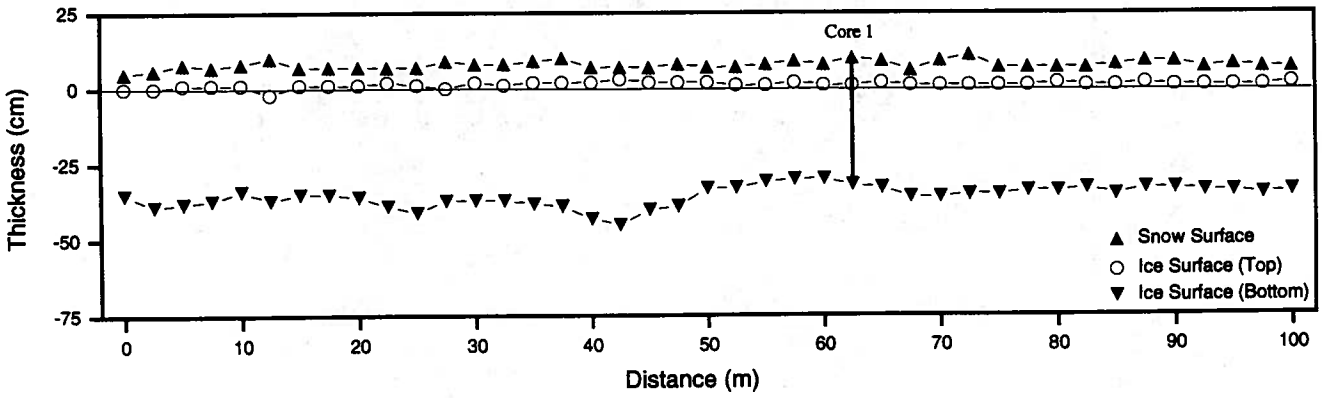

NBP 93-5 FLOE 244

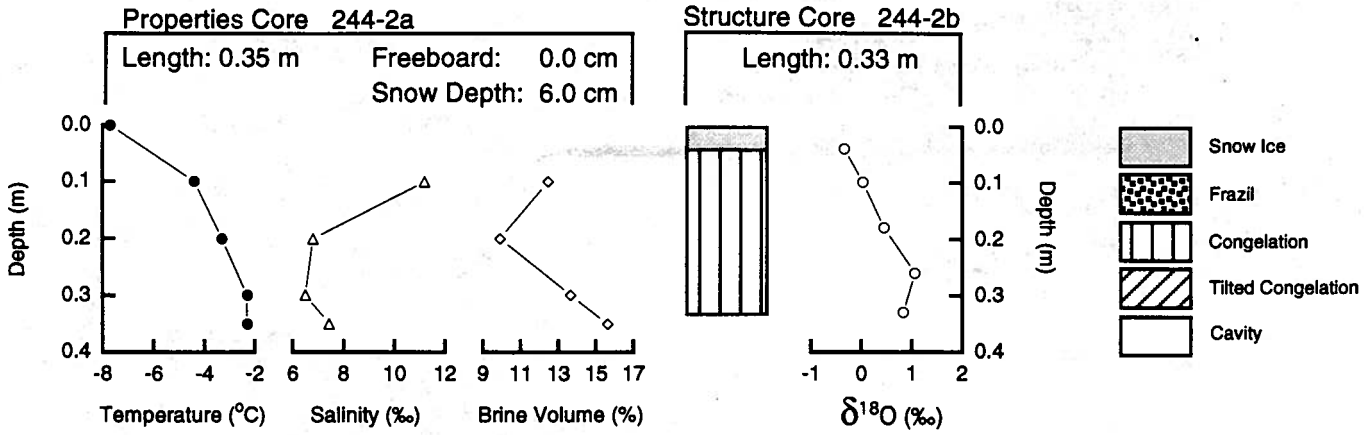

Position: 69° 11.40' S, 94° 10.20' W
Date: 1 September 1993

Mean Ice Thickness: 36.9 ± 3.4 cm
Mean Snow Thickness: 6.6 ± 1.5 cm
Mean Freeboard: 1.2 ± 0.8 cm
Floe Type: A

Salinity min: 6.5 ‰
Salinity max: 11.2 ‰
Salinity mean: 8.0 ‰

$\delta^{18}O$ min: -0.33 ‰
$\delta^{18}O$ max: 1.07 ‰
$\delta^{18}O$ mean: 0.42 ‰

Snow Ice: 12.1 %
Frazil Ice: 00.0 %
Congelation: 87.9 %
Cavity: 00.0 %

Snow Fraction
f_s: 2.50 %
F_m: 0.30 %

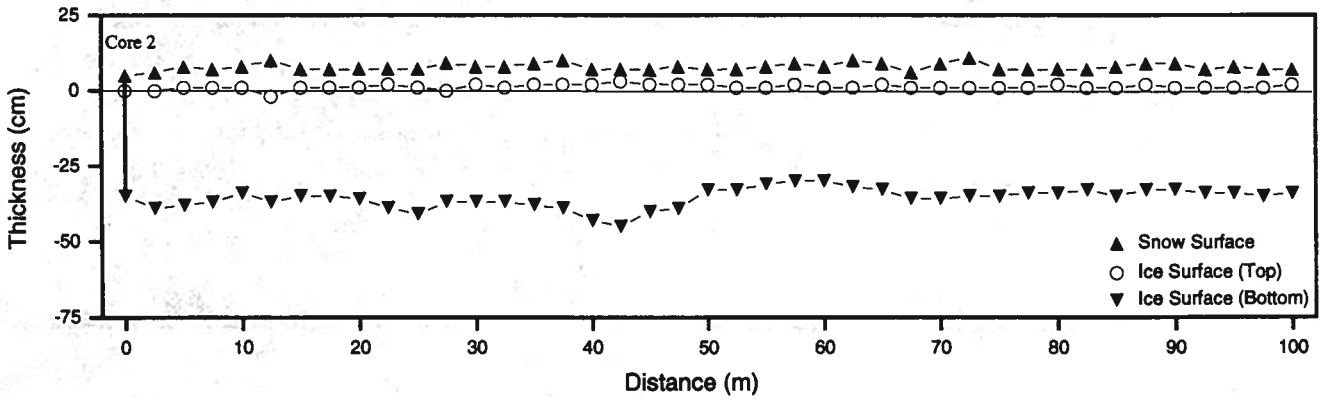

NBP 93-5 FLOE 245

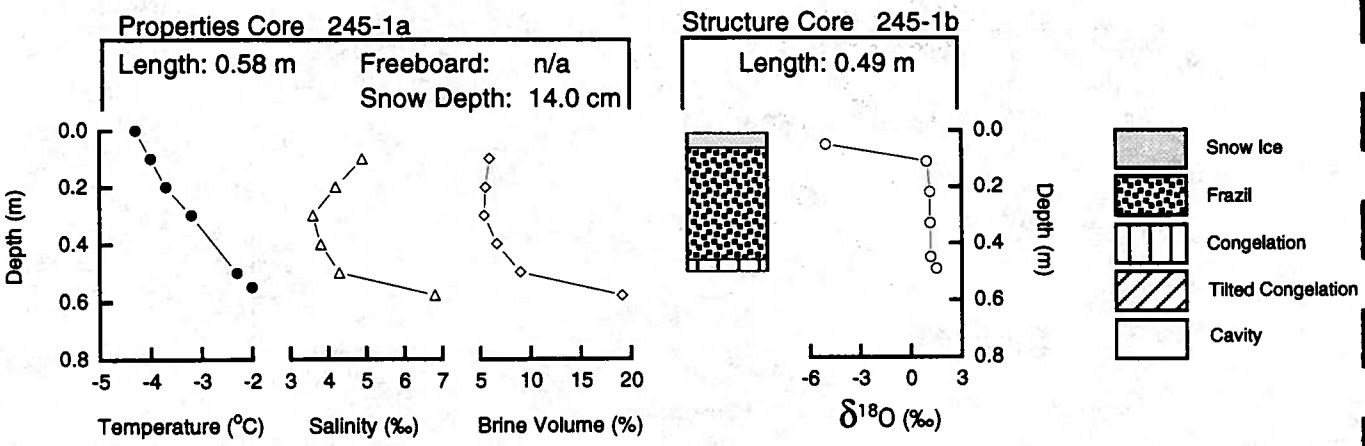

Position: 69° 03.74' S, 96° 07.35' W
Date: 2 September 1993

Mean Ice Thickness: n/a
Mean Snow Thickness: n/a
Mean Freeboard: n/a
Floe Type: n/a

Salinity min: 3.6 ‰
Salinity max: 6.8 ‰
Salinity mean: 4.6 ‰

$\delta^{18}O$ min: -5.08 ‰
$\delta^{18}O$ max: 1.52 ‰
$\delta^{18}O$ mean: 0.13 ‰

Snow Ice: 10.2 %
Frazil Ice: 81.6 %
Congelation: 8.2 %
Cavity: 00.0 %

Snow Fraction
f_s: 38.48 %
F_m: 3.93 %

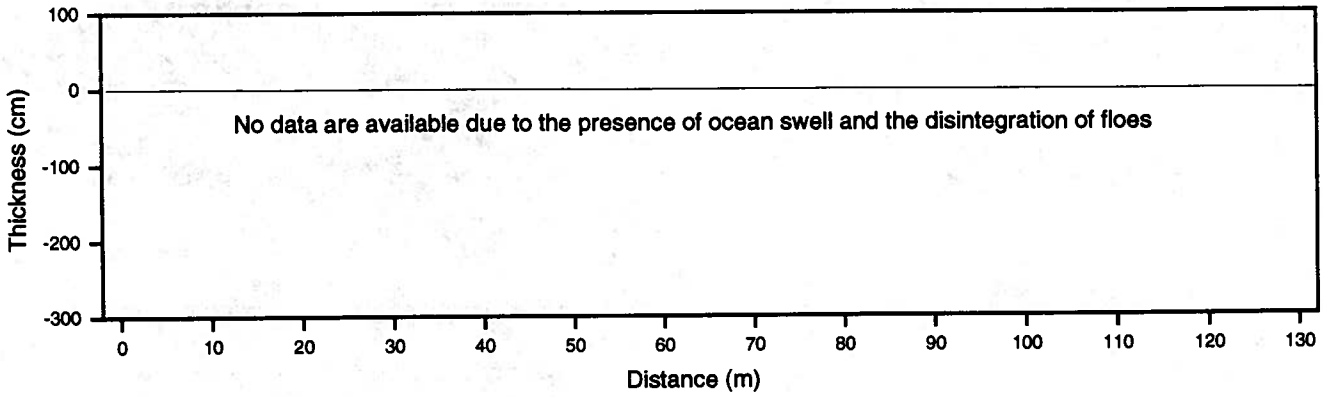

NBP 93-5 FLOE 245

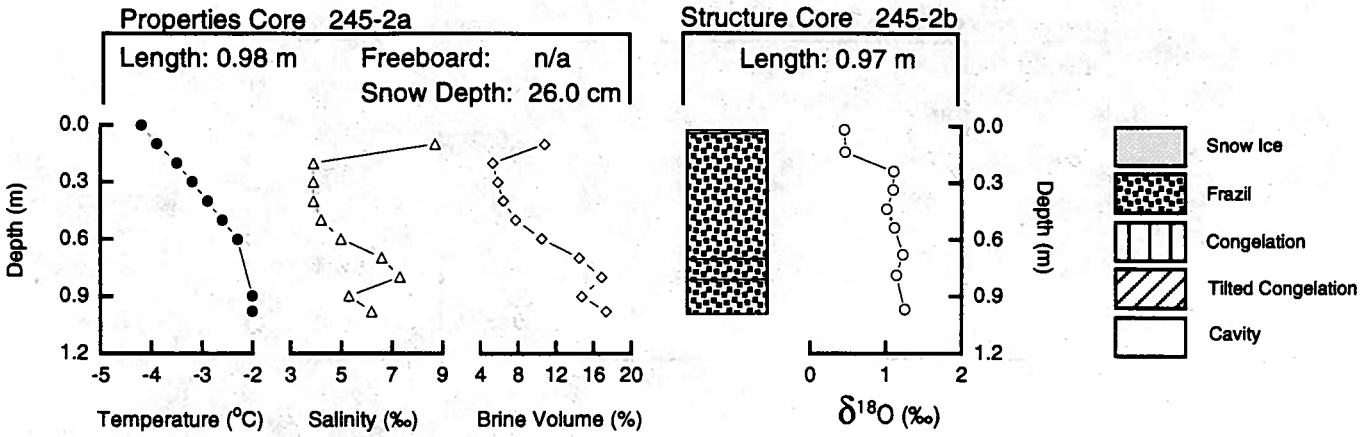

Position: 69° 02.50' S, 96° 11.80' W
Date: 2 September 1993

Mean Ice Thickness: n/a
Mean Snow Thickness: n/a
Mean Freeboard: n/a
Floe Type: n/a

Salinity min: 3.9 ‰
Salinity max: 8.7 ‰
Salinity mean: 5.5 ‰

$\delta^{18}O$ min: 0.46 ‰
$\delta^{18}O$ max: 1.25 ‰
$\delta^{18}O$ mean: 0.99 ‰

Snow Ice: 00.0 %
Frazil Ice: 100.0 %
Congelation: 00.0 %
Cavity: 00.0 %

Snow Fraction
f_s: 0.00 %
F_m: 0.00 %

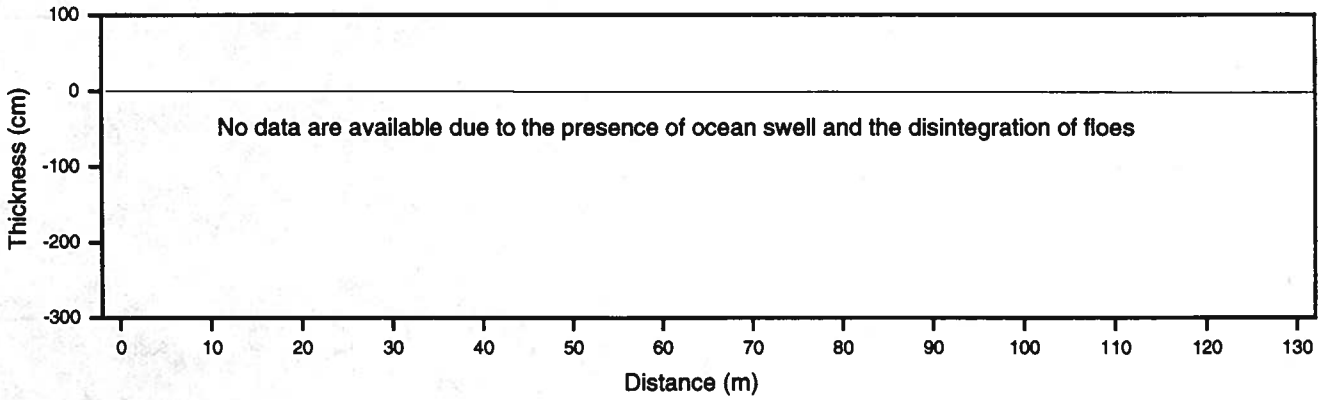

NBP 93-5 FLOE 245

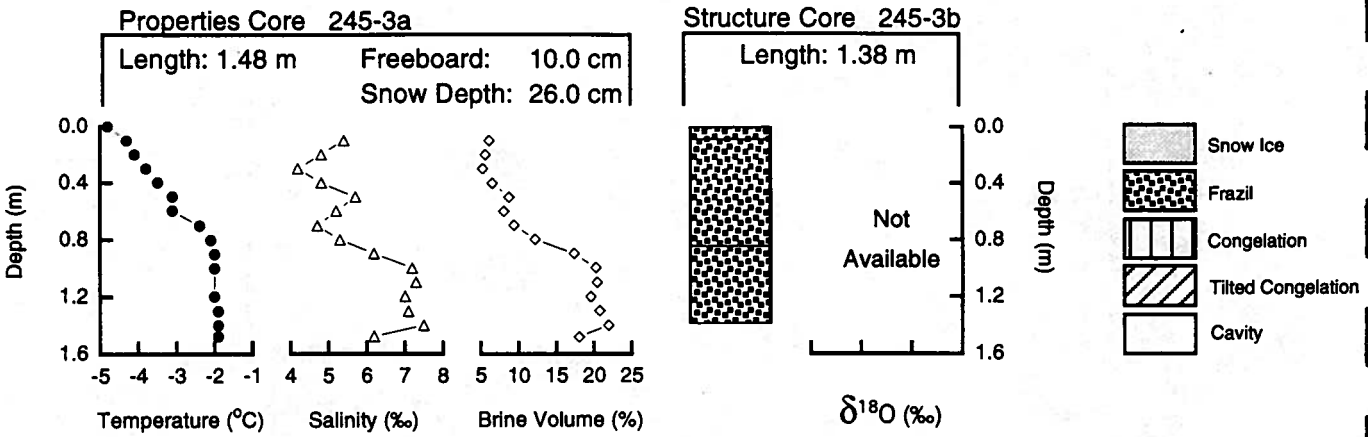

Position: 69° 01.40' S, 96° 14.90' W
Date: 2 September 1993

Salinity min: 4.2 ‰
Salinity max: 7.5 ‰
Salinity mean: 5.9 ‰

Snow Ice: 00.0 %
Frazil Ice: 100.0 %
Congelation: 00.0 %
Cavity: 00.0 %

Mean Ice Thickness: n/a
Mean Snow Thickness: n/a
Mean Freeboard: n/a
Floe Type: n/a

$\delta^{18}O$ min: n/a
$\delta^{18}O$ max: n/a
$\delta^{18}O$ mean: n/a

Snow Fraction
f_s: 0.00 %
F_m: 0.00 %

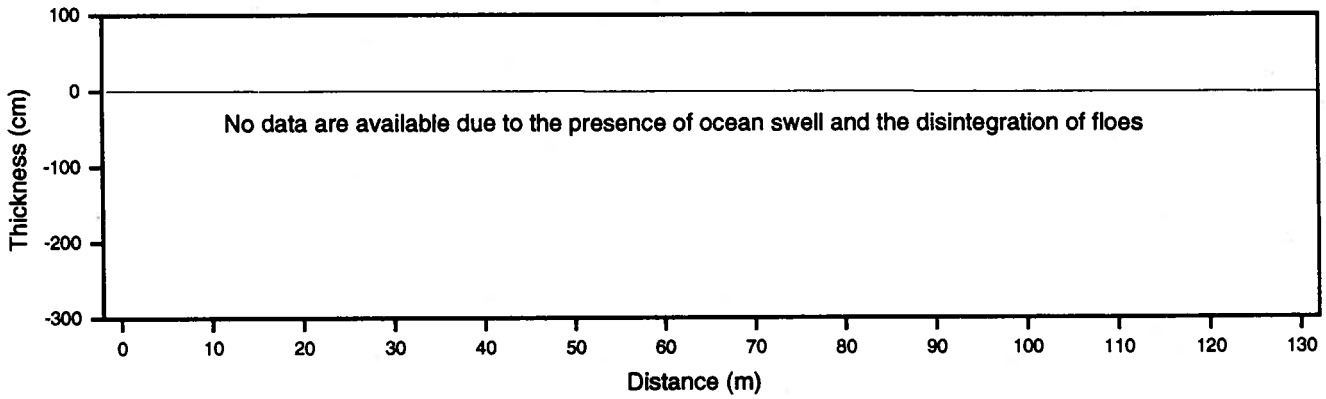

NBP 93-5 FLOE 245

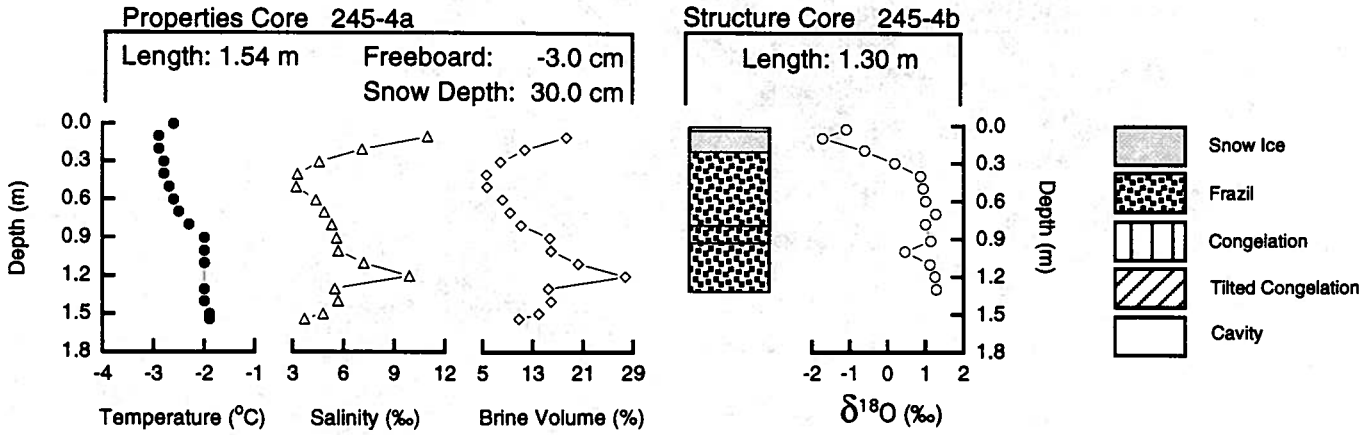

Position: 69° 00.20' S, 96° 20.10' W
Date: 2 September 1993

Mean Ice Thickness: n/a
Mean Snow Thickness: n/a
Mean Freeboard: n/a
Floe Type: n/a

Salinity min: 3.2 ‰
Salinity max: 11.0 ‰
Salinity mean: 5.7 ‰

$\delta^{18}O$ min: -1.73 ‰
$\delta^{18}O$ max: 1.28 ‰
$\delta^{18}O$ mean: 0.50 ‰

Snow Ice: 15.4 %
Frazil Ice: 84.6 %
Congelation: 00.0 %
Cavity: 00.0 %

Snow Fraction
f_s: 8.19 %
F_m: 1.26 %

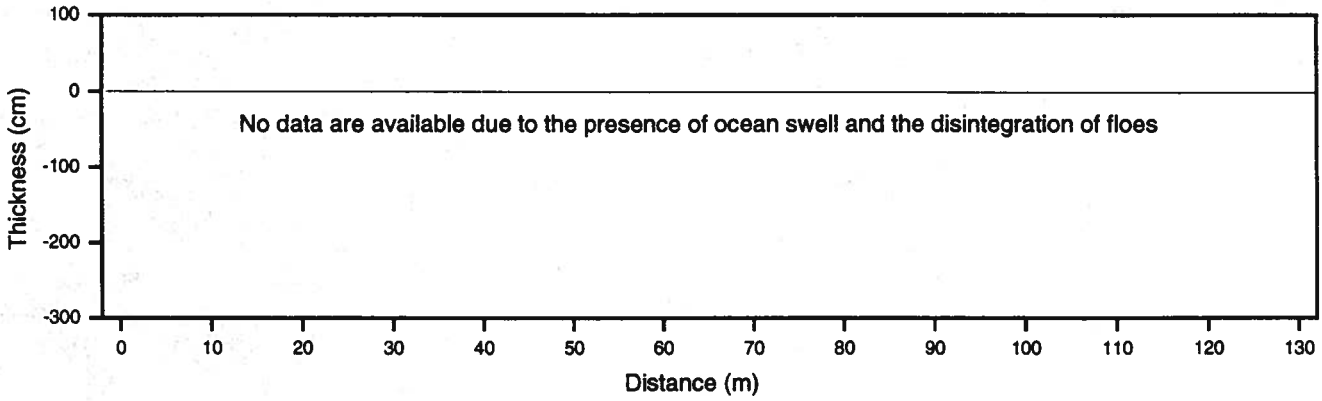

NBP 93-5 FLOE 245

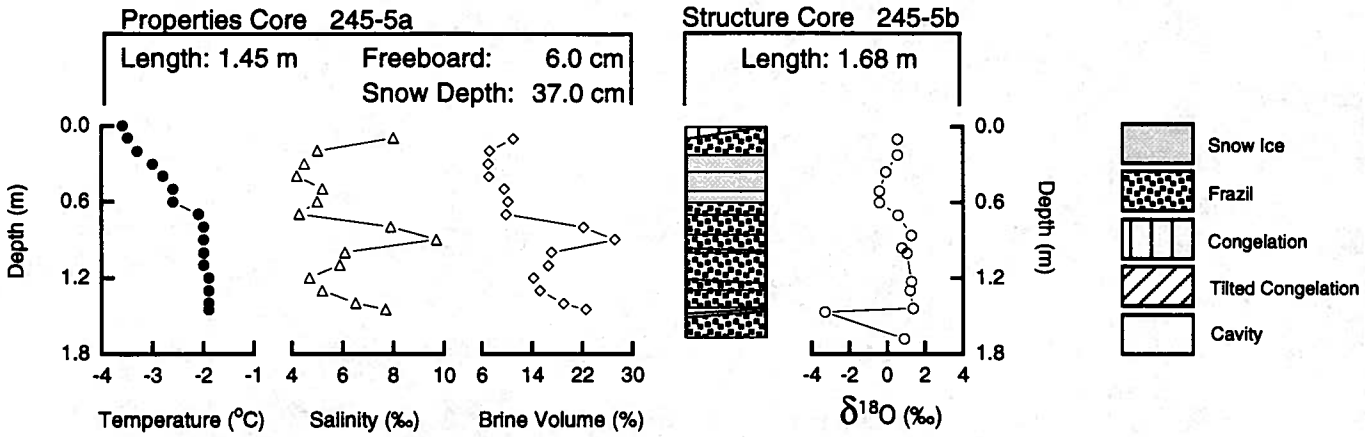

Position: 68° 59.30' S, 96° 24.20' W
Date: 2 September 1993

Mean Ice Thickness: n/a
Mean Snow Thickness: n/a
Mean Freeboard: n/a
Floe Type: n/a

Salinity min: 4.2 ‰
Salinity max: 9.7 ‰
Salinity mean: 6.0 ‰

$\delta^{18}O$ min: -3.30 ‰
$\delta^{18}O$ max: 1.39 ‰
$\delta^{18}O$ mean: 0.38 ‰

Snow Ice: 24.4 %
Frazil Ice: 71.1 %
Congelation: 3.0 %
Cavity: 1.5 %

Snow Fraction
f_s: 3.81 %
F_m: 0.93 %

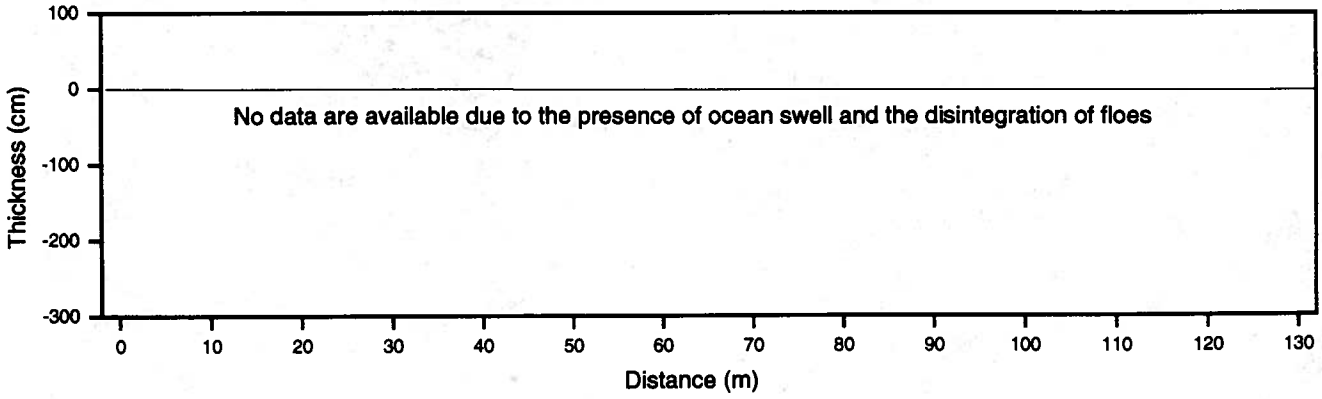

NBP 93-5 FLOE 246

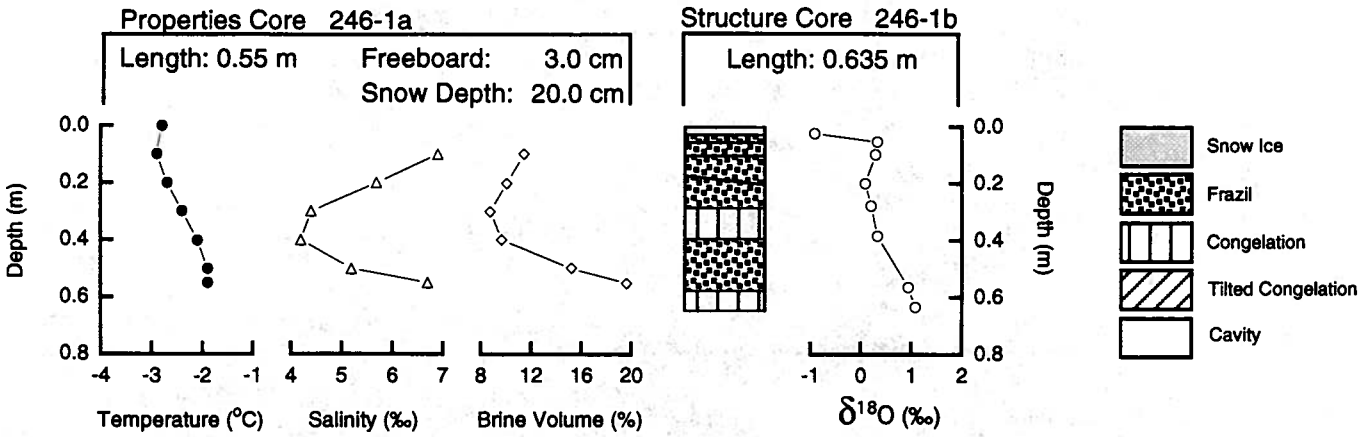

Position: 69° 25.66' S, 96° 13.90' W
Date: 3 September 1993

Mean Ice Thickness: n/a
Mean Snow Thickness: n/a
Mean Freeboard: n/a
Floe Type: n/a

Salinity min: 4.2 ‰
Salinity max: 6.9 ‰
Salinity mean: 5.5 ‰

$\delta^{18}O$ min: -0.91 ‰
$\delta^{18}O$ max: 1.08 ‰
$\delta^{18}O$ mean: 0.30 ‰

Snow Ice: 3.9 %
Frazil Ice: 68.5 %
Congelation: 27.6 %
Cavity: 00.0 %

Snow Fraction
f_s: 6.89 %
F_m: 0.27 %

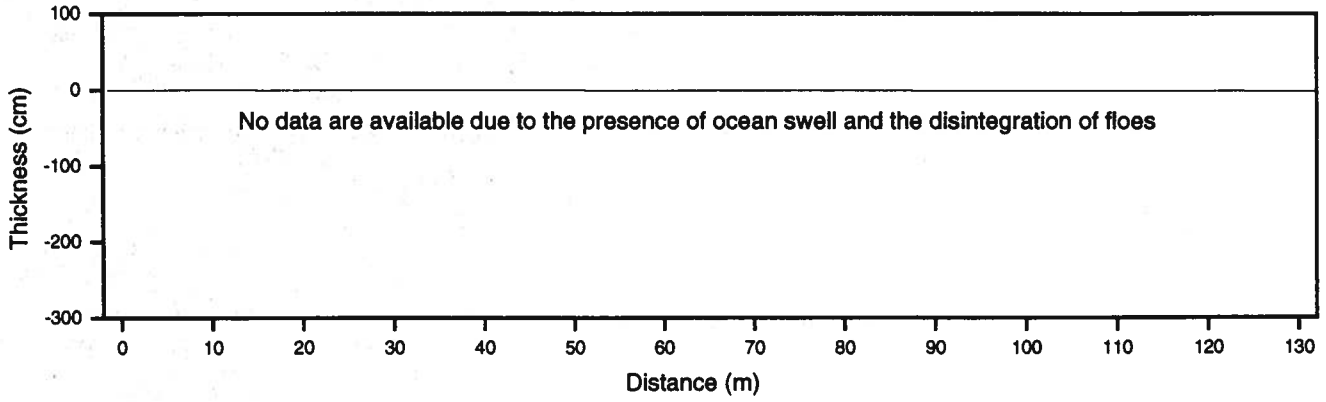

NBP 93-5 FLOE 246

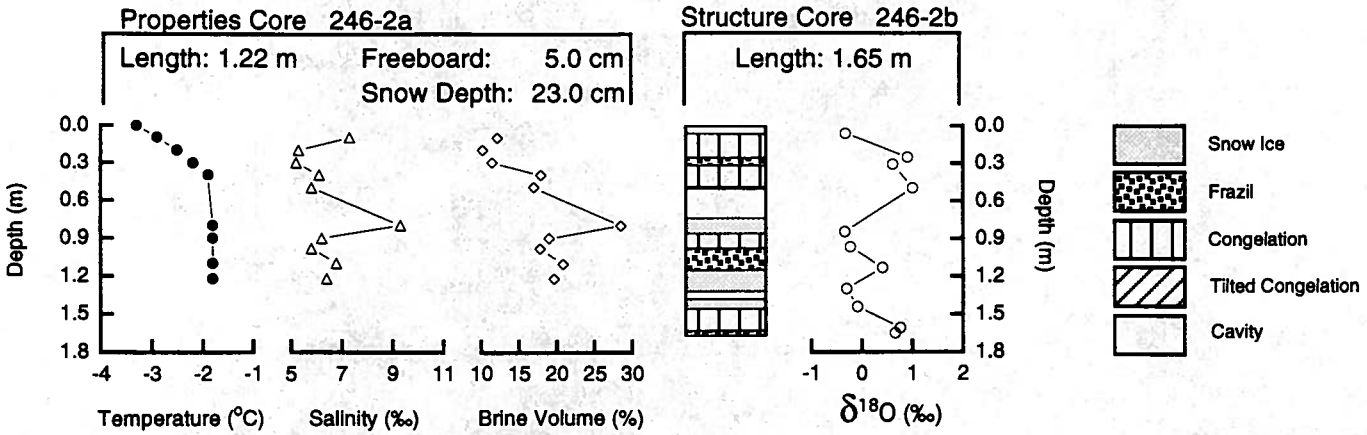

Position: 69° 26.80' S, 96° 07.27' W
Date: 3 September 1993

Mean Ice Thickness: n/a
Mean Snow Thickness: n/a
Mean Freeboard: n/a
Floe Type: n/a

Salinity min: 5.2 ‰
Salinity max: 9.3 ‰
Salinity mean: 6.4 ‰

$\delta^{18}O$ min: -0.34 ‰
$\delta^{18}O$ max: 1.01 ‰
$\delta^{18}O$ mean: 0.28 ‰

Snow Ice: 25.8 %
Frazil Ice: 15.7 %
Congelation: 40.9 %
Cavity: 17.6 %

Snow Fraction
f_s: 2.08 %
F_m: 0.54 %

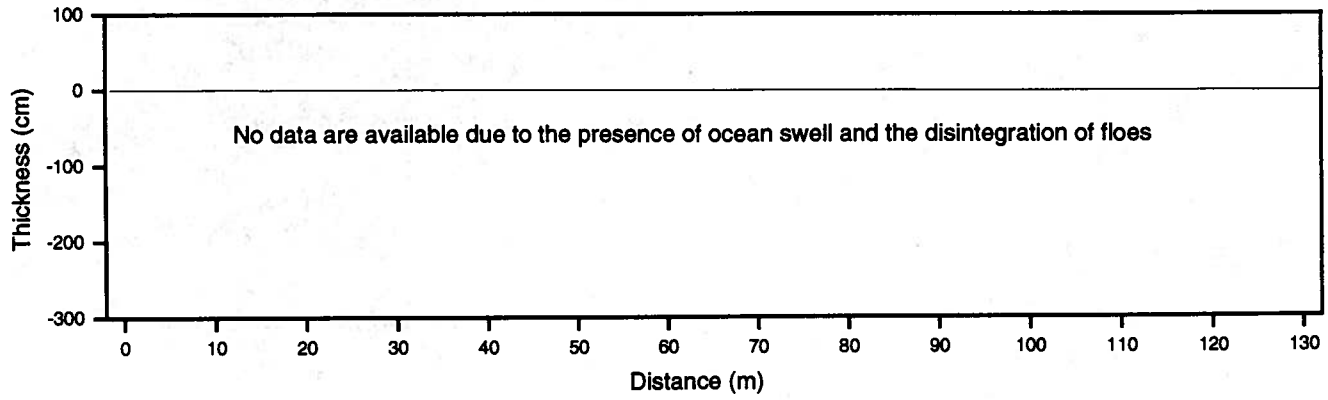

NBP 93-5 FLOE 246

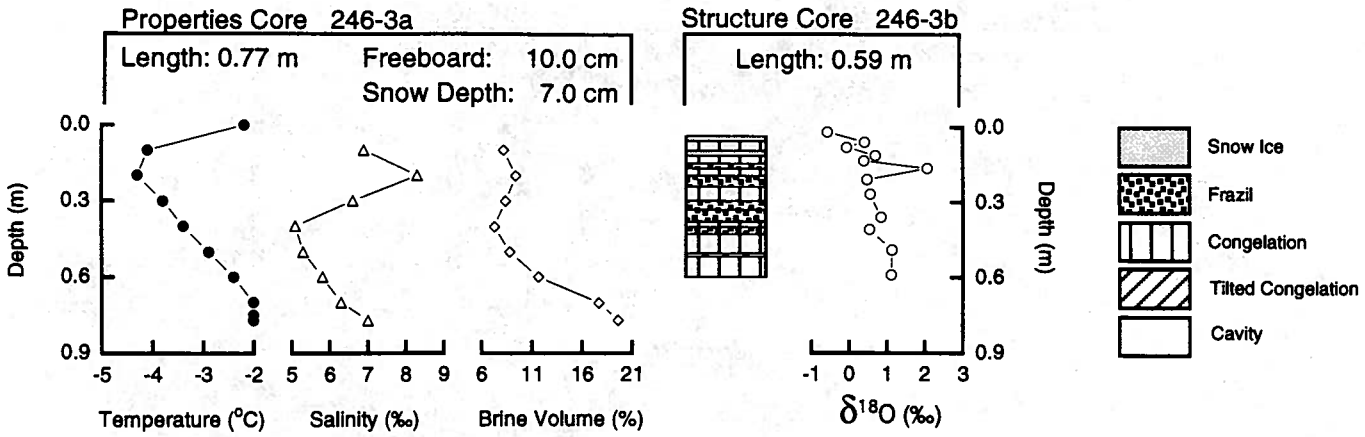

Position: 69° 25.58' S, 96° 03.75' W
Date: 3 September 1993

Mean Ice Thickness: n/a
Mean Snow Thickness: n/a
Mean Freeboard: n/a
Floe Type: n/a

Salinity min: 5.1 ‰
Salinity max: 8.3 ‰
Salinity mean: 6.4 ‰

$\delta^{18}O$ min: -0.58 ‰
$\delta^{18}O$ max: 2.06 ‰
$\delta^{18}O$ mean: 0.63 ‰

Snow Ice: 6.8 %
Frazil Ice: 33.9 %
Congelation: 59.3 %
Cavity: 00.0 %

Snow Fraction
f_s: 2.42 %
F_m: 0.16 %

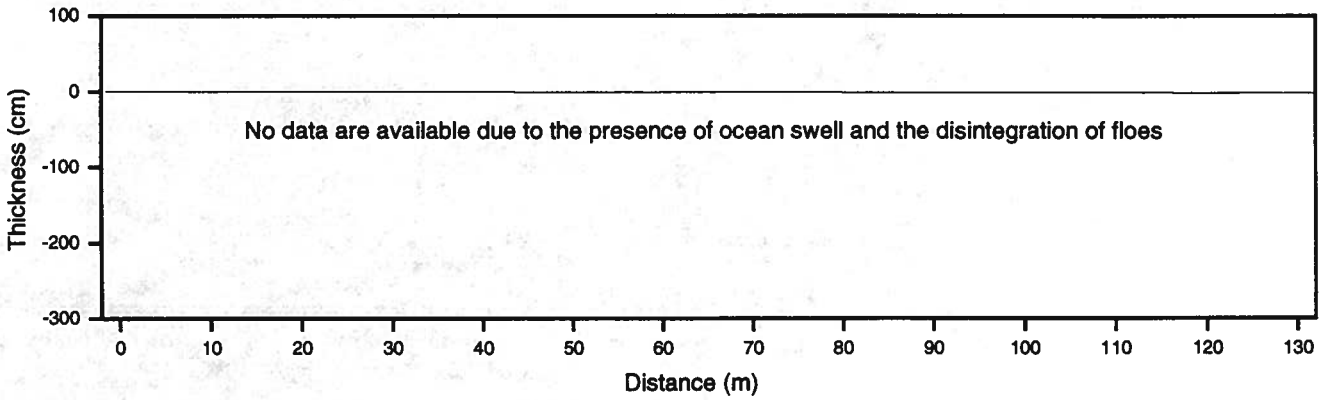

NBP 93-5 FLOE 247

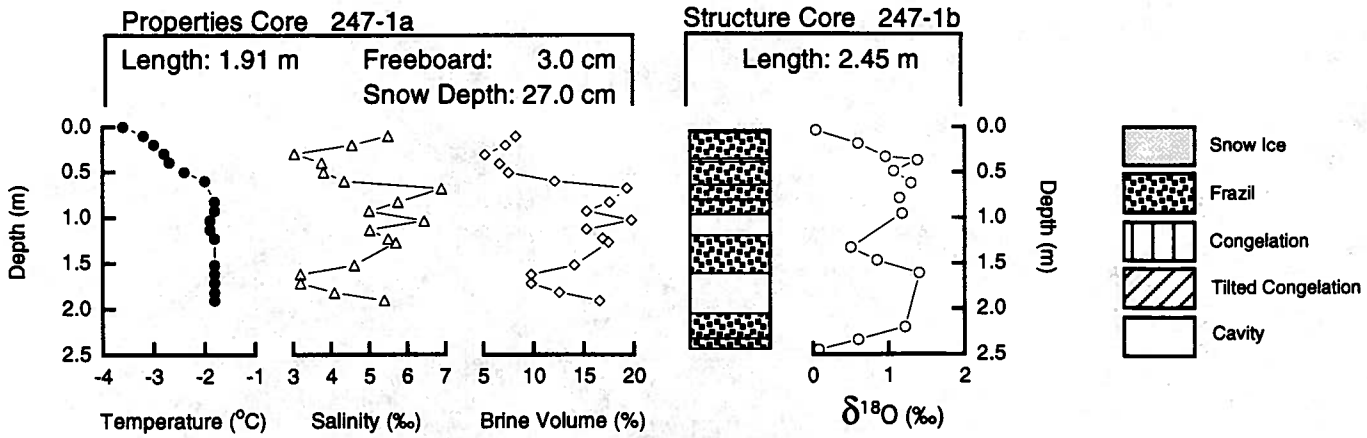

Position: 69° 31.50' S, 96° 18.56' W
Date: 4 September 1993

Mean Ice Thickness: n/a
Mean Snow Thickness: n/a
Mean Freeboard: n/a
Floe Type: n/a

Salinity min: 3.0 ‰
Salinity max: 6.9 ‰
Salinity mean: 4.8 ‰

$\delta^{18}O$ min: 0.04 ‰
$\delta^{18}O$ max: 1.41 ‰
$\delta^{18}O$ mean: 0.88 ‰

Snow Ice: 00.0 %
Frazil Ice: 70.4 %
Congelation: 1.4 %
Cavity: 28.2 %

Snow Fraction
f_s: 0.00 %
F_m: 0.00 %

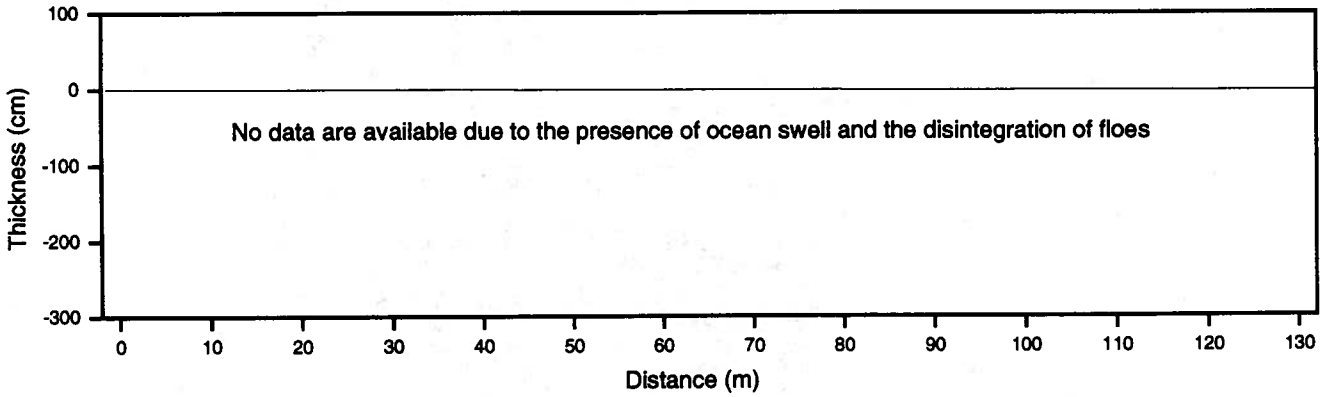

NBP 93-5 FLOE 247

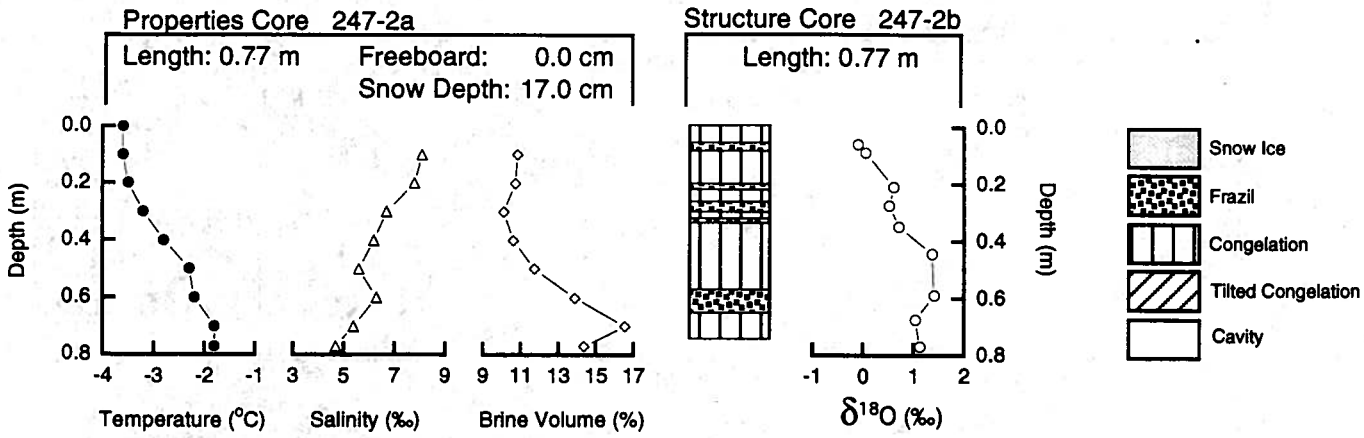

Position: 69° 36.29' S, 96° 21.37' W
Date: 4 September 1993

Mean Ice Thickness: n/a
Mean Snow Thickness: n/a
Mean Freeboard: n/a
Floe Type: n/a

Salinity min: 4.7 ‰
Salinity max: 8.1 ‰
Salinity mean: 6.3 ‰

$\delta^{18}O$ min: -0.10 ‰
$\delta^{18}O$ max: 1.41 ‰
$\delta^{18}O$ mean: 0.75 ‰

Snow Ice: 00.0 %
Frazil Ice: 24.0 %
Congelation: 76.0 %
Cavity: 00.0 %

Snow Fraction
f_s: 0.00 %
F_m: 0.00 %

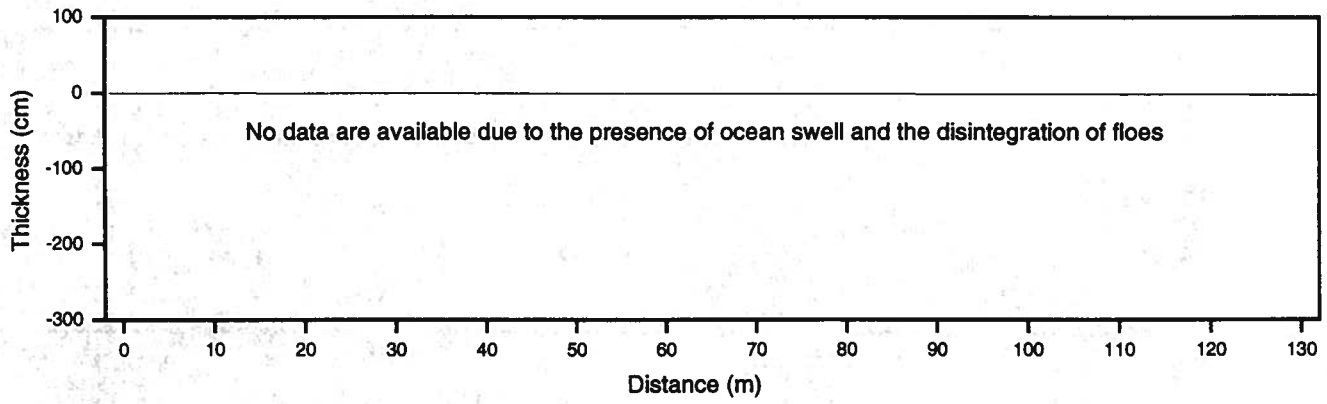

NBP 93-5 FLOE 247

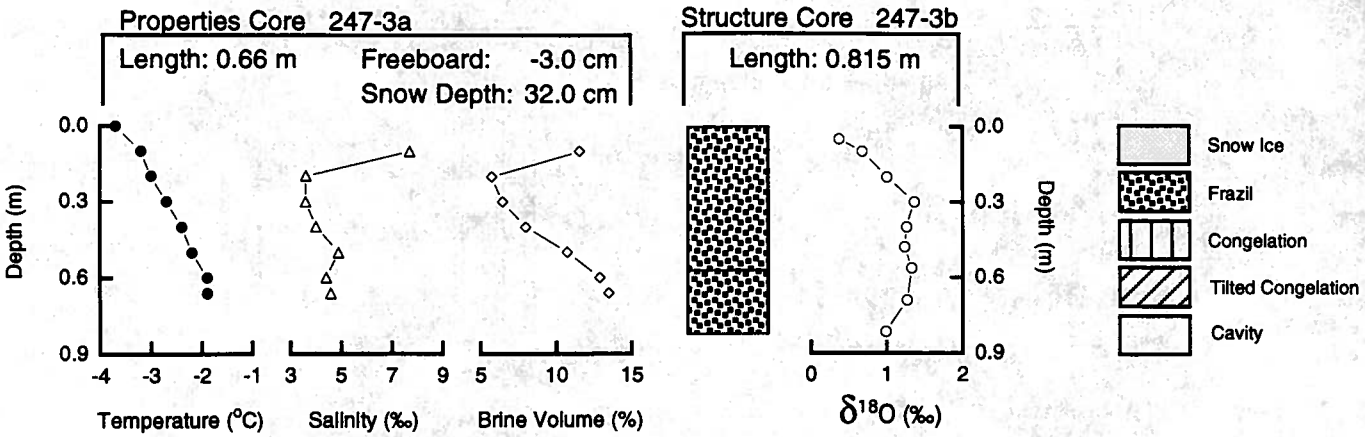

Position: 69° 40.71' S, 96° 20.85' W
Date: 4 September 1993

Mean Ice Thickness: n/a
Mean Snow Thickness: n/a
Mean Freeboard: n/a
Floe Type: n/a

Salinity min: 3.6 ‰
Salinity max: 7.7 ‰
Salinity mean: 4.7 ‰

$\delta^{18}O$ min: 0.37 ‰
$\delta^{18}O$ max: 1.36 ‰
$\delta^{18}O$ mean: 1.06 ‰

Snow Ice: 00.0 %
Frazil Ice: 100.0 %
Congelation: 00.0 %
Cavity: 00.0 %

Snow Fraction
f_s: 0.00 %
F_m: 0.00 %

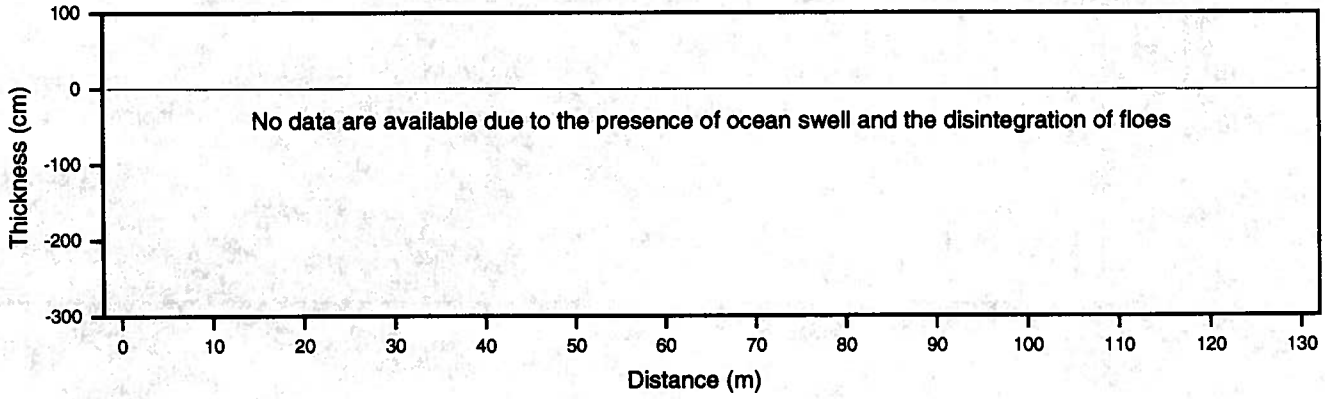

NBP 93-5 FLOE 248

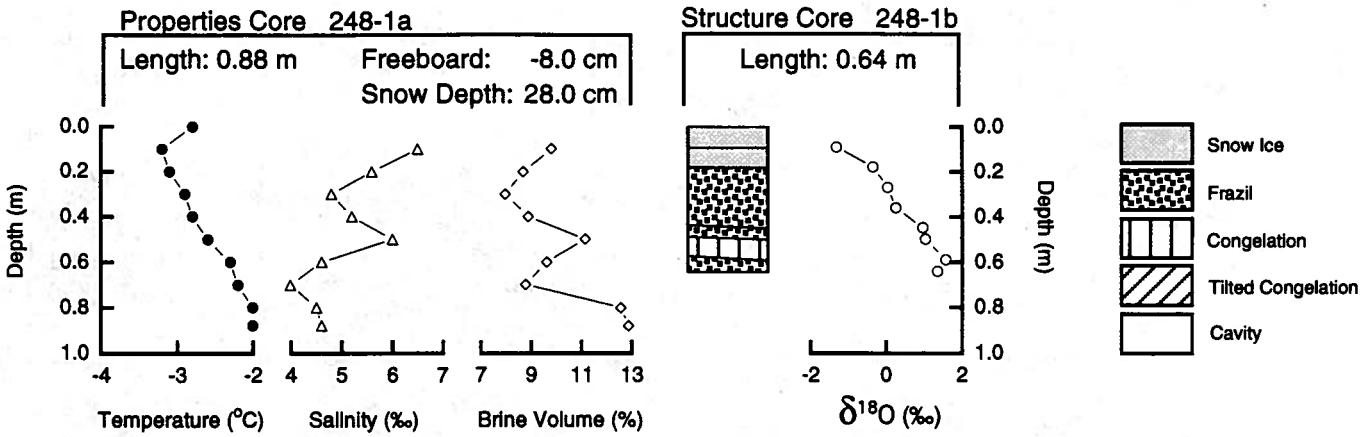

Position: 69° 54.53' S, 96° 22.67' W
Date: 5 September 1993

Mean Ice Thickness: n/a
Mean Snow Thickness: n/a
Mean Freeboard: n/a
Floe Type: n/a

Salinity min: 3.6 ‰
Salinity max: 7.7 ‰
Salinity mean: 4.7 ‰

$\delta^{18}O$ min: 0.37 ‰
$\delta^{18}O$ max: 1.36 ‰
$\delta^{18}O$ mean: 1.06 ‰

Snow Ice: 28.1 %
Frazil Ice: 57.8 %
Congelation: 14.1 %
Cavity: 00.0 %

Snow Fraction
f_s: 6.33 %
F_m: 1.78 %

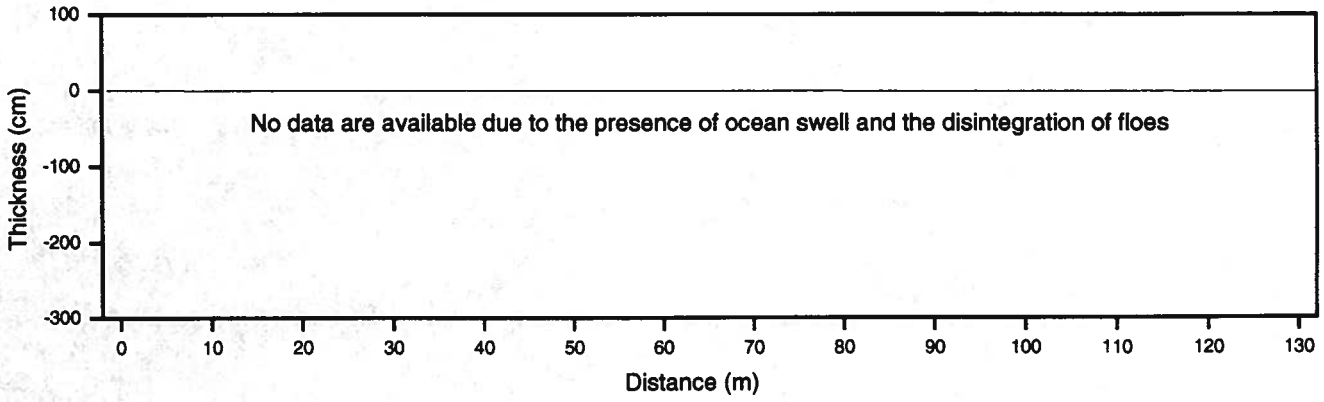

NBP 93-5 FLOE 248

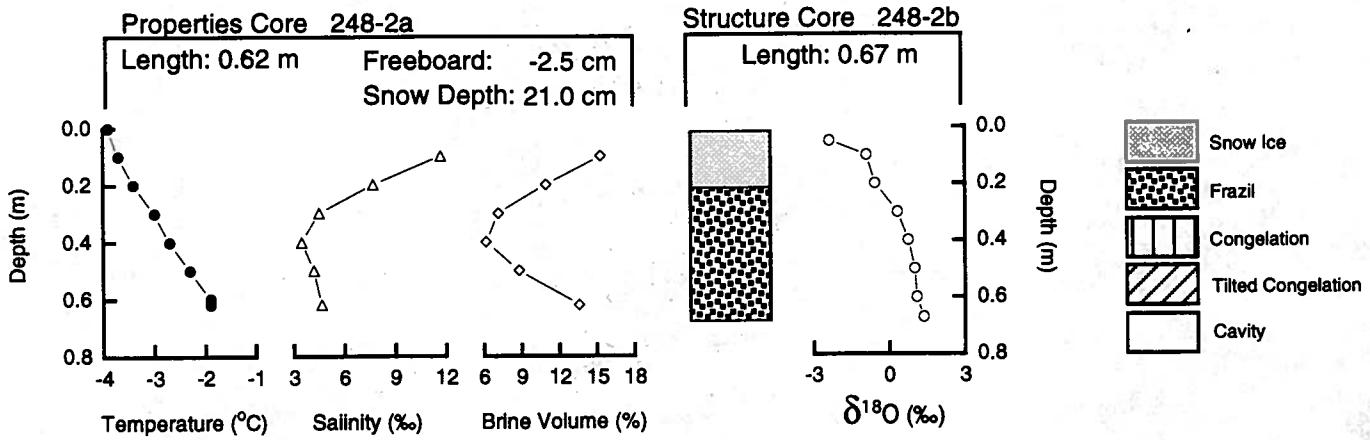

Position: 69° 57.03' S, 96° 11.61' W
Date: 5 September 1993

Mean Ice Thickness: n/a
Mean Snow Thickness: n/a
Mean Freeboard: n/a
Floe Type: n/a

Salinity min: 3.5 ‰
Salinity max: 11.7 ‰
Salinity mean: 6.0 ‰

$\delta^{18}O$ min: -2.35 ‰
$\delta^{18}O$ max: 1.37 ‰
$\delta^{18}O$ mean: 0.10 ‰

Snow Ice: 29.9 %
Frazil Ice: 70.1 %
Congelation: 00.0 %
Cavity: 00.0 %

Snow Fraction
f_s: 8.24 %
F_m: 2.46 %

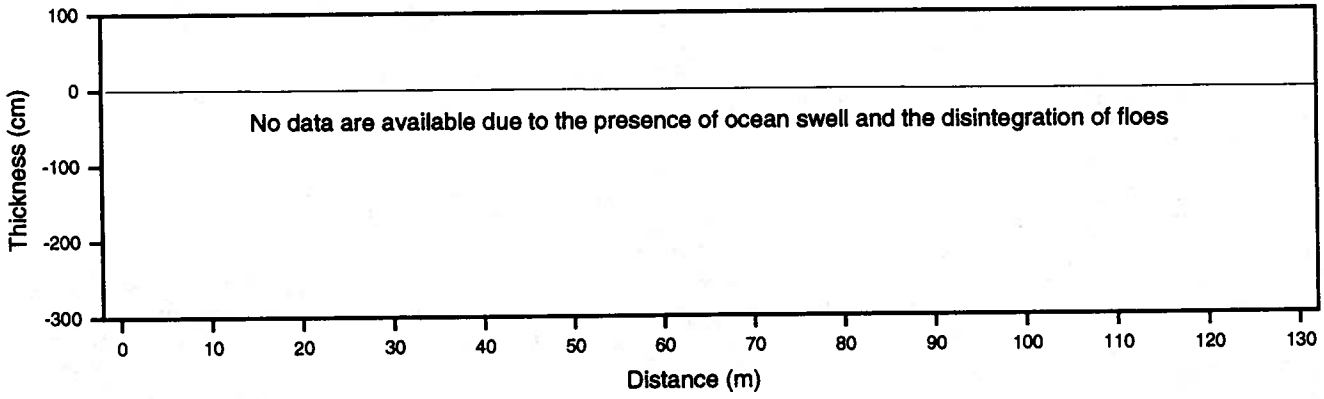

NBP 93-5 FLOE 248

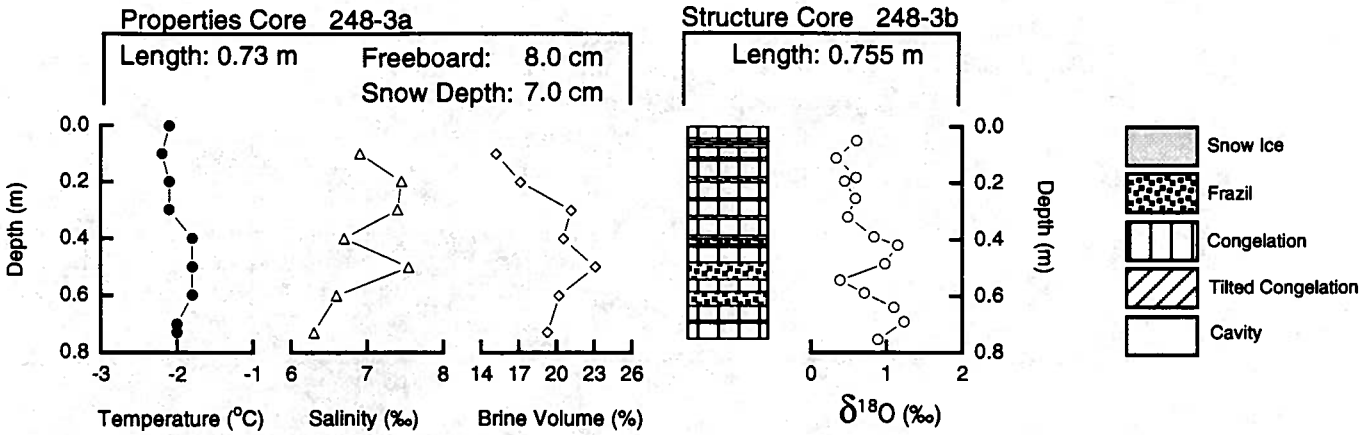

Position: 70° 00.41' S, 95° 58.99' W
Date: 5 September 1993

Mean Ice Thickness: n/a
Mean Snow Thickness: n/a
Mean Freeboard: n/a
Floe Type: n/a

Salinity min: 6.3 ‰
Salinity max: 7.5 ‰
Salinity mean: 7.0 ‰

$\delta^{18}O$ min: 0.34 ‰
$\delta^{18}O$ max: 1.24 ‰
$\delta^{18}O$ mean: 0.74 ‰

Snow Ice: 00.0 %
Frazil Ice: 31.1 %
Congelation: 68.9 %
Cavity: 00.0 %

Snow Fraction
f_s: 0.00 %
F_m: 0.00 %

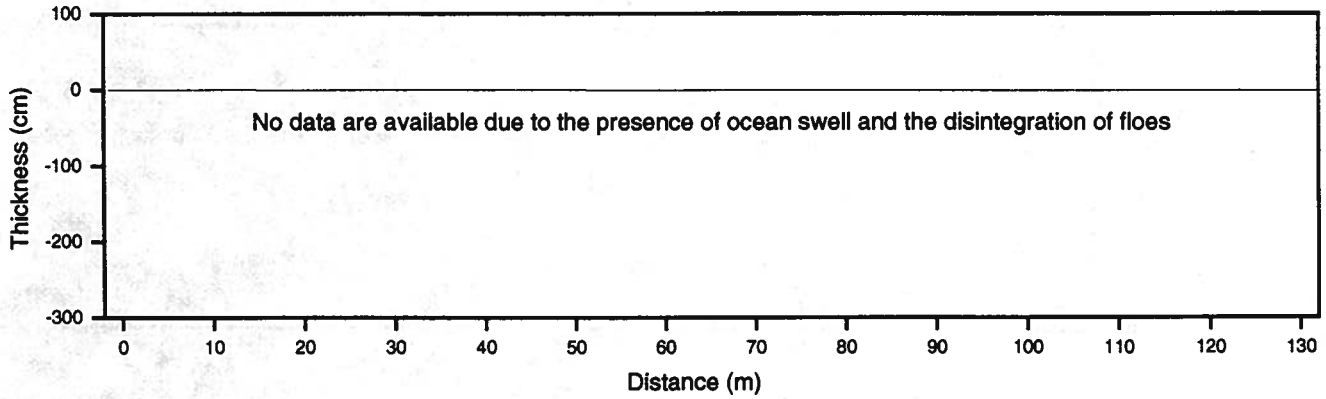

NBP 93-5 FLOE 248

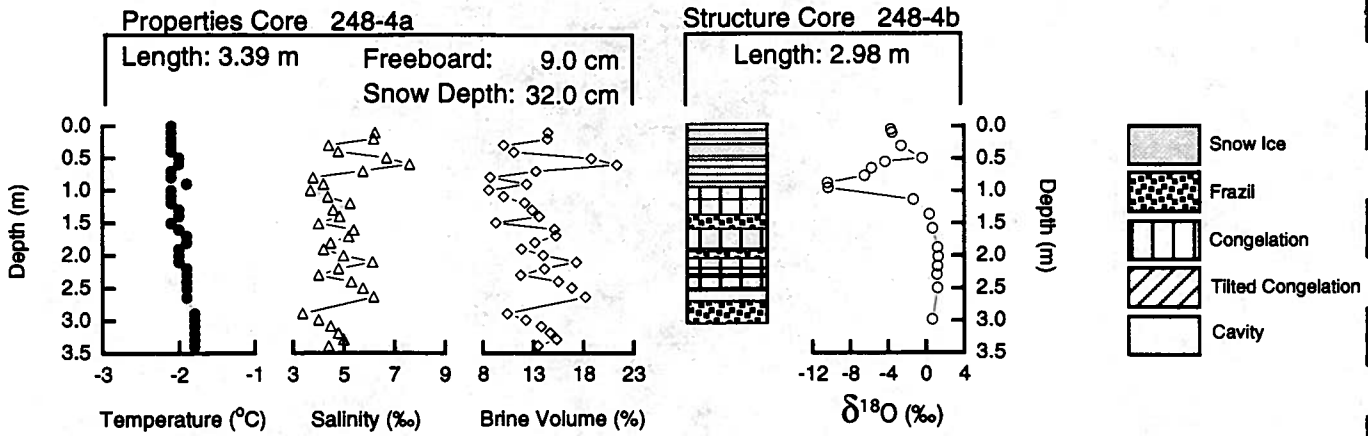

Position: 70° 03.20' S, 95° 48.32' W
Date: 5 September 1993

Mean Ice Thickness: n/a
Mean Snow Thickness: n/a
Mean Freeboard: n/a
Floe Type: n/a

Salinity min: 3.4 ‰
Salinity max: 7.6 ‰
Salinity mean: 5.0 ‰

$\delta^{18}O$ min: -10.41 ‰
$\delta^{18}O$ max: 1.30 ‰
$\delta^{18}O$ mean: -2.30 ‰

Snow Ice: 32.2 %
Frazil Ice: 26.2 %
Congelation: 36.6 %
Cavity: 5.0 %

Snow Fraction
f_s: 36.12 %
F_m: 11.64 %

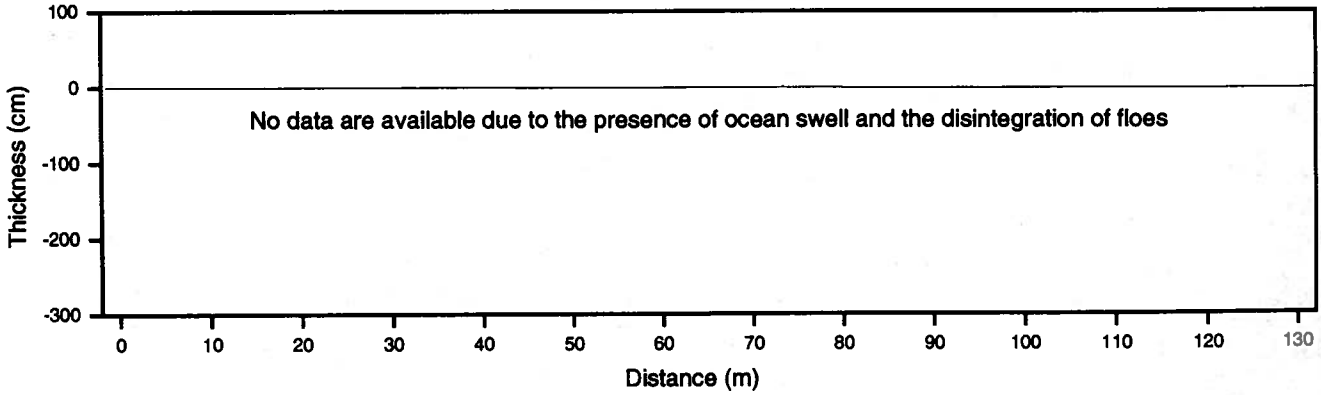

Ice floe 248–4

Ice core 248–4b was the only core to include $\delta^{18}O$ values lower than –6.6‰, the lowest value observed in the first–year cores. Core 248–4b had a single 0.2m thick layer with a mean $\delta^{18}O$ value of –10.4‰ almost 1m below the ice surface (see previous page). This very negative $\delta^{18}O$ value occurred in granular ice with textural characteristics that were significantly different from all other granular ice: the ice was almost inclusion–free with polygonal crystals typically 5–10mm, but sometimes as much as 15mm, across.

The coarse–grained ice with very negative $\delta^{18}O$ values is structurally and isotopically similar to ice observed only at the top of cores obtained at the end of austral summer 1992 (Jeffries et al., 1994a: Figs. 3, 4 and 10), and to ice of glacial origin that has been reported in fragments in sub–surface layers of Bellingshausen Sea ice cores (Haas and Thomas, 1995: Fig. 4). Since cruise NBP 93–5, on three winter cruises throughout the Pacific sector of the Southern Ocean, we have observed such coarse–grained, ^{18}O–depleted ice only occasionally and only in the outer pack ice after the passage of warm, moist air masses that caused melting of the snow cover. Minor amounts of structurally and isotopically similar ice derived from snow melting have been reported also in the East Antarctic pack ice (Worby and Massom, 1995). The ice also strongly resembles the "iced–firn" that contributes to the upward growth of the Ward Hunt Ice Shelf in the Canadian High Arctic where the snow cover is rapidly transformed into ice each summer by melting and refreezing (Jeffries, 1985). Superimposed ice with similar structural and isotopic characteristics has been reported in antarctic landfast ice zones (Panov and Fedotov, 1977; Kawamura et al, 1993, in press).

We interpret the coarse–grained ice with very negative $\delta^{18}O$ values in core 248–4b as superimposed ice. It might have formed earlier in winter 1993 during a warming event and resultant snow melting, which were followed by further snow accumulation, seawater flooding and snow ice formation (the $\delta^{18}O$ values in the granular ice above the superimposed ice are all <0‰ and thus meet the criterion for snow ice [see section 5.5.3 for more details on the differentiation of snow ice from frazil ice]). Or, more likely, the isotopically very negative layer is superimposed ice that formed one summer at the ice surface, which was subsequently flooded leading to snow ice formation. The formation of snow ice upon a summer ice layer indicates that core 248–4b was from a multiyear floe.

NBP 93-5 FLOE 249

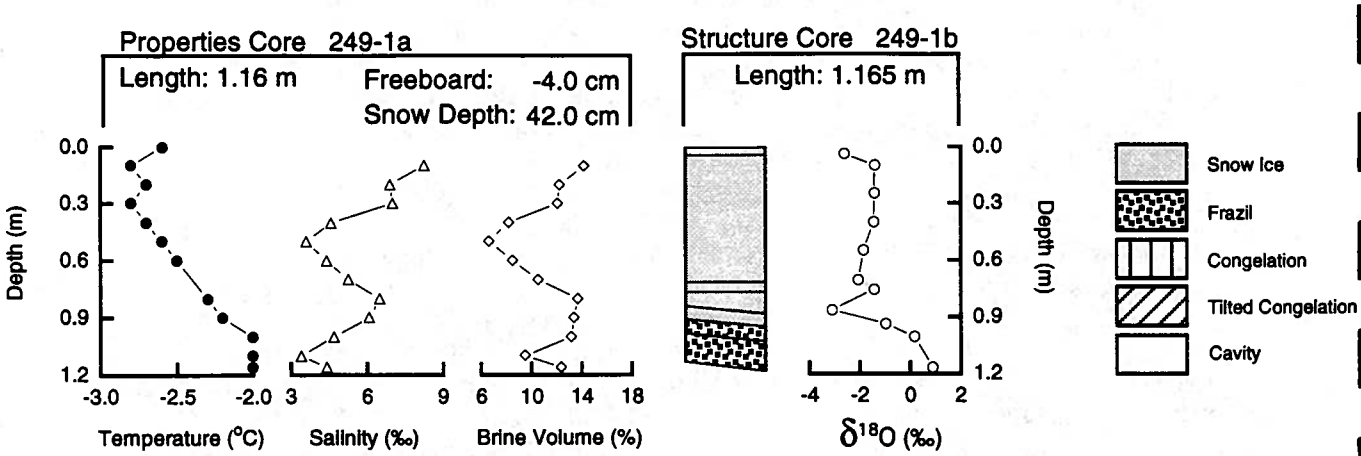

Position: 70° 20.83' S, 96° 11.18' W
Date: 6 September 1993

Mean Ice Thickness: 133.7 ± 73.0 cm
Mean Snow Thickness: 57.5 ± 13.3 cm
Mean Freeboard: -4.1 ± 7.8 cm
Floe Type: C

Salinity min: 3.4 ‰
Salinity max: 8.2 ‰
Salinity mean: 5.4 ‰

$\delta^{18}O$ min: -3.10 ‰
$\delta^{18}O$ max: 0.90 ‰
$\delta^{18}O$ mean: -1.38 ‰

Snow Ice: 81.7 %
Frazil Ice: 18.3 %
Congelation: 00.0 %
Cavity: 00.0 %

Snow Fraction
f_s: 13.71 %
F_m: 11.20 %

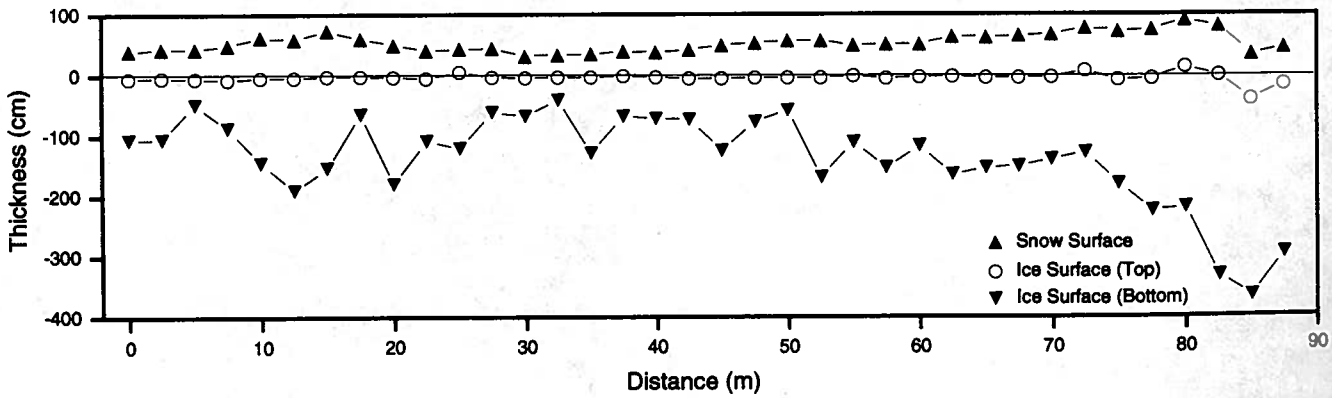

NBP 93-5 FLOE 250

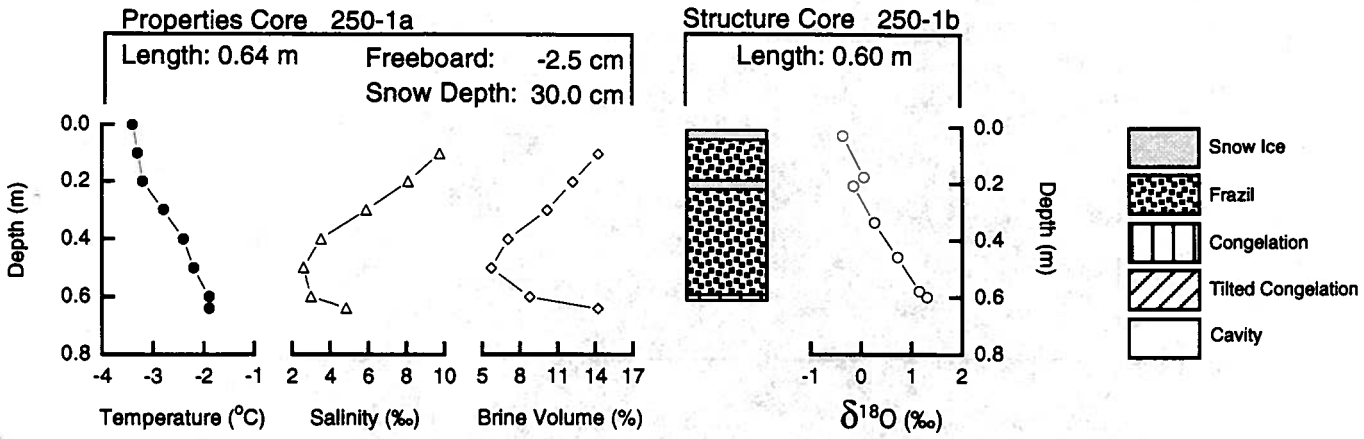

Position: 70° 14.18' S, 97° 59.95' W
Date: 7 September 1993

Mean Ice Thickness: 82.0 ± 24.1 cm
Mean Snow Thickness: 31.6 ± 5.1 cm
Mean Freeboard: -6.6 ± 7.7 cm
Floe Type: B

Salinity min: 2.6 ‰
Salinity max: 9.7 ‰
Salinity mean: 5.4 ‰

$\delta^{18}O$ min: -0.34 ‰
$\delta^{18}O$ max: 1.31 ‰
$\delta^{18}O$ mean: 0.43 ‰

Snow Ice: 10.8 %
Frazil Ice: 85.9 %
Congelation: 3.3 %
Cavity: 00.0 %

Snow Fraction
f_s: 1.88 %
F_m: 0.20 %

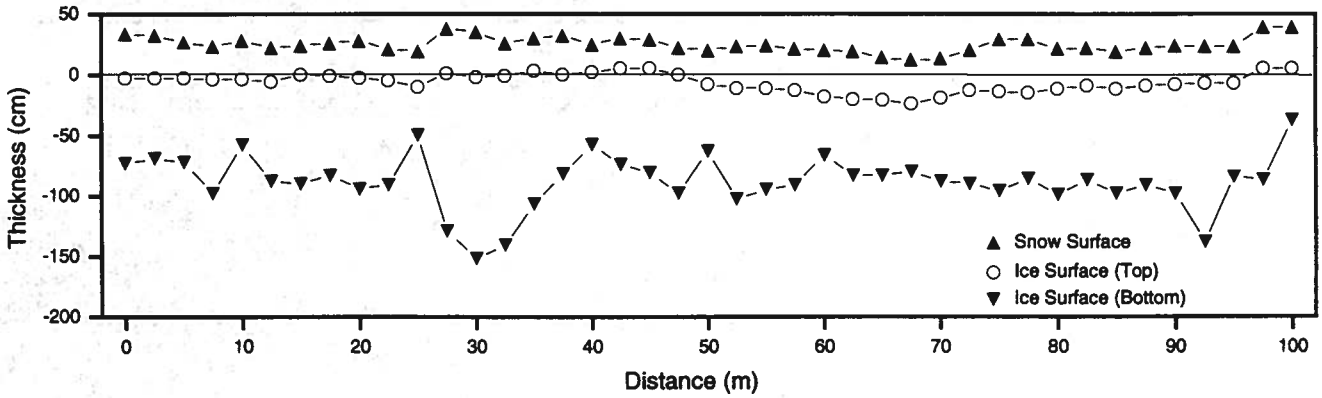

NBP 93-5 FLOE 251

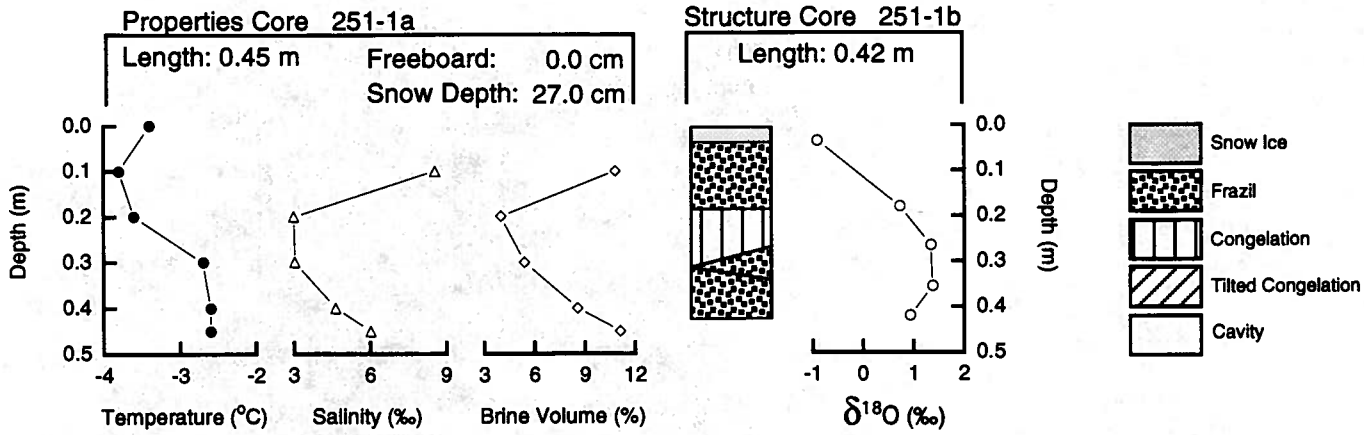

Position: 70° 13.47' S, 99° 39.55' W
Date: 8 September 1993

Mean Ice Thickness: 85.8 ± 51.1 cm
Mean Snow Thickness: 32.1 ± 6.8 cm
Mean Freeboard: -0.6 ± 2.1 cm
Floe Type: C

Salinity min: 3.0 ‰
Salinity max: 8.5 ‰
Salinity mean: 5.0 ‰

$\delta^{18}O$ min: -0.90 ‰
$\delta^{18}O$ max: 1.38 ‰
$\delta^{18}O$ mean: 0.70 ‰

Snow Ice: 8.3 %
Frazil Ice: 66.1 %
Congelation: 25.6 %
Cavity: 00.0 %

Snow Fraction
f_s: 6.82 %
F_m: 0.57 %

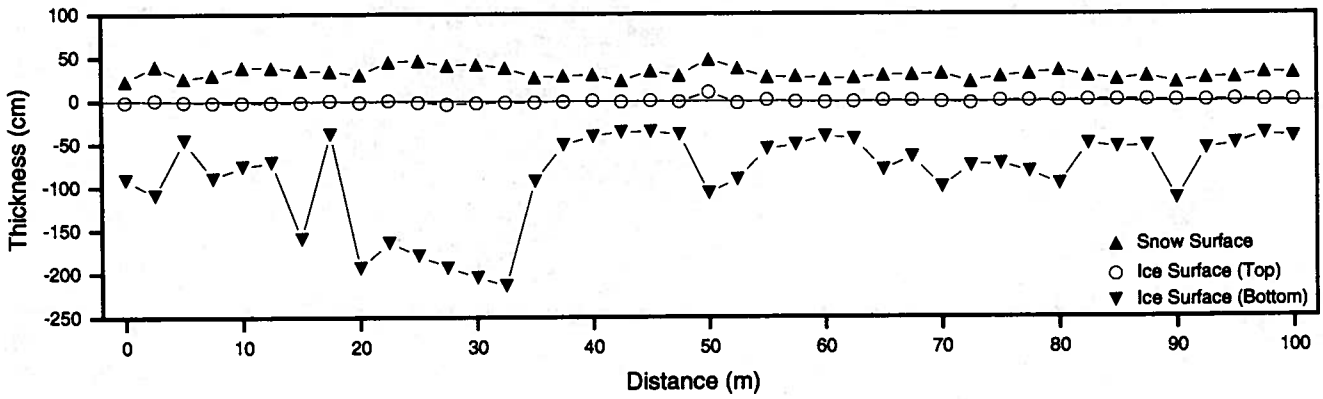

NBP 93-5 FLOE 253

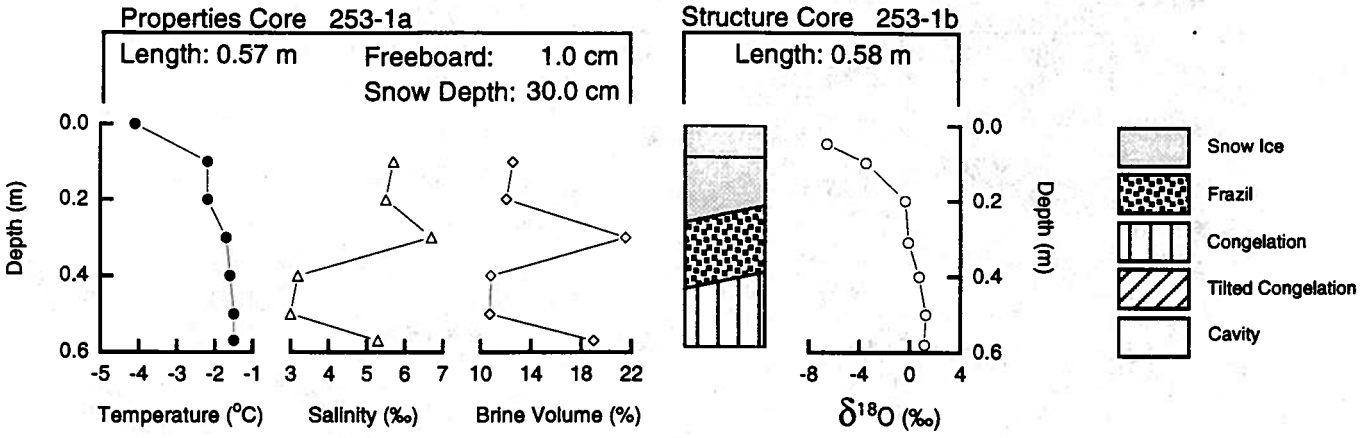

Position: 70° 25.50' S, 100° 55.80' W
Date: 10 September 1993

Mean Ice Thickness: 91.3 ± 26.1 cm
Mean Snow Thickness: 36.8 ± 10.2 cm
Mean Freeboard: 0.5 ± 3.3 cm
Floe Type: B

Salinity min: 3.0 ‰
Salinity max: 6.7 ‰
Salinity mean: 4.9 ‰

$\delta^{18}O$ min: -6.62 ‰
$\delta^{18}O$ max: 1.29 ‰
$\delta^{18}O$ mean: -1.04 ‰

Snow Ice: 53.4 %
Frazil Ice: 32.8 %
Congelation: 13.8 %
Cavity: 00.0 %

Snow Fraction
f_s: 13.33 %
F_m: 7.12 %

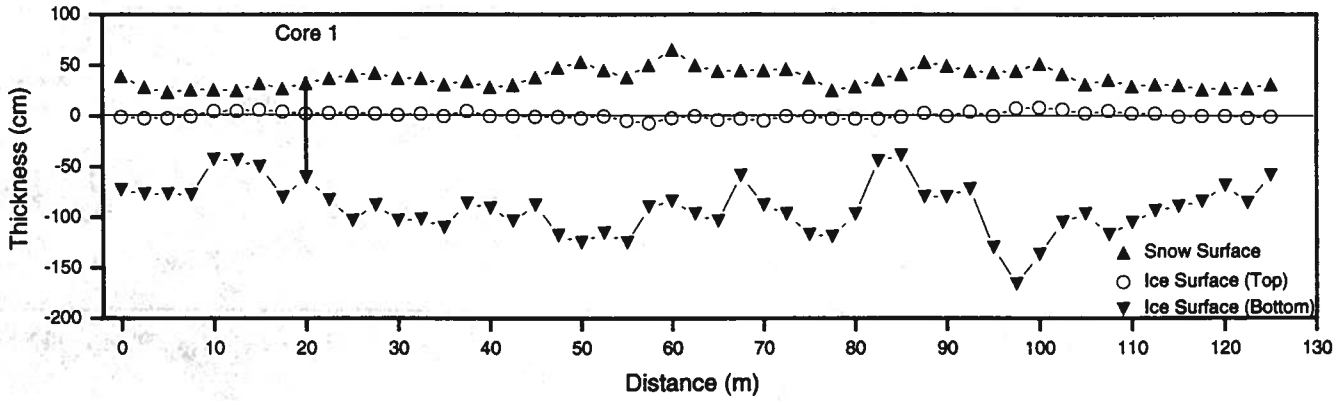

NBP 93-5 FLOE 253

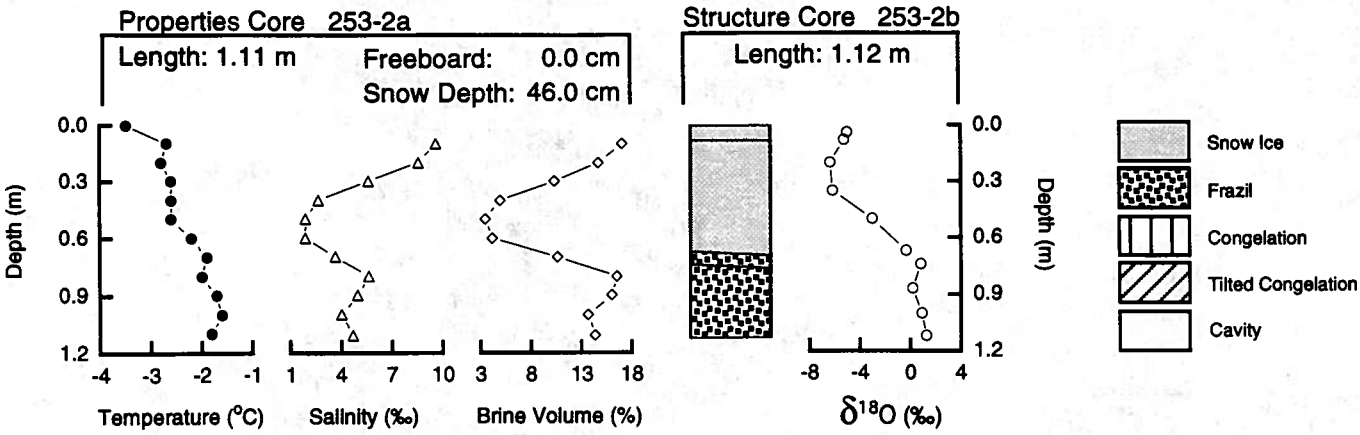

Position: 70° 25.50' S, 100° 55.80' W
Date: 10 September 1993

Mean Ice Thickness: 91.3 ± 26.1 cm
Mean Snow Thickness: 36.8 ± 10.2 cm
Mean Freeboard: 0.5 ± 3.3 cm
Floe Type: B

Salinity min: 1.9 ‰
Salinity max: 9.6 ‰
Salinity mean: 4.8 ‰

$\delta^{18}O$ min: -6.32 ‰
$\delta^{18}O$ max: 1.30 ‰
$\delta^{18}O$ mean: -2.27 ‰

Snow Ice: 59.8 %
Frazil Ice: 40.2 %
Congelation: 00.0 %
Cavity: 00.0 %

Snow Fraction
f_s: 29.26 %
F_m: 17.51 %

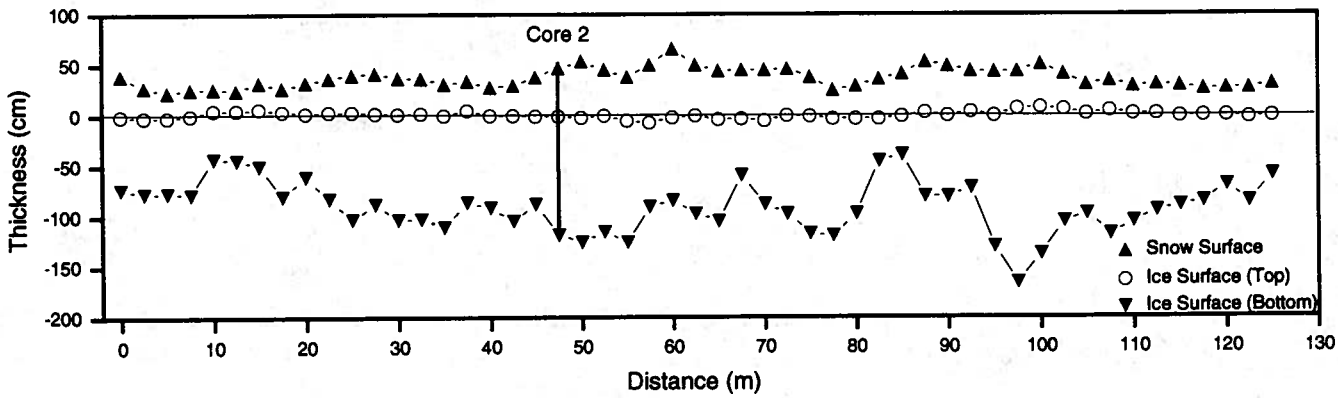

NBP 93-5 FLOE 253

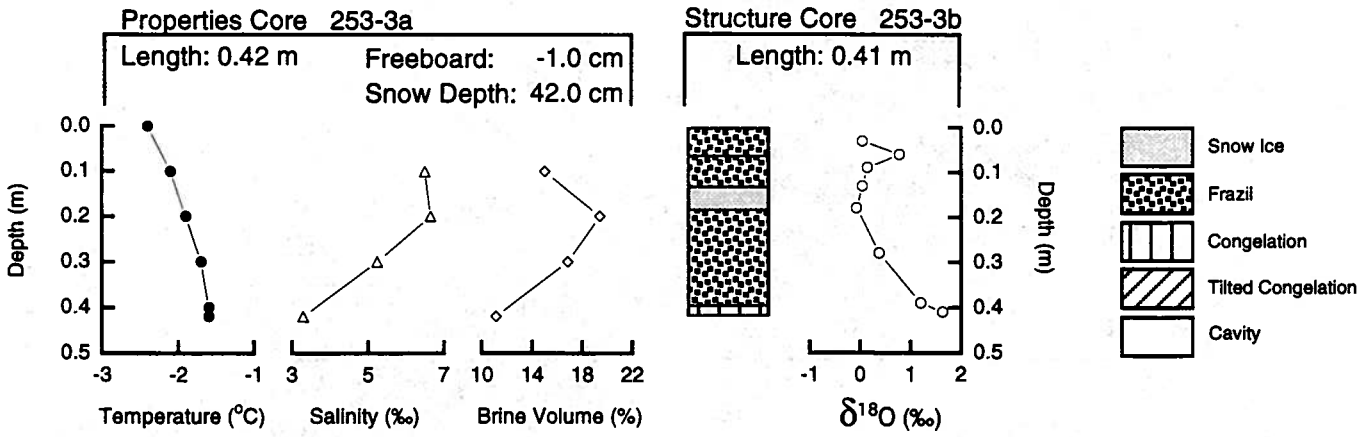

Position: 70° 25.50' S, 100° 55.80' W
Date: 10 September 1993

Mean Ice Thickness: 91.3 ± 26.1 cm
Mean Snow Thickness: 36.8 ± 10.2 cm
Mean Freeboard: 0.5 ± 3.3 cm
Floe Type: B

Salinity min: 3.3 ‰
Salinity max: 6.6 ‰
Salinity mean: 5.4 ‰

$\delta^{18}O$ min: -0.06 ‰
$\delta^{18}O$ max: 1.64 ‰
$\delta^{18}O$ mean: 0.52 ‰

Snow Ice: 12.2 %
Frazil Ice: 82.9 %
Congelation: 4.9 %
Cavity: 00.0 %

Snow Fraction
f_s: 0.45 %
F_m: 0.06 %

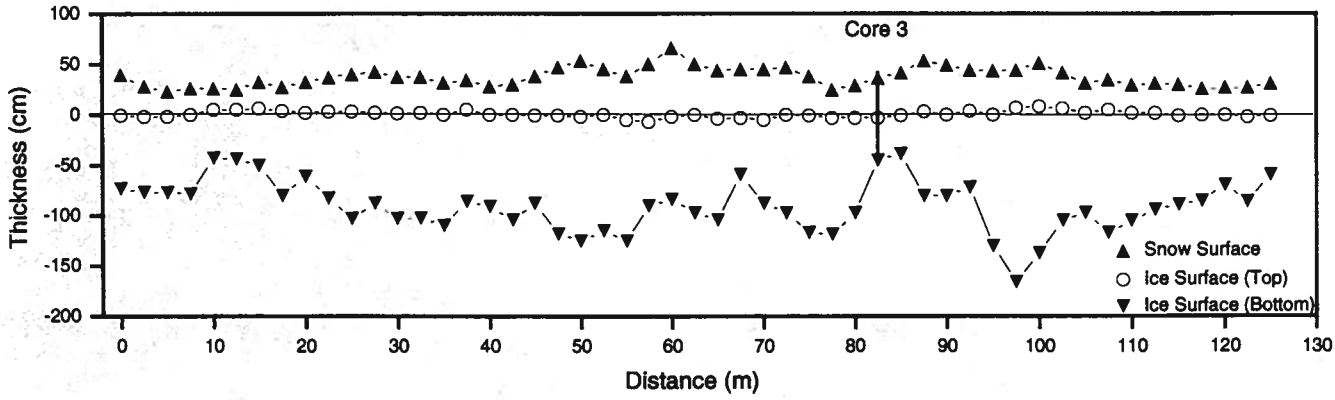

NBP 93-5 FLOE 253

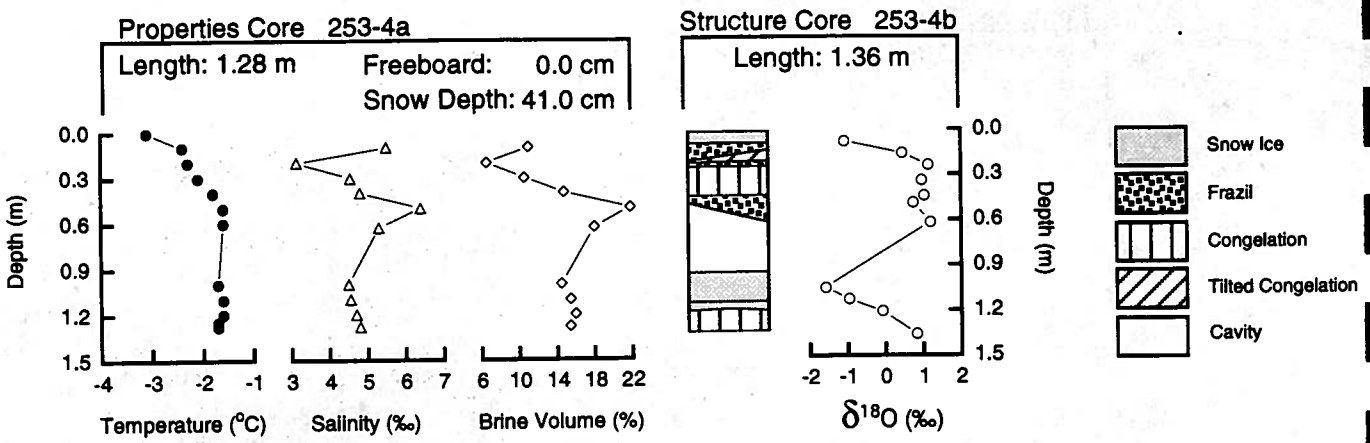

Position: 70° 25.50' S, 100° 55.80' W
Date: 10 September 1993

Mean Ice Thickness: 91.3 ± 26.1 cm
Mean Snow Thickness: 36.8 ± 10.2 cm
Mean Freeboard: 0.5 ± 3.3 cm
Floe Type: B

Salinity min: 3.1 ‰
Salinity max: 6.4 ‰
Salinity mean: 4.8 ‰

$\delta^{18}O$ min: -1.59 ‰
$\delta^{18}O$ max: 1.19 ‰
$\delta^{18}O$ mean: 0.25 ‰

Snow Ice: 24.3 %
Frazil Ice: 19.4 %
Congelation: 26.5 %
Cavity: 29.8 %

Snow Fraction
f_s: 7.16 %
F_m: 1.74 %

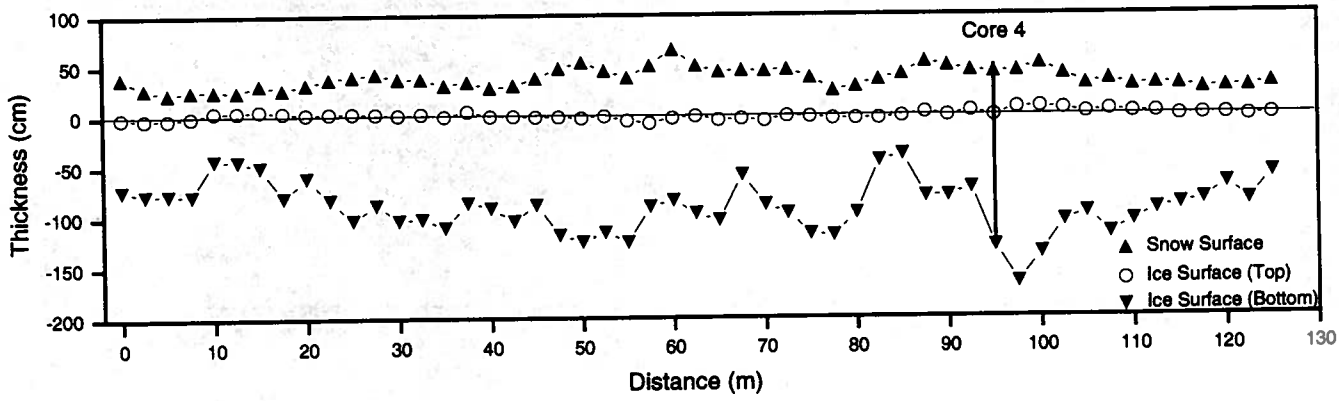

NBP 93-5 FLOE 253

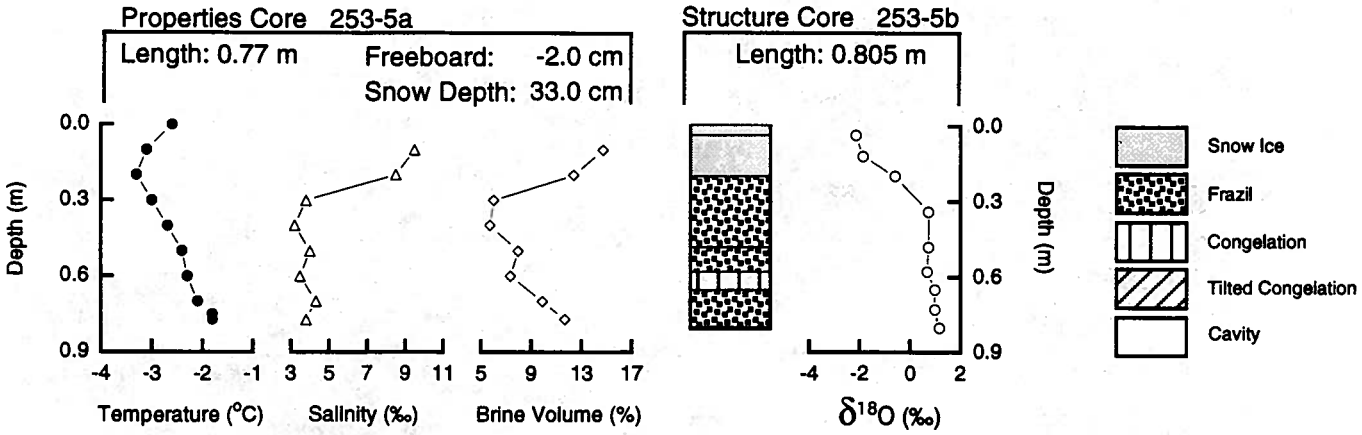

Position: 70° 25.50' S, 100° 55.80' W
Date: 10 September 1993

Mean Ice Thickness: 91.3 ± 26.1 cm
Mean Snow Thickness: 36.8 ± 10.2 cm
Mean Freeboard: 0.5 ± 3.3 cm
Floe Type: B

Salinity min: 3.2 ‰
Salinity max: 9.5 ‰
Salinity mean: 5.1 ‰

$\delta^{18}O$ min: -2.14 ‰
$\delta^{18}O$ max: 1.16 ‰
$\delta^{18}O$ mean: 0.08 ‰

Snow Ice: 24.8 %
Frazil Ice: 65.3 %
Congelation: 9.9 %
Cavity: 00.0 %

Snow Fraction
f_s: 10.64 %
F_m: 2.64 %

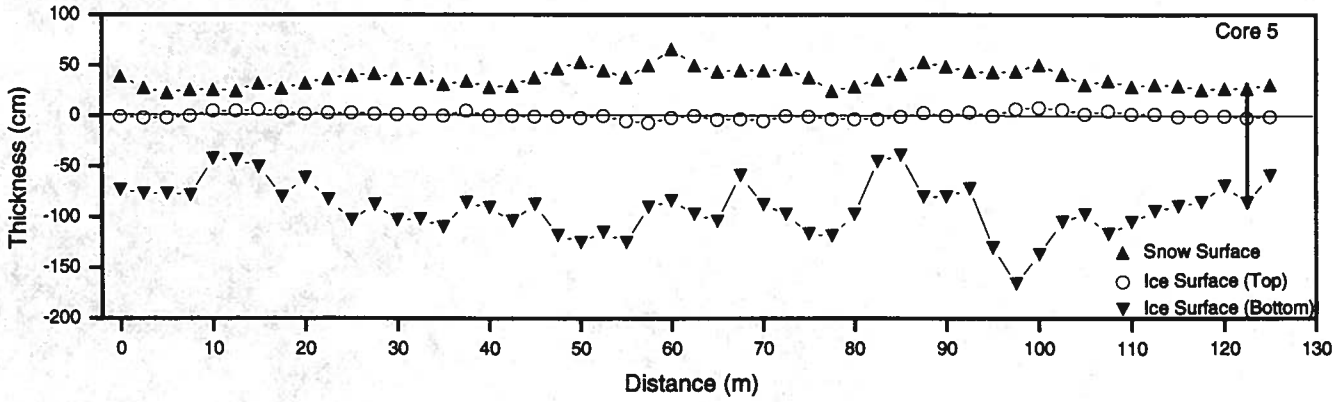

NBP 93-5 FLOE 254

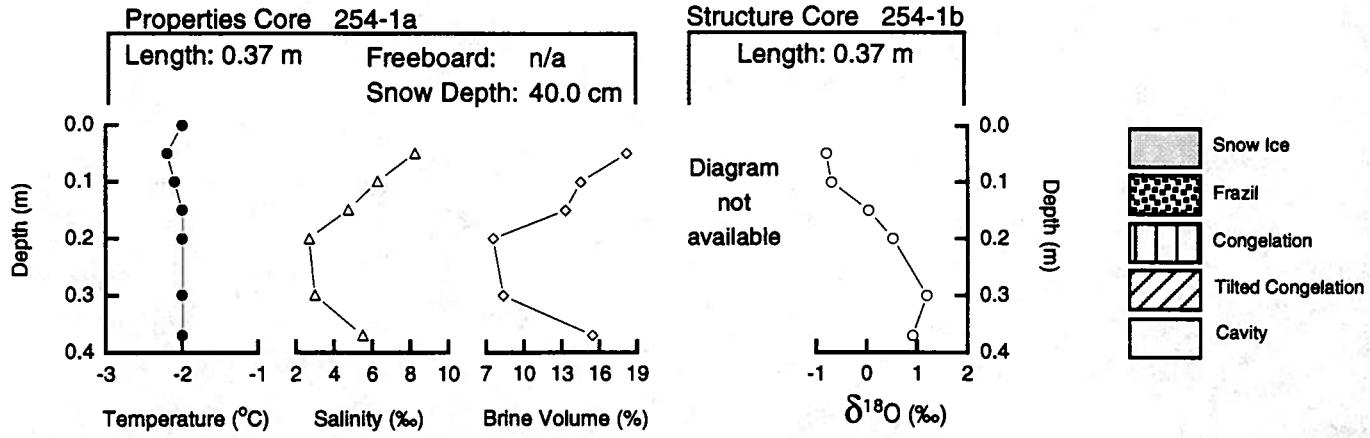

Position: 70° 25.50' S, 100° 55.80' W
Date: 11 September 1993

Mean Ice Thickness: n/a
Mean Snow Thickness: n/a
Mean Freeboard: n/a
Floe Type: n/a

Salinity min: 2.7 ‰
Salinity max: 8.2 ‰
Salinity mean: 5.1 ‰

$\delta^{18}O$ min: -0.80 ‰
$\delta^{18}O$ max: 1.20 ‰
$\delta^{18}O$ mean: 0.20 ‰

Snow Ice: 27.0 %
Frazil Ice: n/a
Congelation: n/a
Cavity: n/a

Snow Fraction
f_s: 5.68 %
F_m: 1.54 %

NBP 93-5 FLOE 254

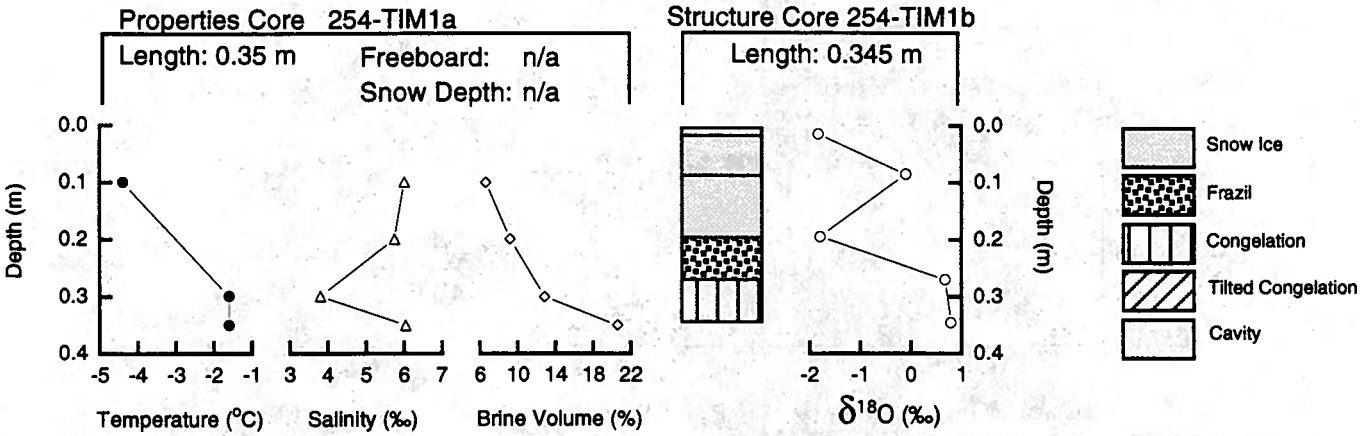

Position: 70° 25.50' S, 100° 55.80' W
Date: 11 September 1993

Mean Ice Thickness: n/a
Mean Snow Thickness: n/a
Mean Freeboard: n/a
Floe Type: n/a

Salinity min: 3.8 ‰
Salinity max: 6.0 ‰
Salinity mean: 5.4 ‰

$\delta^{18}O$ min: -1.83 ‰
$\delta^{18}O$ max: 0.80 ‰
$\delta^{18}O$ mean: -0.45 ‰

Snow Ice: 56.5 %
Frazil Ice: 21.7 %
Congelation: 21.7 %
Cavity: 00.0 %

Snow Fraction
f_s: 9.03 %
F_m: 5.10 %

NBP 93-5 FLOE 254

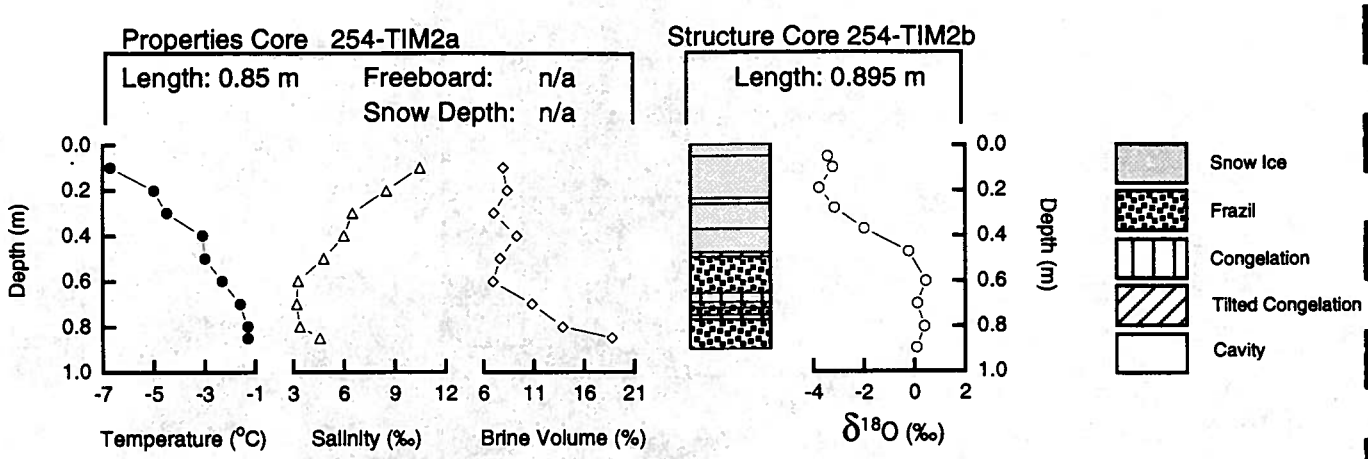

Position: 70° 25.50' S, 100° 55.80' W
Date: 11 September 1994

Mean Ice Thickness: n/a
Mean Snow Thickness: n/a
Mean Freeboard: n/a
Floe Type: n/a

Salinity min: 3.2 ‰
Salinity max: 10.5 ‰
Salinity mean: 5.6 ‰

$\delta^{18}O$ min: -3.78 ‰
$\delta^{18}O$ max: 0.46 ‰
$\delta^{18}O$ mean: -1.48 ‰

Snow Ice: 52.5 %
Frazil Ice: 38.6 %
Congelation: 8.9 %
Cavity: 00.0 %

Snow Fraction
f_s: 18.75 %
F_m: 9.85 %

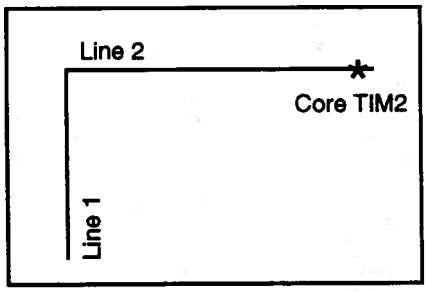

Transect Layout

NBP 93-5 FLOE 255

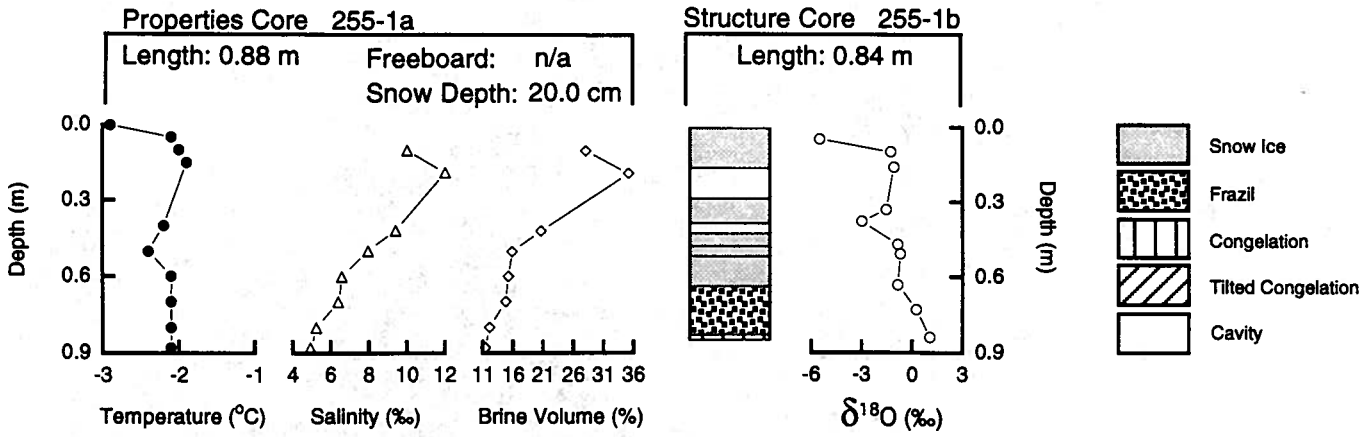

Position: 70° 07.24' S, 101° 57.36' W
Date: 12 September 1993

Mean Ice Thickness: 92.8 ± 45.9 cm
Mean Snow Thickness: 30.1 ± 6.0 cm
Mean Freeboard: 1.8 ± 4.5 cm
Floe Type: C

Salinity min: 4.9 ‰
Salinity max: 12.0 ‰
Salinity mean: 7.8 ‰

$\delta^{18}O$ min: -5.47 ‰
$\delta^{18}O$ max: 1.07 ‰
$\delta^{18}O$ mean: -1.33 ‰

Snow Ice: 56.0 %
Frazil Ice: 22.6 %
Congelation: 2.4 %
Cavity: 19.0 %

Snow Fraction
f_s: 12.76 %
F_m: 7.14 %

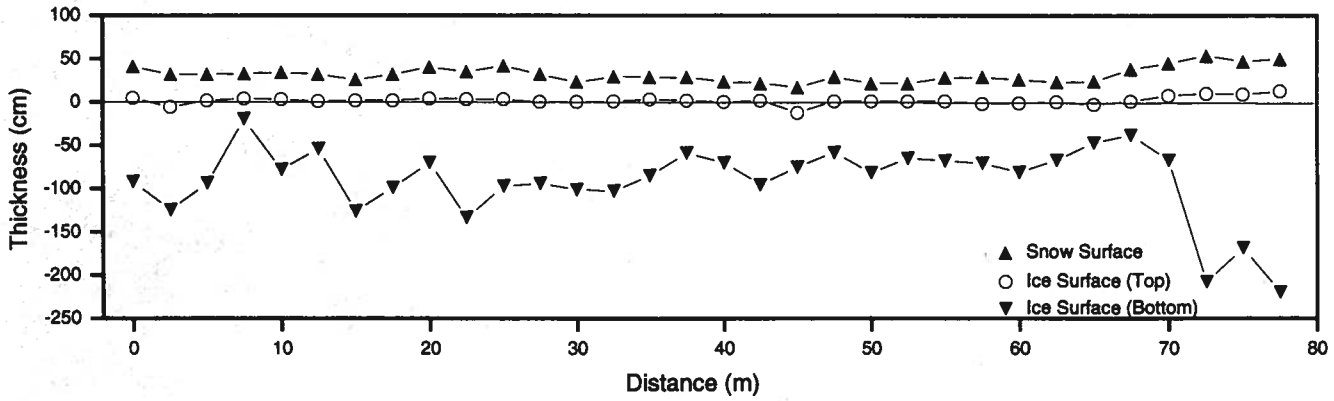

NBP 93-5 FLOE 256

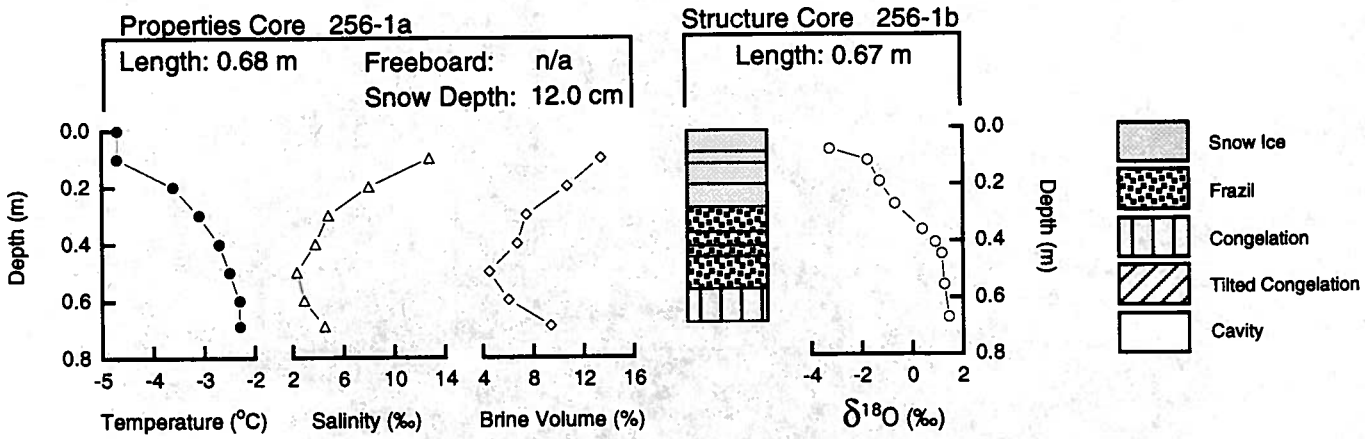

Position: 69° 50.55' S, 102° 50.84' W
Date: 13 September 1993

Mean Ice Thickness: 84.6 ± 29.7 cm
Mean Snow Thickness: 18.8 ± 8.2 cm
Mean Freeboard: 2.7 ± 2.8 cm
Floe Type: B

Salinity min: 2.3 ‰
Salinity max: 12.8 ‰
Salinity mean: 5.6 ‰

$\delta^{18}O$ min: -3.25 ‰
$\delta^{18}O$ max: 1.46 ‰
$\delta^{18}O$ mean: -0.20 ‰

Snow Ice: 40.3 %
Frazil Ice: 42.5 %
Congelation: 17.2 %
Cavity: 00.0 %

Snow Fraction
f_s: 13.08 %
F_m: 5.27 %

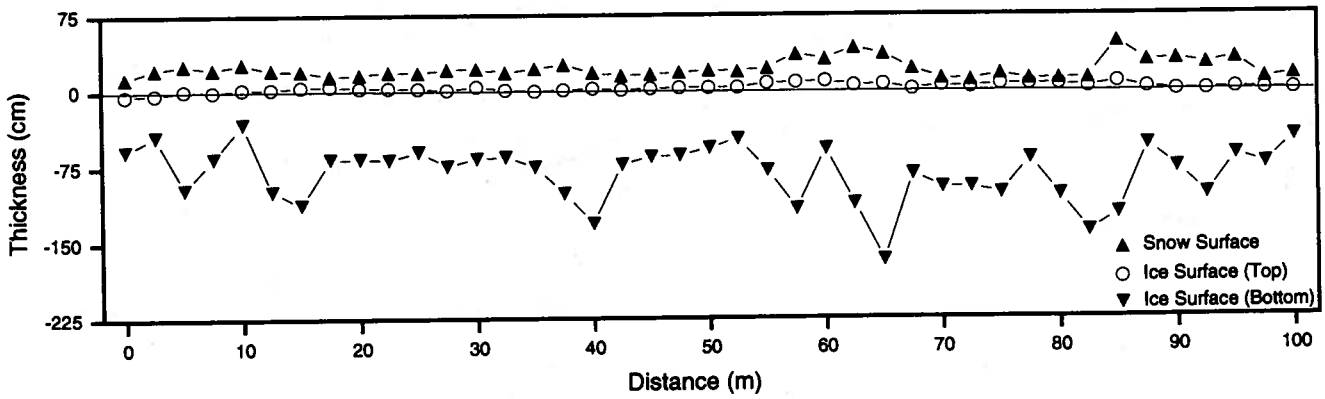

NBP 93-5 FLOE 257

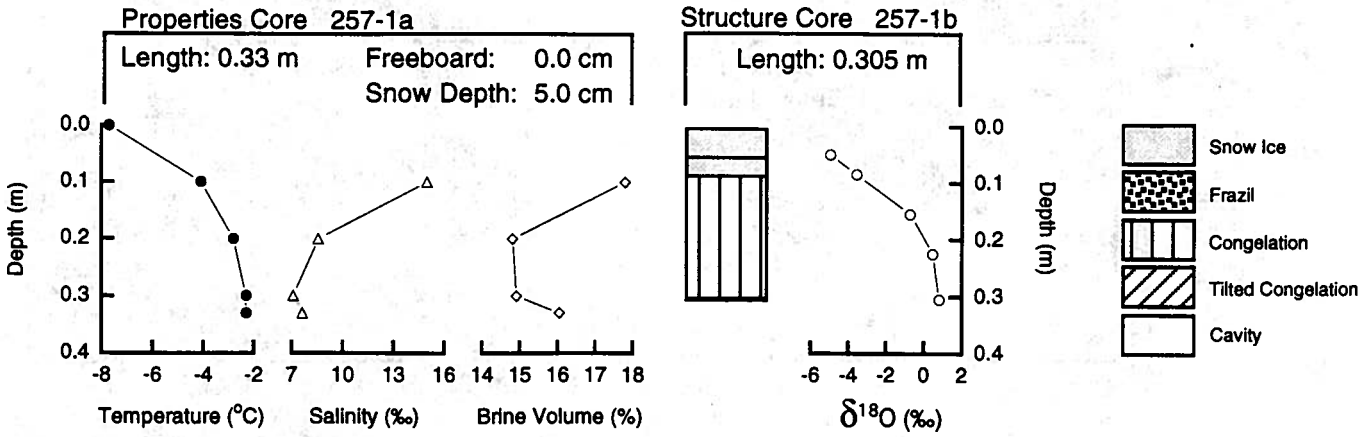

Position: 69° 35.79' S, 103° 47.39' W
Date: 14 September 1993

Mean Ice Thickness: 65.0 ± 37.7 cm
Mean Snow Thickness: 6.9 ± 3.4 cm
Mean Freeboard: 4.3 ± 3.6 cm
Floe Type: C

Salinity min: 7.1 ‰
Salinity max: 15.0 ‰
Salinity mean: 9.6 ‰

$\delta^{18}O$ min: -4.94 ‰
$\delta^{18}O$ max: 0.81 ‰
$\delta^{18}O$ mean: -1.57 ‰

Snow Ice: 27.9 %
Frazil Ice: 00.0 %
Congelation: 72.1 %
Cavity: 00.0 %

Snow Fraction
f_s: 33.06 %
F_m: 9.21 %

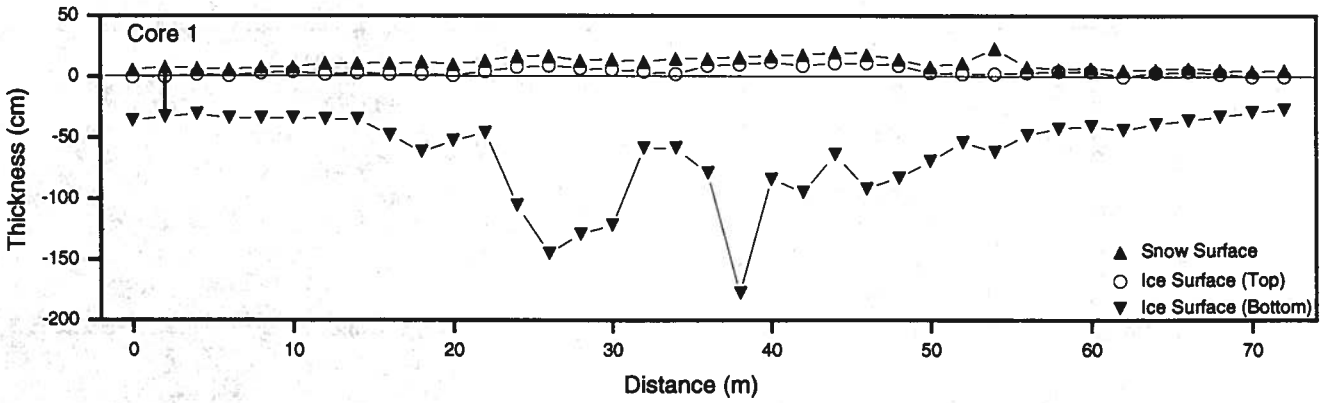

NBP 93-5 FLOE 257

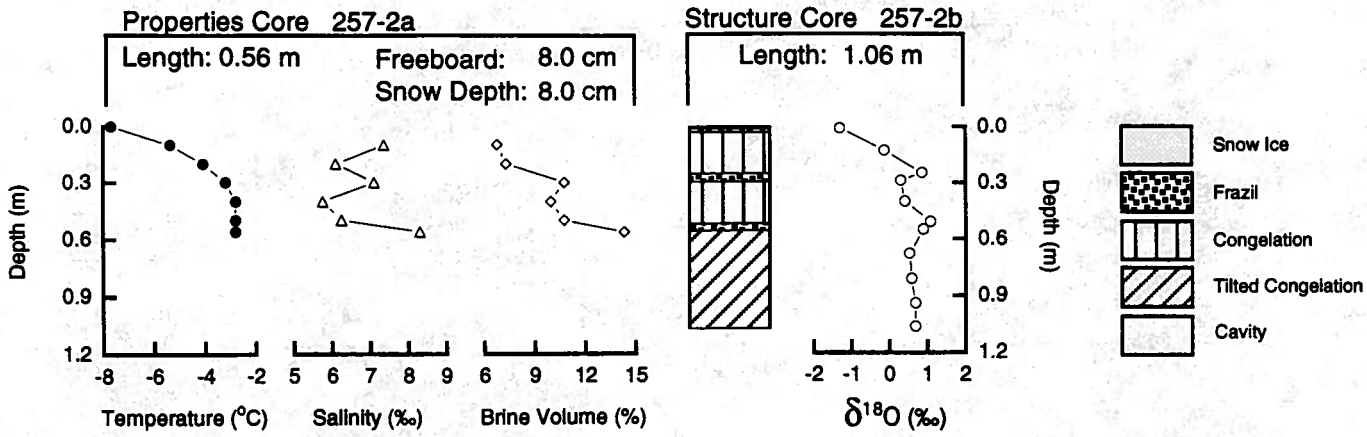

Position: 69° 35.79' S, 103° 47.39' W
Date: 14 September 1993

Mean Ice Thickness: 65.0 ± 37.7 cm
Mean Snow Thickness: 6.9 ± 3.4 cm
Mean Freeboard: 4.3 ± 3.6 cm
Floe Type: C

Salinity min: 5.7 ‰
Salinity max: 8.3 ‰
Salinity mean: 6.8 ‰

$\delta^{18}O$ min: -1.31 ‰
$\delta^{18}O$ max: 1.08 ‰
$\delta^{18}O$ mean: 0.41 ‰

Snow Ice: 0.9 %
Frazil Ice: 9.5 %
Congelation: 89.6 %
Cavity: 00.0 %

Snow Fraction
f_s: 9.92 %
F_m: 0.09 %

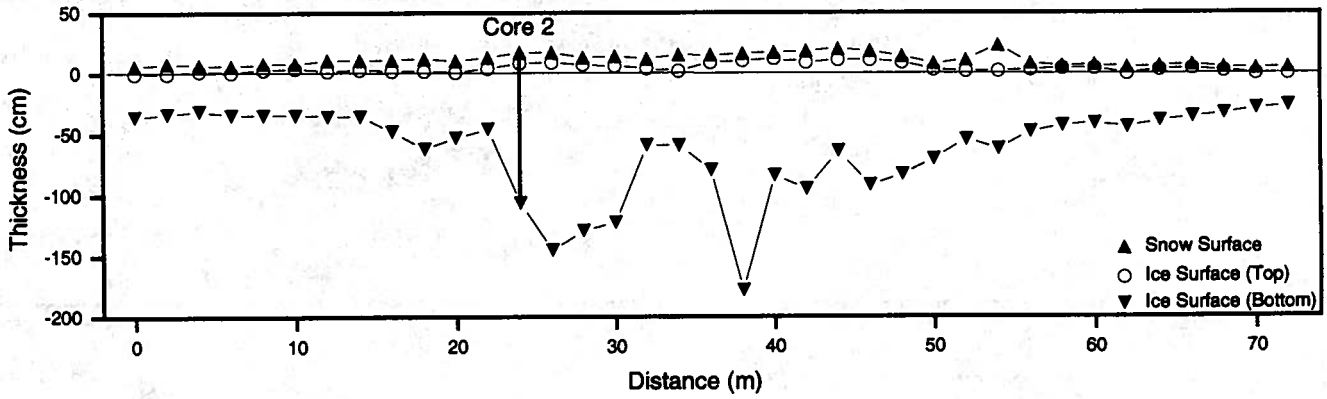

NBP 93-5 FLOE 257

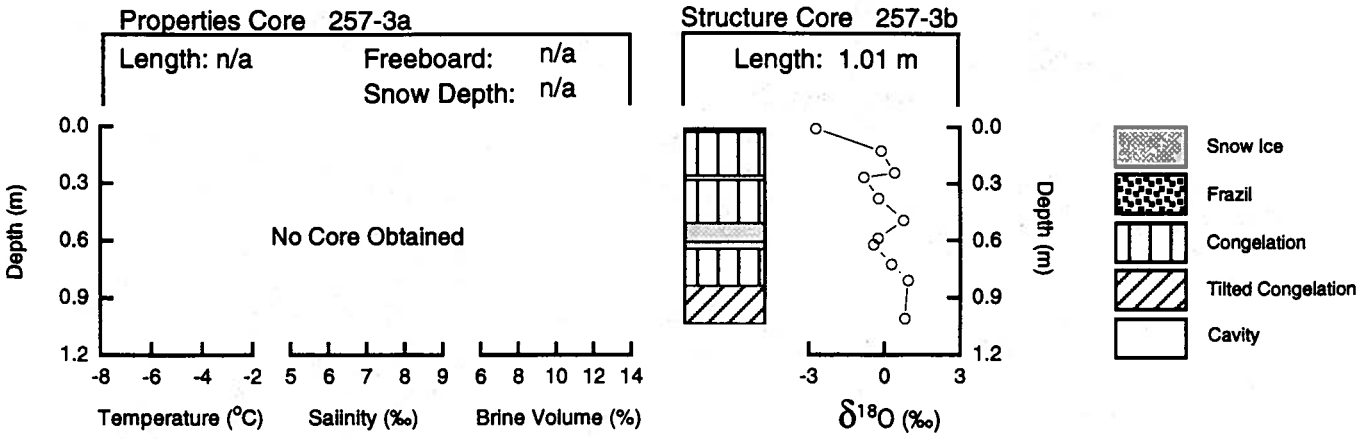

Position: 69° 35.79' S, 103° 47.39' W
Date: 14 September 1993

Mean Ice Thickness: 65.0 ± 37.7 cm
Mean Snow Thickness: 6.9 ± 3.4 cm
Mean Freeboard: 4.3 ± 3.6 cm
Floe Type: C

Salinity min: n/a
Salinity max: n/a
Salinity mean: n/a

$\delta^{18}O$ min: -2.71 ‰
$\delta^{18}O$ max: 0.94 ‰
$\delta^{18}O$ mean: -0.11 ‰

Snow Ice: 17.3 %
Frazil Ice: 00.0 %
Congelation: 82.7 %
Cavity: 00.0 %

Snow Fraction
f_s: 3.91 %
F_m: 0.64 %

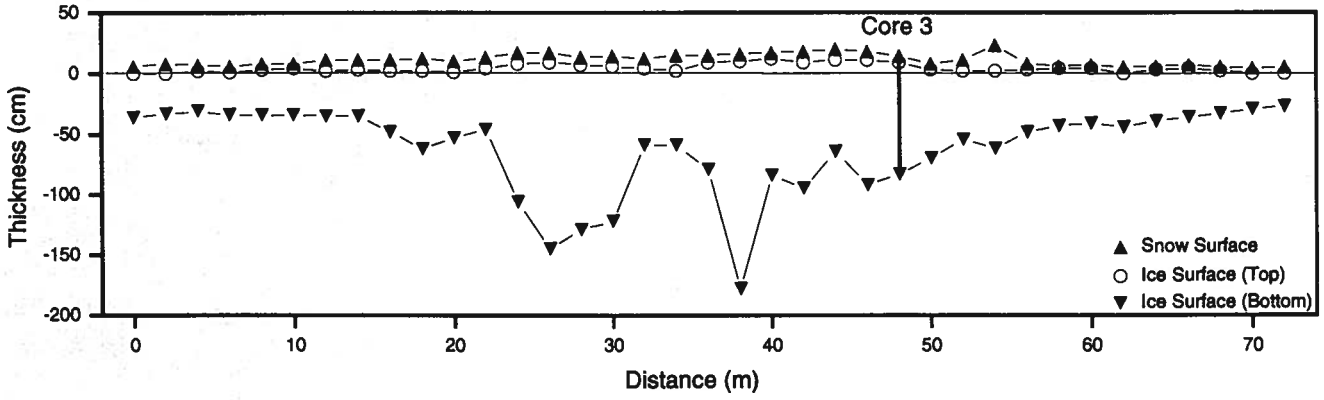

NBP 93-5 FLOE 257

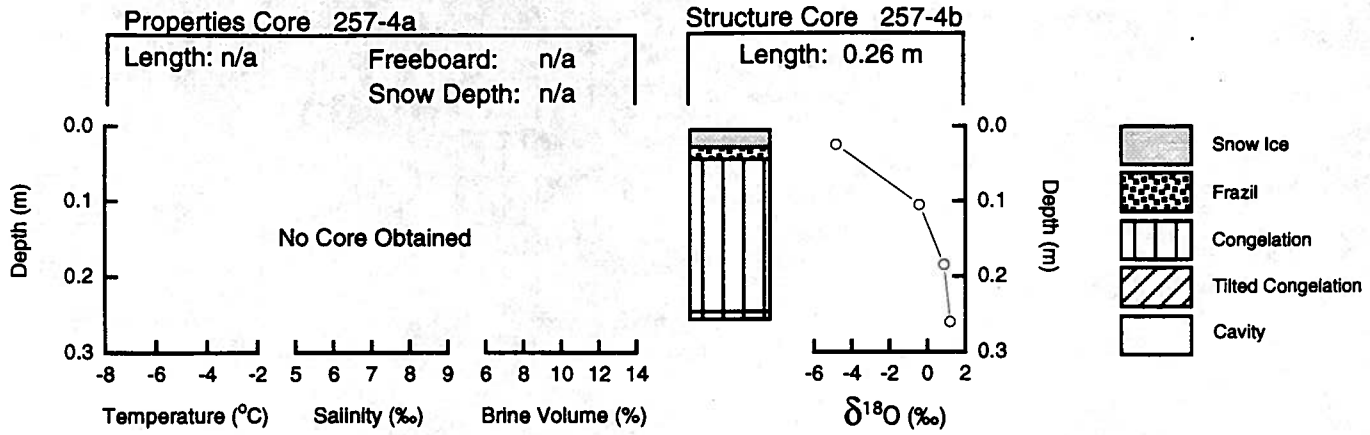

Position: 69° 35.79' S, 103° 47.39' W
Date: 14 September 1993

Mean Ice Thickness: 65.0 ± 37.7 cm
Mean Snow Thickness: 6.9 ± 3.4 cm
Mean Freeboard: 4.3 ± 3.6 cm
Floe Type: C

Salinity min: n/a
Salinity max: n/a
Salinity mean: n/a

$\delta^{18}O$ min: -4.83 ‰
$\delta^{18}O$ max: 1.20 ‰
$\delta^{18}O$ mean: -0.79 ‰

Snow Ice: 9.6 %
Frazil Ice: 5.8 %
Congelation: 84.6 %
Cavity: 00.0 %

Snow Fraction
f_s: 36.59 %
F_m: 3.52 %

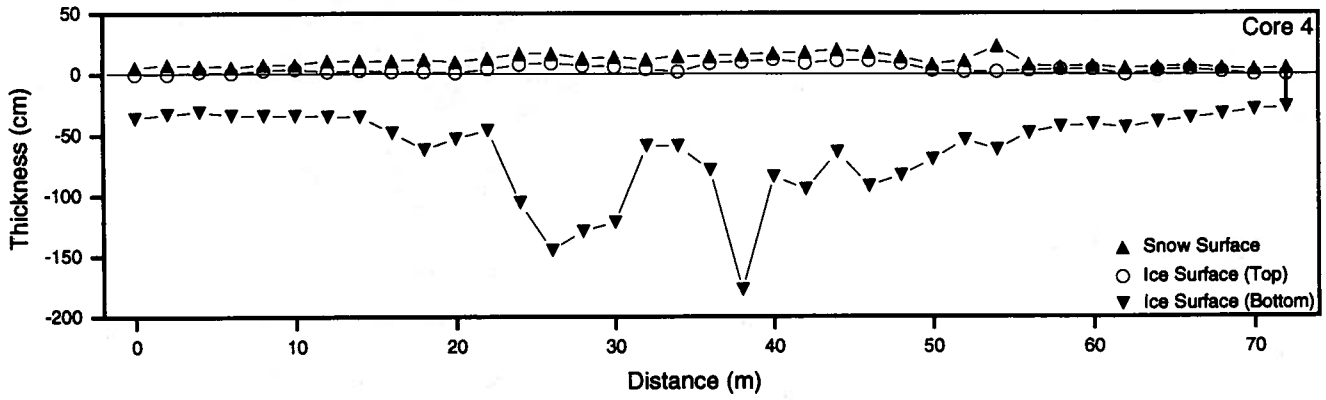

NBP 93-5 FLOE 258

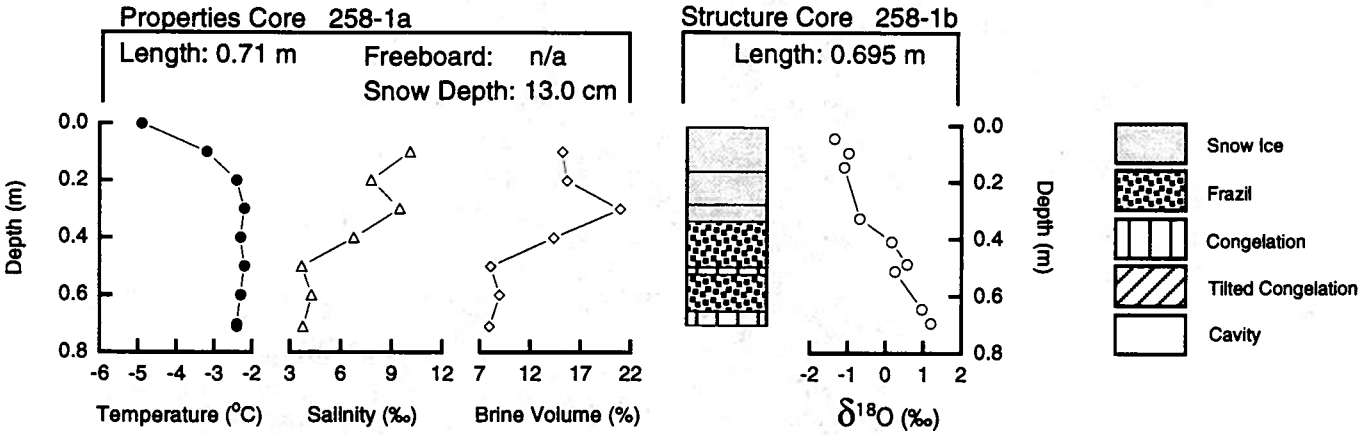

Position: 69° 29.97' S, 105° 01.93' W
Date: 15 September 1993

Mean Ice Thickness: 75.1 ± 17.1 cm
Mean Snow Thickness: 18.1 ± 6.5 cm
Mean Freeboard: 2.9 ± 2.0 cm
Floe Type: B

Salinity min: 3.7 ‰
Salinity max: 10.1 ‰
Salinity mean: 6.6 ‰

$\delta^{18}O$ min: -1.35 ‰
$\delta^{18}O$ max: 1.20 ‰
$\delta^{18}O$ mean: -0.10 ‰

Snow Ice: 47.5 %
Frazil Ice: 41.7 %
Congelation: 10.8 %
Cavity: 00.0 %

Snow Fraction
f_s: 7.57 %
F_m: 2.88 %

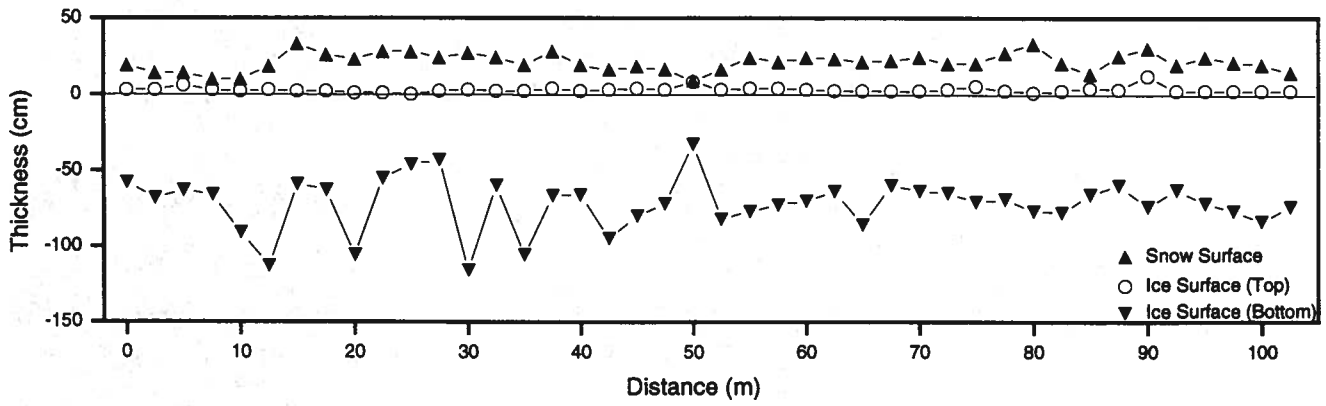

NBP 93-5 FLOE 258

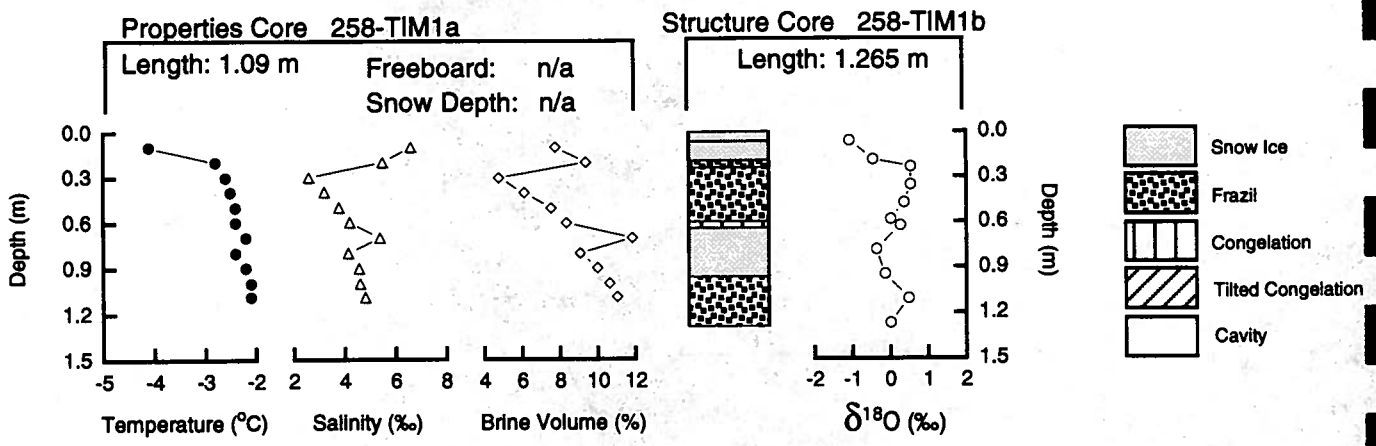

Position: 69° 29.97' S, 105° 01.93' W
Date: 15 September 1993

Mean Ice Thickness: 75.1 ± 17.1 cm
Mean Snow Thickness: 18.1 ± 6.5 cm
Mean Freeboard: 2.9 ± 2.0 cm
Floe Type: B

Salinity min: 2.6 ‰
Salinity max: 6.6 ‰
Salinity mean: 4.5 ‰

$\delta^{18}O$ min: -1.06 ‰
$\delta^{18}O$ max: 0.54 ‰
$\delta^{18}O$ mean: 0.02 ‰

Snow Ice: 40.3 %
Frazil Ice: 56.5 %
Congelation: 3.2 %
Cavity: 00.0 %

Snow Fraction
f_s: 3.05 %
F_m: 1.23 %

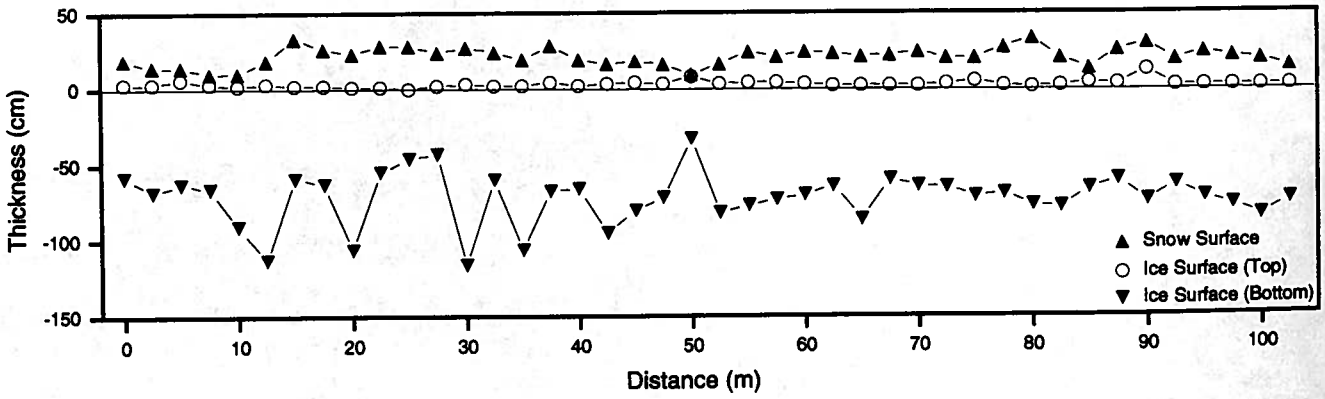

NBP 93-5 FLOE 259

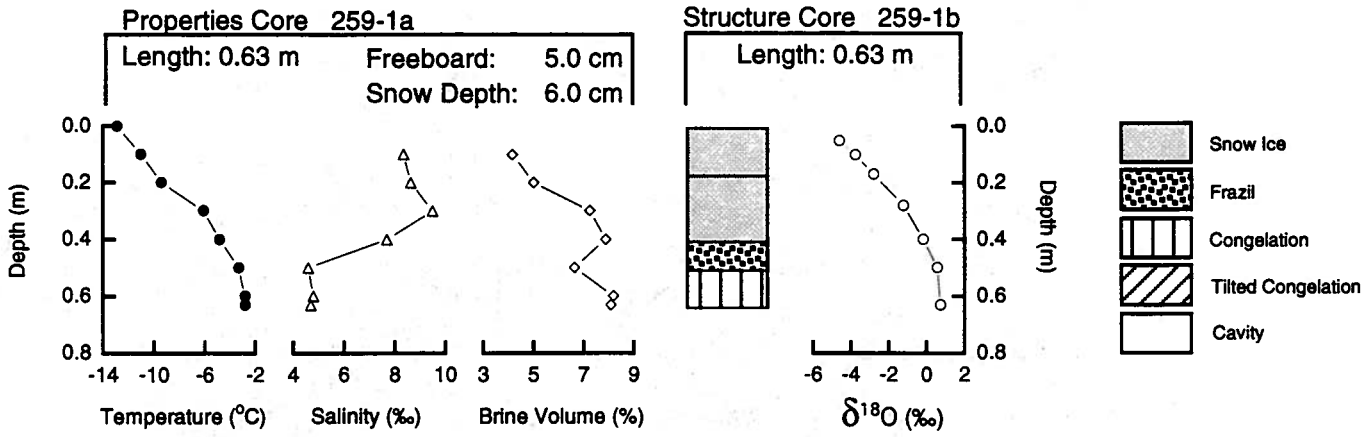

Position: 69° 19.90' S, 106° 10.71' W
Date: 16 September 1993

Mean Ice Thickness: 58.6 ± 11.3 cm
Mean Snow Thickness: 10.7 ± 4.4 cm
Mean Freeboard: 3.7 ± 2.2 cm
Floe Type: A

Salinity min: 4.6 ‰
Salinity max: 9.5 ‰
Salinity mean: 6.9 ‰

$\delta^{18}O$ min: -4.62 ‰
$\delta^{18}O$ max: 0.75 ‰
$\delta^{18}O$ mean: -1.60 ‰

Snow Ice: 63.5 %
Frazil Ice: 15.9 %
Congelation: 20.6 %
Cavity: 00.0 %

Snow Fraction
f_s: 14.52 %
F_m: 9.22 %

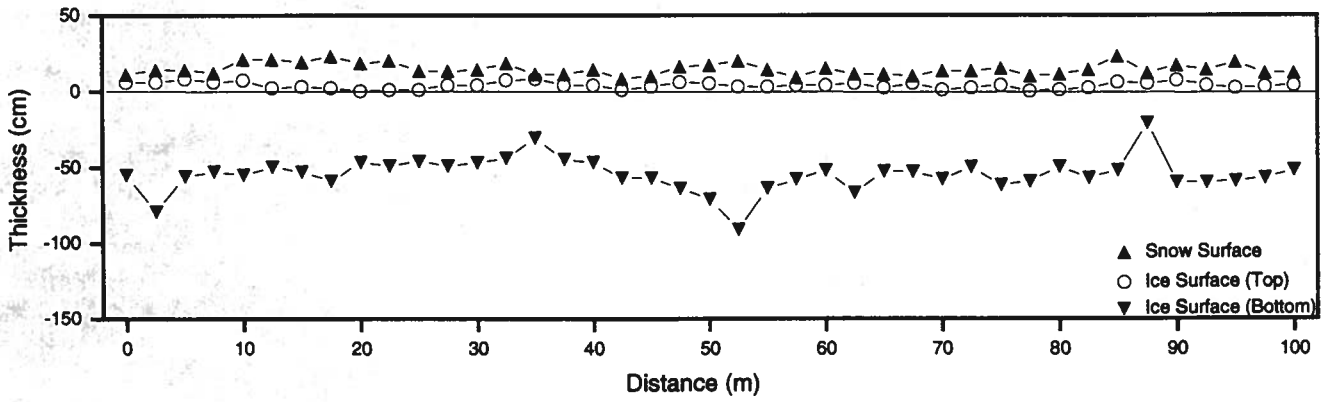

NBP 93-5 FLOE 260

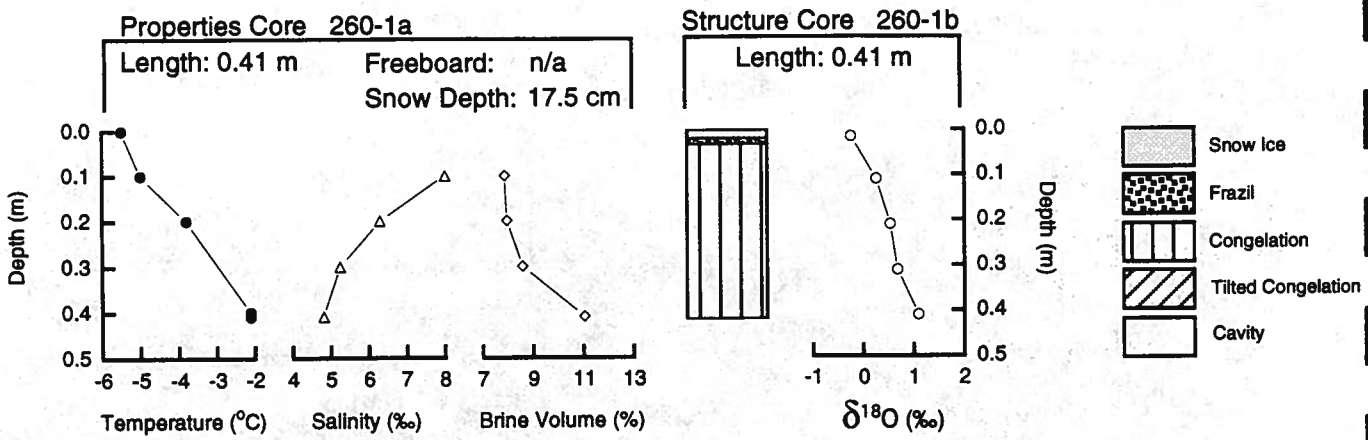

Position: 69° 22.31' S, 107° 39.28' W
Date: 17 September 1993

Mean Ice Thickness: 54.4 ± 24.2 cm
Mean Snow Thickness: 13.8 ± 5.5 cm
Mean Freeboard: 2.1 ± 1.9 cm
Floe Type: C

Salinity min: 4.8 ‰
Salinity max: 8.0 ‰
Salinity mean: 6.1 ‰

$\delta^{18}O$ min: -0.24 ‰
$\delta^{18}O$ max: 1.10 ‰
$\delta^{18}O$ mean: 0.47 ‰

Snow Ice: 3.7 %
Frazil Ice: 3.7 %
Congelation: 92.6 %
Cavity: 00.0 %

Snow Fraction
f_s: 1.82 %
F_m: 0.07 %

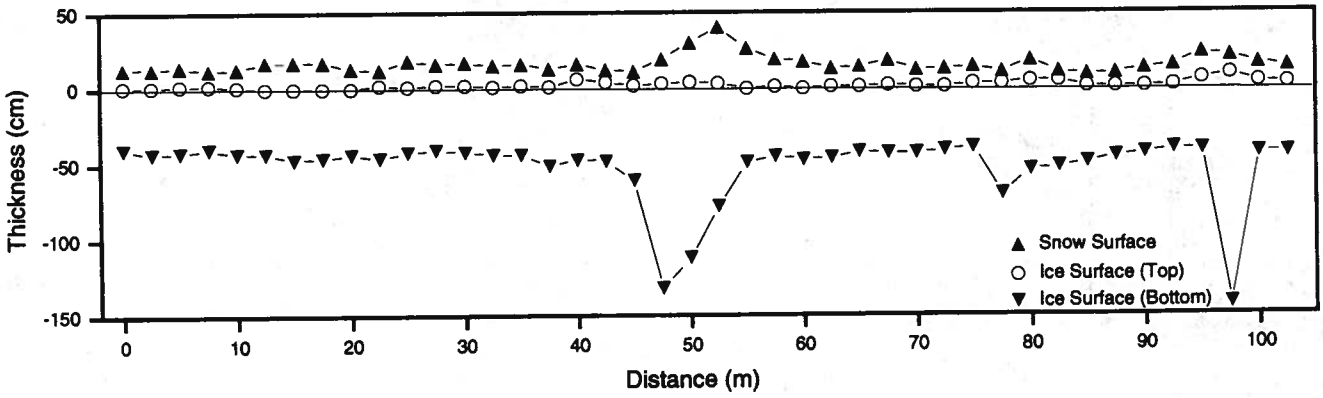

NBP 93-5 FLOE 261

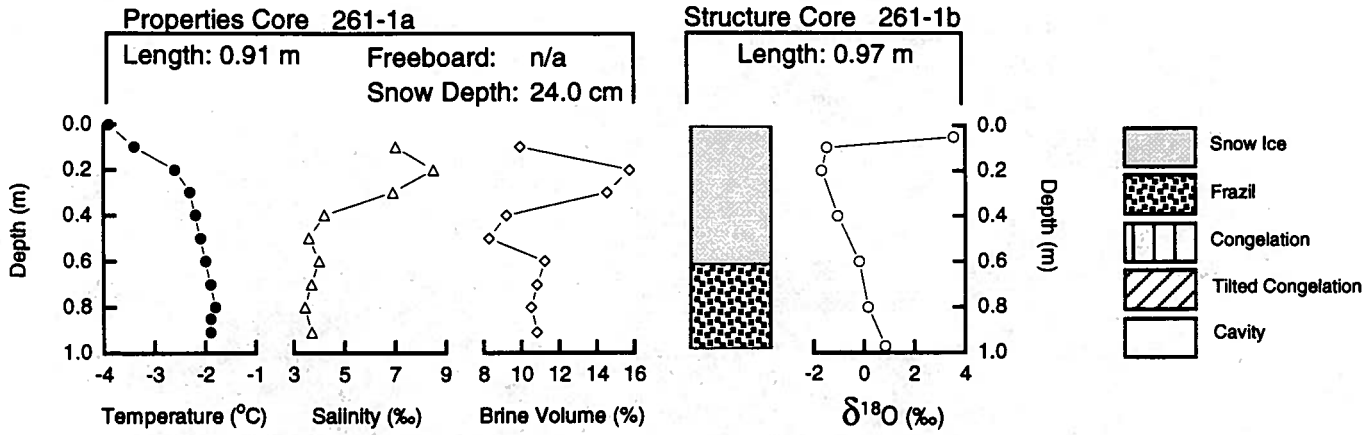

Position: 69° 21.49' S, 108° 47.27' W
Date: 18 September 1993

Mean Ice Thickness: 85.9 ± 41.2 cm
Mean Snow Thickness: 27.7 ± 8.7 cm
Mean Freeboard: 2.0 ± 3.1 cm
Floe Type: C

Salinity min: 3.4 ‰
Salinity max: 8.5 ‰
Salinity mean: 5.0 ‰

$\delta^{18}O$ min: -1.68 ‰
$\delta^{18}O$ max: 3.55 ‰
$\delta^{18}O$ mean: 0.02 ‰

Snow Ice: 56.7 %
Frazil Ice: 43.3 %
Congelation: 00.0 %
Cavity: 00.0 %

Snow Fraction
f_s: 6.79 %
F_m: 3.85 %

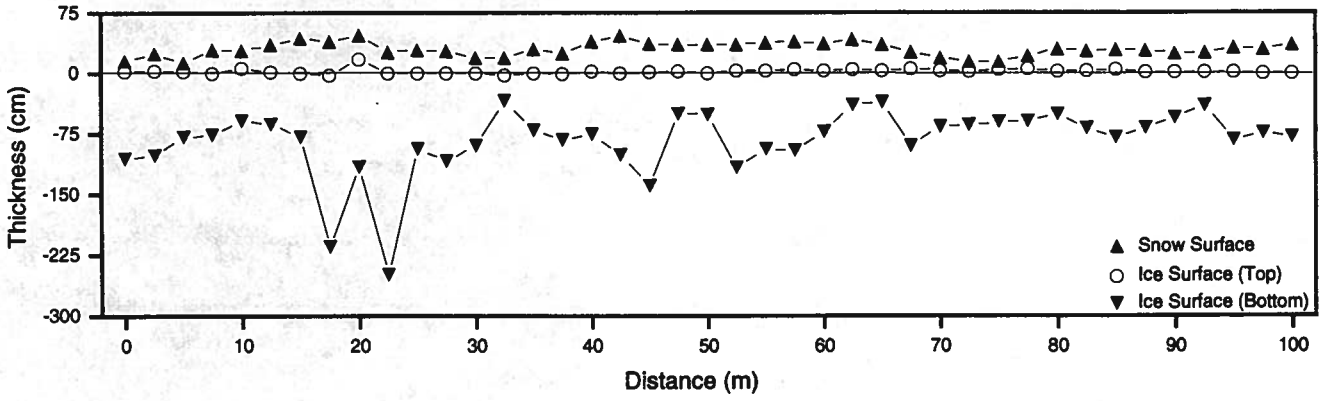

NBP 93-5 FLOE 262

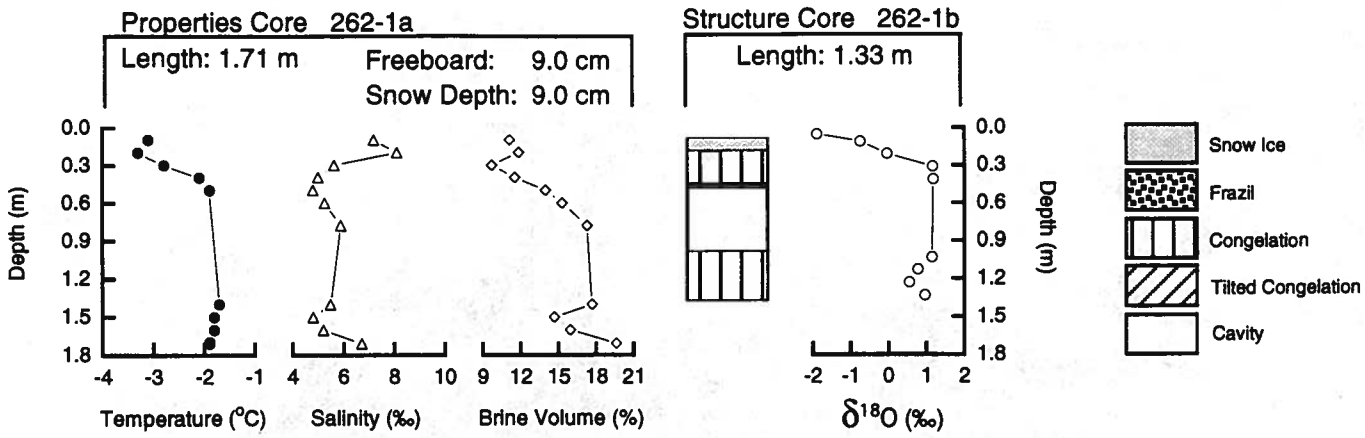

Position: 69° 22.00' S, 109° 46.97' W
Date: 19 September 1993

Mean Ice Thickness: 98.3 ± 48.0 cm
Mean Snow Thickness: 14.0 ± 8.7 cm
Mean Freeboard: 6.1 ± 3.8 cm
Floe Type: C

Salinity min: 4.8 ‰
Salinity max: 8.1 ‰
Salinity mean: 5.8 ‰

$\delta^{18}O$ min: -1.90 ‰
$\delta^{18}O$ max: 1.18 ‰
$\delta^{18}O$ mean: 0.34 ‰

Snow Ice: 8.3 %
Frazil Ice: 0.7 %
Congelation: 51.9 %
Cavity: 39.1 %

Snow Fraction
f_s: 9.64 %
F_m: 0.80 %

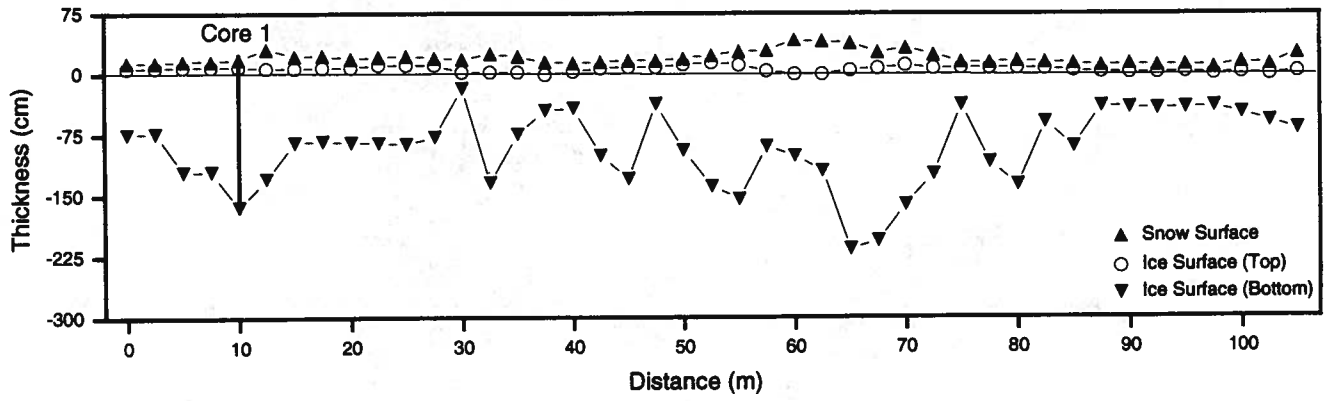

NBP 93-5 FLOE 262

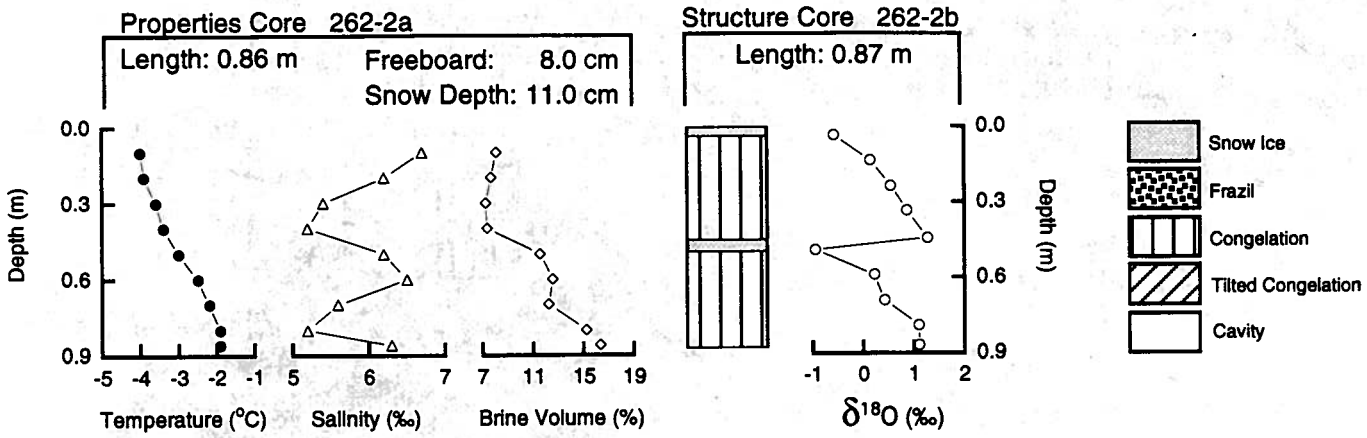

Position: 69° 22.00' S, 109° 46.97' W
Date: 19 September 1993

Mean Ice Thickness: 98.3 ± 48.0 cm
Mean Snow Thickness: 14.0 ± 8.7 cm
Mean Freeboard: 6.1 ± 3.8 cm
Floe Type: C

Salinity min: 5.2 ‰
Salinity max: 6.7 ‰
Salinity mean: 5.9 ‰

$\delta^{18}O$ min: -0.95 ‰
$\delta^{18}O$ max: 1.27 ‰
$\delta^{18}O$ mean: 0.42 ‰

Snow Ice: 9.2 %
Frazil Ice: 00.0 %
Congelation: 90.8 %
Cavity: 00.0 %

Snow Fraction
f_s: 5.97 %
F_m: 0.55 %

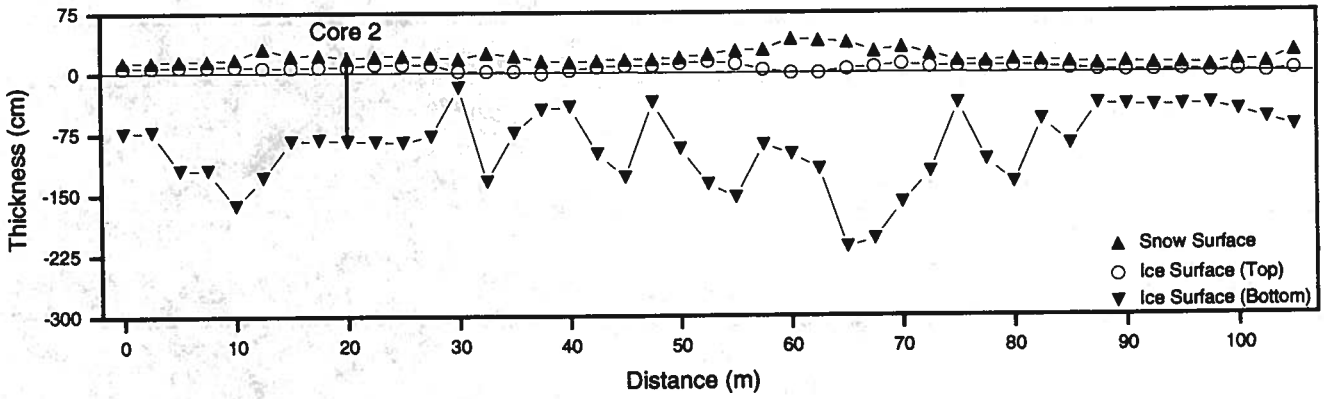

NBP 93-5 FLOE 262

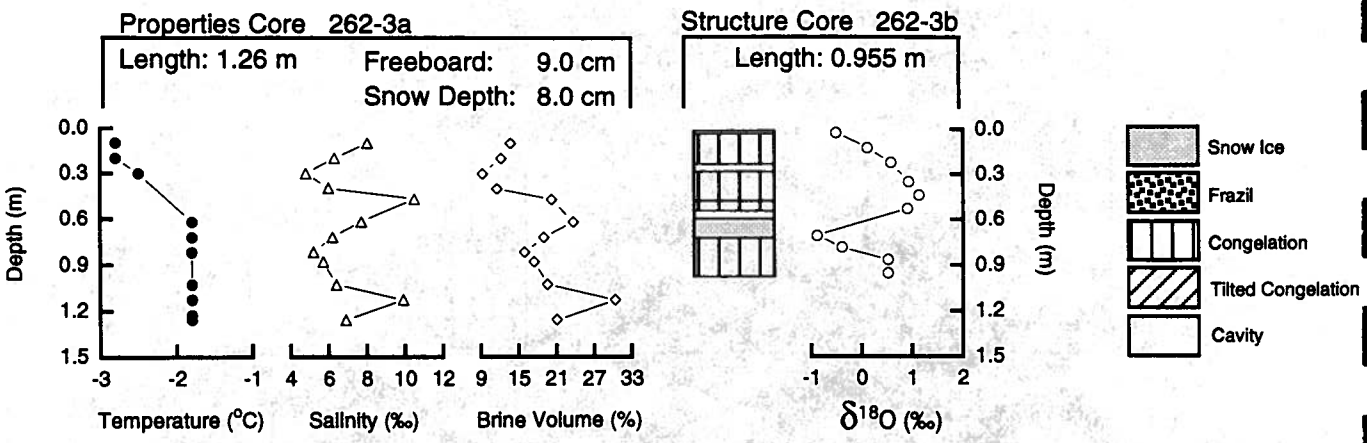

Position: 69° 22.00' S, 109° 46.97' W
Date: 19 September 1993

Mean Ice Thickness: 98.3 ± 48.0 cm
Mean Snow Thickness: 14.0 ± 8.7 cm
Mean Freeboard: 6.1 ± 3.8 cm
Floe Type: C

Salinity min: 4.8 ‰
Salinity max: 10.5 ‰
Salinity mean: 7.0 ‰

$\delta^{18}O$ min: -0.89 ‰
$\delta^{18}O$ max: 1.13 ‰
$\delta^{18}O$ mean: 0.29 ‰

Snow Ice: 15.7 %
Frazil Ice: 0.5 %
Congelation: 73.3 %
Cavity: 10.5 %

Snow Fraction
f_s: 6.25 %
F_m: 0.98 %

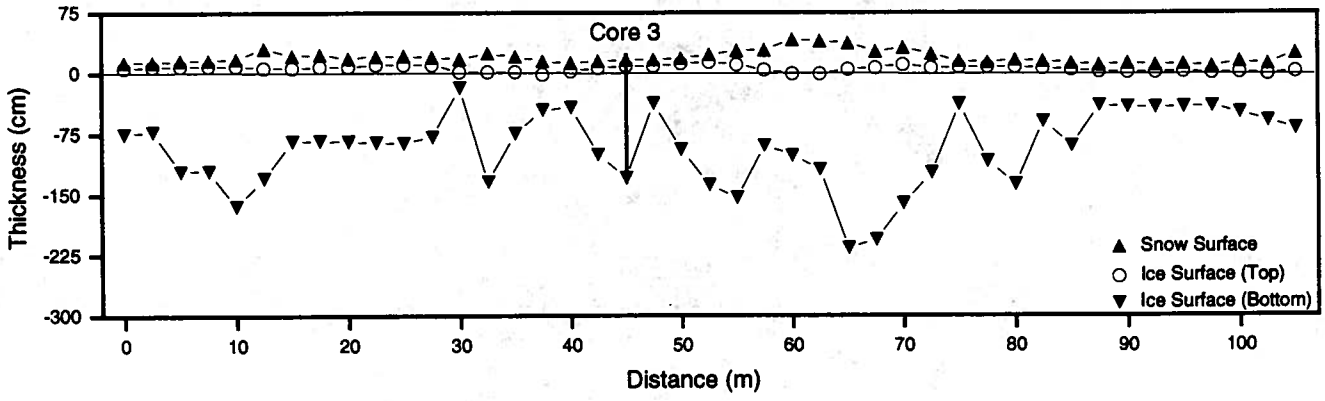

NBP 93-5 FLOE 262

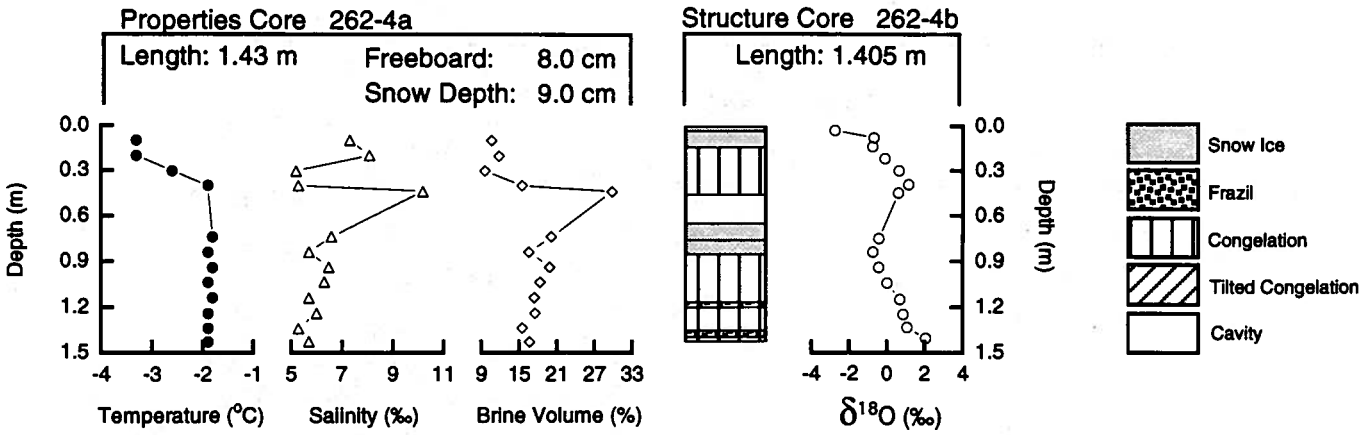

Position: 69° 22.00' S, 109° 46.97' W
Date: 19 September 1993

Mean Ice Thickness: 98.3 ± 48.0 cm
Mean Snow Thickness: 14.0 ± 8.7 cm
Mean Freeboard: 6.1 ± 3.8 cm
Floe Type: C

Salinity min: 5.2 ‰
Salinity max: 10.2 ‰
Salinity mean: 6.4 ‰

$\delta^{18}O$ min: -2.74 ‰
$\delta^{18}O$ max: 2.08 ‰
$\delta^{18}O$ mean: 0.09 ‰

Snow Ice: 24.2 %
Frazil Ice: 5.0 %
Congelation: 57.3 %
Cavity: 13.5 %

Snow Fraction
f_s: 5.99 %
F_m: 1.45 %

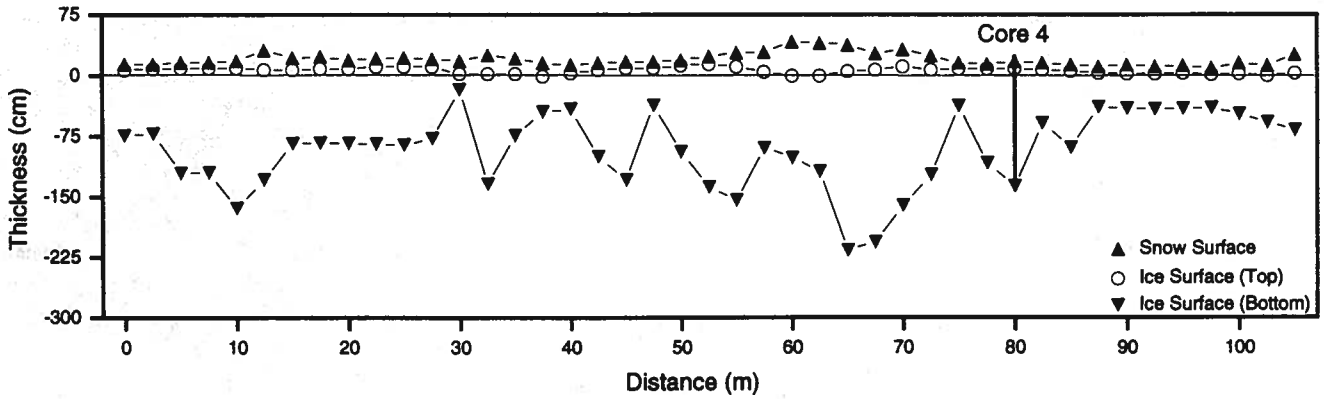

NBP 93-5 FLOE 262

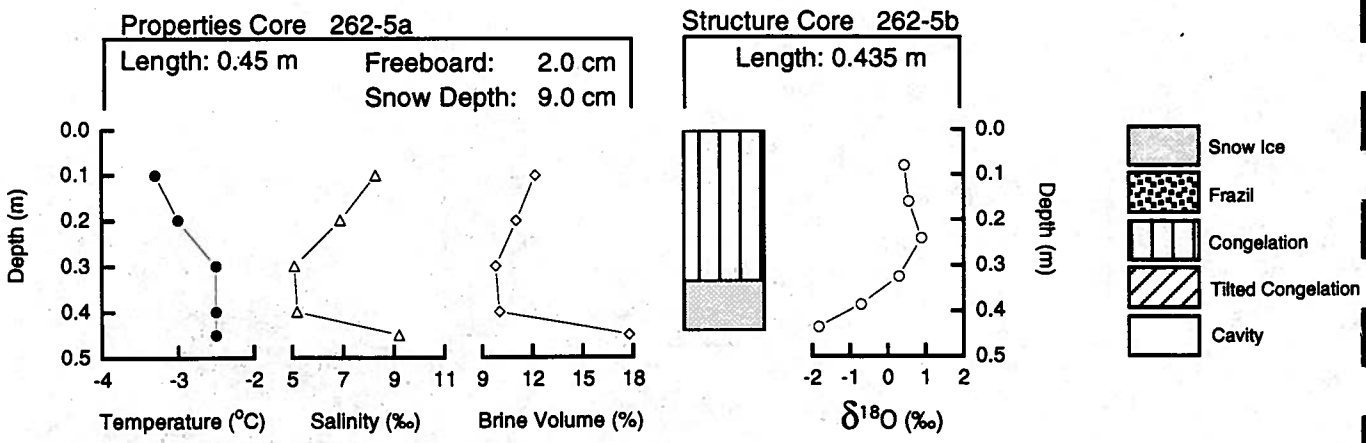

Position: 69° 22.00' S, 109° 46.97' W
Date: 19 September 1993

Mean Ice Thickness: 98.3 ± 48.0 cm
Mean Snow Thickness: 14.0 ± 8.7 cm
Mean Freeboard: 6.1 ± 3.8 cm
Floe Type: C

Salinity min: 5.1 ‰
Salinity max: 9.2 ‰
Salinity mean: 6.9 ‰

$\delta^{18}O$ min: -1.83 ‰
$\delta^{18}O$ max: 0.89 ‰
$\delta^{18}O$ mean: -0.06 ‰

Snow Ice: 25.3 %
Frazil Ice: 00.0 %
Congelation: 74.7 %
Cavity: 00.0 %

Snow Fraction
f_s: 9.19 %
F_m: 2.32 %

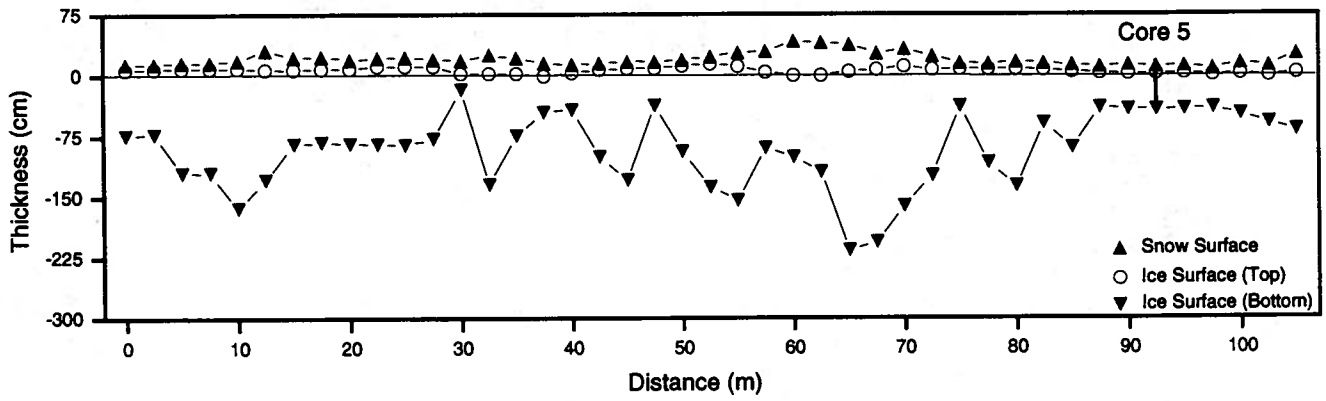

NBP 93-5 FLOE 264

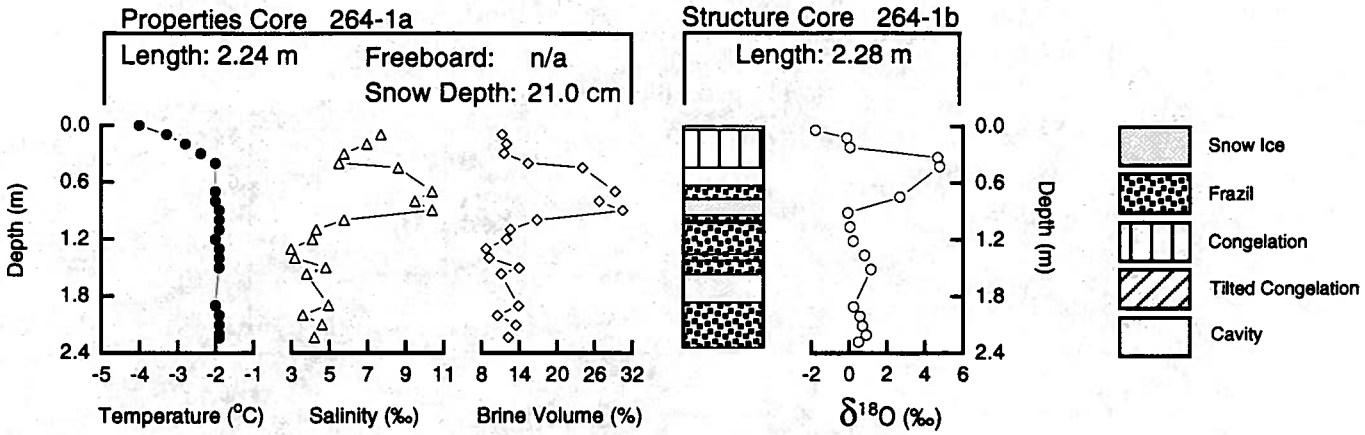

Position: 69° 01.17' S, 109° 58.
Date: 21 September 1993

Mean Ice Thickness: 102.5 ± 72.1 cm
Mean Snow Thickness: 18.8 ± 8.2 cm
Mean Freeboard: 5.2 ± 7.5 cm
Floe Type: C

Salinity min: 3.0 ‰
Salinity max: 10.4 ‰
Salinity mean: 5.8 ‰

$\delta^{18}O$ min: -1.79 ‰
$\delta^{18}O$ max: 4.76 ‰
$\delta^{18}O$ mean: 0.96 ‰

Snow Ice: 9.2 %
Frazil Ice: 52.9 %
Congelation: 16.9 %
Cavity: 21.0 %

Snow Fraction
f_s: 3.38 %
F_m: 0.31 %

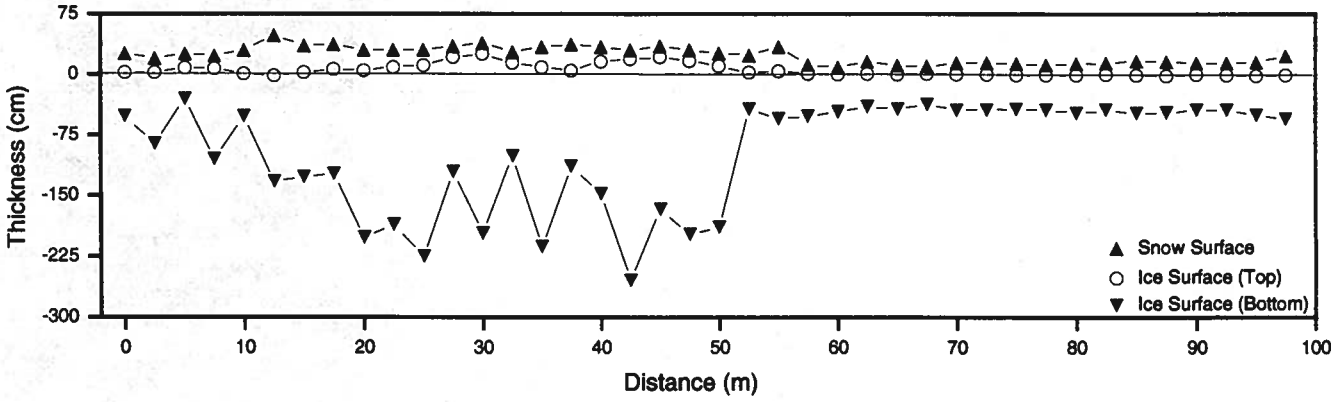

NBP 93-5 FLOE 265

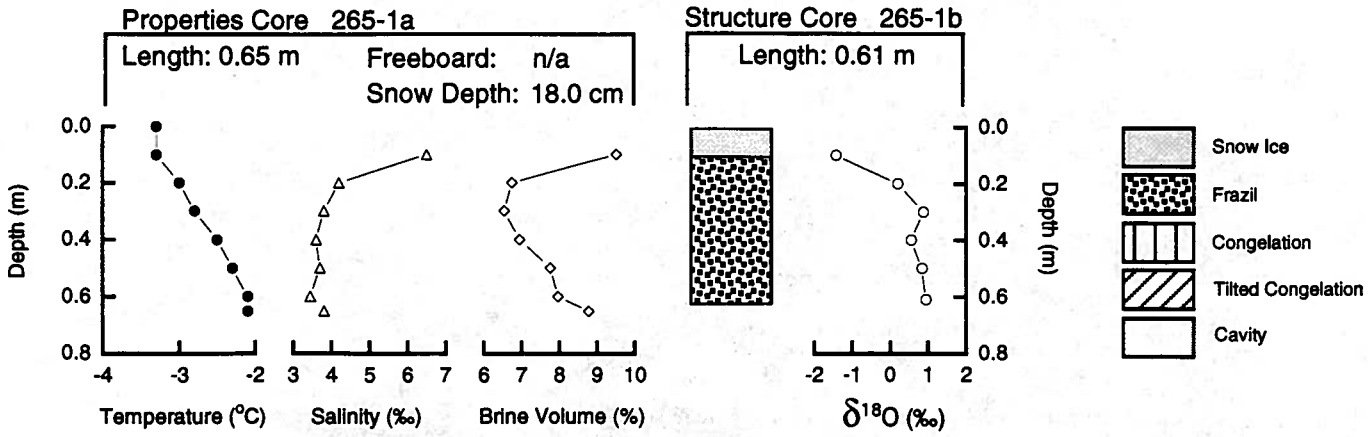

Position: 68° 20.62' S, 110° 08.23' W
Date: 22 September 1993

Mean Ice Thickness: 67.8 ± 14.3 cm
Mean Snow Thickness: 22.1 ± 4.4 cm
Mean Freeboard: 1.2 ± 1.9 cm
Floe Type: B

Salinity min: 3.4 ‰
Salinity max: 6.5 ‰
Salinity mean: 4.1 ‰

$\delta^{18}O$ min: -1.43 ‰
$\delta^{18}O$ max: 0.94 ‰
$\delta^{18}O$ mean: 0.33 ‰

Snow Ice: 16.4 %
Frazil Ice: 83.6 %
Congelation: 00.0 %
Cavity: 21.0 %

Snow Fraction
f_s: 10.83 %
F_m: 1.78 %

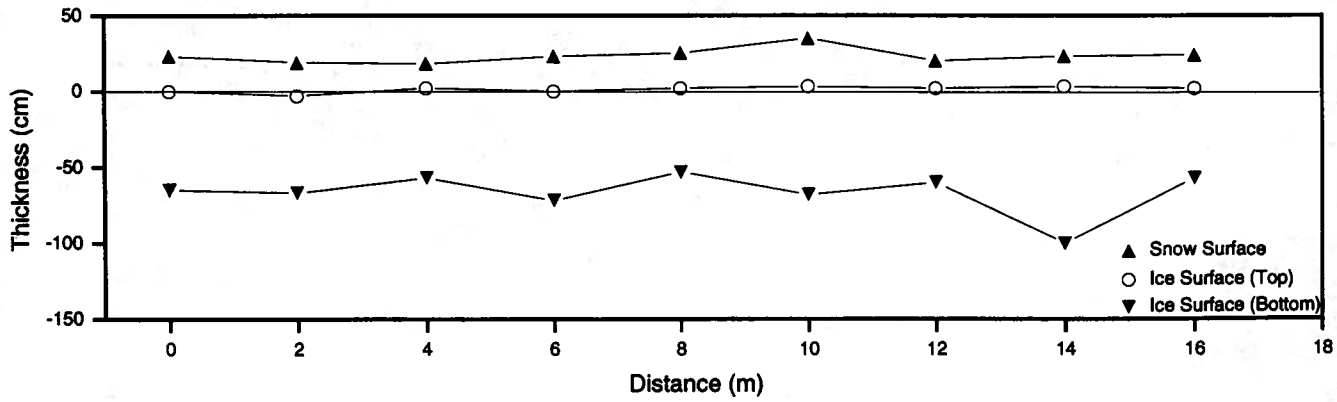

NBP 93-5 FLOE 265

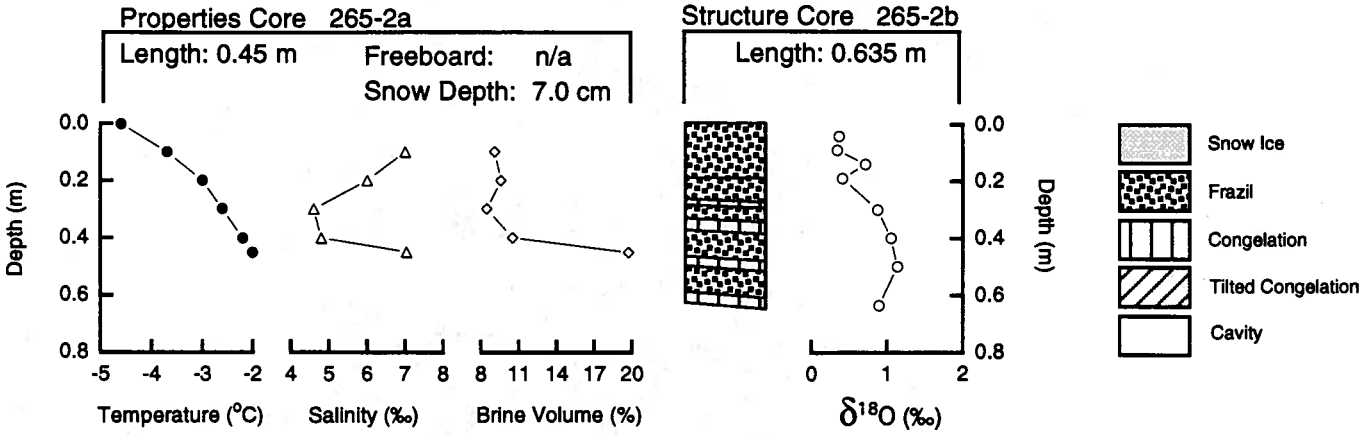

Position: 67° 59.84' S, 110° 00.80' W
Date: 22 September 1993

Mean Ice Thickness: 67.8 ± 14.3 cm
Mean Snow Thickness: 22.1 ± 4.4 cm
Mean Freeboard: 1.2 ± 1.9 cm
Floe Type: B

Salinity min: 4.6 ‰
Salinity max: 7.0 ‰
Salinity mean: 5.9 ‰

$\delta^{18}O$ min: 0.35 ‰
$\delta^{18}O$ max: 1.14 ‰
$\delta^{18}O$ mean: 0.73 ‰

Snow Ice: 00.0 %
Frazil Ice: 78.0 %
Congelation: 22.0 %
Cavity: 00.0 %

Snow Fraction
f_s: 0.00 %
F_m: 0.00 %

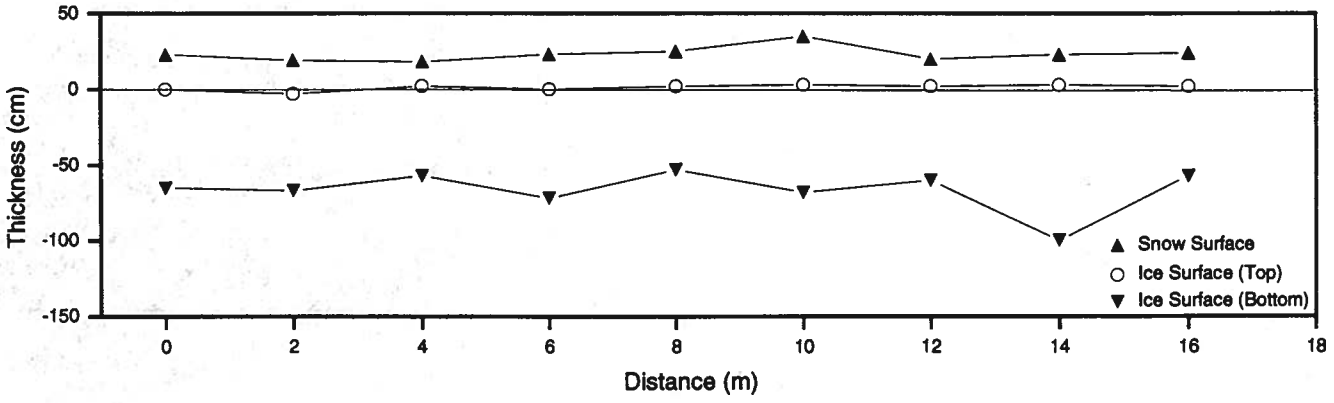

NBP 93-5 FLOE 266

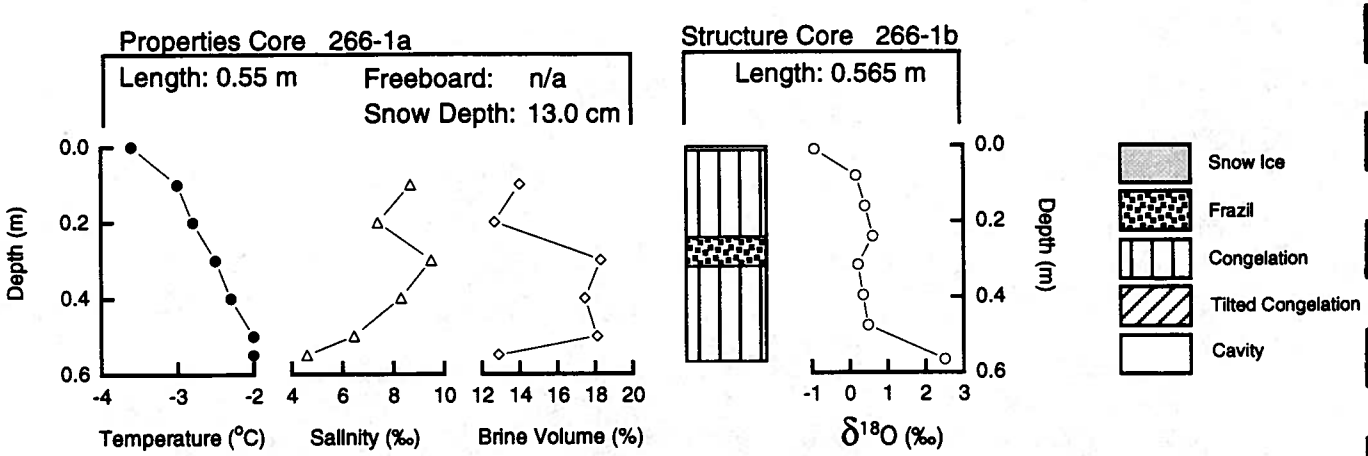

Position: 67° 30.10' S, 109° 33.66' W
Date: 23 September 1993

Mean Ice Thickness: 65.0 ± 20.5 cm
Mean Snow Thickness: 18.4 ± 8.4 cm
Mean Freeboard: 1.3 ± 2.3 cm
Floe Type: B

Salinity min: 4.6 ‰
Salinity max: 9.5 ‰
Salinity mean: 7.5 ‰

$\delta^{18}O$ min: -0.93 ‰
$\delta^{18}O$ max: 2.51 ‰
$\delta^{18}O$ mean: 0.48 ‰

Snow Ice: 1.8 %
Frazil Ice: 13.3 %
Congelation: 84.9 %
Cavity: 00.0 %

Snow Fraction
f_s: 7.05 %
F_m: 0.12 %

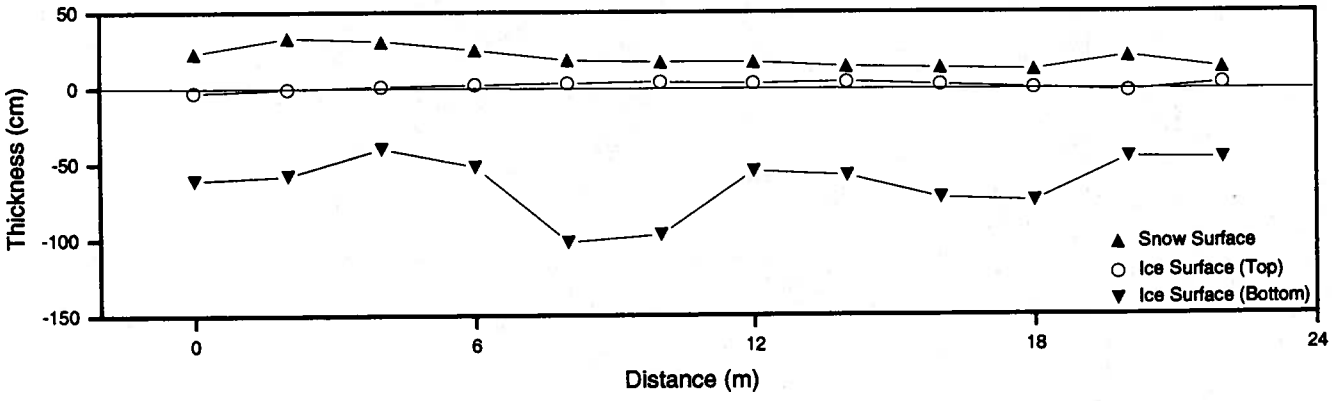

DISTRIBUTION

M. O. Jeffries Geophysical Institute Univ. of Alaska Fairbanks 903 Koyukuk Drive P.O. Box 757320 Fairbanks, AK 99775–7320 U.S.A.	Dr. B. Lettau Manager, Ocean & ClimateSciences Office of Polar Programs National Science Foundation 4201 Wilson Boulevard Arlington, VA 22230 U.S.A.	V. I. Lytle Antarctic CRC University of Tasmania P.O. Box 252C Hobart, TAS 7001 Australia
A. P. Worby Antarctic CRC University of Tasmania P.O. Box 252C Hobart, TAS 7001 Australia	J. H. Triplehorn, Librarian Geophysical Institute Univ. of Alaska Fairbanks 903 Koyukuk Drive P.O. Box 757320 Fairbanks, AK 99775–7320 U.S.A.	R. A. Massom Antarctic CRC University of Tasmania P.O. Box 252C Hobart, TAS 7001 Australia
K. Morris Geophysical Institute Univ. of Alaska Fairbanks 903 Koyukuk Drive P.O. Box 757320 Fairbanks, AK 99775–7320 U.S.A.	N. Liston, Librarian CRREL 72 Lyme Road Hanover NH 03755-1290 U.S.A.	S. F. Ackley CRREL 72 Lyme Road Hanover NH 03755-1290 U.S.A.
W. F. Weeks 6533 SW 34th Avenue Portland, OR 97201 U.S.A.	W. Mills, Librarian Scott Polar Research Institute Cambridge University Lensfield Road Cambridge CB2 1ER England	A. J. Gow CRREL 72 Lyme Road Hanover NH 03755-1290 U.S.A.
B. Hurst–Cushing Geophysical Institute Univ. of Alaska Fairbanks 903 Koyukuk Drive P.O. Box 757320 Fairbanks, AK 99775–7320 U.S.A.	S. Priamikov, Librarian Arctic & Antarctic Research Institute 38 Bering Street St. Petersburg 199397 Russia	W. B. Tucker, III CRREL 72 Lyme Road Hanover NH 03755-1290 U.S.A.
R. Jaña Instituto Antartico Chileno Luis Thayer Ojeda 814 Casilla 16521, Correo 9 Providencia, Santiago Chile	F. Matsusato, Librarian National Institute of Polar Research 9–10, Kaga I–chrome Tokyo 173 Japan	H. Eicken Alfred–Wegener–Institut für Polar– und Meeresforsch. Postfach 12 01 61 D2580 Bremerhaven Federal Republic of Germany
H. R. Krouse Dept. of Physics & Astronomy University of Calgary 2500 University Drive, N.W. Calgary, Alberta Canada T2N 1N4	R. Sbresny, Librarian Alfred–Wegener–Institut für Polar– und Meeresforsch. Postfach 12 01 61 D2580 Bremerhaven Federal Republic of Germany	C. Haas Alfred–Wegener–Institut für Polar– und Meeresforsch. Postfach 12 01 61 D2580 Bremerhaven Federal Republic of Germany
T. Maksym Geophysical Institute Univ. of Alaska Fairbanks 903 Koyukuk Drive P.O. Box 757320 Fairbanks, AK 99775–7320 U.S.A.	I. Allison Antarctic CRC University of Tasmania P.O. Box 252C Hobart, TAS 7001 Australia	S. Harangozo British Antarctic Survey High Cross Madingley Road Cambridge CB30ET England

M. A. Lange Institute for Geophysics Westfälische Wilhelms Universität Münster D-48149 Münster Federal Republic of Germany	T. Kawamura Inst. Low Temperature Science Hokkaido University Kita 19, Nishi 8 Sapporo 060 Japan	Dr. V. P. Gavrilo Arctic & Antarctic Research Institute 38 Bering Street St. Petersburg 199397 Russia
V. E. Squire Dept. of Mathematics and Statistics University of Otago P. O. Box 56 Dunedin New Zealand	P. Wadhams Scott Polar Research Institute Cambridge University Lensfield Road Cambridge CB2 1ER England	N. V. Cherapanov Arctic & Antarctic Research Institute 38 Bering Street St. Petersburg 199397 Russia